



**HAL**  
open science

# Development of implantable antibacterial ePTFE prostheses for soft tissues

Yaëlle Roina

► **To cite this version:**

Yaëlle Roina. Development of implantable antibacterial ePTFE prostheses for soft tissues. Human health and pathology. Université Bourgogne Franche-Comté, 2023. English. NNT : 2023UBFCE002 . tel-04680926

**HAL Id: tel-04680926**

**<https://theses.hal.science/tel-04680926>**

Submitted on 29 Aug 2024

**HAL** is a multi-disciplinary open access archive for the deposit and dissemination of scientific research documents, whether they are published or not. The documents may come from teaching and research institutions in France or abroad, or from public or private research centers.

L'archive ouverte pluridisciplinaire **HAL**, est destinée au dépôt et à la diffusion de documents scientifiques de niveau recherche, publiés ou non, émanant des établissements d'enseignement et de recherche français ou étrangers, des laboratoires publics ou privés.

**THESE DE DOCTORAT DE L'ETABLISSEMENT UNIVERSITE BOURGOGNE FRANCHE-COMTE**

**PREPAREE A UFR Sciences et Techniques | Université de Franche-Comté**

Ecole doctorale n°554

Ecole doctorale Environnements - Santé

Doctorat de Médecine, santé publique, environnement et société

Par

Mme ROINA Yaëlle

Développement de prothèses ePTFE antibactériennes implantables pour les tissus mous

Thèse présentée et soutenue à Besançon, le 01/02/2023

Composition du Jury :

M. Ameduri Bruno	DR à Ecole Nationale Supérieure de Chimie de Montpellier	Rapporteur
Mme Lydie Ploux	DR à Université de Strasbourg	Rapporteur
Mme Goncalvez Anne-Marie	Professeur à Université de Versailles - ILV	Examinatrice
M. Didier Hocquet	PU-PH à CHRU Jean-Minjoz	Examineur
M. Frédéric Auber	PU-PH à CHRU Jean-Minjoz	Examineur
M. Herlem Guillaume	MCF à Université de Bourgogne Franche-Comté	Directeur de thèse



**Titre :** Développement de prothèses ePTFE antibactériennes implantables pour les tissus mous.

**Mots clés :** prothèse, polymère fluoré, fonctionnalisation, biocompatibilité, antibactérien

**Résumé :** Bien que largement utilisé dans le domaine de la chirurgie et du médical plus généralement, le polytétrafluoroéthylène expansé (ePTFE) présente également des inconvénients importants, comme celui de la colonisation de bactéries multirésistantes et la formation de biofilms qui peuvent engendrer de graves conséquences sur la santé des patients. Il existe un besoin urgent d'empêcher ces colonisations bactériennes de survenir sans utilisation d'antibiotiques. C'est à cette fin que notre projet intervient. Ce manuscrit présente une nouvelle méthode de fonctionnalisation de surface du ePTFE consistant à mélanger des composés aliphatiques aminés ainsi qu'un métal alcalin, le lithium. Cette solution conduit à la défluoruration et l'amination de surface du matériau, et caractérisé par spectroscopie XPS et IR-ATR. Ces traitements chimiques entraînent des modifications de

propriétés physico-chimiques importantes comme la rigidification de la surface, ou son changement en surface hydrophile. Ces matériaux aminés sont ensuite fonctionnalisés par physi ou chimisorption de molécules antibactériennes. Par la suite, ces matériaux sont évalués par des tests de cytotoxicité indirecte. Six matériaux ont été sélectionnés par ce moyen comme potentiellement éligibles à une application médicale. Leur efficacité antibactérienne contre 6 souches à l'origine de maladies nosocomiales est enfin évaluée. Selon le composé aminé ou la molécule antibactérienne utilisés, des tendances se dessinent sur le nombre de bactéries affectées par les matériaux. Un des matériaux fonctionnalisés se démarque des autres, avec une probable activité antibactérienne sur toutes les souches testées.

**Title :** Development of implantable antibacterial ePTFE prostheses for soft tissues.

**Keywords :** prosthesis, fluorinated polymer, functionalization, biocompatibility, antibacterial

**Abstract :** Although widely used in the field of surgery and, more generally, medicine, ePTFE also has significant drawbacks, such as the colonization of multi-resistant bacteria which can have serious consequences on the health of patients. There is an urgent need to prevent these bacterial colonizations from occurring, without the use of antibiotics. It is to this end that our project intervenes. This manuscript presents a new surface functionalization method consisting in mixing aliphatic amino compounds and an alkali metal, lithium. This solution leads to defluorination and surface amination of the material, which have been proven by XPS and IR-ATR spectroscopy. These chemical treatments lead to modifications

of important physico-chemical properties such as the stiffening of the surface, or its change into a hydrophilic surface. These amino materials are then functionalized by immersion or grafting of antibacterial molecules. Subsequently, these materials are evaluated by indirect cytotoxicity assays. Six materials were selected by this mean as potentially eligible for medical application. Their antibacterial efficiency against 6 strains causing nosocomial diseases is then evaluated. Depending on the amino compound or the antibacterial molecule used, trends emerge in the number of bacteria affected by the materials. One of the functionalized materials stands out from the others, with probable antibacterial activity on all the strains tested.



## Table of contents:

List of figures .....	7
List of tables .....	9
<b>Introduction .....</b>	<b>10</b>
<b>Presentation of the project .....</b>	<b>10</b>
<b>Abbreviations .....</b>	<b>11</b>
<b>History and presentation of ePTFE .....</b>	<b>13</b>
<b>I. State of the art on medical applications of ePTFE .....</b>	<b>14</b>
<b>I.1. ePTFE improvements needed for medical applications .....</b>	<b>14</b>
<b>I.2. Existing ePTFE functionalization for medical applications .....</b>	<b>16</b>
<b>I.2.1. Covalent bonding .....</b>	<b>16</b>
<b>I.2.2. Non-covalent bonding .....</b>	<b>21</b>
<b>I.3. The assessment of ePTFE-based medical devices in clinical trials .....</b>	<b>26</b>
<b>I.3.1. ePTFE-covered stents .....</b>	<b>27</b>
<b>I.3.2. Haemodialysis and bypass ePTFE grafts .....</b>	<b>35</b>
<b>I.3.3. Guided bone and tissue regeneration procedures for maxillofacial defects .....</b>	<b>38</b>
<b>I.3.4. Hernia repair .....</b>	<b>41</b>
<b>I.3.5. Heart repair .....</b>	<b>43</b>
<b>I.3.6. Other clinical trials .....</b>	<b>45</b>
<b>I.3.6.1. Functional and aesthetic nasal surgery .....</b>	<b>45</b>
<b>I.3.6.2. Bleeding sealant .....</b>	<b>46</b>
<b>I.3.6.3. Ocular non-cancerous surgery .....</b>	<b>46</b>
<b>II. Chemical etching and functionalization of ePTFE using organic solvent and alkaline metal .....</b>	<b>48</b>
<b>II.1. Previous work leading to this study .....</b>	<b>48</b>
<b>II.2. Birch and Benkeser inspired reaction .....</b>	<b>51</b>
<b>II.2.1. Materials and methods .....</b>	<b>51</b>
<b>II.2.2. Reaction description and observations .....</b>	<b>51</b>
<b>II.2.3. Lithium alkylamide formation and characterization .....</b>	<b>52</b>
<b>II.2.4. Defluorination and amination of the fluorinated surface .....</b>	<b>57</b>
<b>II.3. Characterizations of the functionalized surfaces .....</b>	<b>60</b>
<b>II.3.1. Materials and methods .....</b>	<b>60</b>
<b>II.3.2. Spectroscopy analysis .....</b>	<b>60</b>
<b>II.3.3. Imaging .....</b>	<b>62</b>
<b>AFM imaging .....</b>	<b>62</b>

SEM imaging.....	64
II.3.4.    Drop Shape Analysis.....	66
Fowkes' theory <sup>213</sup> method to determine surface energy.....	67
Results and discussion.....	68
II.3.5.    Instrumented Indentation.....	70
Presentation of Oliver and Pharr method.....	70
Results and discussion.....	72
III.    Additional functionalization with bioactive molecules and efficiency evaluation.....	75
III.1.    Selection of antibacterial molecules.....	75
III.1.1.    Chitosan.....	75
III.1.2.    Polyethylenimine.....	78
III.1.3.    Polyvinyl pyrrolidone Iodine complex.....	81
III.2.    Functionalization and characterizations.....	83
III.2.1.    Materials and methods.....	83
III.2.1.    Reaction of functionalization.....	83
III.2.2.    SEM imaging.....	84
III.2.3.    IR-ATR Spectral characterization.....	86
III.3.    Biocompatibility assessment on the samples obtained.....	93
Materials and method.....	93
Results and discussion.....	95
III.4.    Antibacterial evaluation of the biomaterials.....	103
Materials and methods.....	104
Results and discussion.....	106
Conclusion    and outlook.....	109
Résumé en français.....	112
Annexes.....	130
A1.....	130
A2.....	131
Chitosan grafting protocol.....	131
PEI grafting protocol.....	131
PVP soaking protocol.....	132
A3.....	132
A4.....	140
References.....	143



## List of figures

Figure 1. Schematic illustrating the mussel-inspired chemistry of dopamine that is used as a precursor material for the synthesis and deposition of conformal polydopamine (PDA) film. <sup>31</sup> .....	16
Figure 2. Chemical route of surface activation of ePTFE with reduction using UV light and bisphenone/ NaH in DMF; to its UV-induced polymerization grafting of 2-Methacryloyloxyethyl phosphorylcholine, using dipentaerythriol penta-/hexa-acrylate as a cross-linker. <sup>32</sup> .....	18
Figure 3. Concentration of of <i>S. aureus</i> plotted as a function of time for the experimental sequence: control, ePTFE, MA-ePTFE, PEG-MA-ePTFE, PEN-PEG-MA-ePTFE, and PEN-ePTFE <sup>39</sup> .....	19
Figure 4. Chemical route of plasma-induced grafting of penicillin using maleic anhydride (MA) and polyethylene glycol (PEG) as intermediates. <sup>38</sup> .....	20
Figure 5. Numbers of cells attached on unmodified ePTFE, (HEP/COL) <sub>5</sub> modified ePTFE, REDV-(HEP/ COL) <sub>5</sub> modified ePTFE and REVD-(HEP/COL) <sub>5</sub> modified ePTFE (24, 48, and 72 h, *indicates statistically significant difference at the P<0.05 level). <sup>65</sup> .....	24
Figure 6. Distribution and topics of ePTFE studies in clinical trials (values obtained from the Pubmed database). .....	27
Figure 7. Endoleak classification system. <sup>108</sup> .....	28
Figure 8. Kaplan-Meier curves with associated 95 % confidence intervals for (A) freedom from type IA endoleak and type I/III endoleak, and (B) overall survival and freedom from aneurysm-related mortality after endovascular aneurysm repair (EVAR) with the Ovation Abdominal Stent Graft platform in the Effectiveness of Custom Seal with Ovation: Review of the Evidence (ENCORE) cohort. <sup>112</sup> .....	31
Figure 9. Example of percutaneous transluminal angioplasty (PTA) with self-expanding stent placement. <sup>135</sup> .....	34
Figure 10. Overall 1-year primary patency rate of the provisional stenting group. <sup>136</sup> .....	35
Figure 11. Forest plot of risk ratio (RR) of one-year primary patency loss of geometrically modified vs. standard expanded polytetrafluoroethylene (ePTFE) arteriovenous grafts for haemodialysis access based on randomised controlled trials (RCT) and observational studies. The solid squares denote the RRs, the horizontal lines represent the 95 % confidence intervals (CIs), and the diamonds denote the pooled effect size. M-H = Mantel-Haenszel random effects test; df = degrees of freedom. <sup>139</sup> .....	36
Figure 12. Forest plot of risk ratio (RR) of one-year secondary patency loss of geometrically modified vs. standard expanded polytetrafluoroethylene (ePTFE) arteriovenous grafts for haemodialysis access based on randomised controlled trials (RCTs) and observational studies. The solid squares denote the risk ratios, the horizontal lines represent the 95 % confidence intervals (CIs), and the diamonds denote the pooled effect size. M-H = Mantel-Haenszel random effects test; df = degrees of freedom. <sup>139</sup> .....	37
Figure 13. Horizontal attachment levels (mm) and class of furcation involvement. <sup>152</sup> .....	39
Figure 14. Complication during follow-up for patients that have received Ventralex or Cabs'Air device for their hernia repair surgery. <sup>179</sup> .....	43
Figure 15. a) Long-term survival of patients with mitral valve repair and b) Freedom from reoperation for all patients. <sup>190</sup> .....	44
Figure 16. XRD structure of lithium alkylamide LiEDA.....	54
Figure 17. Powder XRD patterns of lithium alkylamides (a) LiDETA and (b) LiDAP.....	55
Figure 18. Reactive centers in the CDFT formalism of the lithium alkylamides. Isosurface maps of the dual descriptors ( $\Delta f$ ) of (a) LiEDA, (b) LiDETA and (c) LiDAP. Positive and negative regions of the dual descriptor $\Delta f$ are represented as blue and red colors, respectively.....	56



Figure 19. First and second derivatives of $E[N;v(r)]$ with respect to $N$ and $v(r)$ , where $E$ is the state energy of a non-degenerate $N$ -electron system, and $v(r)$ the electron nucleus Coulomb interaction. <sup>234</sup> .....	56
Figure 20. XPS analysis on a LiDETA sample and atomic composition of the surface. ....	58
Figure 21. XPS analysis on a LiEDA sample and atomic composition of the surface. ....	59
Figure 22. Vibrational analysis by IR-ATR spectroscopy of (a) PTFE, LiEDA, LiDETA and LiDAP treated samples, (b) LiEDA sample with diamond and Ge crystals and by Raman spectroscopy of (c) ePTFE modified by LiDETA lithium alkylamide dissolved in THF and (d) PTFE, ePTFE modified by THF+LiEDA, THF+LiDETA and LiEDA.....	62
Figure 23. AFM images of samples treated with LiEDA. Image A and C: PTFE, B: ePTFE and D: ePTFE 3D picture. ....	63
Figure 24. AFM image and the corresponding 3D picture of PTFE sample treated with LiDETA .....	64
Figure 25. SEM images of (a) bulk PTFE, (b) LiDETA and (c) LiEDA treated PTFE. ....	65
Figure 26. Transverse direction fracture surface of sintered PTFE irradiated with 200kGy at 335 °C. <sup>255</sup> .....	65
Figure 27. LiEDA sample sliced and observed by SEM imaging. Untreated area width is indicated by the blue arrows.....	66
Figure 28. Surface free energy and corresponding contact angles (in blue), the error bars are calculated with propagation of uncertainty using first order Taylor expansion applied to Fowkes' theory formulas. <sup>214</sup> .....	69
Figure 29. A) Dependence of the PTFE contact angle on the exposure time to Ar plasma. The measurement was accomplished 5 min after the exposure. B) Dependence of the contact angle on the plasma exposure time and on the aging time. The measurements were accomplished immediately after the treatment (0 h) and then after 24, 48, 72 and 96 h aging times. <sup>259</sup> .....	70
Figure 30. Indentation modulus of unmodified ePTFE (a) or PTFE (b) and modified by LiEDA and LiDETA. The error bars represent confidence interval with probability of 95 %. ....	73
Figure 31. Chitosan synthesis through chitin deacetylation. <sup>274</sup> .....	76
Figure 32. Schematic representation of antimicrobial mechanisms of chitosan and its derivatives. <sup>276</sup> .....	76
Figure 33. AFM images of <i>S. aureus</i> (A) and <i>E. coli</i> (B) before and after treatment with chitosan. The top image is from untreated bacteria, and below treatment times are as indicated in the image. Arrows show specific cells referred to in the text. <sup>278</sup> .....	78
Figure 34. Hemolysis induced by PEIs. Each data point represents PEIs as antimicrobial agents with selective activity (Gibney 2012).....	79
Figure 35. Model of the possible bactericidal mechanism of Ag-NP-1, Ag-NP-2, and Ag-NP-3 against <i>A. baumannii</i> . <sup>291</sup> .....	80
Figure 36. Minimum inhibitory and bactericidal concentrations of povidone. <sup>270</sup> .....	81
Figure 37. Grafting of CHI on aminated ePTFE, two steps with two reactions of addition and condensation. ....	84
Figure 38. SEM micrography of ePTFE. White arrow: short distance, orange arrow: long distance.....	86
Figure 39. IR-ATR spectra obtained on ePTFE treated samples with LiEDA PEI, LiEDA CHI, LiEDA and LiEDA PVP. A weak band at 1654 $\text{cm}^{-1}$ is labeled. ....	87
Figure 40. FT-IR absorption spectra of (a) CuO/PVP nanosheets and (b) PVP <sup>302</sup> and FT-IR Peak Assignment of PVP. <sup>303</sup> .....	88
Figure 41. Experimental IR-ATR spectra of LiEDA PVP, LiDETA PVP samples and bulk PTFE; obtained with germanium crystal. ....	89
Figure 42. FT-IR spectra of pristine PEIs <sup>304</sup> .....	90
Figure 43. Experimental IR-ATR spectra of LiEDA PEI, LiDETA PEI samples and bulk PTFE; obtained with germanium crystal.....	90

Figure 44. FTIR spectrum of chitosan with the characteristic signs as evidence. <sup>305</sup> .....	91
Figure 45 Experimental IR-ATR spectra of LiEDA CHI, LiDETA CHI samples and bulk PTFE; obtained with germanium crystal. ....	92
Figure 46. Cell viability of LiHMPA treated samples, with additional grafting of chitosan followed by a reduction (LiHMPA CHI red) or not (LiHMPA CHI imine) with NaBH <sub>4</sub> . LiHMPA CHI red: sample modified with LiHMPA followed by chitosan grafting and NaBH <sub>4</sub> reduction. LiHMPA CHI imine: sample modified with LiHMPA followed by chitosan grafting only. ....	96
Figure 47. Cell viability of LiEDA treated samples, with additional grafting of chitosan followed by a reduction (ECR) or not (ECI) with NaBH <sub>4</sub> . ECR: sample modified with LiEDA followed by chitosan grafting and NaBH <sub>4</sub> reduction. ECI: sample modified with LiEDA followed by chitosan grafting only.....	97
Figure 48. Cell viability vs control (A) and confluency (B) for LiEDA-modified samples. The colors between the two figures correspond. ....	99
Figure 49. Cell viability vs control (A) and confluency (B) for LiDETA-modified samples. The colors between the two figures correspond. ....	101
Figure 50. Images obtained from the IncucyteS3 at t=0 and 4 days for 3 conditions .....	103
Figure 51. Antibacterial activity of eight treatments applied on ePTFE prostheses and tested against a panel of six bacterial strains. <i>S. aureus</i> (Sa), <i>K. pneumoniae</i> (Kp), <i>S. epidermidis</i> (Se), <i>E. coli</i> (Ec), <i>E. faecalis</i> (Ef), <i>P. aeruginosa</i> (Pa). The antibacterial activity of the chemical treatment (A) was calculated by subtracting the bacterial growth after the 22-hour incubation on non-chemically treated samples ( $\log C_{24h} - \log C_{2h}$ ) from that after incubation on chemically-treated samples ( $\log T_{24h} - \log T_{2h}$ ). Each test was carried out in triplicate.....	108

## List of tables

Table 1. Bacterial adhesion assay (colony-forming units of bacteria <i>S. epidermidis</i> on the material surface). <sup>58</sup> .....	23
Table 2. Denomination and structure of silver nanoparticle covered with different PEIs.....	80
Table 3. Mean internodal distances calculated with Gwyddion software. Confidence interval with probability of 95 % (IC95) corresponds to each value. ....	85
Table 4. Correspondence between bonds and peaks in Figure 44. ....	92
Table 5. 10 measurements of mass of Li and EDA used to modify 10 samples of ePTFE for each bottle ....	131

## Introduction

### Presentation of the project

The work described in this manuscript is the result of a reflection on a surgical problem of ePTFE prosthesis and approached in a multidisciplinary way in chemistry and biology. It has received financial support from the region "Franche-Comté" over three years in the form of the DELPHI project for "Développement de prothèses ePTFE antibactériennes implantables pour les tissus mous".

Expanded polytetrafluoroethylene (ePTFE also known as Gore-Tex) is a polymer widely used in surgical repair and replacement, as we'll develop further in the next part presenting the state of the art. This project is rooted in the issue raised of multi-resistant bacteria involved in the treatment of laparoschisis and omphalocele in newborns. These diseases, which have a prevalence of 1 out of 10 000, is treated with ePTFE membranes. These membranes are used to separate the inner organism from the outside, but they can be colonized by bacteria, which leads to severe infections. In this case, 50 % of mortality is observed among the infected subjects. Multiple interventions to change the membrane can be necessary, whereas the healing below is not attained. The use of antibiotics favors the emergence of multi-resistant bacteria that can spread in the hospital unit. This project aims to develop an antibacterial ePTFE membrane to avoid the bacterial spread and thus the use of antibiotics. The material modification process developed and presented here is of course not only designed for this issue as it could be applied in any surgical department using ePTFE (or PTFE) device.

The development of this antibacterial membrane consists in its chemical surface modification with an innovative process patented in 2022 by us. Indeed, until now, there was no known non catalyzed chemical reaction allowing to proceed to a defluorination and a functionalization of a fluorinated polymer (and more generally of a fluorinated carbon bond) in a single experimental step. Once modified, the surface is then grafted with anti-bacterial molecules. Multiple combinations of modification process and antibacterial grafting are elaborated. They are then assessed with cytotoxicity tests, largely thanks to Dr. Gwenaël Rolin and its team, to help us select non-toxic biomaterials and make sure that any antibacterial effect is not due to cytotoxicity itself. The selected biomaterials are then tested against multiple bacteria strains that are usually encountered in the nosocomial diseases mentioned before. These tests are carried out by the hospital hygienist team of Pr. Didier Hocquet in Besancon.

The first chapter of this manuscript focuses on the state of the art regarding ePTFE medical applications. We present first the already existing surface

functionalizations of ePTFE for medical applications, sorted by covalent or non-covalent bonds, for various bioactive improvements of the material. Then, the efficiency assessed in clinical trials of the current medical devices made of ePTFE in the major medical fields is reviewed to understand which aspects of the devices would benefit from improvements such as antibacterial properties but also anti-inflammatory or anti-platelets adhesion. The second chapter presents a new reaction process we developed and patented to modify the surface chemistry of the ePTFE. Numerical simulations of the reaction, as well as experimental characterizations such a spectroscopy, imaging, wetting and mechanical testing are developed. The third chapter focuses on the attribution and assessment of antibacterial properties of the material. The antibacterial molecules selected, chitosan, branched polyethylenimine, and poly(vinylpyrrolidone)–iodine complex are presented with short literature references. The characterizations of the materials obtained by MEB imaging and spectroscopy are then presented. Next, the biocompatibility by the evaluation of the cytotoxicity of the material follows. The last part of this chapter shows the results obtained from the antibacterial evaluation on six bacteria.

### Abbreviations

ePTFE: expanded polytetrafluoroethylene

PTFE: polytetrafluoroethylene

EDA: ethylenediamine

DETA: diethylenetriamine

DAP: 1,3-Diaminopropane

HMPA: hexamethylphosphoramide

Li: lithium

CHI : chitosan

PEI : branched-polyethyleneimine

PVP: polyvinylpyrrolidone-iodine

LiEDA: salt obtained by reaction of Li and EDA and used for surface treatment of ePTFE or PTFE

LiDETA: salt obtained by reaction of Li and DETA and used for surface treatment of ePTFE or PTFE

LiDAP : salt obtained by reaction of Li and DAP and used for surface treatment of ePTFE or PTFE

LiHMPA : salt obtained by reaction of Li and HMPA and used for surface treatment of ePTFE or PTFE

LiEDA CHI : sample modified with LiEDA followed by CHI grafting

LiEDA PEI : sample modified with LiEDA followed by PEI grafting

LiEDA PVP : sample modified with LiEDA followed by immersion in a PVP solution

LiDETA CHI : sample modified with LiDETA followed by CHI grafting

LiDETA PEI : sample modified with LiDETA followed by PEI grafting

LiDETA PVP : sample modified with LiDETA followed by immersion in a PVP solution

LiHMPA CHI red : sample modified with LiHMPA followed by CHI grafting and NaBH<sub>4</sub> reduction

LiHMPA CHI imine : sample modified with LiHMPA followed by CHI grafting only

MTT : 3-(4,5-dimethylthiazol-2-yl)-2,5-diphenyltetrazolium bromide

*S. aureus* : *Staphylococcus aureus*

*K. pneumoniae* : *Klebsiella pneumoniae*

*S. epidermidis* : *Staphylococcus epidermidis*

*E. coli* : *Escherichia coli*

*E. faecalis* : *Enterococcus faecalis*

*P. aeruginosa* : *Pseudomonas aeruginosa*

CI : confidence interval

IR spectroscopy : infrared spectroscopy

IR ATR spectroscopy : Infrared attenuated total reflection spectroscopy

SEM : scanning electron microscope; MEB in french (microscopie électronique à balayage)

### History and presentation of ePTFE

We will now present the history of ePTFE, the discovery of its manufacturing process that is the origin of its main mechanical and chemical properties.

Roy Plunkett discovered PTFE in 1938 at the DuPont company and was kept on secret order for World War II until 1946. In 1950, DuPont was a large producer and provider of PTFE, but offering few manufactured products. Wilbert L. Gore was an employee at DuPont but had greater ideas for PTFE applications. In 1958, he decided to follow his innovative and entrepreneurial spirit and left the DuPont company to create his own business. He started his activity by developing and marketing PTFE-insulated wire and cable, which won his first patent. The products were primarily used for defence and emerging information technology industries. Innovative intentions of Wilbert Gore did not stop, as he intended to develop a new form of PTFE that would include more air in the bulk material, to be lighter and therefore less expensive to produce. Bob Gore, Wilbert Gore's son, tried many ways to turn bulk PTFE into foam by stretching it, but the material was still breaking under slow stretch rates ( $< 50$  mm/min) after heat treatment. A test with a high strain rate after being processed at high temperature suddenly made the polymer elongated by 1000%, while a slow stretch allowed it to stretch by 10-20%.<sup>1</sup> The company W.L. Gore and its associates patented this new form of PTFE, ePTFE under the name Gore-Tex. While John W. Cropper first discovered in 1966 a process for producing ePTFE,<sup>1</sup> a resounding legal battle in the 1970s (known as Gore v. Garlock decision) cancelled any claim to invention. As no public patent was filed, the new form of the material could not be legally recognized. Ultimately, the manufacturing process used by Gore was patented in 1973<sup>2</sup> and 1977<sup>3</sup>.

PTFE is a polymer composed of only carbon and fluorine atoms forming - $(CF_2)_n$ - helical chains where C-C and C-F bonds are very strong.<sup>4-6</sup> This chemical composition and structure give to PTFE remarkable characteristics such as chemical resistance, thermal stability, and hydrophobicity due to low surface free energy (around  $19$  mJ/m<sup>2</sup> at 20°C).<sup>7-8</sup> Indeed, the lower the free surface energy of a material, the more difficult is to wet it with higher surface energy solvents such as water. Some physical treatment of the PTFE surface increases free energy value of the surface.<sup>9-10</sup>

Two main processes are used to obtain ePTFE. The first one starts with pure fine powder of PTFE. A lubricating agent is added until a paste is obtained and

then extruded into a sheet form. The latter is heated and expanded under a high strain rate to produce a microporous sheet. The structure is stabilized in an amorphous locking step without fracture as it is the case with most polymers. Deformation at extremely high rates increases the tensile strength of the resulting ePTFE. The lubricating agent is removed at the end of the process due to its low boiling point, resulting in 100 % ePTFE.

The second one has less impact from the point of view of the pharmaceutical industry than before since the product is less pure. Some steps in this process involve PTFE powder mixed to burnable or fugitive material such as paper fibers or carbonate, respectively. Then, they are removed by heating, but traces of contaminant make them unsuitable for biomedical use. The main application is microporous ePTFE membranes for microfiltration.

Thus, ePTFE is now a well-known material which has proven itself concerning its particular advantages in terms of chemical and mechanical properties. It has been widely used for medical application over the past decades, but bioactive properties might be lacking to really adapt the material to different types of surgeries. In the next part, we will review the state of the art of published methods for functionalizing ePTFE to enhance its bioactive properties. The clinical efficiency of ePTFE-based surgical devices used will also be reviewed, allowing for assessment of missing properties to achieve better results in clinical trials.

## I. State of the art on medical applications of ePTFE

### I.1. ePTFE improvements needed for medical applications

PTFE is used for a variety of medical purposes, and targets different organs and systems (cardiovascular, urinary track, nervous system, etc.).<sup>11</sup> Nosocomial infections occurring in hospitals are the cause of various serious diseases, mainly bacteria and to a lesser extent micro-fungi.<sup>12</sup> Indeed, they have been recognized as a major source of morbidity and mortality. In this context, post implant infections coming from ePTFE prosthesis are quite significant and can be life-threatening with one third of vascular graft infections being fatal.<sup>13-17</sup> Indeed, micropores of ePTFE are large enough to allow bacteria to grow but too small to enable immune cells to reach the microorganisms in the pores. Compared to bioengineered decellularized vessels, ePTFE vascular grafts show five times more colonization by *S. aureus* and *E. coli* two weeks after inoculation than the designed vessels.<sup>18</sup>

Additionally, antimicrobial resistance (AMR) emerged with the use of antibiotics. Aminoglycosides, penicillin, cephalosporins, and carbapenems are examples of antibiotics usually chosen for clinical treatment of infections. As AMR is increasing globally, the threat of population health is considerable. The

predominant resistant bacteria are *Staphylococcus aureus*, *Pseudomonas aeruginosa*, *Klebsiella pneumoniae*, *Escherichia coli*, and *Acinetobacter baumannii*.<sup>12</sup>

Thus, not only are antibacterial functionalizations necessary to eliminate nosocomial infection related to the ePTFE implant, but bactericidal strategies making it possible to circumvent the problem of resistance are also necessary.

In case of contraindicated autologous grafts, synthetic vascular grafts are used for coronary or lower limb replacement. Crucial properties of the graft needed to maintain a sustainable blood flow that sufficiently provides organs are the non-thrombogenicity, the same viscoelasticity as native vessels, and resistance to high blood pressure.<sup>19</sup> Thrombosis is the obstruction of a blood vessel by the formation of a blood clot. The absence of endothelium on ePTFE lumen grafts leads to neointimal hyperplasia which results in total (thrombosis) or partial (stenosis) obstruction. The intimal cells proliferate on the lumen side of the graft and thus thicken its walls, which leads to restenosis of the vessel. The elasticity and compliance of the graft depend on the mechanical properties of the material used. ePTFE is generally chosen for its efficient resistance to high intensity mechanical stresses.

Despite the highly hydrophobic character of ePTFE and fluoropolymers in general, biological reactions can occur on their surfaces.<sup>20</sup> For instance, adhesion of blood components such as serum albumin and fibrin proteins can lead to complement activation, platelet adhesion and activation of coagulation pathways. Such reactions can cause the occlusion of the graft.<sup>21</sup> The difference in compliance between the graft and the host vessel is also involved in the graft occlusion process, as it contributes to activate neointimal hyperplasia. For example, ePTFE is effective with a satisfactory maximal patency of 40 to 50 % for arterial grafts of large diameter, while smaller grafts achieve only 20 to 25 % patency, and grafts of the same diameter for the veins have good patency.<sup>19</sup>

The inertness of ePTFE prevent the cells from adhering to the prosthesis and its microporous structure for cell penetration and tissue in-growth. In treatments for congenital diaphragmatic hernia, ePTFE membranes are used to replace the diaphragm. The poor adhesive property of the polymer is suited to the abdominal face but not the thoracic face, where specific adhesion and tissue integration is required.<sup>22</sup> The bone-bonding property of ePTFE implants is also a lead that has been investigated as a tissue space-filler, for instance.<sup>23</sup> Tissue engineering also requires cell adhesion to ePTFE, allowing scaffolds to be integrated into tissue that is in contact, such as anterior cruciate ligament cells.<sup>24</sup>

---

<sup>1</sup> Parts I.1. and I.2. are directly taken from our review published "ePTFE functionalization for medical applications" <https://doi.org/10.1016/j.mtchem.2020.100412>



## I.2. Existing ePTFE functionalization for medical applications

The surface functionalization of PTFE has been developed with several techniques over the past decades. In the case of ePTFE, the strategies chosen are covalent or non-covalent functionalization. Covalent functionalization generally involves a surface modification of ePTFE through tight bonding to highly reactive species due to its initial inertness, while contact functionalization uses structure properties such as porosity or physical property such as hydrophobicity.

### I.2.1. Covalent bonding

Before conducting the grafting of ePTFE, there is a need to permanently modify the carbon-carbon-fluorine bond. Despite many remarkable properties of PTFE, it is very difficult to introduce functional groups to the surface. Sometimes it is necessary to sacrifice its lubricity in order to be bonded and to further functionalize it. For instance, PTFE can be etched chemically with a commercial etchant (FluoroEtch) comprised of sodium naphthalene complex dissolved in 2-methoxyethyl ether, in few minutes.<sup>25-28</sup> Isopropyl alcohol is used to stop the attack. To continue with alkali metals, PTFE surface can be modified chemically using Billups-Birch reduction reaction too.<sup>29</sup> In this context, the functionalization of PTFE has been achieved with polydopamine in several studies<sup>27,30</sup> using coated ePTFE as medical applications. The mechanism of functionalization is illustrated in Figure 1.

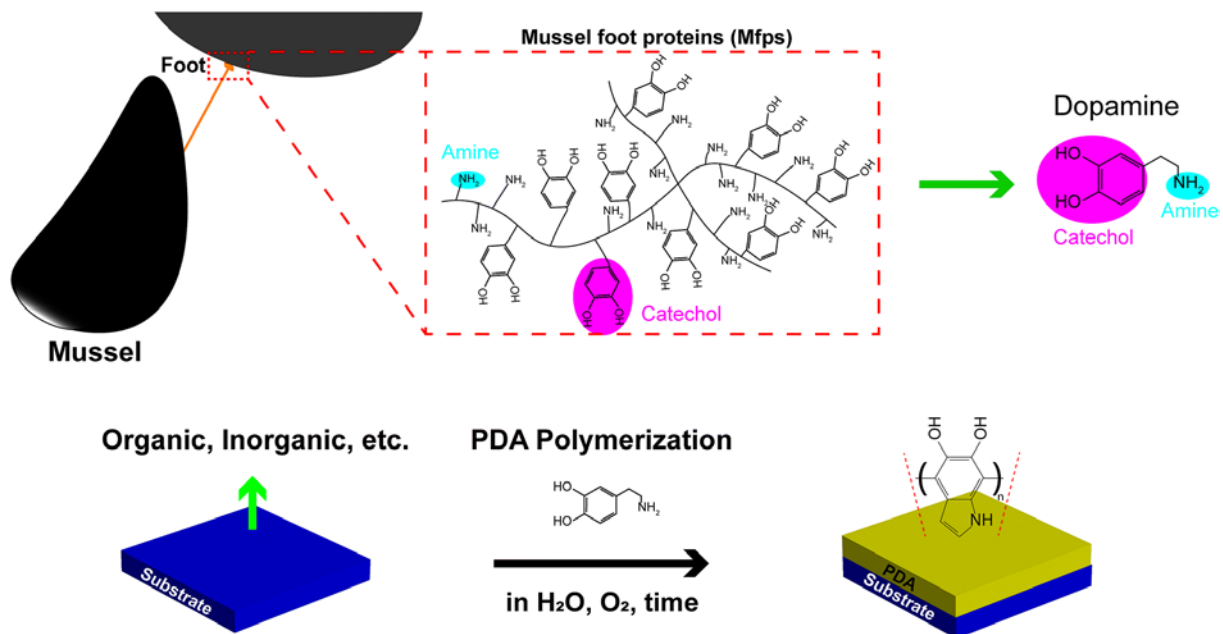


Figure 1. Schematic illustrating the mussel-inspired chemistry of dopamine that is used as a precursor material for the synthesis and deposition of conformal polydopamine (PDA) film.<sup>31</sup>

Another possibility is to chemically reduce the surface of the material according to the suggested process is the chemical treatment of the surface as shown in Figure 2, where the C-F bonds are partially reduced to C-H. This has been applied to improve the antibacterial and anti-inflammatory properties, which is of interest for the problems that ePTFE implants can involve.<sup>32</sup> The process suggested is the chemical treatment of the surface as shown in Figure 2, where C-F bonds are partially reduced into C-H bonds. The chemical route is to treat ePTFE with bisphenone/NaH in DMF under UV light. Then, grafting and polymerization of 2-Methacryloyloxyethyl phosphorylcholine follows under UV on the reduced surface. The modified surface material has been tested *in vitro* and *in vivo* to assess bacterial adhesion and inflammatory response. Protein adhesion of bovine plasma fibrinogen (BPF), adhesion and activation of fibroblasts (NIH3T3) and bacterial adhesion of *S. aureus* were tested *in vitro* and found to be significantly reduced with PMPC-grafted ePTFE, compared to unmodified ePTFE. The quantitative fluorescence intensity results showed that the adhesion and growth of *Staphylococcus aureus* was reduced by 60 % with functionalized plates, compared to unmodified ones. The same molecule was used in combination with Ar plasma treatment on ePTFE to obtain platelet anti-adhesion properties.<sup>33</sup>

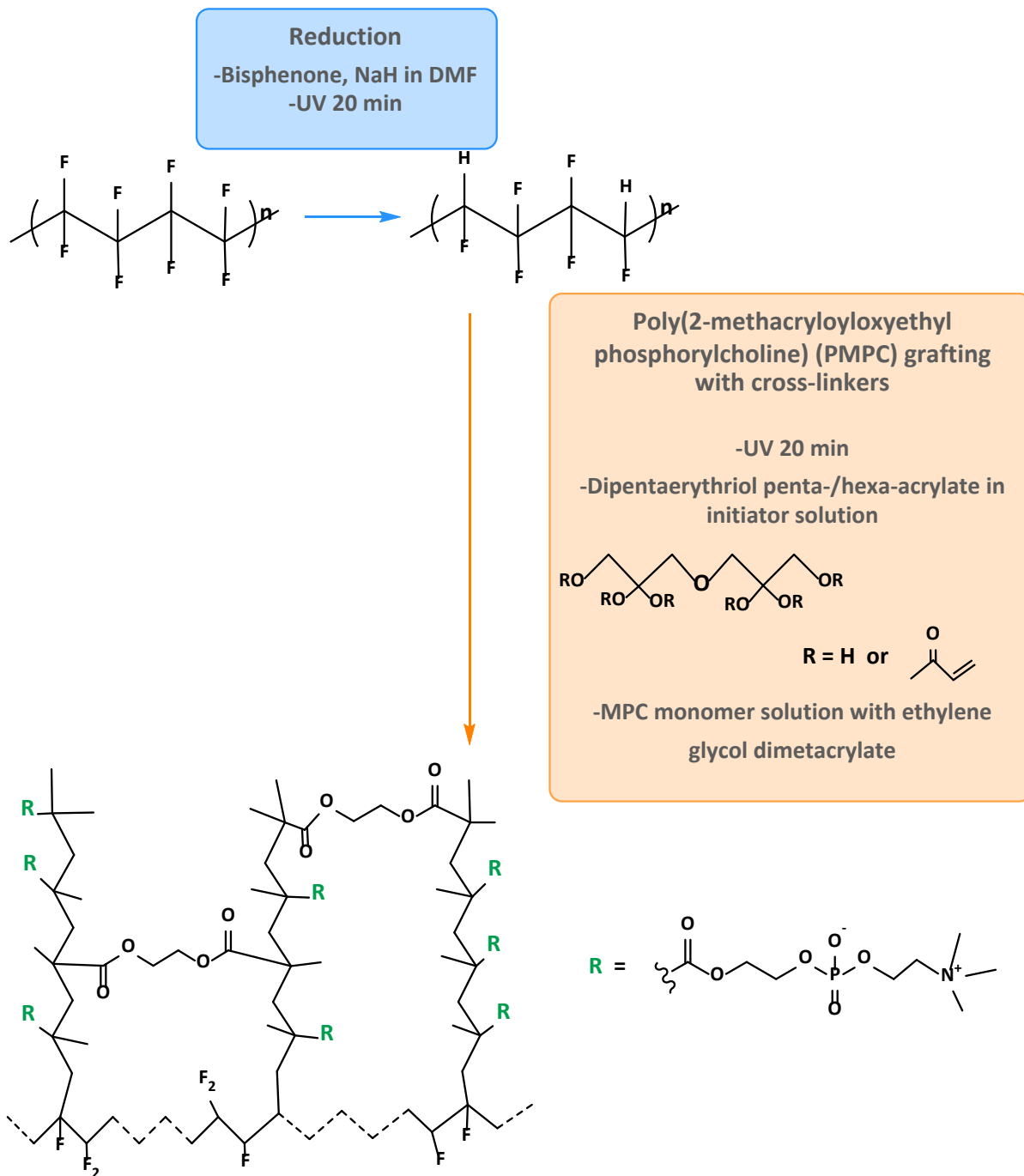


Figure 2. Chemical route of surface activation of ePTFE with reduction using UV light and bisphenone/ NaH in DMF; to its UV-induced polymerization grafting of 2-Methacryloyloxyethyl phosphorylcholine, using dipentaerythriol penta-/hexa-acrylate as a cross-linker.<sup>32</sup>

Indeed, another way of modifying the surface of PTFE or ePTFE comes from the formation of radicals on the surface of the material, with gas plasma,<sup>34-37</sup> or gamma rays' techniques with an initiator molecule. A well-known antibiotic, penicillin (PEN), has been used as antibacterial coating using this technique,

coupling argon plasma with maleic anhydride (MA).<sup>38</sup> Once MA is grafted on the surface of the polymer, the molecules are hydrolyzed and attached to polyethyleneglycol (PEG) molecules which reacts in return with the penicillin (Figure 4). The ePTFE surface becomes antibacterial upon this physicochemical process. It seems that *in vitro* experiments with cultures of *S. aureus* demonstrate that the functionalization PEN-PEG-MA-ePTFE is efficient in eliminating bacteria, compared to ePTFE, MA-ePTFE, PEG-MA-ePTFE or PEN-ePTFE (Figure 3). However, the surface does not predictably eliminate gram-negative bacteria such as *Pseudomonas aeruginosa*. The question of the release of PEN linked to PEG with ester bond can be raised. ATR-FTIR analysis of C=O ester bond over time, with PEN-PEG-MA-ePTFE exposed to PBS buffered solution at 37°C showed a decrease in signal intensity, with a decrease by 30 % after 24h, which corresponds to 32 % of the initial volume of PEN.<sup>39</sup> This interesting study does not deal with the effect of the hydrolysis kinetics on the organism because no other study than *in vitro* has been carried out.

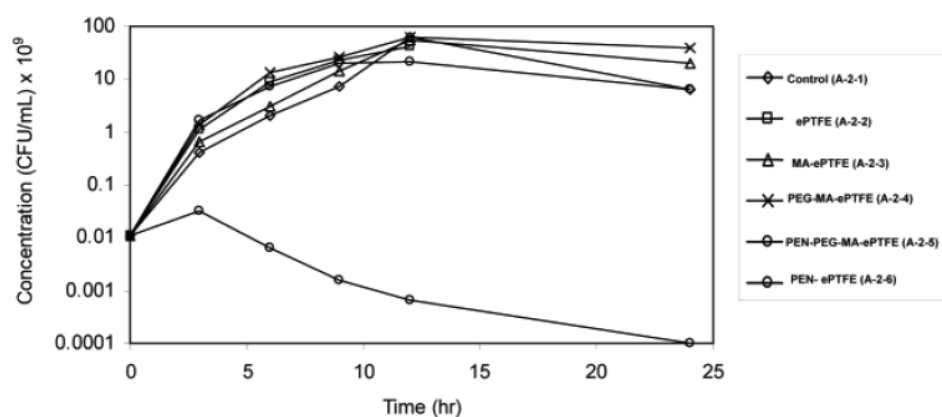


Figure 3. Concentration of *S. aureus* plotted as a function of time for the experimental sequence: control, ePTFE, MA-ePTFE, PEG-MA-ePTFE, PEN-PEG-MA-ePTFE, and PEN-ePTFE<sup>39</sup>

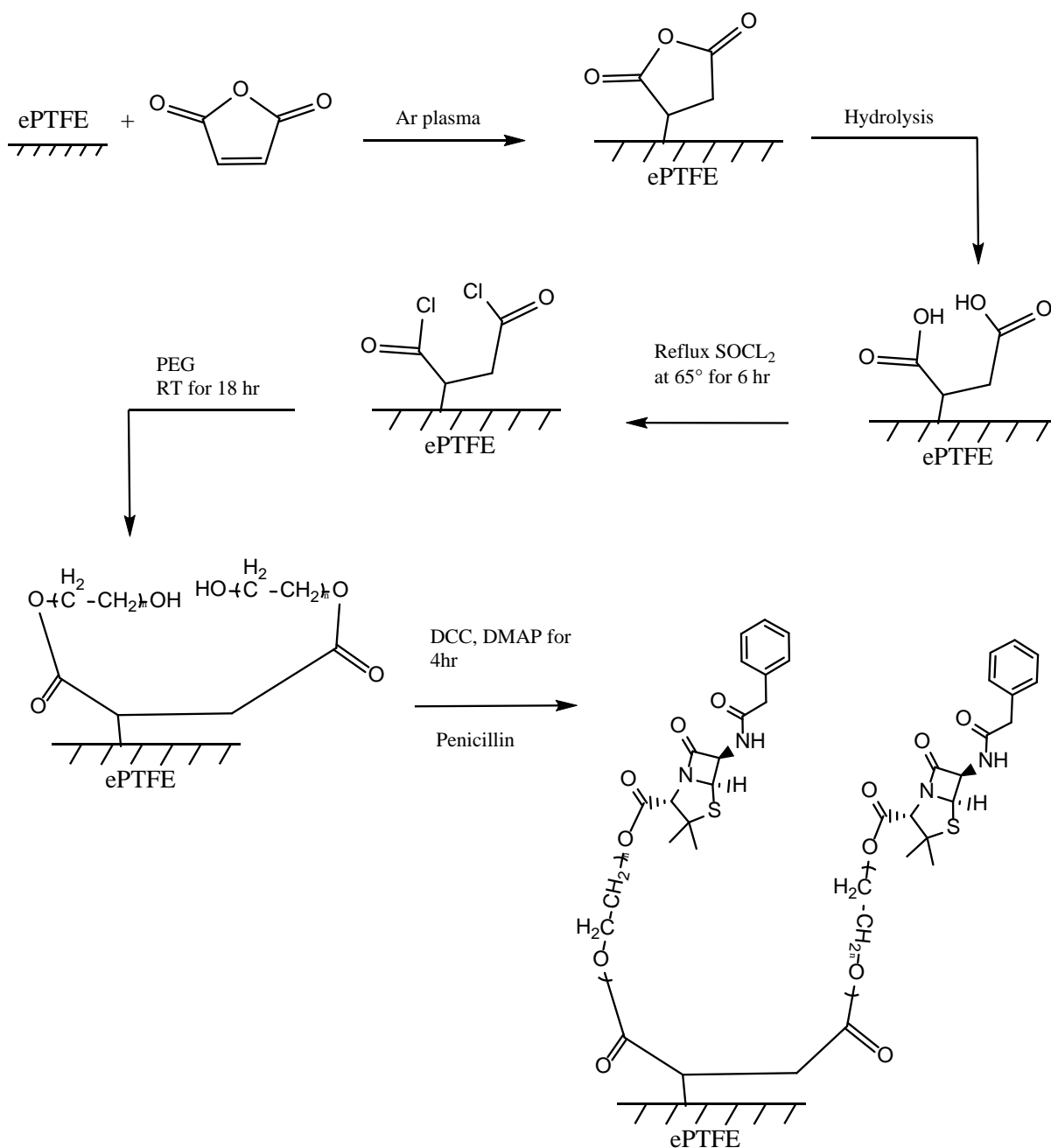


Figure 4. Chemical route of plasma-induced grafting of penicillin using maleic anhydride (MA) and polyethylene glycol (PEG) as intermediates.<sup>38</sup>

Argon plasma induces a low percentage of grafting<sup>40</sup>, which has been attributed to steric hindrance due to the formation of an imidazole ring. Gamma irradiation is a technique with higher grafting yield because the radicals are formed directly on the surface.<sup>41-42</sup> A recent functionalization on PTFE film has been developed with this technique.<sup>43</sup> The process consists in gamma irradiation, following with methyl methacrylate (MMA) grafting. N-vinylimidazole (NVI) is then grafted onto MMA-PTFE by irradiating the grafted material in the presence

of NVI and toluene solution. These previous steps were carried out to fix the silver nanoparticles with sufficient retention with regard to the hydrodynamic physiological condition of organism.<sup>44</sup> An aqueous solution of AgNO<sub>3</sub> is used exposed to the grafted films for immobilization of silver on the previously grafted molecule. An antibiogram study compared the zone of inhibition in presence of *E. coli* or *S. aureus* around the functionalized material MMA-ePTFE, NVI-MMA-ePTFE and Ag/NVI-MMA-ePTFE. The latter presents a distinctive inhibition zone. The amount of NVI grafted was also evaluated by antibiogram and showed that the maximum amount of NVI grafted on the surface (15 %) was the most effective with the largest zone of inhibition. Quantitative measurements of absorbance in TSC medium confirmed that the sample with maximal amount of silver attached to NVI was the most efficient.

Cardiovascular grafts also benefit from an improvement study with a covalent-bonding modification. An interesting study used surface oxidation and grafting of active components coupled to a nanodevice.<sup>45</sup> After surface activation of ePTFE by oxidation with a piranha solution, the PLGA nanoparticles loaded with fluorescein isothiocyanate and dextran are covalently anchored to the surface by glutaraldehyde. The immobilization of nanoparticles has been studied, as well as biocompatibility and cytotoxicity, but no efficiency assay have been performed.

Another oxidation realized for ePTFE to functionalize it with a peptide was recently reported.<sup>46</sup> In this method, the authors used a peptide anchor sequence, Tyr-Lys-Tyr-Lys-Tyr-Lys named YK3 bonded to a ligand sequence for  $\alpha 4\beta 1$  integrin, Leu-Asp-Val (LDV). This molecule, the YK3-LDV, was coated to the polymer surface in oxidative medium, consisting in aqueous solution of copper chloride (II) and hydrogen peroxide (H<sub>2</sub>O<sub>2</sub>). In vitro assays were performed where the coating appeared promising in enhancing properties for endothelial cell adhesion. In vivo model in a rat with ePTFE patch implanted in carotid revealed an acceleration in the formation of neointima-like tissue.

### 1.2.2. Non-covalent bonding

Non-covalent bonding of ePTFE is another way to improve its antimicrobial properties. Fluorinated liquids are used to saturate the pores of ePTFE by physisorption of a thin film of lubricating liquid yielding slippery liquid-infused porous surfaces (SLIPS,<sup>47-49</sup> and LIPS<sup>50</sup>). Thus, the SLIPS created by this technique allow the ePTFE to fill its pores which no longer let bacteria to penetrate and make the material more hydrophobic. The properties obtained upon SLIPS modifications prove to be efficient against the adhesion and colonization of *S. aureus*. Experiments were carried out *in vivo*, with biomaterial contaminated by *S. aureus*. It appears that after three days of inoculation, some SLIPS-ePTFE

substrates were not colonized at all, with rat infection rate of 92.3 % for ePTFE, 33.3 % for perfluoropolyether (PFPE), 0 % for perfluoroperhydrophenanthrene (PFPH) and perfluorodecalin (PFD).

The most common way to do antibacterial functionalization is to soak it in antibiotic solutions. Tetracycline, amoxicillin, rifampicin, vancomycin, or minocycline are examples of antibiotics used for functionalization. These direct impregnations have been exploited to prevent bacteria penetration and colonization of tissue regeneration membranes guided by ePTFE,<sup>51</sup> or by prosthetic vascular grafting.<sup>52-53</sup> However, the question of uncontrolled release of antibiotic and overdose on cell viability may be raised. The benefits of prophylactic pre-soaking of implants may be reassessed, as *in vitro* assay at high dose of rifampicin caused cytotoxicity on vascular cells.<sup>54</sup> In addition, antibiotic resistance is strongly correlated with the use of antibiotics. AMR is estimated to cause at least 23 000 deaths per year in the United States and 25 000 deaths per year in Europe<sup>55-56</sup> Therefore, this solution should be used with caution regarding the increasing AMR worldwide. If there is a risk of graft infection and graft replacement, pre-soaked grafts are prescribed instead.

To reduce bacterial adhesion and promote the biocompatibility of the ePTFE graft, a method called autologous vascularization has been developed. It has already been stated that the parenchyma or the network of blood vessel on a material surface allows the survival of the graft.<sup>57</sup> The idea of this method is to allow tissue growth in the pores of ePTFE and thus avoid bacterial infiltration, since the survival of bacteria on the surface of endothelial cells with biological activity is found to be limited. Studies have evaluated its efficiency against bacterial survival and chronic inflammation at the implantation site in animal models.<sup>58-59</sup> Here we present a study where the ePTFE material is first implanted in blood-rich subcutaneous tissue for four, eight and twelve weeks in 30 rats.<sup>58</sup> The biocomposite is then implanted at the place of interest with injection of *Staphylococcus epidermidis*. The control group received ePTFE without previous implantation. Bacterial adhesion shows that the number of bacteria on the surface of the material is approximately cut by two with AV-ePTFE compared to unmodified ePTFE (Table 1). It also decreases over time. Even if the study appears effective, the question of the morbidity of the procedure with an additional site of intervention can be asked.

Table 1. Bacterial adhesion assay (colony-forming units of bacteria *S. epidermidis* on the material surface).<sup>58</sup>

Times (after surgery)	AV-ePTFE (10 <sup>7</sup> CFU/L)	ePTFE (10 <sup>7</sup> CFU/L)
1 week	7.41 ± 1.30*	19.67 ± 2.51
2 weeks	3.94 ± 1.00*	8.75 ± 1.7
4 weeks	1.97 ± 0.89*	3.66 ± 1.8

\*P < 0.05 compared to the number of adherent bacteria on the normal ePTFE surfaces at the same point in time.

As previously described, thrombosis and restenosis of ePTFE grafts are the main problem encountered after vascular surgery. To this end, a study succeeded in functionalizing ePTFE by its spin-coating of polyurethane (PU) solution and the coverage by centrifugation of a solution loaded with dispersed PU nanoparticles (PU-NP). This coating prevents platelet adhesion, which is a nice improvement over ePTFE or PU-coated ePTFE. The longer plasma recalcification time for PU/PU-NP ePTFE compared to pure PU implies that the functionalization improves the blood compatibility of the graft.<sup>60</sup>

Another method used for the coating of ePTFE is a self-assembling fluoro-surfactant polymer (FSP) incorporating bioactive molecules. These components, heptamaltose (M7-FSP), cell adhesive RGD peptide (RGD-FSP), or the endothelial cell-selective CRRETAWAC peptide (cRRE-FSP), exhibit properties that are expected to prevent thrombosis of ePTFE graft.<sup>61</sup> RGD-FPS and cRRE-FPS allow the formation of endothelial cells in the monolayer of pulmonary artery after soded. After one month, from 50 to 66 % of the modified grafts remain patented.

Aggressive “priming” such as plasma allows further modification to achieve layer-by-layer (LbL) assembly to PTFE.<sup>62-64</sup> The LbL technique has been primarily designed in medical applications to improve cell adhesion. As an example, we present here a method using heparin and collagen multilayers (HEP/COL) to improve reendothelialization and anticoagulation of ePTFE grafts.<sup>65-66</sup> An endothelial cell (EC) adhesive peptide sequence Arginine-Glutamine-Asparagine-Valine (named REDV) is also added after LbL treatment to promote cell adhesion on the surface.<sup>65</sup> The *in vitro* plasma recalcification time method showed longer plasma clotting time for REDV-LbL-ePTFE than the pure one. The REDV-coated and modified ePTFE exhibited 95 % of the surface colonized by venous endothelial cells after 72h of co-culture, while ePTFE alone exhibited eight times fewer adherent cells, and LbL-ePTFE four times. The quantitative results on the number of cells attached on the different versions of ePTFE are shown in Figure 5.



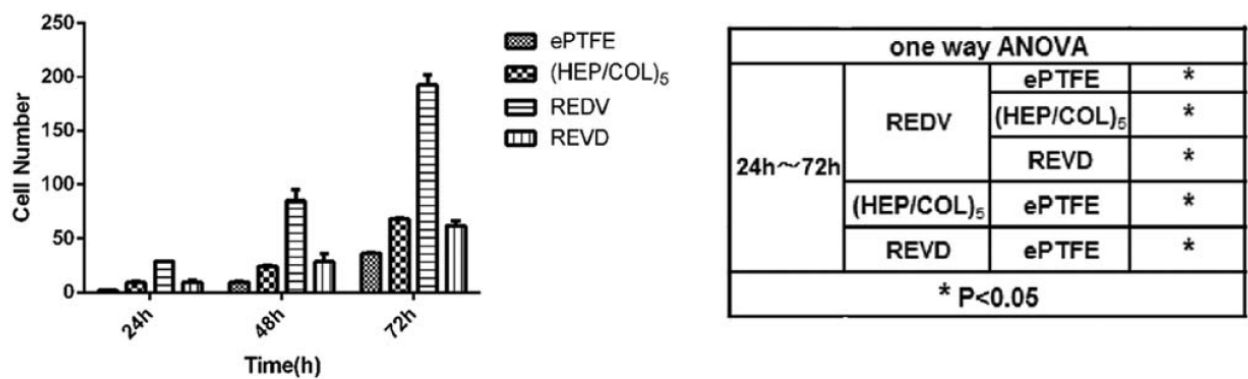


Figure 5. Numbers of cells attached on unmodified ePTFE, (HEP/COL)<sub>5</sub> modified ePTFE, REDV-(HEP/ COL)<sub>5</sub> modified ePTFE and REVD-(HEP/COL)<sub>5</sub> modified ePTFE (24, 48, and 72 h, \*indicates statistically significant difference at the P<0.05 level).<sup>65</sup>

Cell seeding has also been described as an efficient means of *in vitro* or *in vivo* models to avoid vascular graft complication.<sup>67-69</sup> We present here a study on animal model study performed on 12 miniature pigs: 7 control with unseeded grafts and 5 with seeded grafts.<sup>68</sup> Autologous endothelial cells are collected from the saphenous vein of the pigs with cell-seeded grafts. The cells are then seeded on the luminal surface of the graft and cultured for 48 hours. The results showed that after 6 months, 4 seeded grafts (80 %) were patented, while only 2 control grafts (29 %) were. Endothelial cells expression of VEGF165 (growth factor) and fibulin-5 (extracellular matrix glycoprotein) are necessary for their adhesion and proliferation under flow condition, thus transduced cells with enhanced of expression fibulin-5 were developed. Elisa assays verified the expression of these components, and *in vitro* assessment of adhesion under flow conditions showed significantly improved adhesion for transduced cells compared to native ones.

The same strategy was adopted with autologous endothelial cells transduced with enhanced expression of VEGF165 and fibulin-5 or prostacyclin.<sup>70</sup> The same experiments on large animal models showed patency on selective angiography with modified cells seeded in vascular grafts, while a third of native were patented.<sup>70</sup> The complete state of the art on cell seeding in vascular grafts is available.<sup>71</sup> The functionalization of ePTFE during the expansion of the bulk material for the adhesion of endothelial cells of the human coronary artery has also recently been described to improve the patency of small vascular grafts.<sup>72</sup>

However, *in vitro*, or *in vivo* cell seeding and autovascularization experiments in animal models should be interpreted and approached with

caution. Indeed, the animal model does not reflect the human speed of healing and may therefore miss the point of clinical relevance of the studies carried out.<sup>73</sup> All the more, cell seeding for vascular grafts, even if it could theoretically improve grafts patency, has never been adequate when applied clinically. The issue may reside in the incomplete understanding of the complex biology of the vascular wall, the disruption created by the implanted synthetic graft and the interactions with this foreign body.<sup>74</sup>

A patented functionalization process<sup>75</sup> uses a sealant and thermoplastic polymer, the styrene ethylene propylene styrene co-polymer (SEPS). SEPS is used to coat with a thin layer the luminal surface of vascular grafts. The coated surface is then functionalized by a copolymerization process with carboxyl groups, which are then covalently bonded to semisynthetic molecules of heparan sulphate type. Detections of neointimal hyperplasia were carried out by implanting semisynthetic heparan sulphate-coated and non-coated grafts into the carotid of sheep.<sup>54</sup> The uncoated grafts exhibited pseudointima developed in their lumen, while coated grafts exhibited no obstructing tissue.

Ion-beam modified ePTFE also shows promise for improved blood compatibility grafts, promoting cell adhesion and inhibiting the platelet response.<sup>76</sup> He<sup>+</sup> (helium), Ne<sup>+</sup> (neon), Ar<sup>+</sup> (argon) and Kr<sup>+</sup> (krypton) ion beams are used to modify the ePTFE sheets surface at an energy of 150 keV with fluences from  $1 \times 10^{14}$  to  $1 \times 10^{15}$  ions/cm<sup>2</sup>. The platelets adhesion assay was conducted by replenished platelet-rich plasma (PRP) in contact with modified or unmodified ePTFE. Some of the fluence conditions described for He<sup>+</sup>, Ne<sup>+</sup> and Ar<sup>+</sup> ion beams prevented platelet adhesion, while others of these ions, in addition to Kr<sup>+</sup>, promoted adhesion like unmodified ePTFE. It is suggested that the different conditions used lead to different surface structures which are more or less likely to attract platelets. *In vitro* assays of endothelial cell growth on an ePTFE modified surface show that each modified surface promotes endothelial cell growth.

In congenital diaphragmatic hernia, the poor adhesive property of ePTFE is adapted to the abdominal face but not the thoracic, on which specific adhesion and tissue integration is required.<sup>22, 77</sup> The spontaneous adhesion and polymerization of dopamine on the surface of ePTFE under oxidizing conditions<sup>78</sup> is a means of functionalizing asymmetrically the membrane with components favourable to cell adhesion. Indeed Liu et al., described the mechanisms of cell adhesion improved by the modification of polydopamine surface of different materials.<sup>79</sup> Polydopamine (PDA) has also been used in other medical applications such as vascular grafts.<sup>27, 80</sup> A recent study combined PDA with polyethylenimine (PEI) deposition to produce amine groups on the surface.<sup>80</sup> The amine groups from PEI were then coupled with sulphated zwitterionic polymers, as second coating.

A favourable environment for cell attachment and growth can also be created by biochemically-based polymers such as poly(lactic-co-glycolic acid) (PLGA) or polycaprolactone<sup>81</sup>. A study designed an ePTFE scaffold coated with PLGA precipitate.<sup>24</sup> The scaffold was then dipped in a solution of 25 % PLGA dissolved in chloroform, and then immersed in a solution of methanol to effect phase separation. The *in vitro* MTT assay shows that ePTFE coated with PLGA is eight times more colonized by cells than pure ePTFE.

Implants in contact with bone, such as tissue space-fillers, would benefit from a better bone cells-material interaction. Many techniques have already been examined,<sup>82</sup> such as the deposition of hydroxyapatite,<sup>83-84</sup> long pulse, ion implantation treatment by high frequency oxygen plasma immersion (PIII),<sup>85-86</sup> or adsorption of peptides containing dihydroxyphenylalanine (DOPA).<sup>87</sup> Another potential bone-integrating polymer inducing precipitation of hydroxyapatite (HAP) was tested recently under simulated body fluid in attempt to make outcomes more predictable.<sup>23</sup> It appears that the grafting of linear or branched poly acrylic acid or poly acrylic-co-itaconic acid induces a precipitation of HAP, while the crosslinked polymers are in different phases separated of phosphate and calcium. Guided bone regeneration membranes in maxillary surgery have also been subject of an interest for innovative functionalization.<sup>88</sup>

Based on the research conducted in the previous parts, it is noticeable that fewer articles about covalent bonding on ePTFE have been published, compared to non-covalent bonding. This is explained by its strong chemical inertness that only a few aggressive techniques can alter. The functionalization strategy can be chosen according to the degree of hazardousness of the chemical, the pressure, and the temperature with one can work. For further application in medical devices, the strategy must also be industrially viable. This may also explain why non-covalent bonding is more explored to modify the surface properties of ePTFE, as soft chemistry is favored in the industry. In the next part, we will focus on the medical devices made of ePTFE that were evaluated in clinical trials. Their efficiency is evaluated to assess what improvements are still needed to cure the health condition of various patients.

### 1.3. The assessment of ePTFE-based medical devices in clinical trials

The study of ePTFE-based medical devices in clinical trials can be encountered in various fields that can be sorted into five areas. In Figure 6, the clinical trials found in the Pubmed database using the keywords “ePTFE clinical trial” were sorted by field in Figure 6. 228 results were originally obtained. The articles in which ePTFE is considered as a control for another device testing were excluded. It resulted in 134 articles, in which 61 were applied to guided bone regeneration

for maxillofacial diseases, 43 to Stent, haemodialysis and bypass grafts, 8 to hernia repair, 8 to heart repair, and 14 to other application fields, presenting less than 4 % of the total of selected articles.

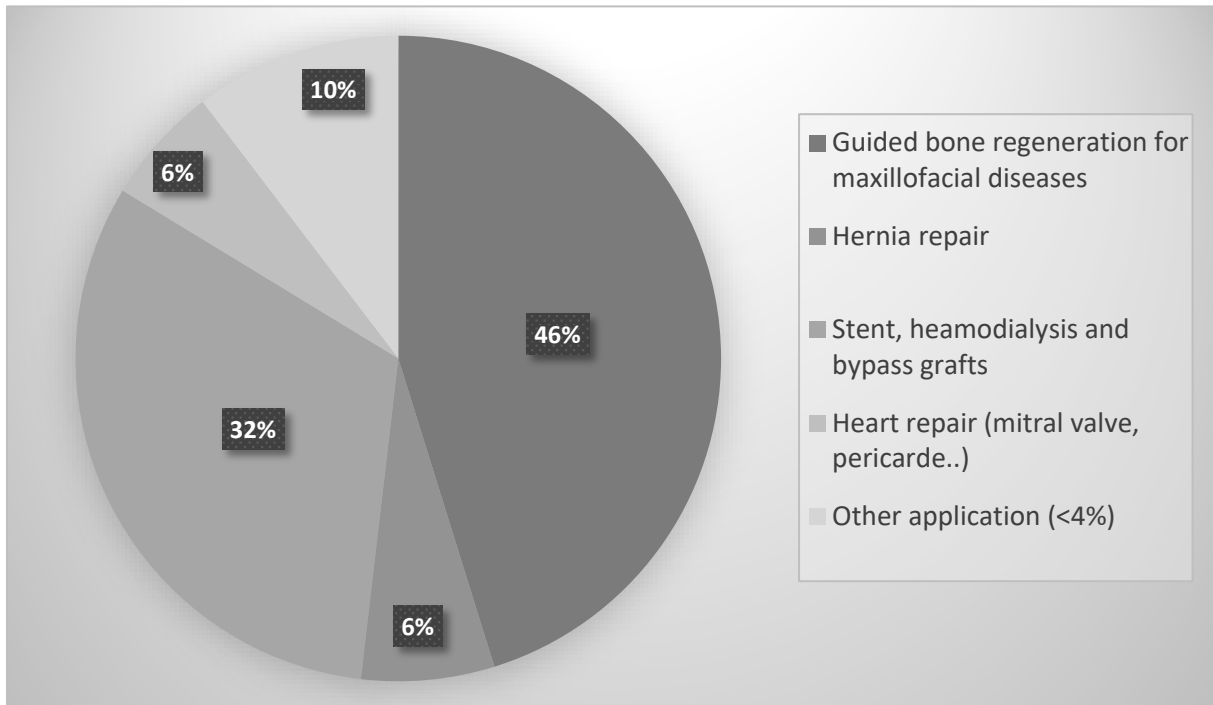


Figure 6. Distribution and topics of ePTFE studies in clinical trials (values obtained from the Pubmed database).

### 1.3.1. ePTFE-covered stents

The risk of occlusion exists with stents whether they are metallic or plastic, which lead to the development of different design strategies to solve this issue.<sup>89</sup> The added value resulting from the functionalization of metal stents with a thin layer of organic polymer (silicone, fluoroethylene, etc.) consists in reducing the rate of occlusion and prolonging the permeability.<sup>61</sup> The application of these stents is mainly used for biliary and blood vessel obstruction. The mainly used are abdominal aortic aneurysm and thoracic stents grafts, but stents for coronary artery or femoropopliteal atherosclerotic lesions can also be encountered. They are also found for transjugular intrahepatic portosystemic shunt.<sup>90-94</sup>

In case of abdominal aortic aneurysm (AAA), management of the aneurysm consists in either replacing it by a synthetic graft while open repair surgery or a

<sup>2</sup> Part I.3. is directly taken from our review "ePTFE-based biomedical devices: An overview of surgical efficiency" <https://doi.org/10.1002/jbm.b.34928>

stent by endovascular aneurysm repair (EVAR). The comparison between the two techniques has been widely studied over the past 30 years. Randomized trials, meta-analysis and observational studies agreed to conclude that EVAR presents lower perioperative mortality and morbidity.<sup>95-97</sup> The available analysis of postoperative years shows however that late survival is inferior compared to open surgery, thus the technique is chosen regarding the individual state of the patient.<sup>98-100</sup> EVAR is recommended however in case of ruptured AAA.<sup>101</sup> Studies regarding thoracic aortic aneurysm management came to similar conclusions.<sup>102-105</sup>

One of the most important and common complications that can be encountered after successful EVAR are endoleaks. They occur in approximately 25 % of the patients undergoing EVAR.<sup>106</sup> Endoleaks can lead to rupture of aneurysm at late stages, that is why regular follow-up is needed as it can occur anytime.<sup>107</sup> The different types of endoleak is detailed in Figure 7.

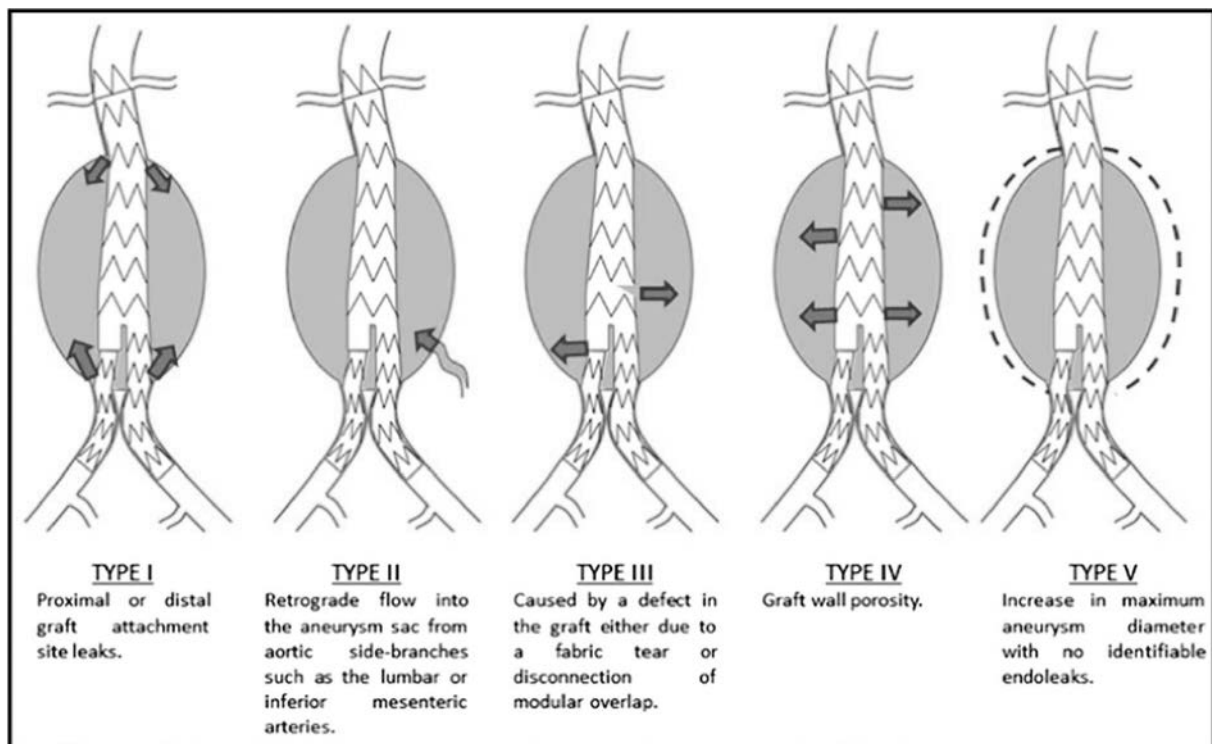


Figure 7. Endoleak classification system.<sup>108</sup>

To focus on the devices used and their effectiveness, many stent devices have been developed since the first launch in 1981, mostly based on ePTFE. EVAR were performed regularly with self-expanding ePTFE-nitinol stents, which were suspected over time to provoke aortic neck dilation (AND).<sup>109</sup> This latter was

proven to induce complications such as further endoleak, graft migration or reintervention. Indeed, a systematic review reported pooled results based on 26 articles published between 1988 and 2015, involving 9721 patients, with median age of 71.8 years and 97 % men.<sup>110</sup> In 7 studies, clinical events such as endoleak type I, migration and reintervention during follow-up were reported. These 1759 patients were divided into AND group and AND-free group. In the AND group (339), 26 % of the patients presented these combined clinical events, while in the group without AND (1420), only 2 % was affected.

Regarding the whole study with the main results, they found out that 24.6 % (95 % CI 18.6 % to 31.8 %) of the patients were affected by AND during follow-up time, from 1.3 to 9 years. The theory currently presented is that the design of EVAR devices is usually oversized by 15 to 30 % of the radius to ensure apposition of the self-expanding stents. It would apply a radial force to the vessel wall, which would be the cause of AND. Proper sealing by these endograft is also an issue that provokes failure within 1 year.<sup>109</sup> Indeed, a comparison study between self-expanding stents (SES) and balloon-expandable stents (BES) endograft proved that radial force applied by SES could be the reason to AND in the infrarenal area. This study involving 49 patients with the Nellix (Endologix, Irvine, Calif) an ePTFE-based BES and 56 with the Endurant II (Medtronic, Minneapolis, Minn), a polyester-based SES. It appeared that the rate of increase in the infrarenal neck diameter was significantly higher in SES patients ( $1.1 \pm 0.1$  mm/y) than in BES patients ( $0.22 \pm 0.04$  mm/y;  $P < .0001$ )<sup>111</sup>. The difference here is obviously due to a difference of design rather than the material composition of the device. However, this is a parameter that could have been considered by using the same polymer that the devices were made of.

An alternative EVAR device was recently developed, called the Ovation Abdominal Stent Graft Platform, composed of three parts with a main aortic body made of PTFE. Its particularity is its inflatable sealing rings set along the main body, in which low-viscosity polymer conform to the neck anatomy before hardening. This innovative design aims to avoid radial forces inducing AND as explained before. A descriptive analysis of the Effectiveness of Custom Seal with Ovation: Review of the Evidence (ENCORE) database allowed to note the midterm efficiency of this device.<sup>112</sup> The pooled studies from the database enable to access to a total of 1296 patient's data for the analysis, with average age of 73.8 years, 81 % of them were male. The results regarding the perioperative and postoperative outcomes are presented on Figure 8. The freedom from endoleaks in the survival proportion of patients was up to 96 % for type IA endoleaks and 94 % for type II and III. Type IA endoleak consists in a persistent blood flow into the aneurysmal sac from proximally.<sup>113</sup> The survival proportion decreased to 79 % at 5 years' follow-up, but 99 % of the mortality was not related to aneurysm. This

study appears to prove a real advance in AAA management regarding the outcomes.

Moreover, a recent study compared the Ovation and Nellix devices, finding them both effective on endoleaks type I and II. Each of their beneficial features could be combined into a promising new device preventing these critical issues of the AAA management.<sup>114</sup>

Open repair surgery can be also realized for AAA management regarding the case. In a prospective randomized study, including 99 patients who underwent implantation of 90 tube of ePTFE Gore-Tex Stretch grafts, 56 tube Dacron grafts (Uni-Graft KDV, polyester, B. Braun, knitted), and 51 tube Dacron grafts (Gelseal Plus, polyester, Vascutek, triaxial knitted). Ultrasound examination was carried out at 12 months and 6 years follow-up. Even if ePTFE appeared to be more resistant to neck dilation, no significant differences were observed between the three grafts for each measure during follow-up.<sup>115</sup> However, a study comparing ePTFE and polyester grafts for EVAR found that polyester grafts were inducing significantly more post implantation syndrome, including fever and inflammation (57 % for polyester vs. 17.9 % for ePTFE in a 149 cohort).<sup>116</sup>

The thoracic portion of aorta is also well concerned by aneurysm. In this case, thoracic endovascular aneurysm repair (TEVAR), similar to EVAR, appears to be the treatment of choice to exclude completely the aneurysm sac and prevent rupture.<sup>117-118</sup>

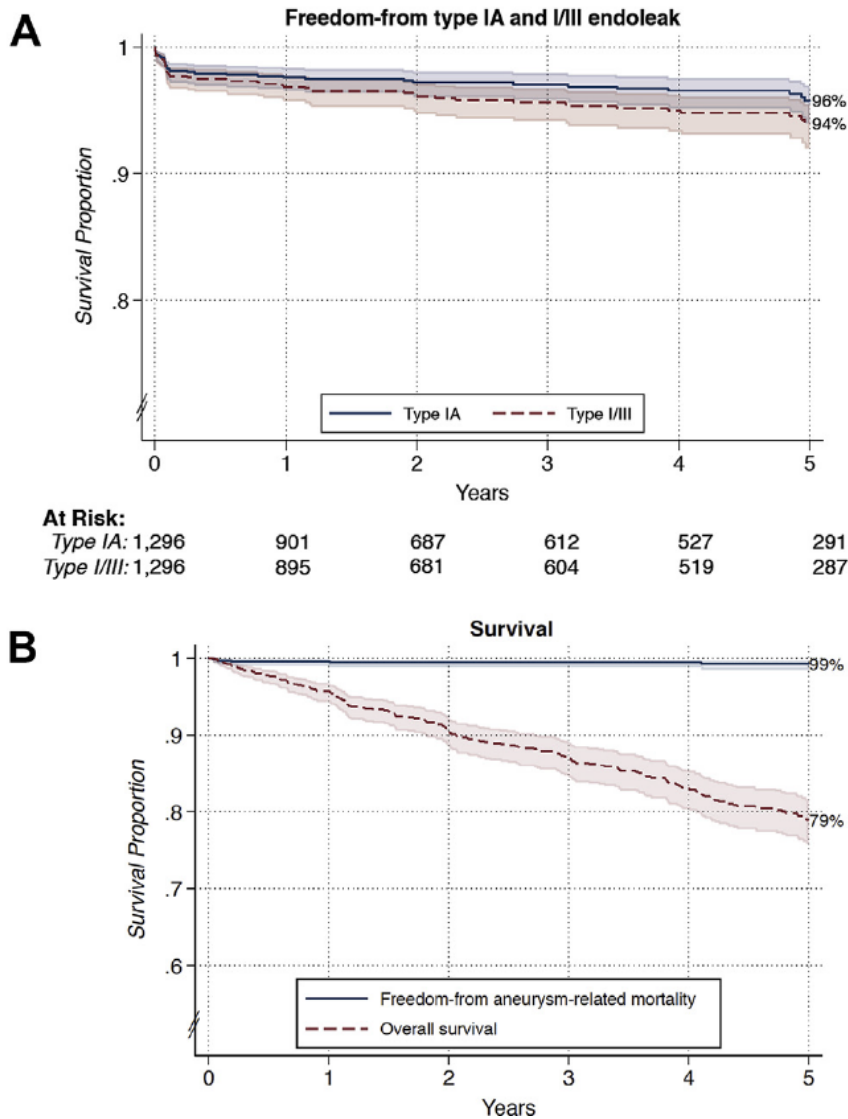


Figure 8. Kaplan-Meier curves with associated 95 % confidence intervals for (A) freedom from type IA endoleak and type I/III endoleak, and (B) overall survival and freedom from aneurysm-related mortality after endovascular aneurysm repair (EVAR) with the Ovation Abdominal Stent Graft platform in the Effectiveness of Custom Seal with Ovation: Review of the Evidence (ENCORE) cohort.<sup>112</sup>

In a recent prospective database study, ePTFE (Gore TAG®) and Dacron (Relay Plus® Bolton) device for TEVAR were compared in term of early and late outcomes.<sup>119</sup> 56 patients were part of the ePTFE group (group A) and 73 of the Dacron group (group B). It appeared that type I, II and III endoleaks were respectively observed in 16.3 %, 10.9 %, and 3.1 % of the patients, with no significant differences between the two groups. Freedom from reintervention was evaluated at 6, 12, 24 and 36 months, comparing group A vs. group B. The values obtained were 94.0 % vs. 97.1 %, 94.0 % vs. 95.5 %, 90.8 % vs. 86.9 %, and



81.1 % vs. 80.4 %, respectively. Thus, both devices are effective and safe, which is a conclusion we will see again in bypass grafts comparison, in the following part.

In case of obstruction of coronary artery bypass, percutaneous coronary interventions reveal to be a challenge because of the fragile composition of saphenous vein wall often used for bypass. The Symbiot coronary stent system is a self-expanding ePTFE-coated stent manufactured by Boston scientific, used in case of obstruction of saphenous vein graft originally set as coronary bypass. This device consists of a nitinol stent covered with two thin ePTFE membranes on each side (inner and outer face of the lattice). The randomized feasibility and safety trial, the Symbiot II trial,<sup>120</sup> was carried out on Symbiot stent in saphenous vein graft lesions. Stent deployment was successful in 97.4 % of the 77 patients, and the procedure success rate was 83 %. Thus, the feasibility of the procedure is proven by the study. Safety was assessed with the rate of major adverse cardiac events (MACE). 30 days after operation, MACE only appears only at the satisfactory rate of 5.2 % of the 75 patients concerned. At 6 months of follow-up, MACE apparition reached 14.3 %. 77.3 % of the patients enrolled underwent angiography and presented no luminal loss at the intervention site. Low occurrences rate of MACE at 30 days and 6 months suggests acceptable device safety.

However, the third Symbiot stent trial failed to prove better efficiency of self-expanding stents covered with ePTFE than bare metal stents (BMS).<sup>121</sup> In this prospective randomized trial, 400 patients were involved, with 201 patients in Symbiot group and 199 un BMS group. At 8 months, a comparable percentage of diameter stenosis was observed between Symbiot (30.9 %) and BMS (31.9 %) group. The same result was observed for the rate of binary restenosis with 29.1 % for the Symbiot group and 21.9 % for the BMS one. Binary restenosis at the proximal edge was even higher for the Symbiot group. Mace incidence was similar, at the rate of 30.6 % for the Symbiot group and 26.6 % for the BMS one. Thus, the Symbiot group obtained a higher MACE incidence rate in this trial of 201 people, than that obtained in the previous Symbiot II trial, which included 77 patients. The rate is doubled from the Symbiot II to III trial.

A recent study focused on nitinol stents passivated by ePTFE and fluorinated ethylene propylene (ePTFE-FEP) to prove their superiority over metal stents to reduce occlusion rate.<sup>122</sup> For this purpose, stents covered with ePTFE-FEP have been used in percutaneous treatment of malignant hilar biliary obstruction. The methodology consisted of comparing the results of the covered nitinol stents (ePTFE-FEP) and the bare nitinol stents. 120 patients were included due to obstructive jaundice caused by an unresectable hilar malignancy after failure of endoscopic intervention in a prospective randomized trial. Certain

exclusion criteria were considered (primary tumors for more than three months, a biliodigestive anastomosis, previous stenting, and a Karnofsky score of less than 50).

As a result, the occlusion rate was similar for covered and bare stents. The median patency was 229 and 130 days, respectively. The median survival in patients with covered stents was 79 days and 92 days with bare stents. Another study focused on covered stents only and describes the results of a 4-year follow-up period.<sup>123</sup> A very similar median patency of the stent was observed, with 173 days, but the median survival time much higher, with 247 days. The progress of the technique and the number of patients involved could explain the difference.

Obviously, no proof of the contribution of functionalization was brought but nothing comes refute either. But ePTFE-FEP resulting in percutaneous palliation of hilar biliary obstruction is achievable with both the bare and covered stents, as well as adjuvant chemotherapy is achievable with both stents.

Another type of ePTFE-covered stent for malignant biliary obstruction was developed early, named Gwon stent.<sup>124</sup> A study was carried out on 24 patients who underwent percutaneous placement of these ePTFE-covered stents in case of malignant obstruction of the hilar bile ducts and occlusion of the unilobar portal vein.<sup>125</sup> The patency of the stent evolved with satisfactory trend, as it decreased slightly from a cumulative rate of 100 % at the first month to 71 % at twelve months. Occlusion only occurred in two cases (8 %) in twelve months. None of the other patients developed cholangitis or jaundice. The article emphasizes that PTFE-covered stent was already compared with bare stents for the palliative treatment of malignant biliary obstruction and showed a significantly better patency for PTFE-covered stents.<sup>126</sup> The different design of Gwon Stents compared to other triple-layered ePTFE-covered stents could be an improvement in device efficiency. In addition, an attempt to improve the Gwon stent with an ePTFE anti-reflux valve was recently evaluated in a multicenter randomized controlled trial. The trial published a comparison of Gwon stents with and without the anti-reflux valve in 104 patients. The study found no significant differences regarding the occurrence of biliary obstruction.<sup>127</sup>

A recent study used Y/T-shaped stents, based on Gwon study, in 10 patients with malignant biliary trifurcation obstruction.<sup>128</sup> They achieved an occlusion rate of 30 % and 20 % of patients experienced late complications. The patency rate at 6 months follow-up was 88.9 %. Comparison with studies evaluating bare stents showed similar technical success (80–100 %), clinical success (90–100 %), and early complication rates (5.7–50.0 %).<sup>129-134</sup> A greater value of median patency period of Gwon type covered stents was observed with 275 days, compared to 83-250 days for the other studies. These results may confirm the efficiency of the

Gwon stents design and explore new possibilities to address malignant biliary trifurcation obstruction.

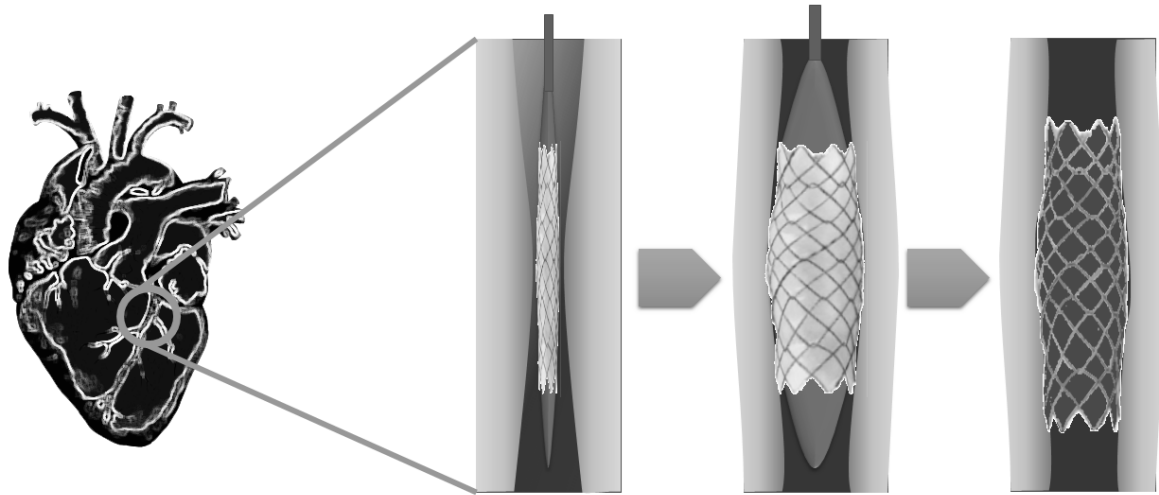


Figure 9. Example of percutaneous transluminal angioplasty (PTA) with self-expanding stent placement.<sup>135</sup>

A recent review and meta-analysis focusing on endovascular treatment of femoropopliteal atherosclerotic lesions by stenting included 3 029 patients from fifty-one studies.<sup>136</sup> The mean length of the lesion of the patients was 269mm, the long lesions (>200mm) being of particular interest to assess their need of reintervention. The mean primary patency, including all stent types in the relevant studies, at 1-, 6-, 12-, 24- and 60-months of follow-up was 98 %, 76 %, 62 %, 55 % and 39 %. The proportion of patients with patent lesion after 1 year is described in Figure 10. Among the included studies, some of the stents used were covered with heparin bonded ePTFE, which had a one-year higher primary patency (69 %) than bare metal stents (55 %) or percutaneous transluminal angioplasty (PTA, Figure 9) with uncoated stenting (54 %) and higher ratings of the rest of this patency. Drug eluting stents with paclitaxel showed the same result with a primary patency of 73 %. This analysis concludes in favor of drug eluting and ePTFE-covered stents for improved patency efficacy and remaining in atherosclerotic femoro-popliteal lesions.

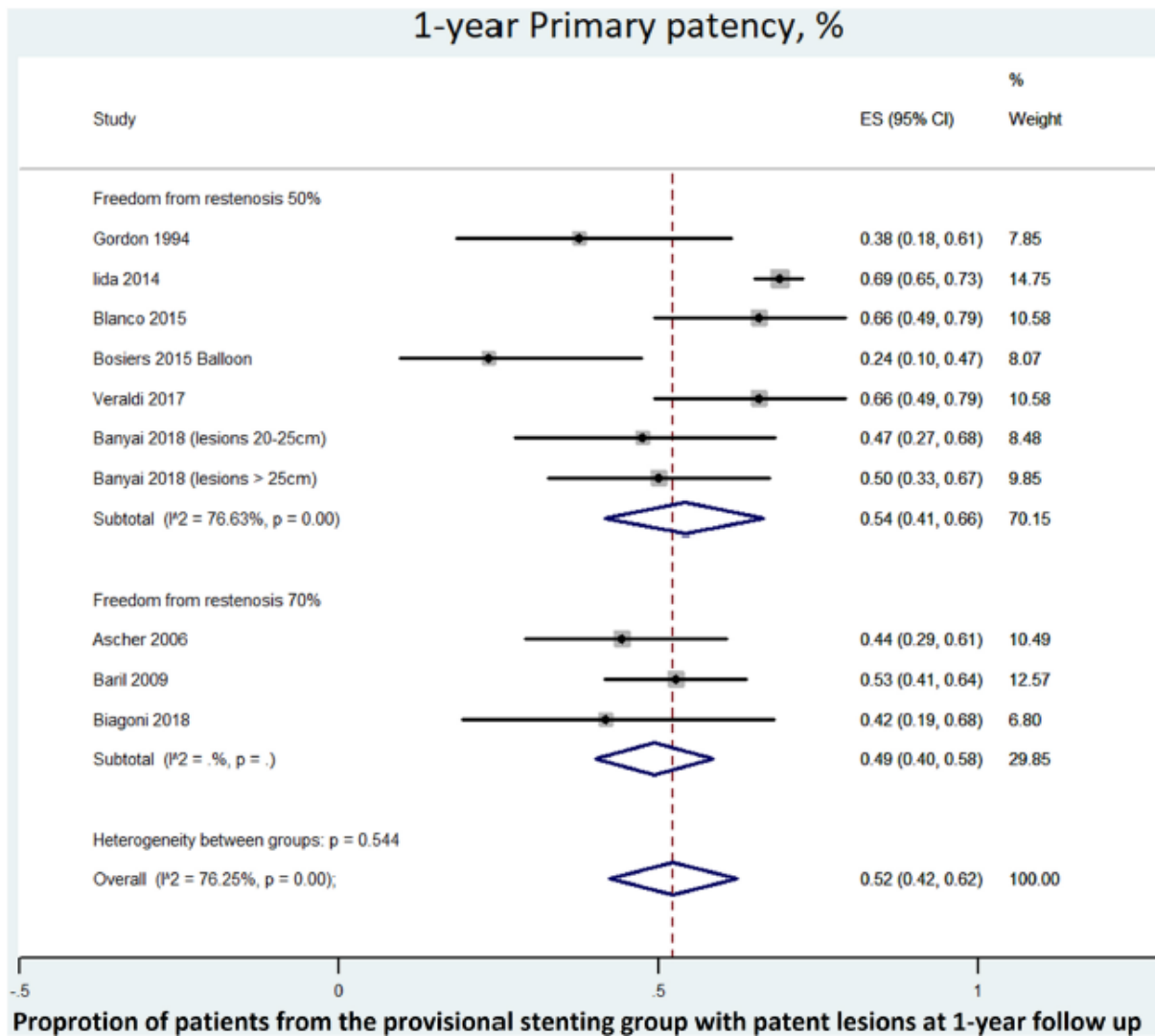


Figure 10. Overall 1-year primary patency rate of the provisional stenting group.<sup>136</sup>

### I.3.2. Haemodialysis and bypass ePTFE grafts

In chronic renal failure, autogenous arteriovenous fistula is generally preferred for haemodialysis treatment. However, if no suitable veins can be used, ePTFE synthetic graft are most used for dialysis. However, the occurrence of stenosis and thrombosis in these grafts due to neointimal hyperplasia remains a major concern. To improve hemodynamic at the anastomotic site and reduce graft obstruction, new models of cuff-shaped graft designs have been recently investigated. A wide range of studies are investigating the efficiency of cuff-shaped ePTFE haemodialysis graft compared to ePTFE standard one. For example, these two consecutive prospective randomized clinical studies were carried out by the same team to assess the efficiency of this design. The first trial published

in 2006 recruited 36 patients,<sup>137</sup> 17 assigned to cuffed grafts group and 19 to standard grafts group. The implanted grafts were placed in the upper part or forearm depending on the availability of vessel access. At 3 months of follow-up, the cuffed grafted group obtained a mean degree of stenosis of 22.76±26.37 %, while the standard graft obtained an average of 44.95±27 %. Since the two results are significantly different, the cuffed shape shows better efficacy against restenosis. The second trial, published in 2009,<sup>138</sup> 98 patients were enrolled for the trial. After applying the exclusion criteria, 89 subjects were randomly divided into two groups: 42 in cuffed grafts group and 47 in non-cuffed graft group. At one and two years of follow-up, cuffed group had a primary patency of 63 % and 45 % and secondary patency of 98 % and 84 %. The non-cuffed group had lower values of 50 % and 32 % for primary patency and 85 % and 61 % for secondary patency, after 1 and 2 years. Significant improvements have been demonstrated with this wider range of patients.

Recently, a review and meta-analysis confirmed that cuffed-shaped ePTFE grafts were led to significantly higher primary and secondary patency on 112 patients at 1-year follow-up than standard grafts on 92 patients (

Figure 11, Figure 12).<sup>139</sup> The ePTFE grafts modified with a venous cuff at the anastomotic site were also evaluated and compared to standard grafts in the review. No improvement in patency rates was noted with a venous patch between the prosthetic graft and the vessel.

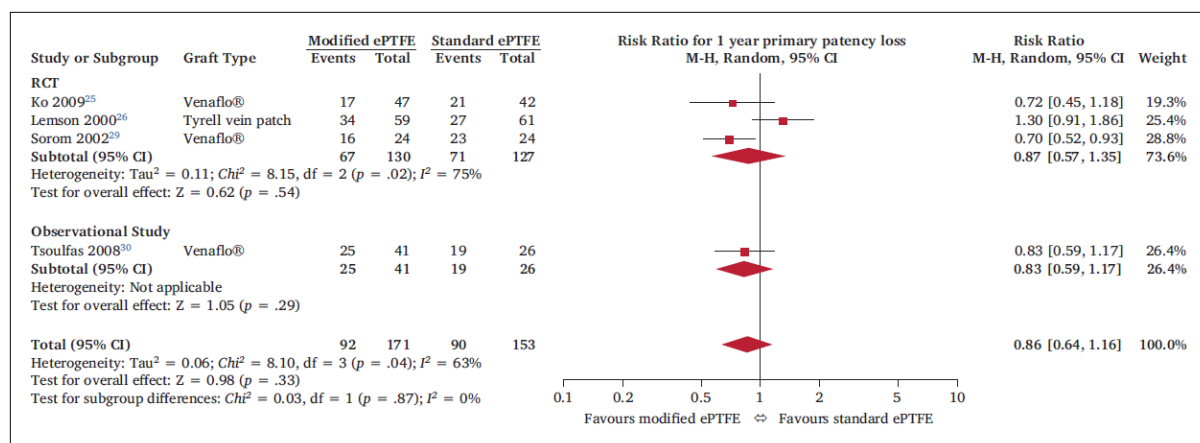


Figure 11. Forest plot of risk ratio (RR) of one-year primary patency loss of geometrically modified vs. standard expanded polytetrafluoroethylene (ePTFE) arteriovenous grafts for haemodialysis access based on randomised controlled trials (RCT) and observational studies. The solid squares denote the RRs, the horizontal lines represent the 95 % confidence intervals (CIs), and the diamonds denote the pooled effect size. M-H = Mantel-Haenszel random effects test; df = degrees of freedom.<sup>139</sup>

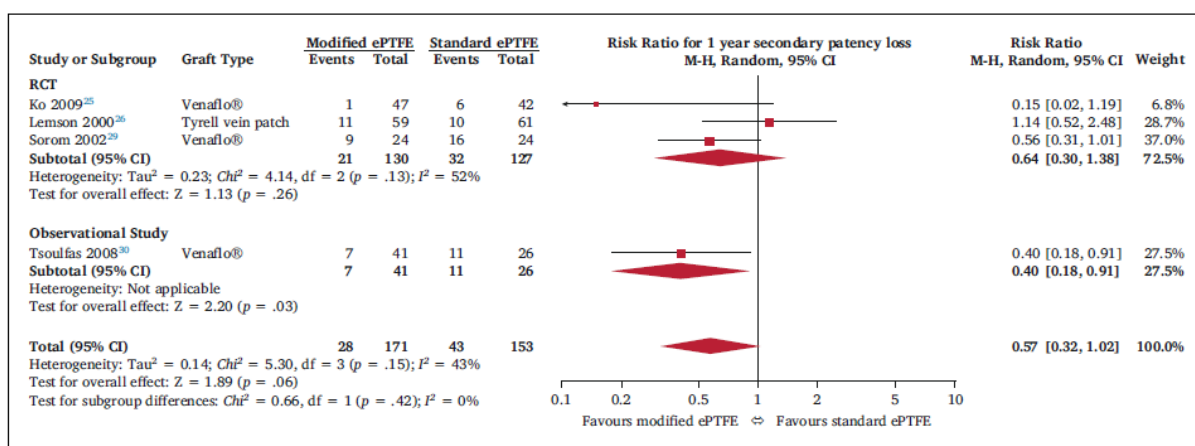


Figure 12. Forest plot of risk ratio (RR) of one-year secondary patency loss of geometrically modified vs. standard expanded polytetrafluoroethylene (ePTFE) arteriovenous grafts for haemodialysis access based on randomised controlled trials (RCTs) and observational studies. The solid squares denote the risk ratios, the horizontal lines represent the 95 % confidence intervals (CIs), and the diamonds denote the pooled effect size. M-H = Mantel-Haenszel random effects test; df = degrees of freedom.<sup>139</sup>

Functionalized ePTFE grafts with heparin bonding for access to haemodialysis have recently been tested in the hope of reducing the occurrence of restenosis and thrombosis.<sup>140</sup> Out of 1394 patients eligible for new vascular access, 160 randomized subjects out of 175 assessed for eligibility for ePTFE grafts were recruited, after application of the exclusion criteria. Two groups of 80 were made at random without any exclusion: one with heparin-bonded ePTFE graft and regular ePTFE graft. The location of the grafts was determined according to access to the vessel in the arm. Primary patency at 6 months and 1 year was 35 % and 14 % for the heparin-related group, and 29 % and 12 % for regular group. Secondary patency reached 83 %, 83 %, and 81 % at 1, 2- and 3-years of follow-up for the heparin-related group and 81 %, 73 % and 68 % for standard group. Another study followed with 105 patients involved, with the same comparison carried out, but with PTFE grafts.<sup>141</sup> For heparin-related PTFE, the 1-year patency was 34.9 %, for the standard group, 32.7 %. These results present higher patency rates than the first ones, as they are approximately doubled. This latest study also performed a meta-analysis involving 1209 patients. No significant difference could be obtained with this sample of patients. They estimated that the optimal sample would be 3800 subjects. This could explain the difference of patency observed previously.

The graft occlusion potential ePTFE was compared to that of Dacron grafts in trials. In one of them, 85 patients suffering from above-knee vascular disease were recruited and randomized into two groups.<sup>142</sup> After the Dacron or ePTFE above-knee femoropopliteal bypass placement, 1-year follow-up, the primary patency of Dacron group was 100 % and ePTFE 88.37 % and secondary patency was 83.3 % and 75 % respectively, with no significant differences. Dacron or ePTFE proved as effective here.

Studies on the improvement of ePTFE by the heparin-binding functionalisation of bypass grafts for better patency have been carried out.<sup>143-146</sup> In an prospective, non-randomized early study, the primary and secondary patency obtained at 1-year of follow-up with 86 patients enrolled were 82 % and 97 % respectively.<sup>143</sup> Results from other studies show the same range of patency, and hence the effectiveness of the heparin coating for bypass grafts.

### I.3.3. Guided bone and tissue regeneration procedures for maxillofacial defects

In maxillary surgery, when the volume and dimensions of bone and soft tissue are not sufficient, surgical procedures have been developed using membrane barriers to guide the growth of the hard or soft tissue required. These procedures, called guided bone regeneration (GBR) and tissue regeneration (GTR), are typically used for edentulous area and around the teeth bone and soft tissue regeneration, respectively. These techniques were developed to ensure dental or implant stability and regeneration of horizontal periodontal attachment.

Early clinical trials used PTFE as a membrane barrier for GTR in furcation disease.<sup>147</sup> After the discovery and use of ePTFE, it became and still is considered the gold standard for comparison and validity assessments with other biomaterials in GTR and GBR. Indeed, as the PTFE and ePTFE barriers involve a second intervention to remove them, the bioabsorbable membranes have been tested over years in comparison with ePTFE to evaluate which one would be most suitable for GTR in furcation defects.<sup>148-151</sup> A randomized clinical trial with a 10-year follow-up in nine patients compared the two types of membranes to analyse the results over time.<sup>152</sup> Nine patients with two sites affected by periodontitis were recruited. Each patient site was randomly assigned a polyglactin 910 bioabsorbable or non-resorbable ePTFE membrane. The horizontal clinical attachment level (CAL-H) gain has already been evaluated before at 6, 24 and 60, and 120 months in this paper.<sup>153-155</sup> At 120 months follow-up, tooth loss and regression were noted in 22 % of patients. Other patients gained the same amount of bone between the two sites treated differently. The gain appeared

significant at 120 months compared to 12 months, with  $0.8 \pm 1.0$  mm for ePTFE membrane and  $1.1 \pm 1.1$  mm for the polyglactin membrane. But no significant differences were observed between the two membranes (

Figure 13).

Patient	Polyglactin 910			ePTFE		
	Baseline	12 Months	120 Months	Baseline	12 Months	120 Months
1	4.0	3.0 I	3.0 I	4.0	2.5 I	5.0 II
2	4.5	2.5 I	*	5.0	3.0 I	*
3	5.0	2.5 I	4.0 II	5.0	3.0 I	4.0 II
4	5.0	2.5 I	3.0 I	4.5	2.5 I	3.0 I
5	4.0	3.0 I	2.5 I	4.0	3.0 I	3.0 I
6	5.0	3.0 I	1.0 I	5.5	3.0 I	3.0 I
7	6.0	2.5 I	2.5 I	4.0	2.0 I	1.0 I
8	5.0	3.5 II	4.0 II	5.5	4.0 II	5.5 II
9	4.0	2.5 I	4.0 II	5.0	2.5 I	4.0 II
Mean $\pm$ SD	$4.7 \pm 0.7$	$2.8 \pm 0.4$	$3.0 \pm 1.0$	$4.7 \pm 0.6$	$2.8 \pm 0.6$	$3.6 \pm 1.4$
Change to baseline		$1.9 \pm 0.8^\dagger$	$1.7 \pm 1.4^\ddagger$		$1.9 \pm 0.5^\dagger$	$1.1 \pm 1.3^\ddagger$
Change 12 to 120 months			$-0.2 \pm 1.1$			$-0.8 \pm 1.1$

\* Tooth lost.  
 †  $P < 0.01$ .  
 ‡  $P < 0.05$ .

Figure 13. Horizontal attachment levels (mm) and class of furcation involvement.<sup>152</sup>

A more recent article compared the use of PTFE and collagen membrane on chronic periodontitis on a larger sample of patients (20) but with shorter follow-up time (3 and 6 months). The study compared the two membranes with a control group. It appeared that both of the membranes were significantly efficient for the treatment of the furcation, but there was no difference of efficacy between them.<sup>151</sup> Thus, as the results remains the same over the years



of follow-up, it might be recommended to use absorbable membrane instead of ePTFE to avoid second surgical intervention.

Other issues highlighted by publications are the possible contamination and infection of regenerated tissues by the ePTFE membrane in contact with oral cavity. The results of GTR can be affected by bacterial contamination. Two options can be considered: to find another material with fewer issues involved or improve the existing material by functionalization.

A study addressed this question by comparing treatment with enamel matrix derivative (EMD) and GTR with ePTFE membrane in a randomized clinical trial.<sup>156</sup> This study recruited 98 patients with infrabony defects caused by periodontitis. The level of probing attachment at 1-year after surgery was not significantly different between the two procedures compared, with a value of  $4.1\pm 1.8$ mm for EMD and  $4.3\pm 1.9$  mm for GTR.

The other approach involving functionalization of ePTFE for the treatment of periodontitis by GTR was considered in a clinical trial associating the adjunction of enamel matrix proteins (EMP) on the defects of an ePTFE membrane coated with tetracycline.<sup>157</sup> The study compared the device to the EMP adjunction alone, in 11 patients with 2 defects each. At 1-year follow-up, EMP treatment with ePTFE membrane led to a mean gain in attachment level of  $1.28\pm 2.04$  mm. The only EMP-treated group obtained a mean level attachment of  $1.65\pm 1.29$  mm. The gain in attachment level is not significantly different between the two procedures. However, it can be noted that the values are much smaller than other studies that use GTR procedure,<sup>158</sup> EMP,<sup>159-160</sup> or both,<sup>161-162</sup> including the one mentioned above. The difference would be due to the choice of the treatment before the trial. Indeed, if the presence of *A. actinomycetemcomitans* was detected, treatment was applied which involved scaling and root planning, with the use of systemic amoxicillin and metronidazole. The purpose of the procedure was to improve the results of GBR. However, in the presence of such poor results, it is suggested that the pre-trial treatment would have reduced the inflammation at the site and thus led to a weaker regenerative response. In addition, a study functionalizing the ePTFE membrane with a natural bone mineral with or without platelet-rich plasma against bacteria did not observe any clear improvements against bacteria colonization.<sup>163</sup> A recent systematic review highlighted the heterogeneity of the published trials on GTR and EMD. No meta-analysis was feasible, so no clear conclusion on whether EMD or GTR has the better beneficial effect on healing.<sup>164</sup>

These studies proved that no biomaterials have shown better results than ePTFE, functionalized or not.

In GBR, vertical regeneration of the alveolar bone is the main object of interest, usually to ensure the stability of the dental implant. For this purpose, bone graft material is used to replace the missing structure around an implant or tooth and recovered by a biocompatible membrane to prevent rapidly growing gum tissue and allow bone to grow. ePTFE is generally used as a membrane for this kind of surgery. A prospective randomized controlled clinical trial compared two types of membrane: ePTFE or dense PTFE.<sup>165</sup> Indeed, PTFE had already been tested in clinical trials for other GTR or socket preservation procedures, but not for GBR around implants in comparison with ePTFE. The study enrolled 23 patients with atrophic posterior mandibles, where 26 sites were treated, and a total 78 dental implants were inserted. Defects were filled with composite bone graft around the implant and randomly covered with an ePTFE or PTFE membrane. After 6-7 months of healing, the membrane removal procedure was found by the surgeon to be easier with PTFE than ePTFE. The level of the bone crest increased in both membrane groups and bone regeneration in vertical defects was achieved around the implants. The quantitative results regarding the mean defect fill did not show a significant difference between the two groups, with  $5.49 \pm 1.58$  mm at PTFE sites and  $4.91 \pm 1.78$  mm at ePTFE sites. No obvious advantage can be drawn from these results. However, a recent *in vitro* assay compared ePTFE and dense PTFE regarding *Streptococcus oralis* development.<sup>166</sup> The results favored ePTFE with fewer layers of colonizing bacteria. However, dense-PTFE was frequently used for GBR.<sup>167</sup>

Other biomaterials than collagen, PTFE or ePTFE, such as aliphatic polyesters (PLA, PLGA, PCL) membranes are also commercially available. They are used for GBR procedures and have the advantage of inducing less inflammation and the possibility to be used as carrier for drug delivery.<sup>168</sup> However their results in bone regeneration are inferior to those of collagen membranes.

A new bioabsorbable membrane is under development with promising results.<sup>169-172</sup> The first tests are only beginning to be performed and several steps must be completed before clinical trial. So far, the efficacy and predictability after years of use make ePTFE a reliable material for bone and tissue regeneration treatments.<sup>173</sup>

#### 1.3.4. Hernia repair

Hernia defects are defined as tissue or organ that abnormally protrude through the wall of the cavity that includes it. The most common types of defects are inguinal, hiatal, umbilical, and ventral hernia. Incisional hernia refers to a

ventral hernia that occurs after abdominal surgery, it is a major complication with a reported frequency of 2-20 %.<sup>174</sup>

For hernia repair, ePTFE was found to be a material of choice very early because of its high biological tolerance, lower inflammatory and better peritoneal response compared to polypropylene.<sup>175</sup> The ePTFE developed by Gore involves a special method of expanding the PTFE which preserves its microstructure and improve its mechanical resistance. In the late 1950s, polypropylene had become a revolutionizing material thanks to its much lower strength than the titanium mesh used previously.<sup>176</sup> Thus, ePTFE-polypropylene composite patches have been developed to combine these advantages. Recent short and long-term results from a double-blind randomized controlled clinical trial reported significantly lower discomfort after surgery for PTFE than polypropylene, which would encourage adoption it.<sup>177</sup> It has been reported that the use of ePTFE is currently decreasing though.<sup>178</sup> A recent study compared two of these composite devices: the Ventralex<sup>®</sup> Hernia Patch (Bard USA) and the Cabs'Air<sup>®</sup> Composite (Cousin Biotech France).<sup>179</sup> Both devices were installed via laparoscopic hernia repair, which has been shown to reduce surgical site infection in primary ventral hernia.<sup>180</sup> In this randomized clinical study, 83 patients presenting primary epigastric or umbilical hernia and an incisional hernia were enrolled, after application of the exclusion criteria. Two groups were formed, each received a different device. The Cabs'Air device was deployed intraperitoneally with a balloon to help mesh deployment. The Ventralex<sup>®</sup> Hernia Patch is installed manually by the surgeon, which involves positioning the prosthesis so that it completely covers the defect.<sup>181</sup> The result is that the difference in design leads to a difference of efficiency. Indeed, the Ventralex<sup>®</sup> Hernia Patch was associated with 15.7 % of reoperation with explant of the device due to a mesh infection, bowel obstruction and severe pain resulting from shrinkage (mass syndrome). No recurrence or complication have been associated with the Cabs'Air group (Figure 14). Thus, the combination of polypropylene with ePTFE and the adequate design helps to ensure successful postoperative results.

	Ventrex® (n = 38)	Cabs' Air® (n = 39)	P Value
Mean follow-up (months)	36 (10–54)	36 (8–53)	NS
Mesh infection	1 (2.6%)	0 0%	NS
Bowel obstruction	1 (2.6%)	0 0%	NS
Severe pain (VAS > 60)	6 (15.7%)	0 0%	0.01
Mass sensation	6 (15.7%)	0 0%	0.01
Feeling body foreign	6 (15.7%)	0 0%	0.01
Total comorbidity	8/38 (21.05%)	0/39 0%	0.01
Recurrence	4 (15.7%)	0 0%	0.01
Reoperation (explantation)	6 (15.7%)	0 0%	0.01

VAS, visual analog scale; NS, nonsignificant.

Figure 14. Complication during follow-up for patients that have received Ventrex or Cabs' Air device for their hernia repair surgery.<sup>179</sup>

A recently published review described the process of development of hernia devices to obtain optimal behavior and biomaterials that were introduced over the years.<sup>182</sup>

Other directions of research have previously been directed towards structural changes in ePTFE to improve tissue incorporation and reduce the rate of recurrence.<sup>183</sup> However, v the multiple devices developed over the past decades such as MycroMesh<sup>184</sup> or DualMesh plus<sup>185</sup> have shown no improvement in mechanical strength or tissue behavior at the peritoneal interface compared to regular ePTFE or polypropylene patch on animal experiments. No clinical trials have been published on these devices. However, MycroMesh and DualMesh antibacterial functionalization with silver carbonate and chlorhexidine diacetate has been shown to be efficient *in vitro*, and may be a direction to follow in further studies.<sup>186</sup>

### 1.3.5. Heart repair

ePTFE is usually a suitable material for the replacement or repair of three dysfunctional elements of the heart: mitral valve chordae, pericardium, and ventricular septum. Degenerative mitral valve regurgitation could be managed with chordal replacement or repair, but chordal repair was quickly chosen as the most effective and safe procedure,<sup>187-188</sup> and therefore widely practiced, most often using the ePTFE Gore-Tex suture. Early mitral surgery has been shown to be more effective than initial medical management in terms of long-term survival and the risk of heart failure.<sup>189</sup>

Long term results of mitral valve repair with ePTFE chordae were reported in one study. In 20 years, 608 patients were followed after mitral repair with

artificial chordae.<sup>190</sup> The majority of them suffered from degenerative valve disease (91.3 %), and half of them had already undergone chordae replacement. ePTFE sutures from W. L. Gore & Associates were used. The results showed cumulative survival rate up to 84 % (Figure 15). The obtained 95 % confidence interval is between 75 and 90 %. Infectious endocarditis occurred in 7 cases (1.1 %), thromboembolic events in 21 (3.5 %) and mitral regurgitation in 12 (2 %). Atrial fibrillation was more common (12.5 %). To conclude, the publication has proved in this successful long-term clinical trial that ePTFE is a very well-suited material that meets all the characteristic required for chordae repair, such as mechanical strength, flexibility, inertness, and good tissue reaction.

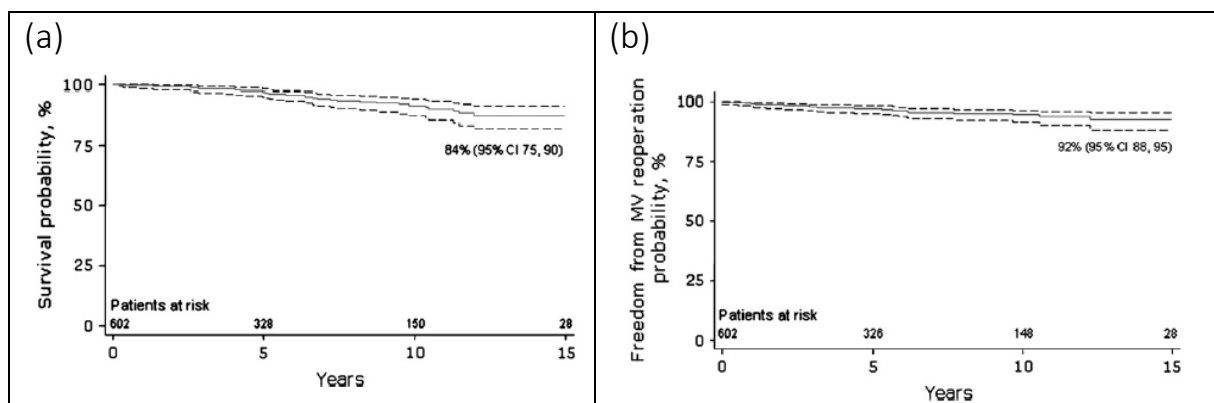


Figure 15. a) Long-term survival of patients with mitral valve repair and b) Freedom from reoperation for all patients.<sup>190</sup>

Pericardial replacement or closure is typically performed for patients after heart surgery or due to congenital heart disease. After heart surgery, primary pericardial closure can put stressful forces on the heart or the graft. This may also not be possible with an autologous pericardium graft used for heart repair. Indeed, adhesion of the cardiac structures to the overlying sternum is dangerous because it limits the total compliance of the cardiac volume and the filling function during diastole.

Early clinical trials were conducted to evaluate the use of the ePTFE membrane for this application. In a prospective randomized trial, 302 patients requiring isolated coronary bypass grafting were enrolled to test the efficacy of the ePTFE membrane in preventing dangerous adhesion.<sup>191</sup> 138 received an ePTFE membrane and 164 had the pericardial cavity left open, as control. The total mortality rate was 1.25 % with 2 patients in each group. No statistically difference was observed regarding the occurrences of complication, with rates of 21 and 14 %, for control and implant patients, respectively.

Otherwise, the ePTFE membrane for pericardial replacement has been shown to be useful for children with congenital heart disease.<sup>192-193</sup> In a clinical

trial involving 61 children, 23 underwent successful membrane removal surgery, and 35 kept the implant without removal.<sup>192</sup> No major complications were encountered.

More recently, a cardiac septal occluder has been developed for patent foramen ovale (PFO). The Spider™ PFO occluder has been proven to be clinically safe,<sup>194</sup> as well as the GORE® CARDIOFORM Septal Occluder based on ePTFE and nitinol only.<sup>195</sup> The latter began to be studied in comparison with antiplatelet therapy for reduction of recurrent stroke or new brain infarct in patients who have already suffered a cryptogenic stroke, in a large clinical trial involving 664 patients. The study is expected to be completed by 2028.<sup>196</sup> However, a recently published review with meta-analysis showed that PFO closure involves for patients to have higher risks of atrial fibrillation than medically treated patients.<sup>197</sup>

### 1.3.6. Other clinical trials

#### 1.3.6.1. Functional and aesthetic nasal surgery

Functional nasal surgery (FNS) is carried out for patients with traumatic nasal deformity and obstruction. The risks associated with the use of an autogenous extranasal graft make the benefit risk ratio negative under certain circumstances, which leaves the solution of synthetic implants.

A 13-year clinical trial involved 404 patients who required FNS.<sup>198</sup> The trial was specifically focused on patients requiring ePTFE implants for traumatic injury. The required use of ePTFE was for 40 patients, 35 of whom suffered from traumatic nasal injury. The ePTFE implants were used at the nasal dorsum. No postoperative complication occurred in 33 of the 35 patients (94 %). One of the two patients who remained presented postoperative infection, the other with irregularities in the shape of the nose.

Aesthetic application also meets ePTFE surgical use. The strong demand in Asian countries for nasal tip and dorsum augmentation led to early use of alloplastic implants which were found to be available, easy to shape and prevent donor site morbidity.

Gu et al. in 2018, reported the efficient, safe, and little-studied solution of using ePTFE as nasal tip and dorsum augmentation, in a randomized clinical trial.<sup>199</sup> Out of a sample of 150 people seeking rhinoplasty, 129 were eligible for dorsum and tip nose augmentation. Patients were randomly enrolled into two groups: one with ePTFE attached to conchal cartilage at the distal end, and one with only an increase in ePTFE. After 9 years, 76 people were available for follow-up, including 39 in the ePTFE alone group and 37 in the ePTFE with conchal cartilage group. The rates of infection, inflammatory reaction or cosmetic irregularity were very low or null for the two groups. Extrusion did not occur in any of the groups. The results lead to the conclusion that the cartilage used as a

shield is not required and the ePTFE used alone for nasal tip and dorsum augmentation is a new technique that can be used safely with high levels of acceptable success. Paranasal augmentation with multi-folded ePTFE is also a technique that has been shown to be clinically safe and effective with a follow-up of 3 to 10 years.<sup>199</sup>

#### **1.3.6.2. Bleeding sealant**

ePTFE patches present many advantages with their strength and elasticity but tend to bleed the suture line after carotid endarterectomy (CEA) longer than other device. An ePTFE improved with fibrin sealant in the event of CEA was tested.<sup>200</sup> This study compared ePTFE with fibrin sealant (Quixil) and as control, a fibrous patch of calcium-sodium alginate (Kaltostat). This randomized trial enrolled 10 people in each group with 7 men and 3 women in each. The rate of hemostasis was measured, which is defined as 1 minute after stopping bleeding from the suture line. The Quixil group appeared to have a significantly low hemostasis time, 1 - 4 minutes, median 2.5, compared to Kaltostat group, with a range of 7-59 minute and median at 17 minutes.

However, some studies have chosen to focus on the fibrin sealant, comparing its efficiency to manual compression. In a randomized clinical trial, 140 patients with bleeding at the suture-line were randomly treated with a fibrin sealant or manual compression.<sup>201</sup> The rate of hemostasis at the suture line at 4 minutes appeared to be significantly different, with 62.9 % with fibrin sealant treatment and 31.4 % in the control group. The fibrin sealant also appeared safe, as no serious adverse events were detected. A systematic review and a meta-analysis evaluated the efficiency of the fibrin sealant in vascular and cardiac surgery. It described this as a significantly reduction in blood loss but clinically not enough to reduce the need for blood transfusion.<sup>202</sup>

#### **1.3.6.3. Ocular non-cancerous surgery**

ePTFE membranes have been successfully tested as a treatment for non-cancerous ocular diseases. A recent clinical study reported 8 cases of perforated corneal ulcer that were treated with ePTFE membrane fixed with Prolene® sutures.<sup>203</sup> In all cases, reconstruction of the ocular anterior chamber was successful. Pressure reduction therapy was required in two cases due to increased intraocular pressure. The cornea had a satisfactory aspect of a thin, stable and in some cases vascularized membrane. It was concluded from these observations that the use of ePTFE membrane was safe and efficient for this application. However, no quantified results or statistical analysis were available, which would have been advisable to support the conclusions drawn.

Another non-cancerous ocular issue is complicated multicurrent pterygia. Pterygium is a tissue growth on the cornea that grows from the inside of the eye to the pupil. In a prospective randomized trial, the ePTFE membrane is used to prevent the application of mitomycin, amniotic membrane and conjunctival autograft after pterygia excision.<sup>204</sup> The membrane is used to prevent the graft tissue from adhering to adjacent ones. 62 patients were involved in the study, 30 had an ePTFE membrane placed to cover the graft and 32 had not. At the mean follow-up period, the group with ePTFE membrane, symblepharon significantly regressed, with no other unwanted adhesion to the eyeball. A significant improvement in motility and binocular diplopia was observed in 80 % of the group. For the group without membrane, the same improvements were noted for symblepharon. In contrast, no improvement in motility recovery or diplopia regression were observed.

Refractory glaucoma is a disease that involves uncontrolled intra-ocular pressure which cannot be cured with surgical treatment or with high risk of trabeculectomy failure. This leads to deterioration of the optic nerve and visual field. A clinical trial compared ePTFE membrane-tube implant with Ahmed implant. The study on 20 eyes showed no significant difference between the two devices, with the same efficacy on the reduction of intraocular pressure. The ePTFE membrane-tube implant is described as a better option due to its soft texture and small volume that avoid large conjunctival incision, unlikely widely used implants that have large and rigid reservoirs.<sup>205</sup>

To conclude, ePTFE medical devices have been clinically tested with an increase over the years of successful interventions and postoperative follow-ups since the early 1990s. Significant advances have been made in the fields of vascular, guided bone and tissue regeneration, hernia repair and heart repair surgery, although clinical trial failure rates may remain high according to the field (up to 40% and more). Additionally, ePTFE appears to be a more or equally effective material than other materials used for the same purposes, such as Dacron for vascular graft, bioabsorbable polymers for GTR or nitinol for stents. Improvements in success rates could be achieved with the functionalized ePTFE. Indeed, functionalization is an interesting path of investigation to improve the performance of devices and make them suitable for a larger number of cases requiring specific medical properties. Clinical trials of functionalized ePTFE maintain a marginal presence that could be changed by innovative solutions.

In the next part, we will present an innovative functionalization that we have developed to modify the chemical composition of the surface of ePTFE by defluorination and amination. The method is characterized and its potential for a medical application is evaluated with primary assays.



## II. Chemical etching and functionalization of ePTFE using organic solvent and alkaline metal

### II.1. Previous work leading to this study

Before presenting our innovative functionalization method, we will present the various existing strategies used to achieve the defluorination of fluoropolymers among different fields of chemistry and physics, as well as the previous work using organic solvent and alkaline metal that inspired our work.

It was recently proved that the antibacterial fluorinated molecule 4-fluoro-L-threonine produced by *streptomyces cattleya* could be defluorinated by another bacteria's enzyme: the threonine deaminase.<sup>206</sup> This enzyme originally deaminates of the amino acid L-Threonine in bacteria, yeast or plants.

Another study focused on the metabolism of the autotroph strain *acidimicrobium sp. A6* in presence of only Perfluorooctanoic acid (PFOA) and perfluorooctane sulfonate (PFOS) as the only organic carbon source.<sup>207</sup> It was found that the bacterium was responsible for buildup of fluoride and perfluorinated products, among others. A decrease in Fe(III) reduced per ammonium or dihydrogen oxidized was also constated. The concentration measures of the different species in the medium led to the conclusion that PFOA and PFOS may be an alternative to Fe(III) as electron acceptor during the oxidation-reduction reaction. This would result in a reductive defluorination of the compounds. However, the author found experimentally that the fluorinated molecules cannot be used as electron acceptor alone.

A photochemical defluorination of per- and polyfluoroalkyl substances (PFAS) was developed.<sup>208</sup> The PFAS, dissolved in an aqueous solution containing  $\text{Na}_2\text{SO}_3$  and  $\text{NaHCO}_3$  are placed in a closed photoreactor system. The concentration measurement of  $\text{F}^-$  in the system showed that according to the length of the carbonated chain, the defluorination can be either partial or total, the shorter the chain, the higher the defluorination obtained.

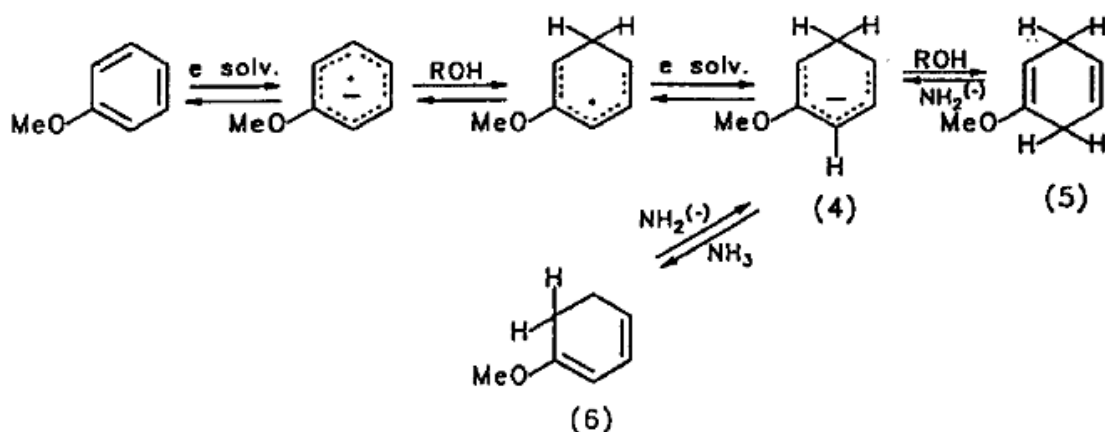
A new method called mineralization that uses alkaline hydroxide to obtain a defluorination by decomposition of PTFE was recently reported.<sup>209</sup> Molten sodium hydroxide in contact with PTFE under atmospheric pressure and elevated temperature leads to the formation of NaF. NaF is then solubilized, the pH is adjusted to 6-6.5 and  $\text{CaCl}_2$  is then added to obtain  $\text{CaF}_2$ . This latter product is indispensable to initiate the synthesis of almost all organofluorine compounds. This process is part of a recycling approach of PTFE, that is also applicable to other fluorinated polymer such as d poly(vinylidene fluoride) (PVDF),

poly(chlorotrifluoroethylene) (PCTFE), and the poly(vinylidene fluoride-co-hexafluoropropylene) copolymer (poly(VDF-co-HFP)).

Among the functionalization methods adopted for medical application as presented previously and the existing defluorination methods, we will now focus on effective strategies to covalently functionalize fluoropolymers, requiring only chemistry equipment.

Copolymerization of monomers is efficient but involves multiple steps of reaction to achieve fluoropolymer crosslinking. In this objective, sodium-based etching solution have been reported to enable bonding with other materials or to itself. Alkali metals such as lithium and sodium are the most reactive elements with ammonia to produce solvated electrons, alkali earth in a lesser extent.<sup>195</sup> The solubility and reactivity of alkali metals in liquid ammonia are known for a long time and lead to amide formation.<sup>210-211</sup>

At first, it was performed by dissolving lithium or sodium in liquid ammonia, according to the Billups-Birch reaction. This latter reaction consists in adding to liquid ammonia an alkali metal, an aromatic compound and alkyl alcohols. The ammonia molecules solvate the metal electrons (solvated electron noted  $e_{\text{solv}}$  in Equation 1), and the strong base sodium amide is produced in liquid ammonia. This strong base leads to reduction of the alkyl alcohols, and the substituted aromatic molecule, showed in Equation 1.

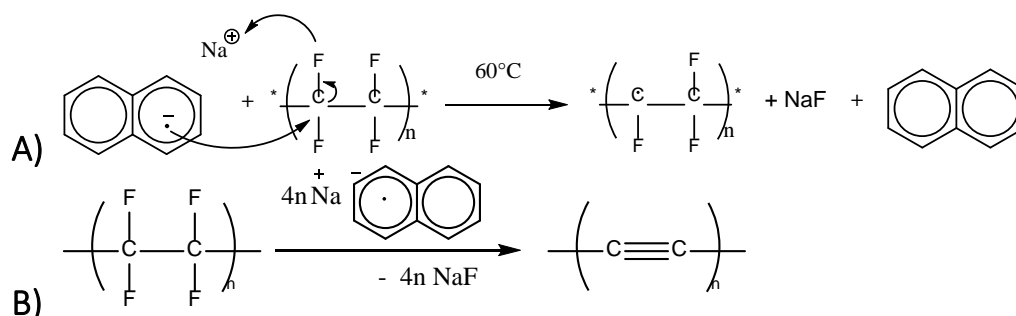


Equation 1 Birch reduction : example of the reduction of methoxybenzene in liquid ammonia in presence of an alkali metal and an alkyl alcohol. The production of solvated electrons is noted  $e_{\text{solv}}$ .<sup>212</sup>

Then, an alternative method was to use sodium naphthalenide dissolved in an ether such as tetrahydrofuran (THF) or benzoin in dimethylsulphoxide<sup>213</sup>. More

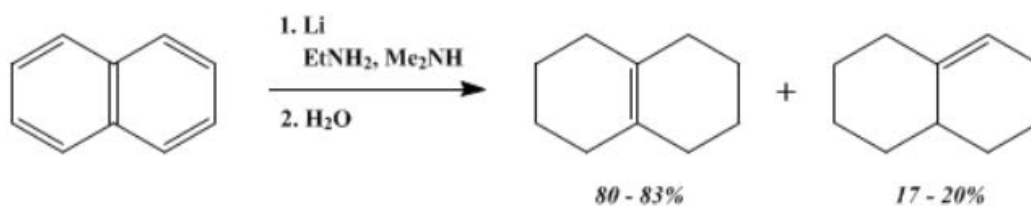
recently, glycol ethers (diglyme) dissolving sodium naphthalenide have replaced THF to reduce health risks.<sup>214</sup>

This commercially available product enables to reduce the fluorinated chain by attacking the carbons. NaF salt is produced as pictured in (Equation 2A) and the polymer chain is gradually defluorinated until the polyyn is obtained (Equation 2B).



Equation 2 A) Balance equation of the reaction of sodium naphthalenide on PTFE. Equation 2 B) Full defluorination of PTFE.<sup>214</sup>

Alkali metals are known to be soluble in light amines in a less extent than in ammonia, but the reaction rate decreases drastically as the length of the alkyl chain of the solvent increases. As reported in the literature, ethylenediamine improves the solubility of alkali metals in light amines. Extensive work with lithium in light amines or a mixture of light amines and ethylenediamine (in a small amount) has been dedicated to the reduction of several types of aromatic compounds. Especially, the Benkeser reduction (Equation 3) which is a fork of the Billups-Birch reaction<sup>215</sup>, overcomes the drawbacks of handling ammonia when run on kilograms or even industrial scale.<sup>216</sup> It consists in reducing aromatic solvents (toluene, cumene, butylbenzene..) using lithium in light amines such as ethylamine, methylamine or ethylenediamine. But there was no mention of the lithium amide in EDA and explanation of its reactivity<sup>217-222</sup>, nor more recently for the alkylation or hydrogenation of single-walled carbon nanotubes and graphene<sup>223-225</sup>.



Equation 3. Benkeser reduction : example of the reduction of naphthalene using lithium and light amines (ethylenediamine and dimethylamine).<sup>226</sup>

Despite many studies reporting the functionalization of fluoropolymers<sup>227</sup> through defluorination, there is no direct chemical conversion of carbon-fluorine bonds in fluorinated materials to any functionality<sup>228</sup>. This is why we developed a Birch and Benkeser inspired method that enables defluorination as well as amination of the surface and will be presented in the next parts.

## II.2. Birch and Benkeser inspired reaction

### II.2.1. Materials and methods

The materials used to carry out the functionalization presented in this part were obtained from W.L. Gore & Associates (Paris, France) for the ePTFE and Goodfellow (Lille, France) for the PTFE. Lithium, Sodium, EDA, and DETA were obtained from Sigma-Aldrich (Saint Quentin Fallavier, France).

The glovebox used was bought from Jacomex (Bagneux, France). The detailed protocol with the exact proportion and durations is detailed in the annex **A1**.

### II.2.2. Reaction description and observations

The idea of this method is to use ethylenediamine both as solvent and as a precursor of the lithium alkylamide source to produce as a one-pot experiment a liquid etchant with respect to fluorinated polymers and bring amination. Consequently, we carried out the synthesis in a glovebox under argon stream. The reaction starts as soon as the lithium is dropped in the solvent. Immediately, a dark blue coloration of the reaction medium takes place, characteristic of the formation of the solvated electrons. Solvated electrons in amines are the anions of electride salts which are intermediate species written in Equation 5. In case of stoichiometric proportion, in less than 1h we observe that the blue color disappears, and the solution gives way to a white solid consuming all the reagents completely in a total reaction, as no solvent or metal remains in the medium. White crystals of millimeter size are formed with EDA, while smaller ones are obtained with DETA. So far, Beumel *et al.* obtained only a white suspension, by an

equimolar synthesis between lithium and EDA, but without achieving a total reaction of a completely solid lithium amide.<sup>229</sup>

When lithium is below the stoichiometric proportions according to the reactions (1), (2) and (3) (Equation 4), the solvent is not entirely consumed. In this configuration, the reaction medium containing the lithium alkylamide remains liquid, which ensure the best contact liquid-solid with the material to be modified.

The drastic changes in the surface of fluoropolymers immersed in this solution are striking not only in color, but also in morphology. Indeed, the color changes from white to black under LiEDA treatment after a few hours of soaking. For LiDETA, colors range from white to dark brown with a metallic sheen depending on the soaking time too.

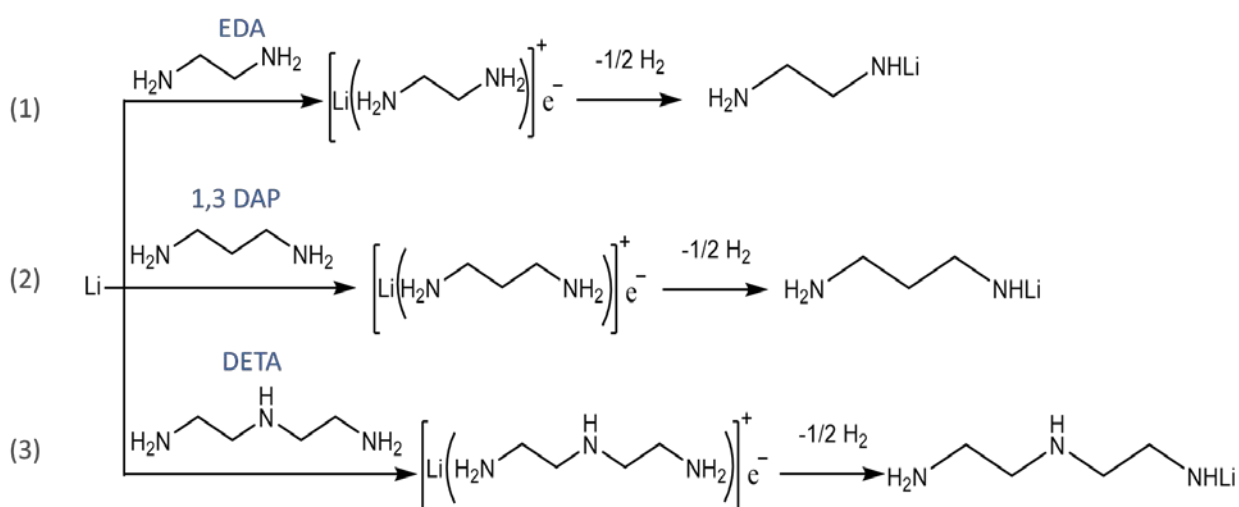
Visible deformations can be noticed on the treated samples. These deformations are all the more visible when the material is soft or in a thin layer such as ePTFE which buckle. This might be attributed to stress-induced chain shortening and rearrangement due to chemical etching.

The different steps of the occurring chemical reaction will be detailed below, based on characterizations and numerical simulations that enable us to achieve the most accurate description possible.

### II.2.3. Lithium alkylamide formation and characterization

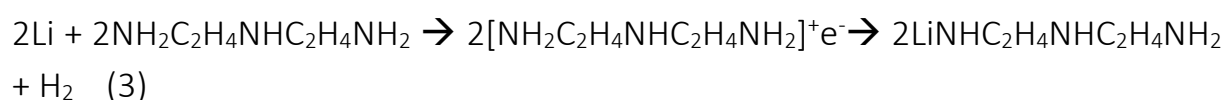
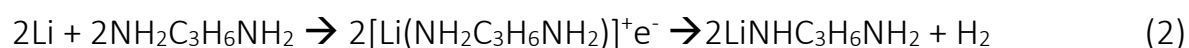
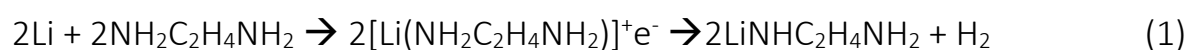
As presented before, our original approach is based on etching and functionalizing fluoropolymers in a one-pot experiment. Numerical simulations and XRD structure were carried out and used to establish the equations below with the structure of the lithium alkylamides formed (Equation 5).

Equation 4. Reactions between lithium and (1) EDA, (2) DAP and (3) DETA, the metal and the solvent added in amount below the stoichiometric proportions.



Organolithium compounds are of great importance in organic asymmetric synthesis<sup>230</sup>, but remain little studied in the case of lithium alkylamides because few crystallographic data exist. They are more soluble and reactive than their sodium or potassium counterparts, hence the use of lithium<sup>231-232</sup>. According to reactions (1), (2) and (3), the following chiral lithium alkylamides LiNHC<sub>2</sub>H<sub>4</sub>NH<sub>2</sub>, LiNHC<sub>2</sub>H<sub>4</sub>NHC<sub>2</sub>H<sub>4</sub>NH<sub>2</sub> and LiNHC<sub>3</sub>H<sub>6</sub>NH<sub>2</sub> can be directly synthesized when reactants are in equimolar proportions of lithium with EDA, DETA and DAP, respectively. This extends the portfolio of chiral lithium alkylamides and amination for covalent functionalization of fluoropolymers.

Equation 5. Reactions (1), (2) and (3) correspond to the reactions in Equation 4 but in stoichiometric proportions.



The X-ray diffraction (XRD) analysis of the crystals obtained by the total reaction of lithium and EDA leads to the chemical formulae C<sub>8</sub>H<sub>28</sub>Li<sub>4</sub>N<sub>8</sub> in the unit cell (space group P2<sub>1</sub>/n) and corresponds to LiNHC<sub>2</sub>H<sub>4</sub>NH<sub>2</sub>, as expected and according to reaction (1) in Equation 5. This is in total agreement with the only known structure of a lithium amide obtained exclusively with a diamine by the reaction of Li<sub>3</sub>N with EDA for 3 days, instead of 1 h in our case<sup>233</sup>. Only XRD patterns were performed for LiDETA and LiDAP as shown in Figure 17(a) and (b), respectively.

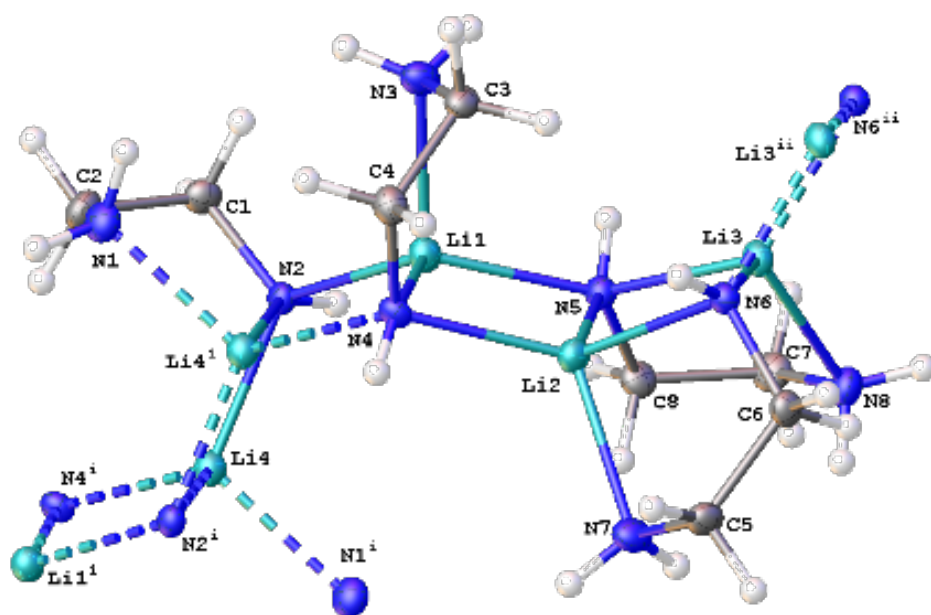


Figure 16. XRD structure of lithium alkylamide LiEDA.

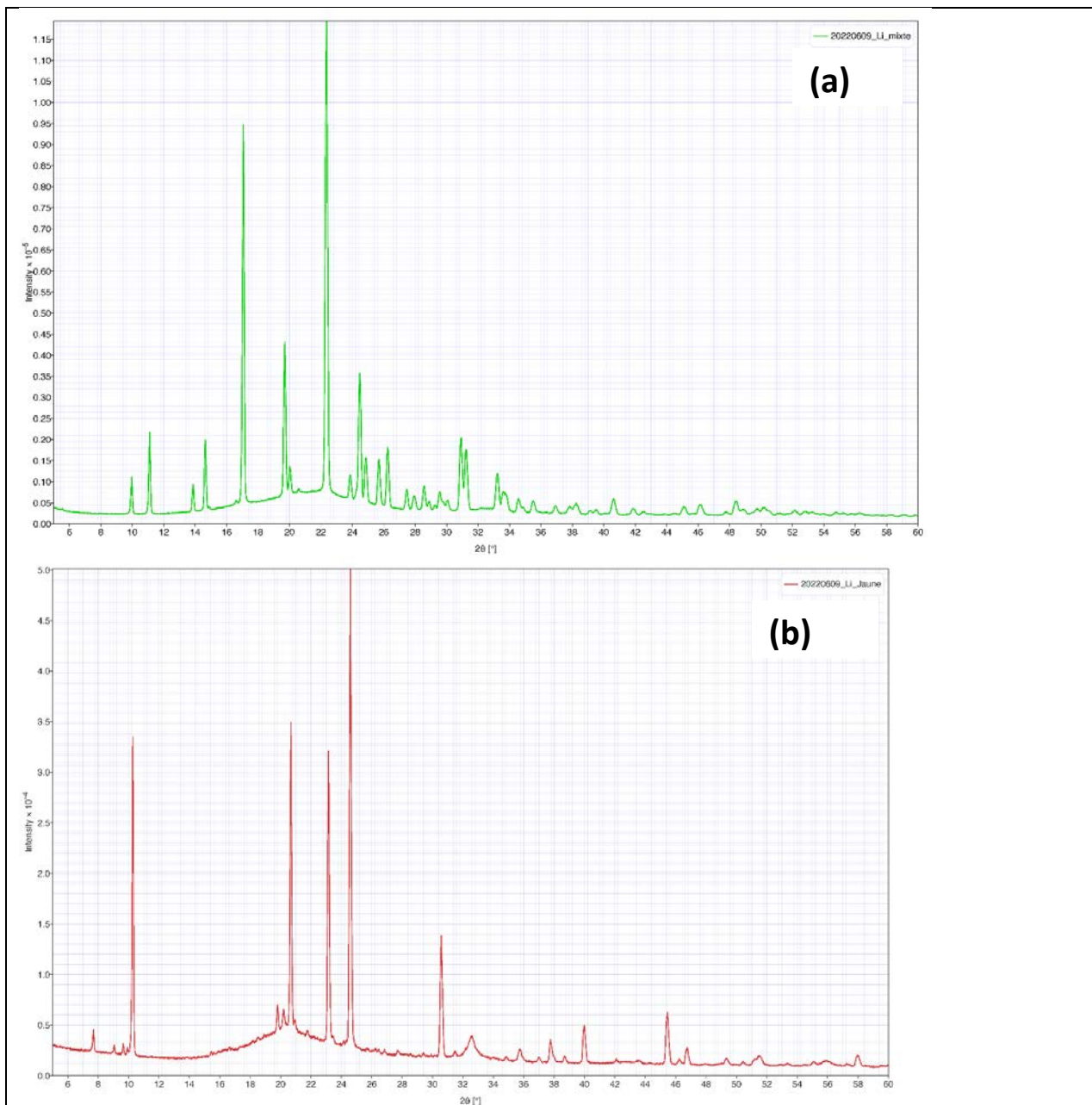


Figure 17. Powder XRD patterns of lithium alkylamides (a) LiDETA and (b) LiDAP.



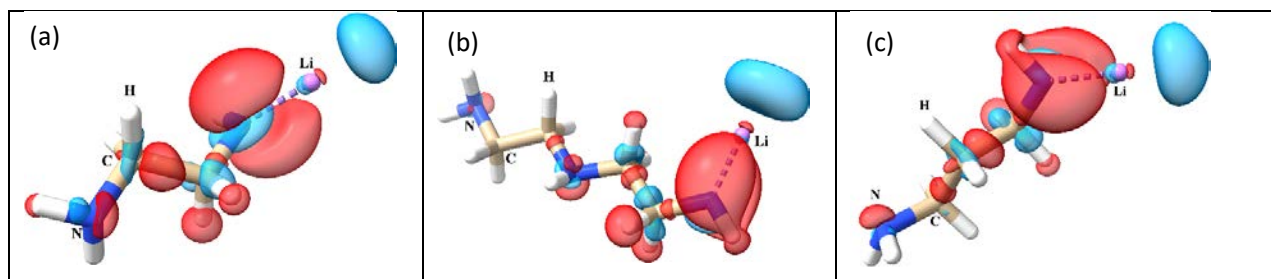


Figure 18. Reactive centers in the CDFT formalism of the lithium alkylamides. Isosurface maps of the dual descriptors ( $\Delta f$ ) of (a) LiEDA, (b) LiDETA and (c) LiDAP. Positive and negative regions of the dual descriptor  $\Delta f$  are represented as blue and red colors, respectively.

The reactivity of this new compound formed, the lithium alkylamide, is evaluated within the framework of conceptual DFT (CDFT).<sup>234</sup>

CDFT is a predictive method relying on the hypothesis that the external potential felt by the electrons changes according to the kind of reaction (nucleophilic or electrophilic attack); because the electrons are attracted to the nuclei and repelled by the electrons of the attacking molecule. Thus, the reactivity of a molecule is described by its response to change in the number of electrons and the external potential. A hierarchy of molecular reactivity determined by indicators can be summarized as shown in Figure 19.

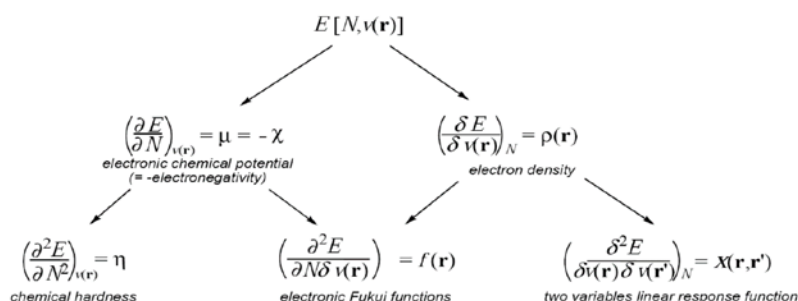


Figure 19. First and second derivatives of  $E[N;v(r)]$  with respect to  $N$  and  $v(r)$ , where  $E$  is the state energy of a non-degenerate  $N$ -electron system, and  $v(r)$  the electron nucleus Coulomb interaction.<sup>235</sup>

As expected and confirmed theoretically by the dual descriptor isosurfaces related to the three lithium amides (Figure 18) within the framework of conceptual density functional theory (CDFT)<sup>234, 236-237</sup>, the alkylamide group (bearing the biggest red lobe) is a favorable site for an electrophilic attack. On the contrary, lithium (blue lobe) is a favorable site for a nucleophilic attack. Indeed, the local reactivity descriptors  $f^+$ ,  $f^-$  and  $f^0$  (Fukui indices) related to nucleophilic, electrophilic, and radical attack can be gathered via  $\Delta f$  to reveal reactive sites at

a glance<sup>238-239</sup>. However, the biggest contribution of the blue isolated lobe in front of lithium atom comes from  $f^+$ , but  $f^o$  contribution is not negligible at all (no contribution from  $f^-$ ). Lithium alkylamides can promote radical coupling by electron transfer for many reactions including alkylation and amination but are highly dependent on their aggregation<sup>240-245</sup>.

Thus, the lithium alkylamides formed present a high reactivity that enables an electrophilic attack. We will now approach the second step of the reaction: the attack of the ePTFE surface by the lithium alkylamide.

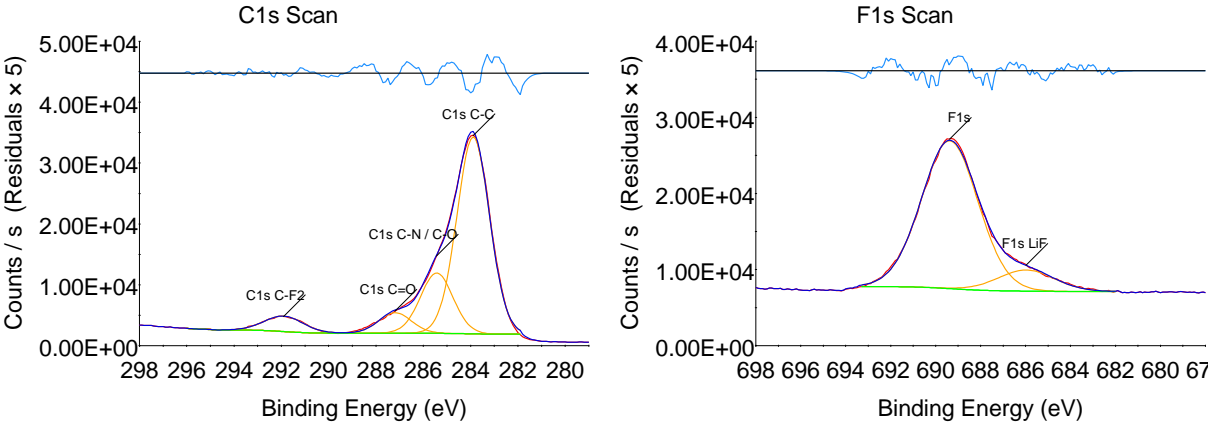
#### II.2.4. Defluorination and amination of the fluorinated surface

In the rest of this study, we will refer the method used to modify a sample in a solution of lithium dissolved in an excess of EDA or DETA (according to the protocol in the annex A1) as LiEDA or LiDETA, respectively. If a functionalization named "X" is added after this first modification, we will refer the whole method as LiEDA X or LiDETA X. This nomenclature will be frequently used to distinguish the different samples studied.

Halocarbons (haloalkane, halo-alkene or alkyne, haloaromatic) can undergo amination with lithium alkylamides, in addition to being of prime importance in asymmetric reactions.<sup>246-253</sup> Amination of fluoropolymers has never been reported while this reaction on halogenated compounds by lithium alkylamides exists. The amination of fluoropolymers depends on the amide reactivity (discussed previously with local descriptors), but also its concentration conditioning its aggregation, for a given halogen (fluorine here). The concentration of lithium amides obtained in EDA or DETA increases with that of lithium to be dissolved.

Whatever the solvent used, it is observed for fluoropolymers that the higher the lithium alkylamide concentration, the faster the modification reaction gets at room temperature. In amines, X-ray photoelectron spectroscopy demonstrates that defluorination and amination are achieved during the one-pot experimental process. Modified PTFE by LiDETA exhibits the major C1s peak at 284.89 eV relative to C-C bonding (carbon sp<sup>3</sup>). The other C1s peak positions (Figure 20) are 284.25 eV for sp<sup>2</sup> carbon, 285.82 eV for C-O-, 287.65 eV for -O-C=O, and 292.73 eV for -CF<sub>2</sub> obviously. The peaks obtained with LiEDA treatment are rather resemblant, with 284.8 eV for C-C bonding, 285.9 eV for C-O and C-N, 287.7 eV for C=O and 292.8 eV for -CF<sub>2</sub>. Untreated PTFE samples contain C and F atoms in a 1:2 ratio in the form of -CF<sub>2</sub>- bonds while this ratio is about 7:1 for LiDETA modified PTFE and 1:1 for LiEDA. Impurities in LiEDA sample is due to the use of water filtered with ion-exchanging resin, while LiEDA sample was rinsed with Millipore water. Amination can be observed in both of the analysis, with C-N

peaks at 285.43 eV for LiDETA treatment with 4.4% for the atomic composition of N1s on the surface and 285.71 eV for LiEDA with 7.73%.



Position (Pos)	C1s	Ca2p	F1s	Li1s	N1s	O1s
	Atomic % (%)	Atomic % (%)	Atomic % (%)	Atomic % (%)	Atomic % (%)	Atomic % (%)
Pt #001	73.1	0.7	8.7	1.1	4.5	12.0
Pt #002	74.5	0.4	5.7	0.0	4.6	14.8
Pt #003	76.7	0.6	4.7	0.0	4.0	14.1

Figure 20. XPS analysis on a LiDETA sample and atomic composition of the surface.

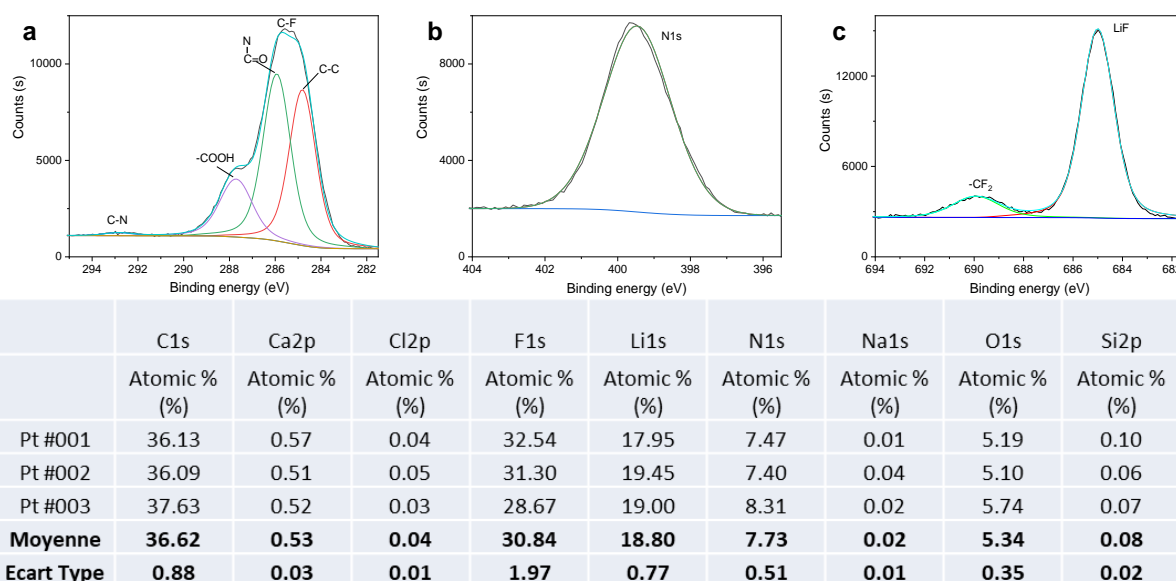
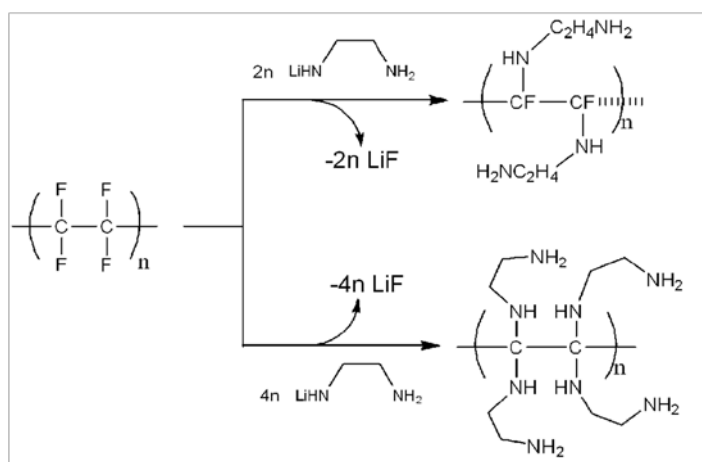


Figure 21. XPS analysis on a LiEDA sample and atomic composition of the surface.

Thus, based on these characterizations as well as additional numerical simulations, we can establish Equation 6 considering the reaction of a PTFE chain attacked by 2 or 4 equivalents of lithium alkylamide, resulting in the precipitation of LiF and the partial or total nucleophilic substitution of fluorine atoms by the alkylamide chain.

Equation 6. Defluorination and amination of PTFE chain by LiEDA, leading to a partial or total nucleophilic substitution according to the number of equivalents of lithium alkylamide reacting.



To confirm our theory and better understand the effects of this new reaction on the material properties, we characterized the surface chemical functions, the morphology, the surface energy, and the mechanical properties of the materials obtained. This will be presented in the next part.

## II.3. Characterizations of the functionalized surfaces

### II.3.1. Materials and methods

The spectroscopy analysis was made using the FR/IR-4X from Jasco to obtain IR-ATR spectra. ePTFE-treated samples were analyzed.

The AFM imaging was obtained with the Nano-observer AFM from CSI and the SEM used was the SU8230 from Hitachi.

AFM imaging was conducted on PTFE-treated samples using resonant mode with a silicon pyramidal tip (FORT tips bought from ScienTec, France).

The contact angles were measured on PTFE-treated samples in air using an Easy Drop DSA100 (KRUSS), and the images were acquired using the Drop Shape Analysis software. The measurements were performed at room temperature with a series of ten deionized water (W) and diiodomethane (DIM, Sigma-Aldrich) drops of 10  $\mu\text{L}$  as testing liquids in order to evaluate contact angles.

The mechanical testing was obtained using the Nanoindenter from CSI instruments. Each sample is glued with a cyanoacrylate adhesive on a steel support. After one night drying, it is tested with a Berkovich tip. The same program as follow was applied to every sample after its optimization:

Maximal load: 1.00 mN

Loading rate: 1.00 mN/min

Unloading rate: 4.00 mN/min

Pause: 120.0 s

Sinus Frequency: 5.0 Hz

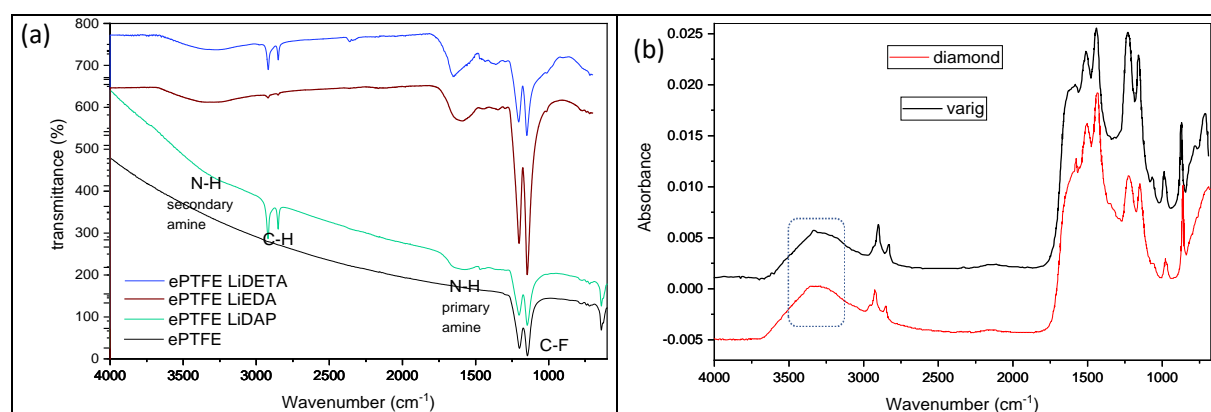
Sinus Amplitude: 0.10 mN

### II.3.2. Spectroscopy analysis

Spectroscopy analyses were carried out to characterize the functional groups present after chemical treatment and corroborate our equations previously presented. Prior to any etching, PTFE and ePTFE has  $-\text{CF}_2$  bands at 642, 1147 and 1204  $\text{cm}^{-1}$  in IR-ATR mode (Figure 22a) and Raman bands at 290, 381, 574, 730, 1214, 1299 and 1380  $\text{cm}^{-1}$ . When chemically etched, PTFE (Figure 22a)

shows characteristic IR bands of  $-CH_2$  from alkanes ( $2919$  and  $2850\text{ cm}^{-1}$ ) and  $-NH$  (around  $1600$  and  $3300\text{ cm}^{-1}$ , visible for LiEDA, Figure 22a). Notice that primary amine bands are better revealed by Ge crystal than diamond one in IR-ATR mode (Figure 22b). According to penetration depth of infrared light (at  $3000\text{ cm}^{-1}$ ) in the sample with Ge crystal, the surface modification is less than  $220\text{ nm}$ .  $-CF_2$  bands remain visible in IR-ATR mode due to larger penetration depth than the thickness of the modification. In contrast, the Raman  $-CF_2$  bands of pristine PTFE fade after etching or disappear (Figure 22d). However, the indirect modification of PTFE by a lithium alkylamide such as LiDETA dissolved in THF evidences active vibration modes (Figure 22c) at  $1657$ ,  $3270$  and  $3300\text{ cm}^{-1}$  assigned to aliphatic primary amines and at  $2926\text{ cm}^{-1}$  for C-H stretching mode. These bands correspond to defluorinated and functionalized ePTFE decorated with aliphatic primary amines.<sup>254</sup> These results can be compared to those obtained by Raman in Figure 22d. Indeed, these lithium alkylamides are soluble in THF and keep their reactivity towards fluoropolymers as observed by their surface state. For instance, the chemical modification of ePTFE surface during 24h by LiEDA or LiDETA dissolved in anhydrous THF and observed by Raman spectroscopy ( $785\text{ nm}$  laser excitation) is shown Figure 22c. The intensity of the Raman bands of PTFE assigned to C-F bonds have drastically decreased or even disappeared for LiDETA. In addition, the band around  $2125\text{ cm}^{-1}$  could be assigned to C=C stretching mode.

Even though significant fluorescence occurs, the ePTFE surface modified with either LiEDA or LiDETA shows a drastic change compared to bare ePTFE, the decrease or disappearance of the C-F bands. Unfortunately, direct etching of PTFE by either LiEDA, LiDETA or LiDAP gives rise to fluorescence background in Raman ( $785\text{ nm}$  excitation) making observation difficult excepted for surfaces modified by lithium alkylamides in THF. Raman spectroscopy gives surface information while IR-ATR on Ge crystal which has a depth of penetration of  $0.66\text{ }\mu\text{m}$  at  $1000\text{ cm}^{-1}$  and  $0.33\text{ }\mu\text{m}$  at  $2000\text{ cm}^{-1}$ , shows surface and underlying layers or even the bulk. As a result, IR-ATR still shows the presence of C-F despite the chemical surface modification.



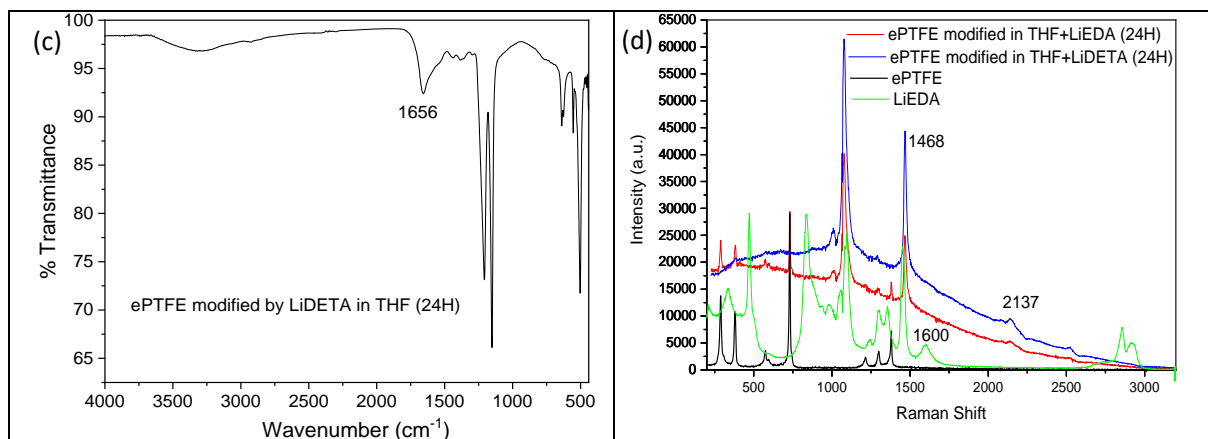


Figure 22. Vibrational analysis by IR-ATR spectroscopy of (a) PTFE, LiEDA, LiDETA and LiDAP treated samples, (b) LiEDA sample with diamond and Ge crystals and by Raman spectroscopy of (c) ePTFE modified by LiDETA lithium alkylamide dissolved in THF and (d) PTFE, ePTFE modified by THF+LiEDA, THF+LiDETA and LiEDA.

Thus, the irreversible modification of PTFE during its reduction by lithium alkylamides LiEDA and LiDETA can be confirmed by IR-ATR and Raman bands, especially with the presence of C-H, C-C and N-H bonds.

### II.3.3. Imaging

#### AFM imaging

Atomic force microscopy observations were carried out on PTFE surfaces modified by LiEDA (Figure 23) and LiDETA (Figure 24). We use the PTFE surfaces for the measures to avoid the large waviness of the ePTFE structure, as we can observe on Figure 23 D, and thus measure the roughness obtained from the treatment only.

As we can observe, both of the LiEDA and LiDETA treated materials present spherical forms on their surface. We can see them closer for LiEDA in Figure 23 C, as spheres joined to each other. The diameter of the spherical forms was measured via image analysis embedded in the gwyddion software. It appears that LiEDA forms smaller spheres than LiDETA on PTFE, with mean diameters of  $105 \pm 24$  nm and  $605 \pm 80$  nm respectively. It appears also that ePTFE have bigger diameter spheres than PTFE, with  $239 \pm 61$  nm for ePTFE LiEDA. In addition, we obtained with the software the roughness average (Ra) of the PTFE surfaces modified by the two methods. For the LiEDA treated surface,  $Ra = 7,5 \pm 1,0$  nm and

for LiDETA,  $R_a = 1,0 \pm 0,1$  nm. As a comparison point, for bulk PTFE,  $R_a = 1,8 \pm 0,5$  nm. Thus, the  $R_a$  obtained from LiEDA treatment is significantly higher than the  $R_a$  of the two other samples. This treatment seems to be more aggressive, as it significantly modifies the surface morphology. LiDETA otherwise does not involve a significant change of roughness compared to bulk PTFE, even if the morphology is visibly different.

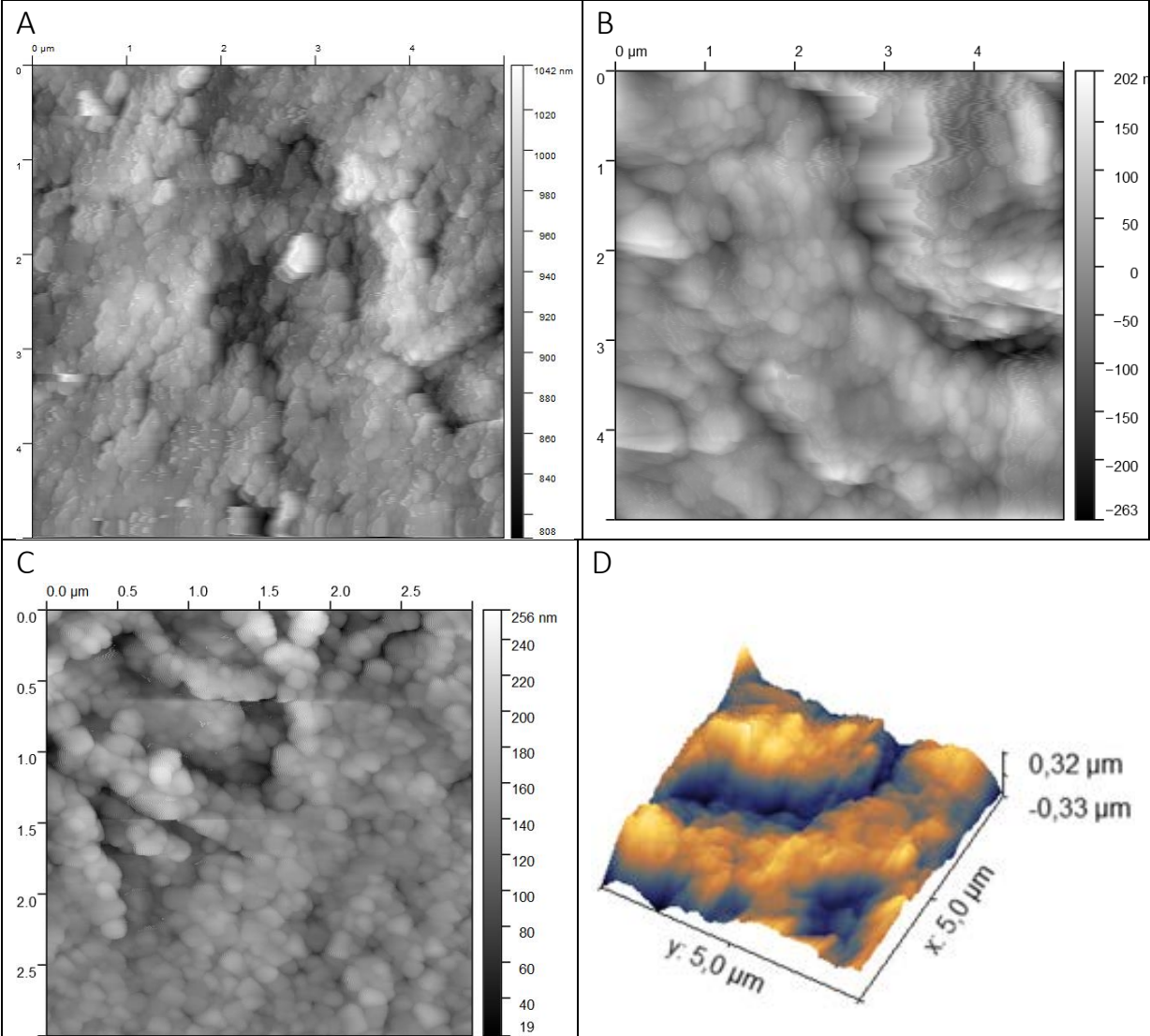


Figure 23. AFM images of samples treated with LiEDA. Image A and C: PTFE, B: ePTFE and D: ePTFE 3D picture.



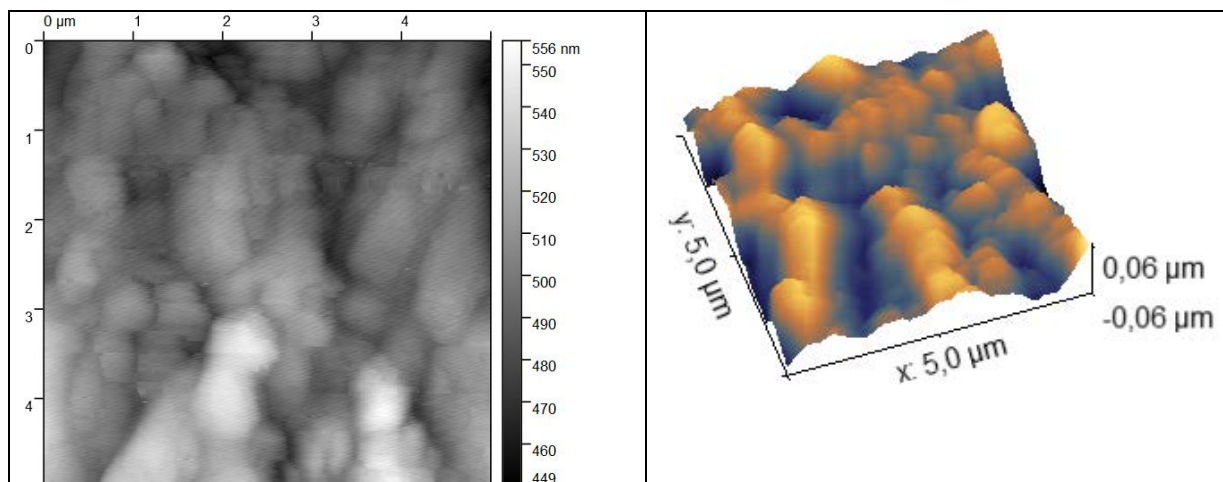


Figure 24. AFM image and the corresponding 3D picture of PTFE sample treated with LiDETA

### SEM imaging

SEM images were obtained on PTFE samples treated with LiEDA and LiDETA. As we can observe on Figure 25, the surface structure in both samples appears disorganized with fibrillar structure and pores showing, compared to the bulk PTFE that only shows scratches from machining. The LiEDA sample presents a larger number of pores than LiDETA sample, which could be interpreted as a more disrupted appearance. Porosity is also obtained in irradiated PTFE as we can see on Figure 26 C, with a similar range of diameters between 50 and 100nm.<sup>255</sup> Patterns named “spherulite” have already been noticed for a sodium naphthalene-based etchant solution or after PTFE irradiation without further functionalization<sup>214, 255-256</sup> (Figure 26 A,B), but such structures are not encountered in LiEDA or DETA samples at the same scale because of the difference in the process used.

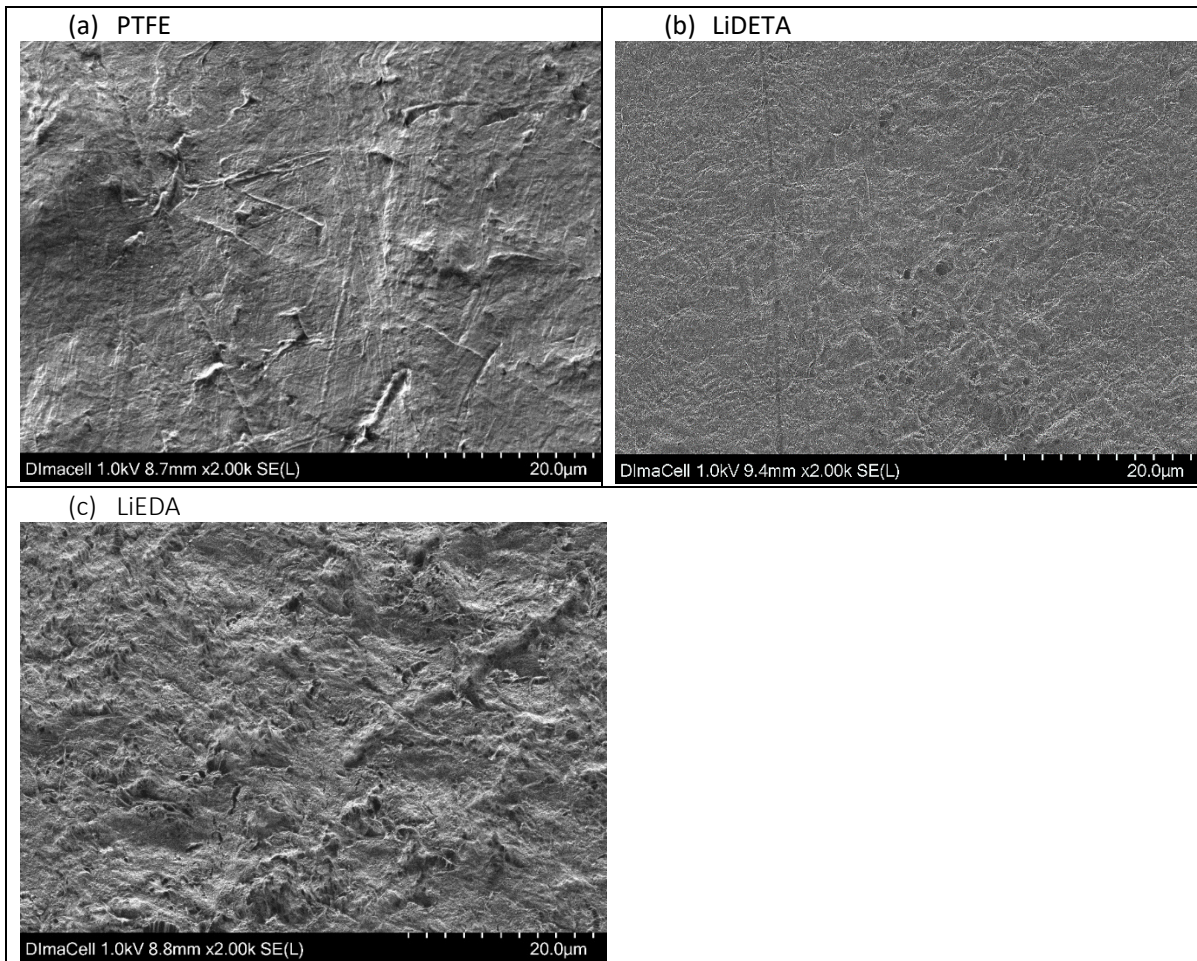


Figure 25. SEM images of (a) bulk PTFE, (b) LiDETA and (c) LiEDA treated PTFE.

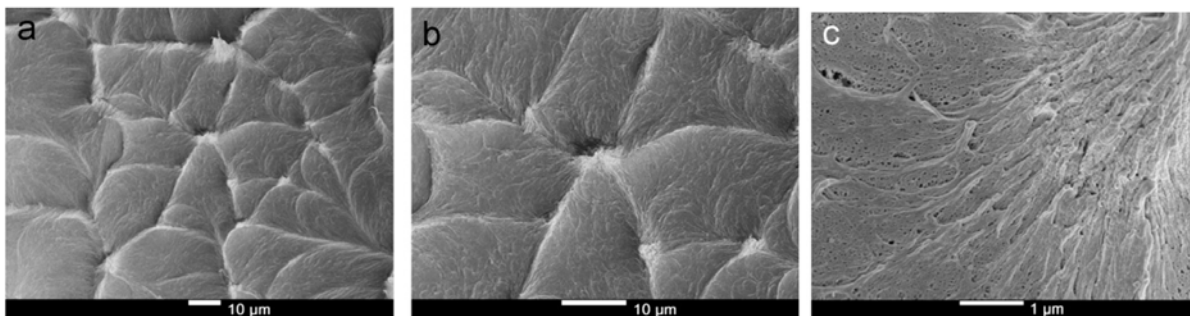


Figure 26. Transverse direction fracture surface of sintered PTFE irradiated with 200kGy at 335 °C.<sup>255</sup>

Additionally, SEM images were realized of ePTFE treated with LiEDA cut after being frozen in liquid nitrogen, to access to a clean slice and observe the width attacked by the treatment. We can see the slice on Figure 27. The untreated width of the sample measures  $1.4 \pm 0.1$  mm on average, the upper dark part, supposedly the treated part,  $120 \pm 1$   $\mu\text{m}$ , and the lower part  $103 \pm 8$   $\mu\text{m}$ . The width

of the sample is originally of 2 mm, we can assume that the cutting, even after frozen in liquid ammonia, has flattened the material as the total width of the sample is  $1.6 \pm 0.1$  mm on this image. But the chemical treatment might also have reduced the thickness. This gives us a more precise description on how the sample is affected by the treatment and how this latter operates.

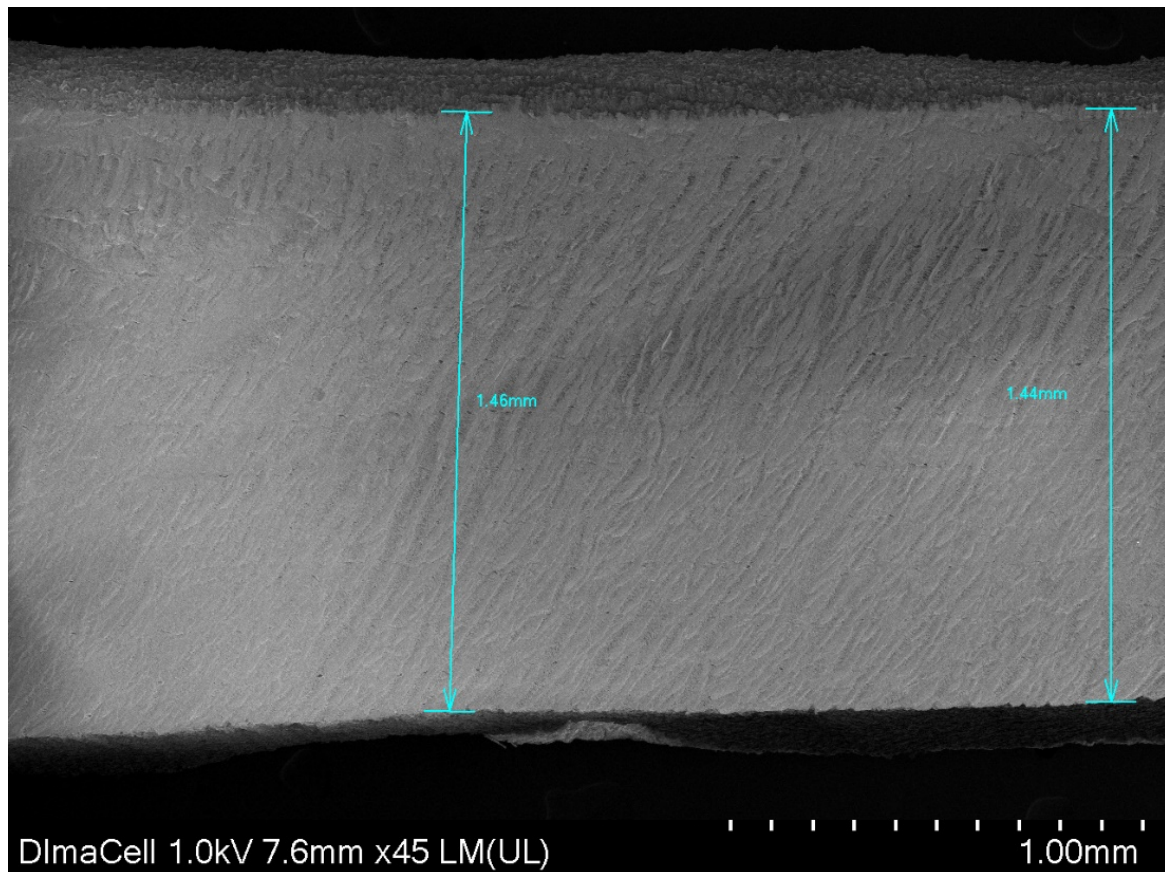


Figure 27. LiEDA sample sliced and observed by SEM imaging. Untreated area width is indicated by the blue arrows.

#### II.3.4. Drop Shape Analysis

Drop shape analysis was carried out to evaluate the impact of the chemical treatments on the physical properties of the material. The contact angle and the surface energy are interesting characteristic properties to give information on the hydrophilicity of the material. ePTFE presents high hydrophobicity, and this analysis will show how it is modified by the different treatments. Several methods exist to calculate the surface energy based on the measured contact angles. We present here the Fowkes' theory that we used in our study.

### Fowkes' theory<sup>214</sup> method to determine surface energy

Contact angles obtained as described before are used to calculate the total surface energy ( $\sigma_s$ ), by the determination of its polar ( $\sigma_s^P$ ) and dispersive ( $\sigma_s^D$ ) terms according to the Fowkes' theory.<sup>257</sup> Fowkes' theory is the most widely used method to determine surface energy, as it uses only two liquids, contrary to Owens/Wendt or Owens Wendt Rabel and Kaelbel theory which requires multiple liquids at choice.

Fowkes's theory is based on a two-component model, which supposes that the surface energy is the result of the addition of its dispersive and polar component.

The method and the theory presented here are extracted from the well-described KRUSS technical note TN306e. Fowkes' theory is based on three fundamental equations that describe interactions between solids and liquids. First, Young's equation:

$$\sigma_s = \sigma_{SL} + \sigma_L \cos\theta \quad \text{EQUATION 7}$$

Wherein  $\sigma_L$  = overall surface tension of the wetting liquid,  $\sigma_s$  = overall surface energy of the solid,  $\sigma_{SL}$  = the interfacial tension between the solid and the liquid, and  $\theta$  is the contact angle between the liquid and the solid. From Dupre's definition of adhesion energy:

$$I_{SL} = \sigma_s + \sigma_L - \sigma_{SL} \quad \text{EQUATION 8}$$

wherein:  $I_{SL}$  = energy of adhesion per unit area between a liquid and a solid surface.

And Fowkes' theory that assumes that the adhesive energy between a solid and a liquid can be interpreted as interactions between the dispersive components of the two phases and interactions between the non-dispersive (polar) components of the two phases.

$$I_{SL} = 2 [ (\sigma_L^D)^{1/2} (\sigma_s^D)^{1/2} + (\sigma_L^P)^{1/2} (\sigma_s^P)^{1/2} ] \quad \text{EQUATION 9}$$

Wherein:  $\sigma_L^D$  = dispersive component of the surface tension of the wetting liquid,  $\sigma_L^P$  = polar component of the surface tension of the wetting liquid,  $\sigma_s^D$  = dispersive component of the surface energy of the solid, and  $\sigma_s^P$  = polar component of the surface energy of the solid.

The combination of these equations leads to the primary equation of the Fowkes' surface energy theory:

$$(\sigma_L^D)^{1/2} (\sigma_s^D)^{1/2} + (\sigma_L^P)^{1/2} (\sigma_s^P)^{1/2} = \frac{\sigma_L (\cos\theta + 1)}{2} \quad \text{EQUATION 10}$$

From this latter equation, a two-step determination is used. First, the component  $\sigma_s^D$  is determined with non-polar solvent, the one most used and used here is diiodomethane. It is assumed that  $\sigma_L^P = 0$  and  $\sigma_L = \sigma_L^D$ . The Equation 10 becomes:

$$\sigma_s^D = \frac{\sigma_L (\cos\theta + 1)^2}{4} \quad \text{EQUATION 11}$$

with  $\sigma_L$  value taken from the Kruss DSA database and  $\theta$  obtained by experiment.

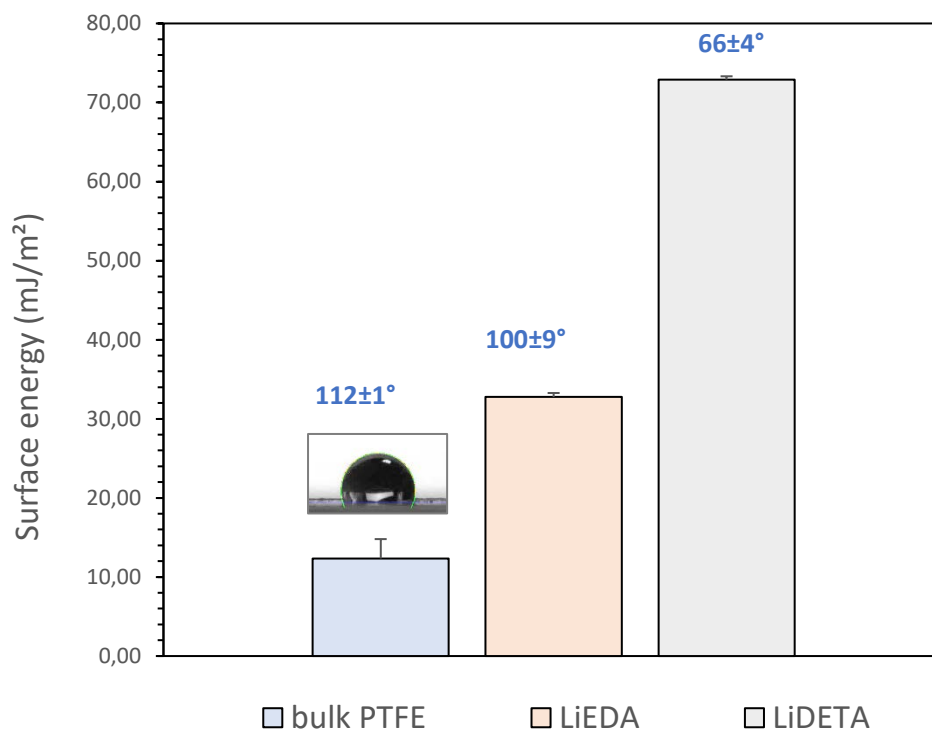
The second step defines the polar component  $\sigma_S^P$  using water as testing liquid. The Equation 10 becomes:

$$\sigma_S^P = \frac{\sigma_L^2 (\cos\theta + 1)^2 - 4 \sigma_L^D \sigma_S^D}{4 \sigma_L^P} \quad \text{EQUATION 12}$$

with  $\sigma_L$ ,  $\sigma_L^D$ ,  $\sigma_L^P$  are know from Kruss DSA database and  $\sigma_S^D$  calculated before.  $\theta$  is obtained experimentally.

## Results and discussion

The surface energies obtained in Figure 28 describes the change of the bulk material into less hydrophobic surfaces regarding the changes caused by LiEDA, and hydrophilic caused by LiDETA. Indeed, bulk PTFE sees its surface energy increased by 3 for LiEDA and 6 for LiDETA.



	Surface energy (mJ/cm <sup>2</sup> )	Corresponding error bar value
bulk PTFE	12,34	2,45
LiEDA	32,76	0,51
LiDETA	72,90	0,42

Figure 28. Surface free energy and corresponding contact angles (in blue), the error bars are calculated with propagation of uncertainty using first order Taylor expansion applied to Fowkes' theory formulas.<sup>214</sup>

Some studies of PTFE plasma treatments found that the elimination of fluorine atoms and addition of oxygen or polar groups were directly linked to higher hydrophilicity and thus higher surface energy. Interestingly, Chen *et al.*<sup>258</sup> found that plasma treatments induce a lower PTFE/water contact angle that does not go below 90°, the limit that distinguishes between a hydrophilic and a hydrophobic material. Kolska *et al.* found that plasma exposition time was decreasing the contact angle (Figure 29 A).<sup>259</sup> The amount of polar groups and oxygen on the surface with increasing exposure time would be, according to the authors, an obvious explanation.<sup>260-261</sup> However, as shown in Figure 29 B, contact angle surprisingly increases with aging time. They supposed first that molecular reorganization and interaction with ambient oxygen while material is aging would explain this phenomenon, but this hypothesis is not consistent with the increase of contact angle.<sup>262-263</sup> Then, the authors observed that the surface roughness increases with time, probably due to molecular segments rearrangements, which might be the cause of the changes of contact angle with aging.

As our process also involves strong conditions as a lithium alkylamide is formed and reacts with the polymer, and surface roughness is observed, we could draw a parallel between the two techniques. Surely, our method does not enable to obtain low contact angle such as 10° or 20°. But the remaining high contact angle might be explained by the increase of surface roughness among time as presented. The defluorination ratios obtained by XPS can explain such a difference of hydrophobicity, LiDETA material with a C:F ration of 7:1, whereas LiEDA presents a ratio of 1:1. The difference between EDA and DETA chemical chain structures might also be important as DETA contains three amine groups against two for EDA, which increases the number of polar groups grafted on the surface.

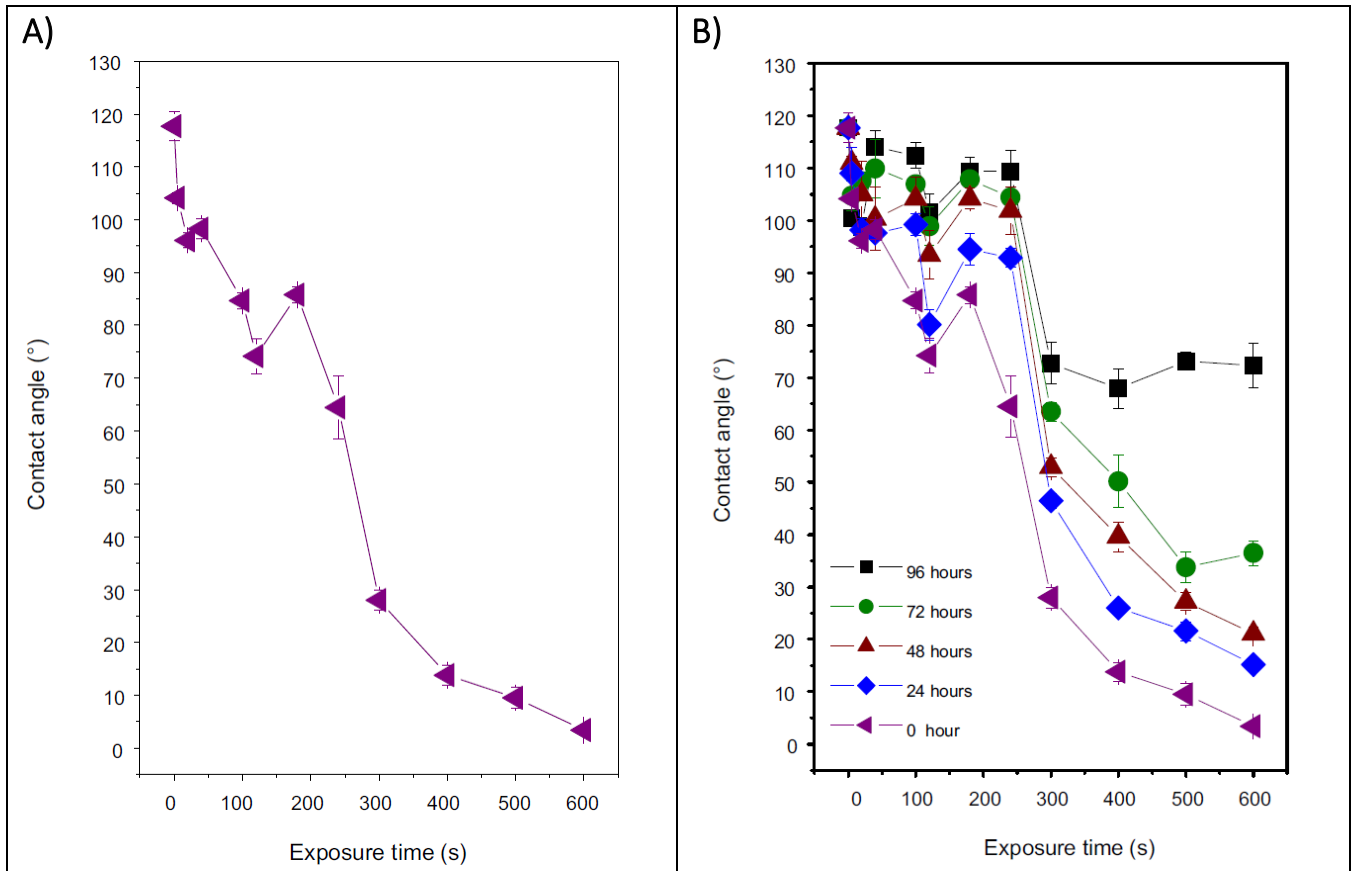


Figure 29. A) Dependence of the PTFE contact angle on the exposure time to Ar plasma. The measurement was accomplished 5 min after the exposure. B) Dependence of the contact angle on the plasma exposure time and on the aging time. The measurements were accomplished immediately after the treatment (0 h) and then after 24, 48, 72 and 96 h aging times.<sup>259</sup>

### II.3.5. Instrumented Indentation

#### Presentation of Oliver and Pharr method

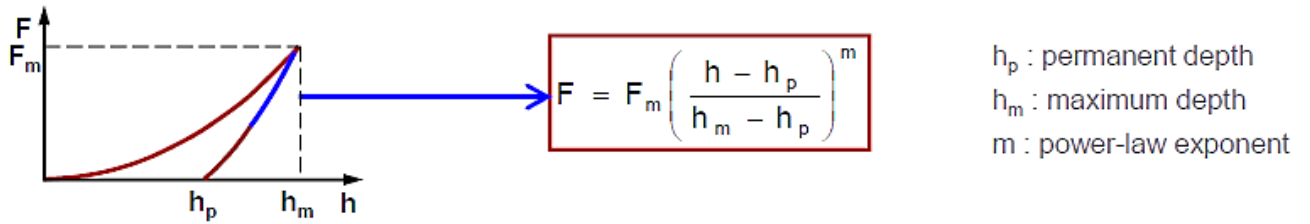
To measure elastic modulus, a nanoindenter is used. Indentation consists in applying force with a tip onto a surface during a load-unload cycle. The applied force and the indentation depth are measured by the instrument and the data obtained is used by the software to calculate hardness and elastic modulus, also called indentation modulus. Force-displacement curve is used for their calculation.

To calculate the indentation modulus EIT, the reduced modulus  $E_r$  is first calculated.

$$E_r = \frac{\sqrt{\pi}}{2\beta} \frac{S}{\sqrt{A_p}} \text{ Equation 13}$$

$\beta$  is a constant which the value depends on the geometry of the tip. For a Berkovich tip, a triangular based pyramid geometry, this value is  $\beta=1.034$ .

In Oliver&Pharr method,<sup>264</sup> the contact stiffness,  $S$ , is related to the tangent of the unloading curve. The fitting of the unloading portion of the force versus indentation depth data enable to obtain the power-law relation, giving the fitting parameters  $h_p$ ,  $h_m$  and  $m$ .

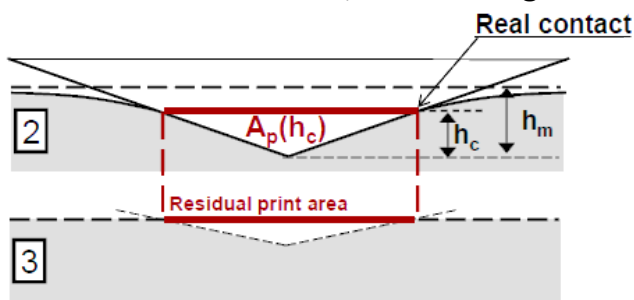


Equation 14

Which leads to the stiffness formulation by differentiation of this equation and evaluating at the maximum indentation depth:

$$S = \left( \frac{dF}{dh} \right)_{h=h_m} = m \cdot F_m \cdot (h_m - h_p)^{-1} \text{ Equation 15}$$

The projected contact area  $A_p$ , is determined from the indentation depth. It is considered as a good approximation to the projected residual print area.  $h_c$  is then the real contact depth, different from  $h_m$ , the depth between the tip and the surface of the material, considering a sink-in effect on both sides of the tip.



$$A_p = C_0 \cdot h_c^2 \text{ Equation 16}$$

with  $C_0=24.5$  for a Berkovich tip, and  $h_c$  calculated as follow:

$$h_c = h_m - \varepsilon \frac{F_m}{S} \text{ Equation 17}$$



The geometric constant  $\epsilon$  is obtained from the Woigard & Co. table, which gives the value of  $\epsilon$  according to the  $m$  value.

Finally, we obtain the elastic modulus  $E_{IT}$  (Equation 18) using reduced modulus of the sample  $E_r$ , the modulus of the indenter  $E_i$ , the Poisson's ratio of the sample ( $\nu_s$ ) and the indenter tip ( $\nu_i$ ).

$$E_{IT} = \frac{(1 - \nu_s^2)}{\frac{1}{E_r} - \frac{(1 - \nu_i^2)}{E_i}}$$

Equation 18

### Results and discussion

Mechanical testing of the surface using nanoindentation device provides relevant information regarding the core and the surface of the material. Young's modulus measurements using nanoindentation testing is known to create significant challenges in polymeric materials.<sup>265</sup> Indeed, the analysis of depth sensing indentation (DSI) testing is usually based on elastic model, which leads to uncertainties with polymers such as PTFE or ePTFE which present viscoelasticity.<sup>266</sup> The use of conventional nanoindentation methods as performed here are supposed to be limited to linear, isotropic and homogeneous materials to enable any calculus of the modulus using the unloading curve. These hypotheses, when could be applied on PTFE with approximations, are clearly not matching with ePTFE. But, we use Oliver and Pharr method as a first-order quantitative comparison, as it was done in previous work.<sup>267</sup>

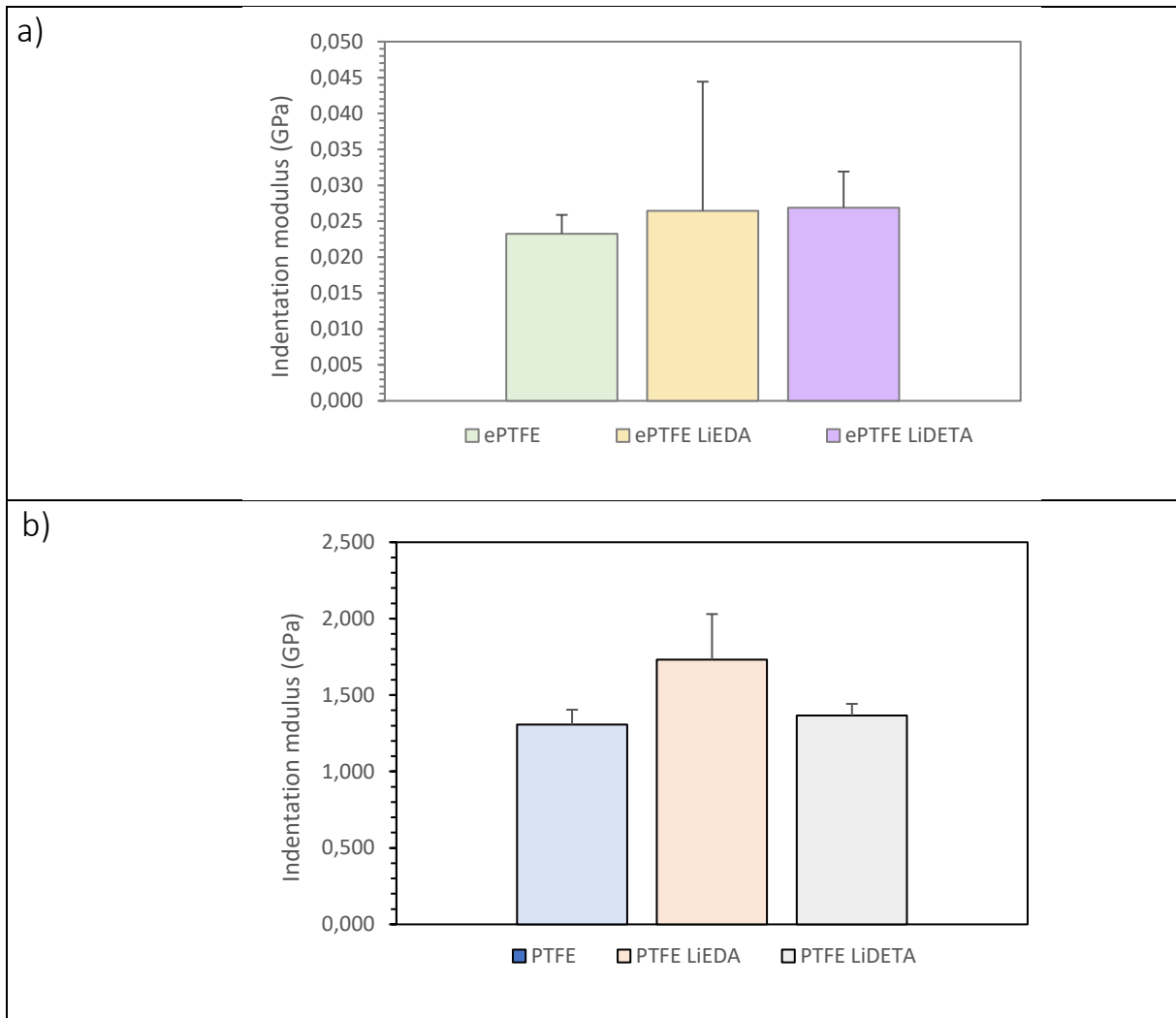


Figure 30. Indentation modulus of unmodified ePTFE (a) or PTFE (b) and modified by LiEDA and LiDETA. The error bars represent confidence interval with probability of 95 %.

Moreover, the Oliver and Pharr method can make it difficult to determine the Young's modulus of viscoelastic materials. Indeed, the beginning of the unloading curve presents a "nose", which makes a linear fitting impossible. PTFE and ePTFE present this kind of behavior during indentation measurement. However, including a holding period at the maximum load is a solution often used to avoid this problem. Even if it was found that the loading time has a significant influence by increasing modulus and hardness error, it was also determined that above 45 seconds of hold, this error became negligible.<sup>268</sup> The tests made here revealed that a holding period of 120 s enabled to obtain a linear-fitting unloading curve for both PTFE and ePTFE.

One feature of ePTFE is its negative Poisson's ratio that is explained by its auxetic structure. Indeed, Poisson's ratio for this kind of material changes according to the strain applied<sup>1</sup>. In nanoindentation, as the vertical strain (calculated as maximal displacement, % of thickness) induced is very low (below

1 %), the Poisson's ratio of the ePTFE is included between -0.5 and 0. The indentation device, when implemented with a negative Poisson's ratio, replaces it by default with 0.001. As this case of figure is not expected in Oliver and Pharr method, a Poisson's ratio as close as 0 is the most accurate way to consider the specificity of this material. PTFE, on the contrary, has a positive Poisson's ratio. The approximation in the calculation of Young's modulus should be considerably reduced. Ten measurements of indentation modulus were made on LiEDA, LiDETA and unmodified ePTFE. While ePTFE nanoindentation results show no differences between modified and unmodified material, PTFE shows significative differences between LiEDA and bulk material.

Indeed, no significant differences are noted between modified and unmodified ePTFE surfaces, with mean modules between 0.023 and 0.27GPa (Figure 30a). LiEDA presents however a wider confidential interval.

PTFE LiEDA appears to present a stiffer surface, with a modulus of  $1.73 \pm 0.30$  GPa, compared to bulk PTFE with a modulus of  $1.31 \pm 0.10$  GPa (Figure 30b). This latter is higher than the tensile Young's modulus we can find in the literature (0.4 GPa). This phenomenon and value of indentation modulus were already described before<sup>269</sup> which enable comparison between the two types of PTFE we study here. PTFE LiDETA shows no significative differences with the bulk material, with a modulus of  $1.37 \pm 0.08$  GPa.

Thus, we could suppose that the particularity of the auxetic structure weighs mostly in the mechanical response of the ePTFE surface, with no clue to report on the alteration of the mechanical properties of the surface. PTFE presents the same chemistry but in bulk form, with a more classic behavior towards indentation tests. Contrary to Fluoroetch etchant, LiEDA PTFE presents a higher modulus than bulk PTFE, which could be explained by the grafting of the aminated chains, creating hydrogen bonds and disorganized the polymer chains by defluorination. These modifications increase the stiffness of the material at a macroscale. LiDETA does not appear to have such a radical effect on the mechanical behavior of the PTFE surface, since no significant differences were observed. Thus, LiDETA seems to be a milder etchant than LiEDA in term of mechanical properties.

To conclude the second part of this manuscript, the characterizations presented indicate that the LiEDA treatment induces a more important structural modification of the ePTFE surface, increasing its stiffness and roughness. They also indicate that LiDETA modifies far differently the material surface, as it changes from hydrophobic to hydrophilic; but its roughness and stiffness are not impacted. Thus, according to the alkylamidure reacting with the fluorinated polymer, the properties of the surface will be different. This can be linked to the

defluorination and amination that occur with both treatment but with different ratios, conduction to different properties. An additional characterization with thermogravimetric analysis could complete the chemical surface description indicating the physisorbed chemicals on the surface. We will see in the next part if this difference has an impact on the cytotoxicity and the antibacterial property of the material. This next part will firstly focus on the functionalization of the treated material, enabled by the presence of the amine groups formed, and the second part will present the cytotoxicity and antibacterial evaluation of the materials obtained.

### III. Additional functionalization with bioactive molecules and efficiency evaluation.

#### III.1. Selection of antibacterial molecules

Multiple molecules were selected to make the modified ePTFE surface antibacterial. Bactericidal molecules are selected according to their ability to be grafted with glutaraldehyde cross-linking, biocompatibility, and effectiveness.

##### III.1.1. Chitosan

Chitosan (CHI) is a linear polysaccharide composed of randomly distributed  $\beta$ -(1 $\rightarrow$ 4)-linked D-glucosamine (at least 60 % of deacetylated unit) and N-acetyl-D-glucosamine (Figure 31). It is a polymer derived from chitin, a macromolecule found in fungi or exoskeleton of arthropods. Its antibacterial properties were investigated quite early for medical purposes. Pharmacological and clinical use of chitosan in the past 20 years were possible because of its safety, biocompatibility, and biodegradability.<sup>270-273</sup>

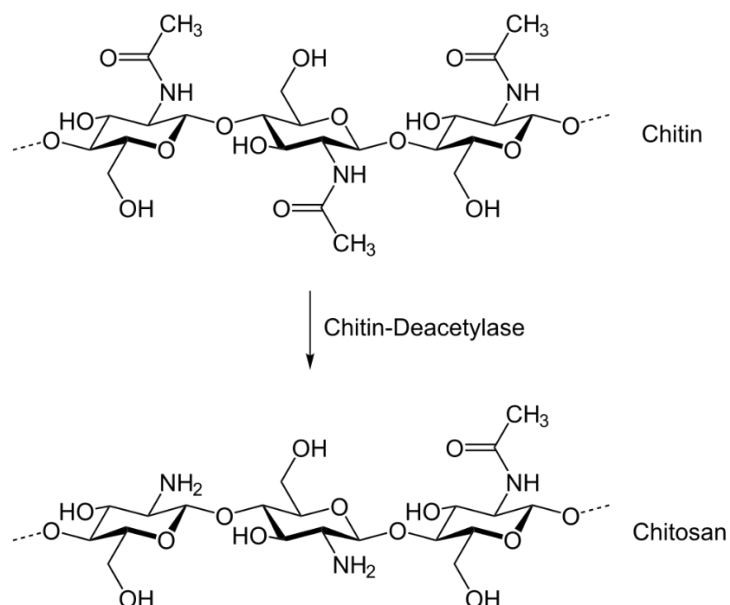


Figure 31. Chitosan synthesis through chitin deacetylation.<sup>274</sup>

Chitosan antibacterial mechanisms are still not fully understood. The most described one considers that the positive charges from amine groups bind to the negatively charged bacterial cell wall, which alters the permeability of the membrane in bacteria (Figure 32). DNA is then attached to the chitosan molecules, which leads to inhibition of DNA replication and thus bacterial death.<sup>275-276</sup> A higher intracellular material leakage is observed in gram-negative compared to gram-positive bacteria, which does not present the same dramatic morphological changes.<sup>277-278</sup>

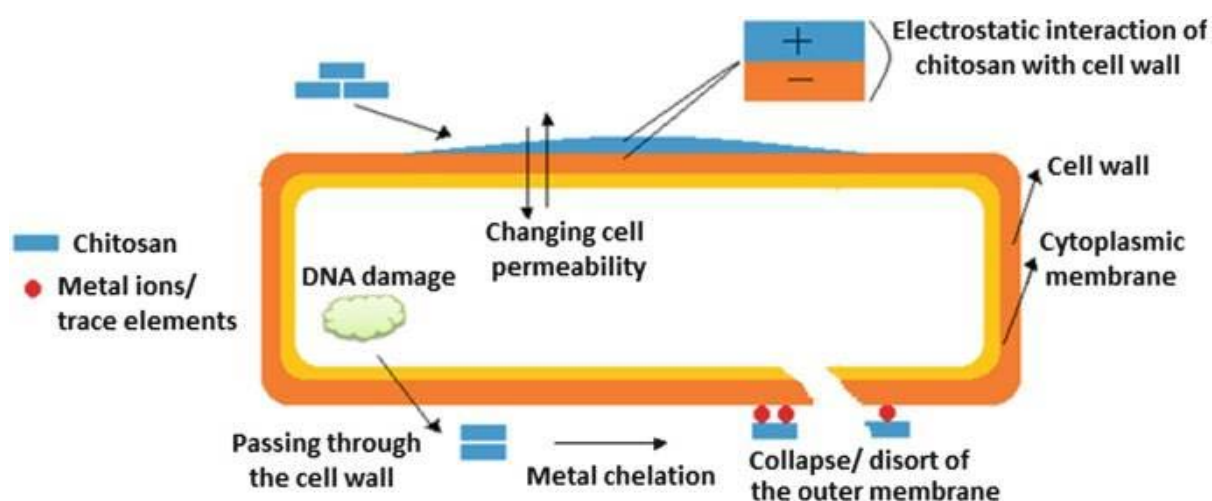


Figure 32. Schematic representation of antimicrobial mechanisms of chitosan and its derivatives.<sup>276</sup>

Indeed, AFM images on chitosan-treated bacteria showed these qualitative results. In Figure 33 we can easily observe cells' shape being drastically altered on *E. coli*, while *S. aureus* does not present these obvious changes. However, quantitative results on viable cell number showed significant reduction of CFU in both *E. coli* and *S. aureus* strains.<sup>278</sup>

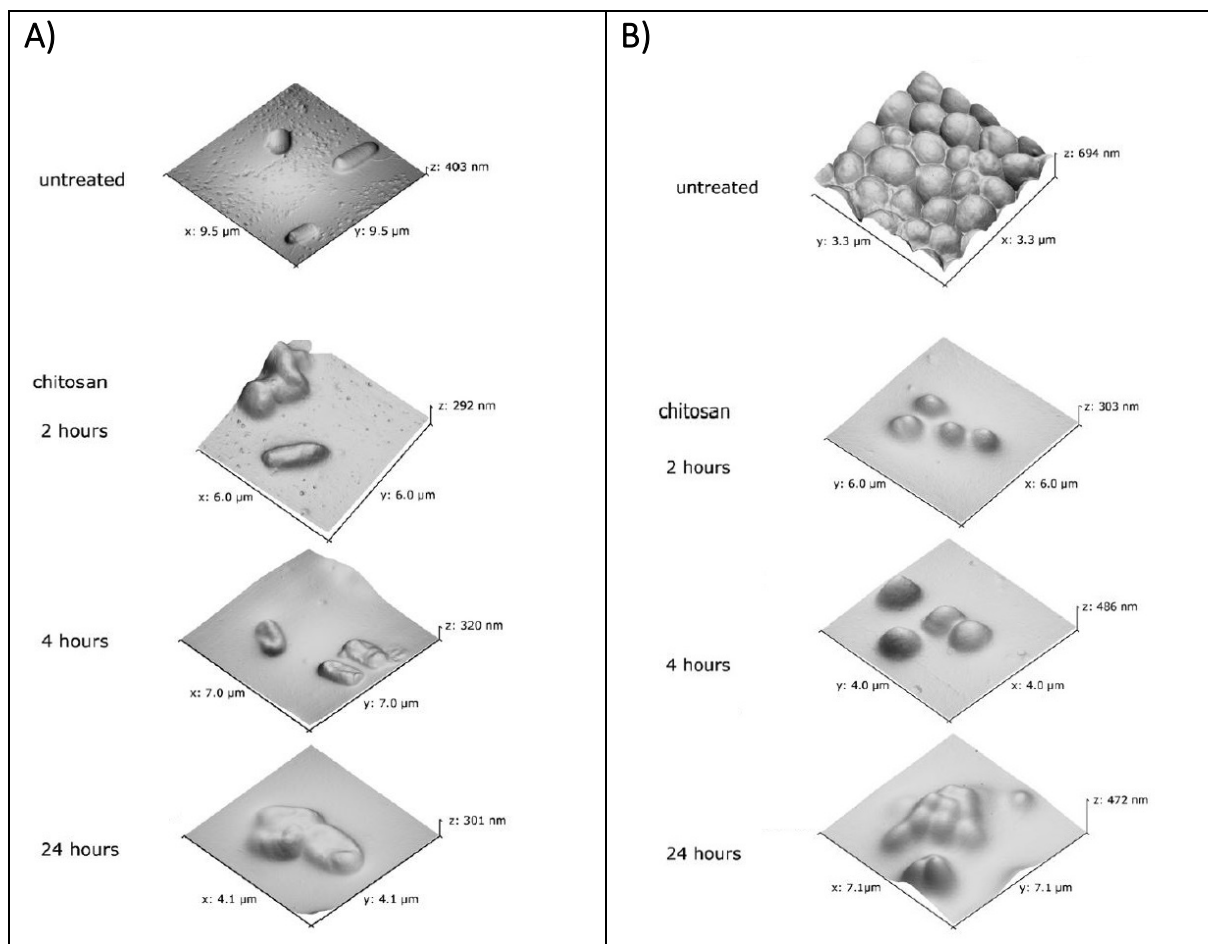


Figure 33. AFM images of *S. aureus* (A) and *E. coli* (B) before and after treatment with chitosan. The top image is from untreated bacteria, and below treatment times are as indicated in the image. Arrows show specific cells referred to in the text.<sup>278</sup>

### III.1.2. Polyethylenimine

Polyethylenimine (PEI) is a cationic polymer that can be branched (B-PEI) or linear (L-PEI). Non-cytotoxicity is not an inherent property of PEI. Several works demonstrate biocompatibility of the molecule, such as those from Vancha et al. They published about the effective attachment factor for weakly anchoring cell line and primary cells.<sup>279</sup> Other works found an improvement in metabolic activity of human neuroblastoma cell line.<sup>280</sup> PEI can cause apoptosis and cytotoxicity.<sup>281-282</sup> This cytotoxicity can reach a quite acceptable low threshold as it increases with the rise of molecular weight (Mw) and concentration.<sup>281</sup> Ultra-thin deposition with low concentration solution (1 mg/mL) is advised to reduce cytotoxicity to an acceptable level.<sup>283</sup>

<sup>3</sup> Part III. is highly inspired from our research article “Development of implantable antibacterial ePTFE prostheses for soft tissues.”

The structure of PEI seems indeed to change its cytotoxicity: B-PEI appeared to be less toxic than linear, with a low molecular weight as well.<sup>284</sup> This was evaluated by the use of solutions with increased concentration of B-PEI or L-PEI (Figure 34). Six PEIs with 3 different values of average molar mass ( $M_n$ ) were tested. In Figure 34,  $M_n = 470, 1100$  and  $12000$  g/mol. In this graph we can notice that hemolysis occurs only when solutions of L-PEI is used.

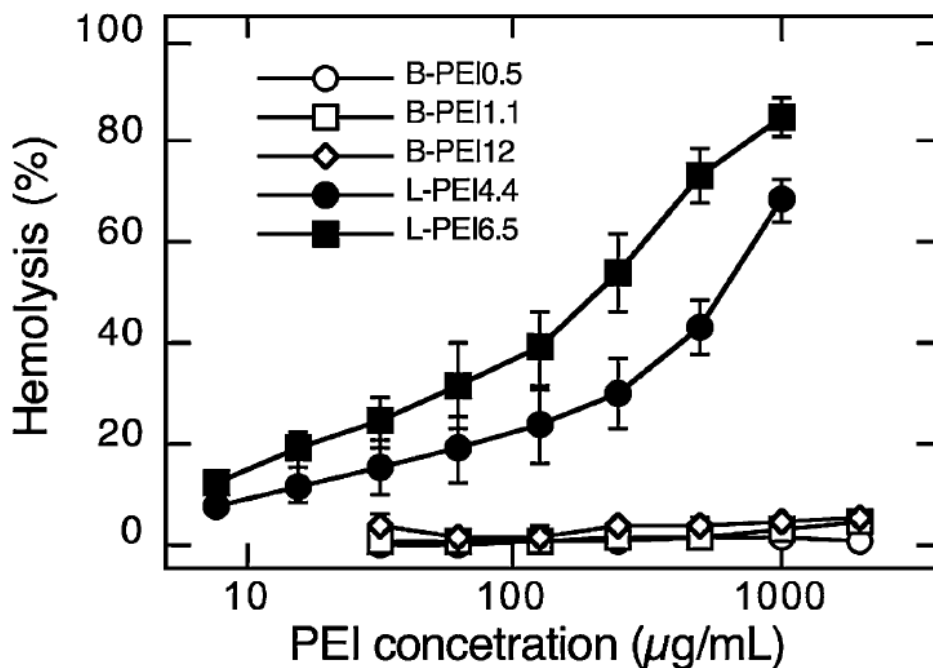


Figure 34. Hemolysis induced by PEIs. Each data point represents PEIs as antimicrobial agents with selective activity (Gibney 2012)

Another study using higher molecular weights, between  $800$  and  $25\,000$  g/mol, but also higher concentrations ( $0.5$  to  $1\,000$  mg/ml), showed that the branched PEIs was more toxic than the linear ones.<sup>282</sup>

Branched and linear PEI with low molecular weight seem to have both an antibacterial effect on *S. aureus* and *E.coli*,<sup>284</sup> while others conclude that only linear PEI is effective against *S. aureus*, *Pseudomonas aeruginosa*, and *Candida albicans*.<sup>285-286</sup> However, the development of high molecular PEI-based materials (with Mw from  $25$  to  $750\text{kg/mol}$ ) for biomedical purposes can be found in case of combination with other molecules.<sup>287-290</sup> Though, no cytotoxicity assays were carried out in these studies.



The antibacterial mechanism of PEI also depends on its molecular weight. A recent study focused on developing B-PEI-covered silver nanoparticles (NP) with different Mw (Table 2) against Gram-negative bacteria *A. baumannii*. Their study on fluorescein interaction with bacteria and NP led them to elaborate a mechanism theory of the interaction between PEI and bacteria wall according to molecular weight.<sup>291</sup>

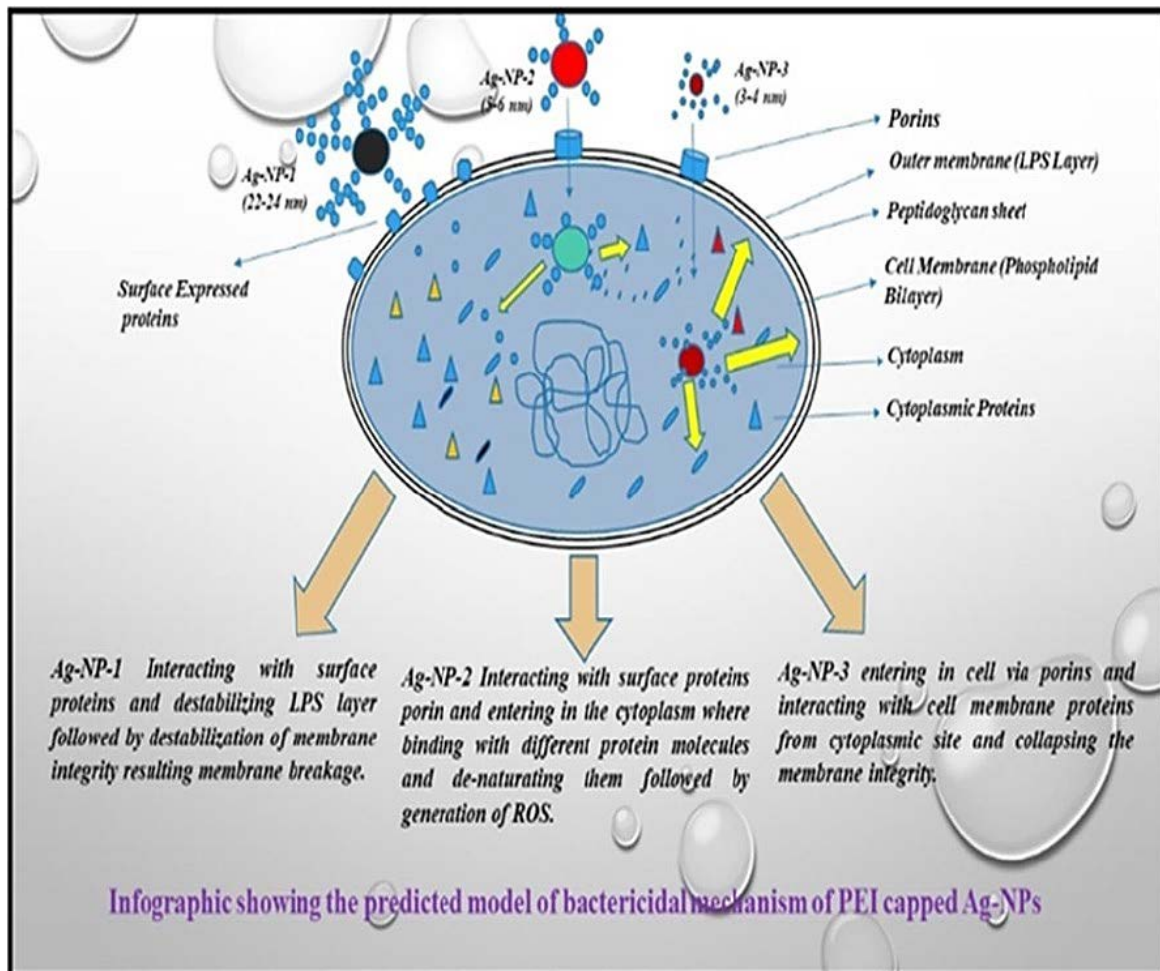


Figure 35. Model of the possible bactericidal mechanism of Ag-NP-1, Ag-NP-2, and Ag-NP-3 against *A. baumannii*.<sup>291</sup>

Table 2. Denomination and structure of silver nanoparticle covered with different PEIs.

Name	Structure	Molecular weight (g/mol)
Ag-NP-1	Branched	750 000
Ag-NP-2	Linear	1300
Ag-NP-3	Branched	60 000

As shown in Figure 35 the high molecular weight PEI covering the NP1 would interact with the surface proteins and destabilize the outer membrane of the bacteria, leading to membrane breakage. The two others would enter in the bacteria cytoplasm through the porins of the membrane. Porins are membrane proteins present on bacterial membranes. They allow passive diffusion of small molecules.

### III.1.3. Polyvinyl pyrrolidone iodine complex

Polyvinylpyrrolidone-iodine (PVP), also known as povidone iodine, was studied early as an antimicrobial agent and an alternative for antibiotics. It is widely known as a common antiseptic but also considered recently in biomaterial engineering to develop new antimicrobial materials.

An early study evaluating inhibitory and bactericidal properties of PVP showed proof of efficiency on 5 problematic bacteria species.<sup>292</sup> These tests were carried out on suspensions of bacteria in saline solution. The results show that a PVP concentration of 5 mg/L enables the inhibition of all the strains of every species and a bactericidal effect on most of them.

Species	No. of strains tested	No. of strains inhibited by povidone iodine (mg/l)		No. of strains killed by povidone iodine (mg/l)		
		2.5	5	2.5	5	10
<i>Staphylococcus aureus</i>	40	32	40	14	40	
<i>Escherichia coli</i>	34		34	33	34	
<i>Klebsiella aerogenes</i>	22		22	18	22	
<i>Proteus vulgaris</i>	10		10	10		
<i>Pseudomonas aeruginosa</i>	36		36	31	36	

Figure 36. Minimum inhibitory and bactericidal concentrations of povidone.<sup>270</sup>

PVP is a water-soluble iodophor, also named iodine-releasing agent, which means it is a complex between iodine and polyvinylpyrrolidone, a solubilizing

polymer carrier. A dynamic equilibrium is installed in aqueous solution, where the active bactericidal agent, iodine ( $I_2$ ) is free and coexists with PVP complex. The antibacterial function resides in the ability of small molecules such as iodine to rapidly penetrate microorganisms, oxidize their key proteins, nucleotides and fatty acids which can lead to the cell's death.<sup>293</sup>

Innovative strategies have been using this molecule to develop antibacterial materials, such as bioelastomeric composite made of polydimethylsiloxane and starch. PVP is incorporated in the composite without any covalent bonding. The authors found out that the iodine was complexed with the starch once immersed in aqueous solution. The povidone iodine was gradually released in the medium for a month. This new composite presents low cytotoxicity and a sustained antibacterial effect against *E. coli* up to a month.<sup>294</sup>

Covalent photografting of PVP was carried out on polypropylene under UV light. Efficient antibacterial properties against *E. coli*, *S. aureus* and *C. albicans* were proven, as 99.9 % of the initial concentration of viable bacteria decreased within 5 hours.<sup>295</sup>

PVP is a common antiseptic used every day. However, clinical studies have reported over absorption of iodine in case of newborns in intensive care. A study reported severe iodine overloading of the thyroid after multiple surgery procedures, from 20 to 40 in 5 days, that required the use of iodine alcohol as antimicrobial agent.<sup>296</sup> Another study, including healthy newborns with povidone iodine application for umbilical cord healing, reported elevated plasma iodine levels with no alteration of thyroid function.<sup>297</sup> The skin permeability of newborns may be the cause of the diffusion of iodine, in opposition to adults. PVP in case of early aged patients is advised to be used with precaution.

These three antimicrobial agents will be used in the following part to functionalize the ePTFE samples treated by LiEDA or LiDETA.

## III.2. Functionalization and characterizations

### III.2.1. Materials and methods

After a first treatment with LiEDA or LiDETA, PTFE and ePTFE samples were functionalized according to the protocols detailed in the annex A2 . CHI, PEI (Mn ~60 000, average Mw ~750 000 by, 50 wt. % in H<sub>2</sub>O), PVP, glutaraldehyde (50 % wt % in H<sub>2</sub>O) and absolute ethanol were purchased from Sigma-Aldrich (Saint Quentin Fallavier, France). The spectroscopy analysis was made using the FR/IR-4X from Jasco to obtain IR-ATR spectra. The SEM used for imaging was the SU8230 from Hitachi.

### III.2.1. Reaction of functionalization

The functionalizations with PEI and CHI were carried out using glutaraldehyde cross-linker. This is a common technique,<sup>298-299</sup> using the reductive power of glutaraldehyde to proceed to an addition with amine groups such as those obtained on aminated ePTFE modified with LiEDA or LiDETA. As a symmetric compound, glutaraldehyde can react with an another aminated molecule such as PEI, or CHI present in the medium. At the end, we should obtain an ePTFE grafted with CHI or PEI. The reactions involved and the hypothetical product obtained are presented in Figure 37 with the example of CHI. The functionalization with a PVP solution by immersion relies on the formation of hydrogen bonds between the primary amines on the surface of the modified material and the polar groups on PVP such as the carbonyl groups.

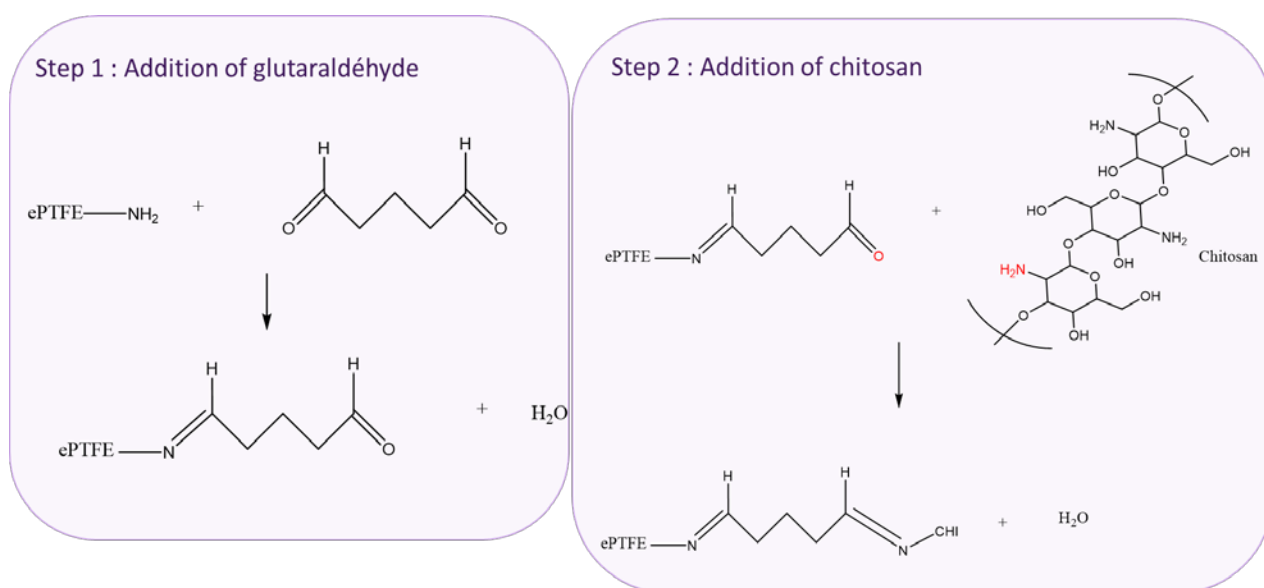


Figure 37. Grafting of CHI on aminated ePTFE, two steps with two reactions of addition and condensation.

To evaluate if this hypothetical reaction occurs, IR-ATR spectroscopy was carried out and will be presented in the following part; after observing the impact of these modifications on the morphology of the ePTFE samples using SEM imaging.

### III.2.2. SEM imaging

ePTFE is a complex structure composed of randomly distributed nodes connected with fibrils, noticeable on Figure 38. SEM imaging of bare ePTFE (Figure 38) and functionalized samples presented in annex A3, reports noticeable structure modifications of the surface after treatment. Indeed, the fibrils seem to break at some points, mostly at their attachment site to a node. Other described treatments lead to fibrils breaking in ePTFE structure, such as argon or oxygen plasma at high radio-frequency (RF) power.<sup>300-301</sup> Porosity with a web-like appearance as described by the authors can also be noticed in the LiEDA treated samples batch.

In the grafted samples by glutaraldehyde, the fibrils seem to be particularly extended, and the nodes bundled. We measured the internodal distances in each picture, considering two different sizes. We made a distinction between the long distance, characterized by a tangle of fibrils between two nodes and the short distance, characterized by nodes directly linked with the same fibrils. This

characterization enables to have less scattered data. An example of the two different sizes is shown in the Figure 38 with the orange and white arrows. This structure is particularly noticeable in ePTFE alone and is extrapolated for the treated samples. Many authors have measured internodal distances of ePTFE mostly to study cell adhesion behavior, but nothing is mentioned in the literature about the modification of internodal distances by chemical treatments.

Distances were measured as a mean of 10 measures each and reported in Table 3, distinguishing the long and short internodal distances. For long internodal distance, only the treatment with LiEDA leads to a significantly longer distance than bare ePTFE. However, this is not the case for the additionally functionalized samples, LiEDA CHI, PEI and PVP. This might be due to intermolecular crosslinking with glutaraldehyde for CHI and PEI that changes the structure and involves a wider variance, notably with the breakage of the fibrils. PVP functionalization also modifies the structure, which presents more tightened nodes and broken fibrils. LiDETA sample presents no significant differences either for long internodal distance in spite of the visible lengthen of the fibrils, and their breakage. This could be linked to the previous result that the resulting structure from LiDETA treatment does not involve an alteration of the mechanical properties. The short internodal distance is however significantly lower than ePTFE, which could reinforce the structure.

Table 3. Mean internodal distances calculated with Gwyddion software. Confidence interval with probability of 95 % (IC95) corresponds to each value.

nodal distances ( $\mu\text{m}$ )	ePTFE	EDA	DETA	EDA PVP	DETA PVP	EDA CHI	DETA CHI	EDA PEI	DETA PEI
long	21,83	32,61	16,80	26,03	19,34	17,19	23,83	27,20	19,29
short	10,72	9,79	6,79	10,30	8,98	4,82	7,67	12,35	8,65
IC95	ePTFE	EDA	DETA	EDA PVP	DETA PVP	EDA CHI	DETA CHI	EDA PEI	DETA PEI
long	4,19	2,61	0,98	4,60	1,52	3,00	2,84	3,86	4,59
short	3,07	2,93	1,67	2,87	2,15	0,77	1,13	2,48	1,44

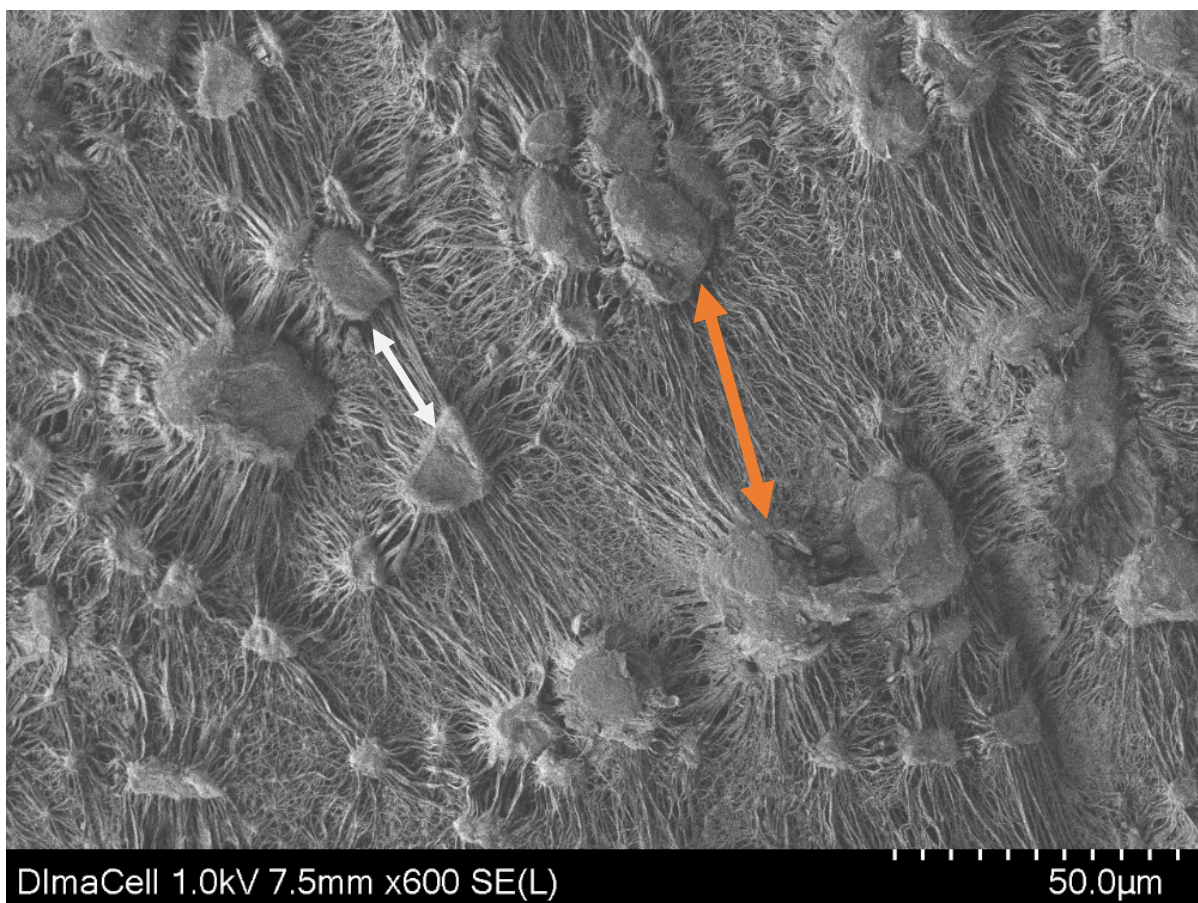


Figure 38. SEM micrograph of ePTFE. White arrow: short distance, orange arrow: long distance.

### III.2.3. IR-ATR Spectral characterization

IR-ATR analysis was carried out to identify the chemical functional groups on the material resulting from the functionalization. This analysis will enable to validate or not the hypothetical reactions of functionalization we presented in Figure 37. At first sight, the spectra seem to be quite identical from one to another. We precisely analyzed each spectrum by comparing it to the spectrum of the molecule alone, found in the literature. Most bands overlap with the ones present on LiEDA and LiDETA samples' spectra.

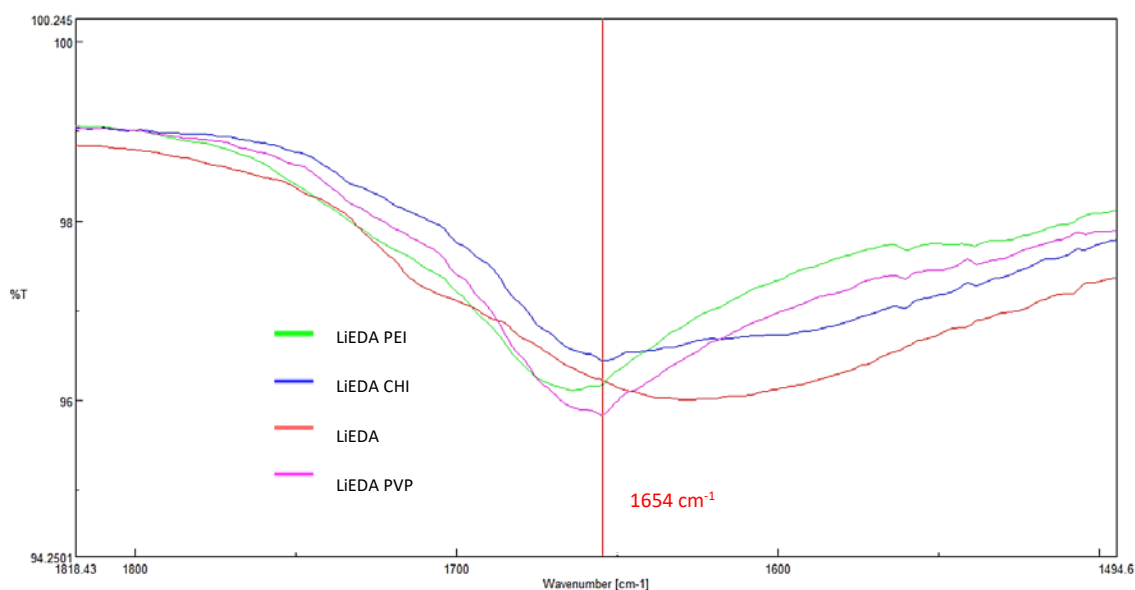
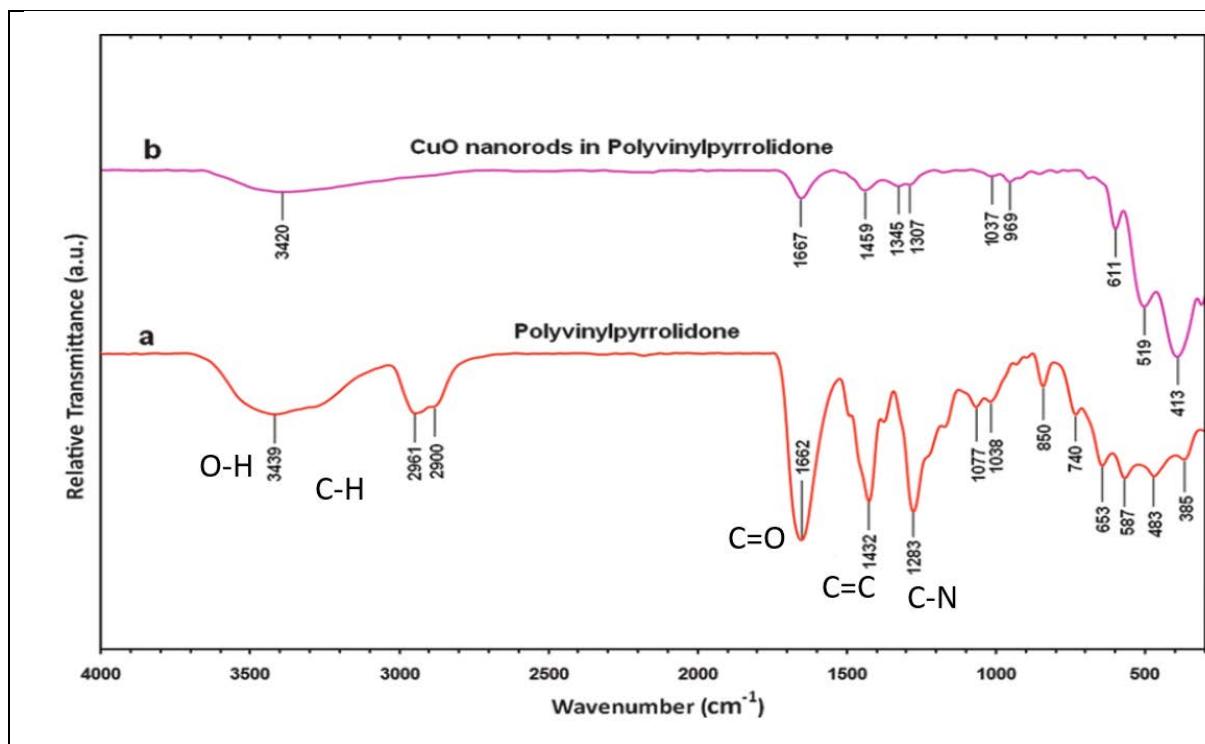


Figure 39. IR-ATR spectra obtained on ePTFE treated samples with LiEDA PEI, LiEDA CHI, LiEDA and LiEDA PVP. A weak band at  $1654\text{ cm}^{-1}$  is labeled.

Firstly, we can compare PEI, PVP or CHI functionalized samples with LiEDA and LiDETA samples alone. Interestingly, a weak band at  $1654\text{ cm}^{-1}$  seems to be present in every functionalized sample, which may correspond to an imine vibration that is present after the attachment of glutaraldehyde and the following grafting of PEI or CHI molecule. PVP presents an imine as one of its mesomere forms.

The PVP presents characteristic peaks that slightly varies from one article to another. We can take as a comparison point the ones at  $3439$ ,  $2961$ ,  $2900$ ,  $1662$ ,  $1432$  and  $1283\text{ cm}^{-1}$ <sup>302</sup> corresponding respectively to O-H<sup>303</sup>, C-H twice, C=O, C=C and C-N (Figure 40). Only peaks corresponding to O-H, C=O and C=C could be attributed as a correspondence between the experimental spectrum of the LiEDA PVP sample (Figure 41) and the PVP molecule from the literature. The peaks near  $1200\text{-}1150\text{ cm}^{-1}$  may be overlapped by the  $\text{CF}_2$  bands of PTFE, as well as O-H in the same area as N-H secondary amine near  $3400\text{ cm}^{-1}$  and C=O in the same area as N-H primary amine near  $1650\text{ cm}^{-1}$ . For LiDETA PVP samples, the spectrum is similar to the LiEDA PVP one, except for the double bands at  $2919$  and  $2850\text{ cm}^{-1}$  that was associated to  $\text{CH}_2$  from alkanes in LiDETA, which could coincide with the  $\text{CH}_2$  peaks from pyrrole ring of PVP.<sup>303</sup>





FT-IR peaks ( $\text{cm}^{-1}$ )			Vibrational mode
Pure PVP	PC5	PCT5	
3396	3409	3381	$\nu(\text{O-H})^{30)}$
2950	2951	2951	Asymmetric $\nu(\text{CH}_2)$ of pyrrole ring <sup>31)</sup>
2922	2922	2921	Symmetric $\nu(\text{CH}_2)$ of chain <sup>31)</sup>
2349	2350	2355	
1646	1655	1650	$\nu(\text{C=O})^{31)}$
1373	1374	1374	$\delta(\text{C-H})^{31)}$
1286	1289	1288	$\text{CH}_2$ wagging $\nu(\text{C-N})^{31)}$
1017	—	—	C-C, $\text{CH}_2$ rock <sup>31)</sup>
933	933	933	C-C bond <sup>31)</sup>
843	844	843	$\delta(\text{CH}_2)^{31)}$
572	576	569	$\delta(\text{N-C=O})^{31)}$

$\delta$ =in-plane bending;  $\nu$ =stretching; —=the peak was absent.

Figure 40. FT-IR absorption spectra of (a) CuO/PVP nanosheets and (b) PVP<sup>302</sup> and FT-IR Peak Assignment of PVP.<sup>303</sup>

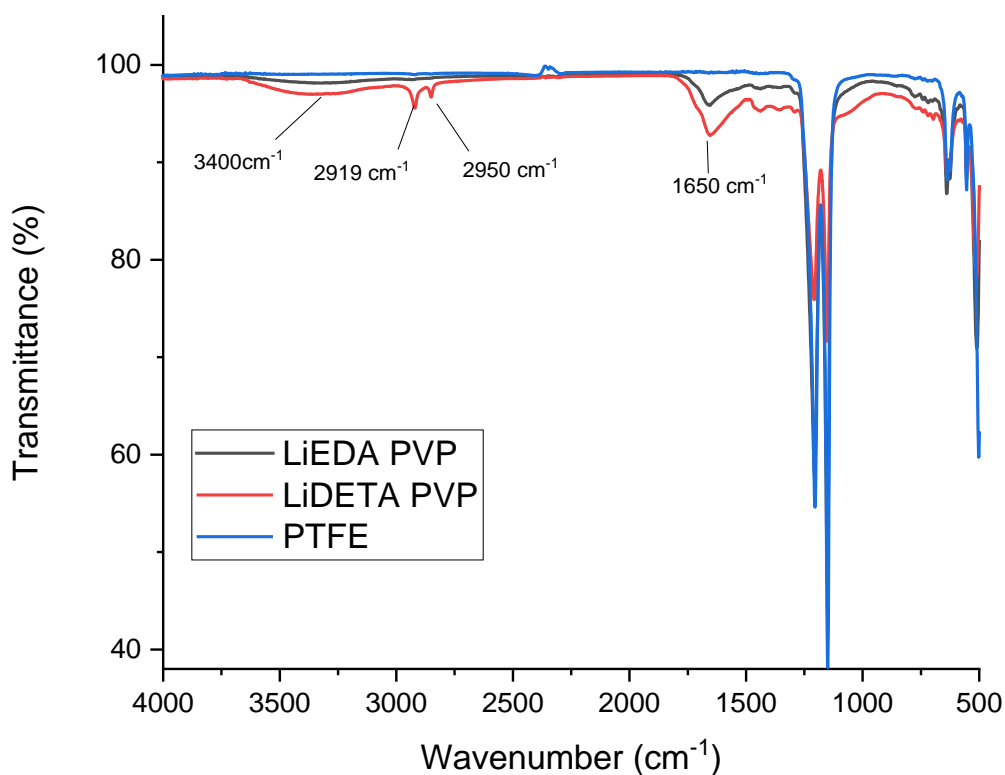


Figure 41. Experimental IR-ATR spectra of LiEDA PVP, LiDETA PVP samples and bulk PTFE; obtained with germanium crystal.

Similar case is encountered for PEI functionalized samples. PEI presents characteristic peaks at 3450, 2930, 2810, 1580, 1460, 1300, 1120 and 1040  $\text{cm}^{-1}$ ,<sup>304</sup> corresponding respectively to N-H, C-H twice, N-H twice, with  $\text{CH}_2$  at the same time for 1460  $\text{cm}^{-1}$  and the following three C-N. Once again, overlapping with existing signal from prior functionalization with LiEDA or LiDETA makes the spectrum lecture less accurate. Taking this into consideration, we might notice some PEI characteristic moiety in LiEDA and LiDETA PEI samples such as N-H, C-H, and  $\text{CH}_2$  and N-H detected at the same peak in the molecule. In LiEDA PEI, we can also notice a weak peak at 1039  $\text{cm}^{-1}$  which could be attributed to PEI C-N bond.

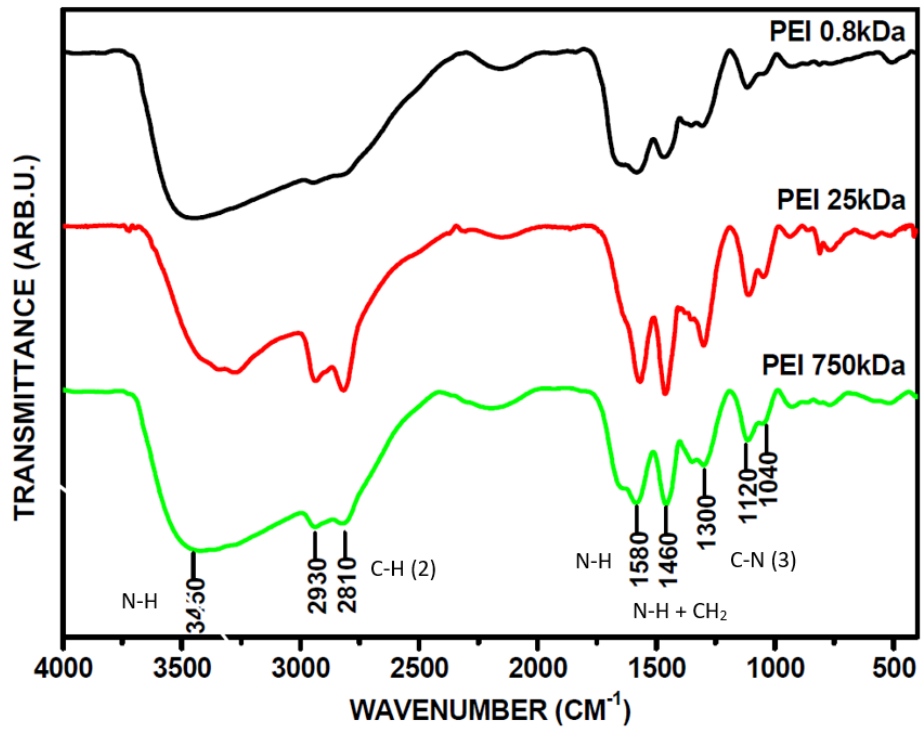


Figure 42. FT-IR spectra of pristine PEIs<sup>304</sup>

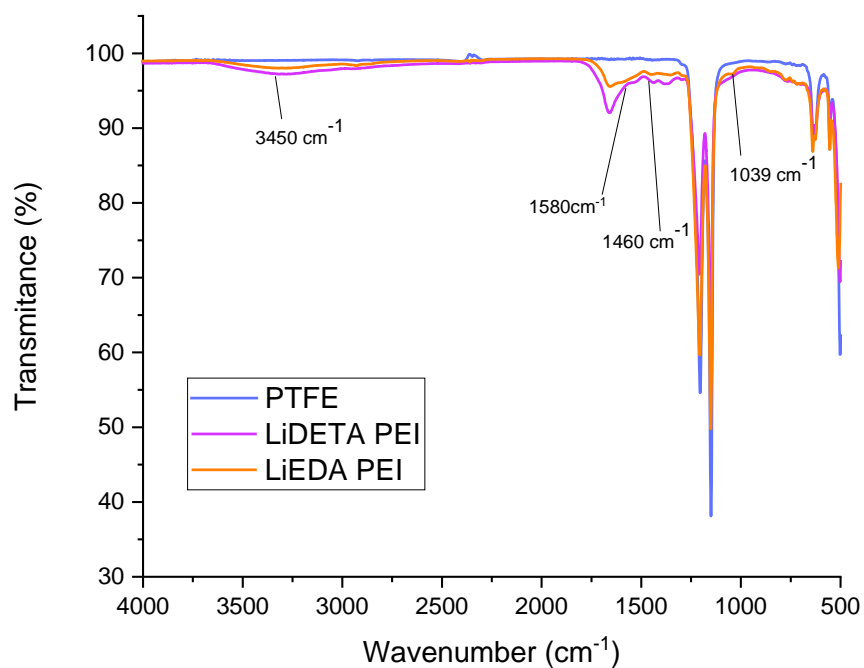


Figure 43. Experimental IR-ATR spectra of LiEDA PEI, LiDETA PEI samples and bulk PTFE; obtained with germanium crystal

Concerning CHI functionalization, the complex structure of this polysaccharide provides a large number of characteristic bands as shown in Figure 44. Compared to our experimental spectrum of LiEDA CHI and LiDETA CHI in Figure 45, we might associate bonds to functionalization, considering the previous observations. Thus, considering the bonds found in the literature in Table 4, we may meet the following groups : N-H and O-H with intramolecular hydrogen bonds near  $3300\text{ cm}^{-1}$ , C-H at  $2923\text{ cm}^{-1}$ , C=O from amide I at  $1655\text{ cm}^{-1}$ , CH<sub>2</sub> and CH<sub>3</sub> near  $1430$  and  $1370\text{ cm}^{-1}$ , and C-O at  $1061\text{ cm}^{-1}$  for LiDETA CHI. In LiEDA CHI we can also notice a band at  $1588\text{ cm}^{-1}$  which can represent N-H from primary amine.

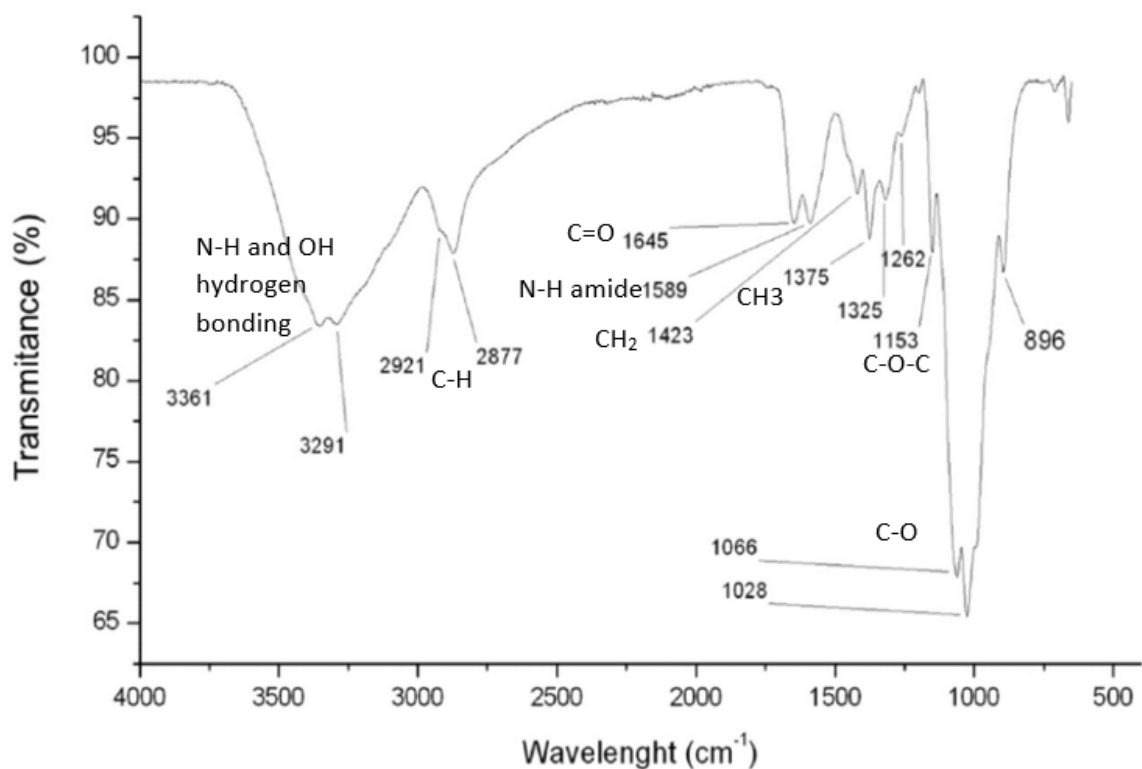


Figure 44. FTIR spectrum of chitosan with the characteristic signs as evidence.<sup>305</sup>

IR ATR Peaks (cm <sup>-1</sup> )	Corresponding bonds
3361-3291	N-H and O-H stretching + intramolecular hydrogen bond
2921-2877	C-H sym and assym stretching
1645	C=O amide I
1589	N-H bending primary amine
1423-1375	CH <sub>2</sub> and CH <sub>3</sub> sym deformation
1325	C-N stretching amide III
1153	C-O-C asym stretching
1066-1028	C-O stretching

Table 4. Correspondence between bonds and peaks in Figure 44.

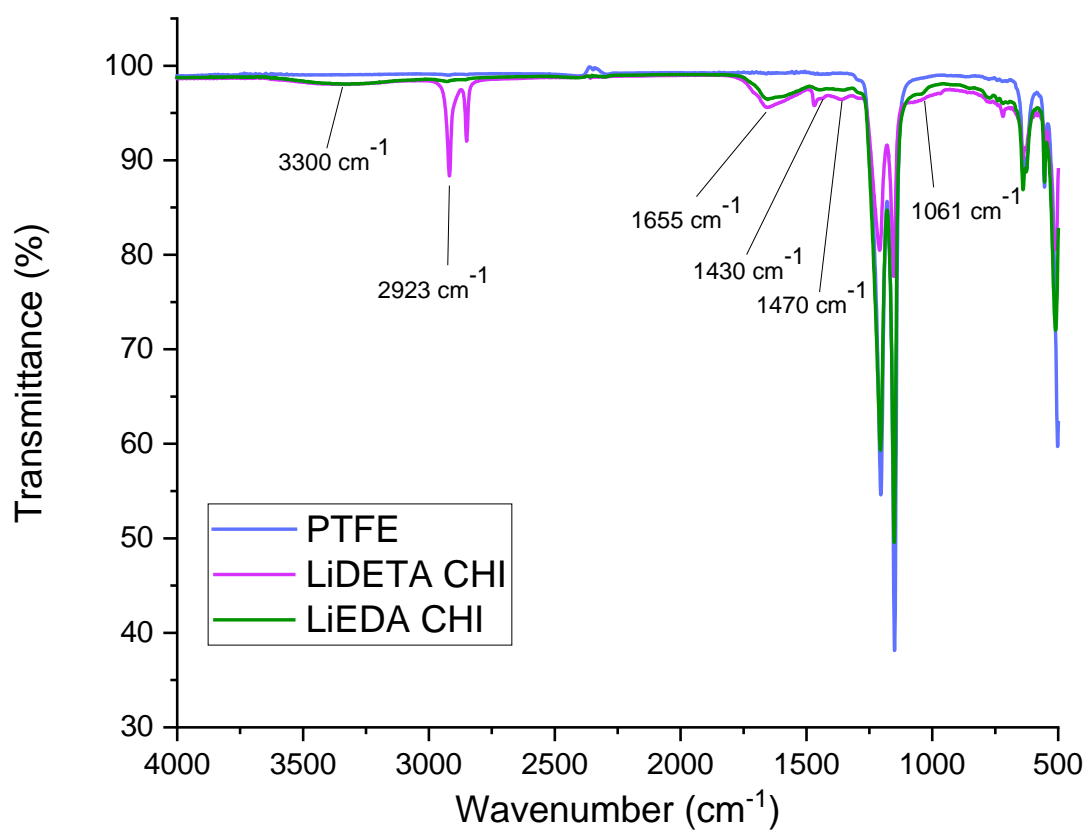


Figure 45 Experimental IR-ATR spectra of LiEDA CHI, LiDETA CHI samples and bulk PTFE; obtained with germanium crystal.

Based on these characterizations, we obtained important clues in favor of the validation of the reaction presented previously with the antibacterial agents. More detailed IR spectroscopy such as function mapping would have been beneficial to get more details on the surface chemistry obtained. Once the functionalization step carried out, the samples are then evaluated in term of cytotoxicity and antibacterial properties, that will be developed in the following part.

### III.3. Biocompatibility assessment on the samples obtained

#### Materials and method

Indirect cytotoxicity assessment was chosen to evaluate the materials functionalized. Indeed, ePTFE is a hydrophobic material that floats when immersed in a solution. The use of glue to stick the sample at the bottom of wells to enable cells to proliferate on the material would have required a long technical optimization. It would have also introduced the possibility of releasing compounds by the glue that can alter the results. At the end, an indirect assay was chosen as a simpler way to obtain preliminary results on this new functionalization method.

#### Reagents

Phosphate buffer saline (P04-36500), Dulbecco Modified Eagle's Medium (P04-05540), penicillin-Streptomycin\_ (P06-07100), trypsin-EDTA (P10-023100) and fetal calf serum (S1810-500) were purchased from Dutscher (Brumath, France); MTT (M5655) and DMSO (D4556) were obtained from Sigma-Aldrich (Saint Quentin Fallavier, France).

#### Cell culture

Murine dermal fibroblasts (L929, ATCC) were routinely cultured in complete medium [DMEM supplemented with 10 % FCS, penicillin (100 U/mL) and streptomycin (0.1 mg/mL)] in cell culture incubator (37°C, 5 % CO<sub>2</sub>). The culture medium was renewed every 3 days. Prior to confluence, fibroblasts were detached from culture flask with trypsin (0.05 %) - EDTA (0.02 %) solution and sub-cultured for cell expansion. For further experiments, cells were used between the fifth and ninth passages.

#### Extract cytotoxicity assay

Extract preparation from material was conducted following ISO 10993-5 and ISO 10993-12 recommendations<sup>306-307</sup>. Each material was sterilized by incubation into ethanol for 15 min followed by two washes in PBS. After sterilization, samples were pre-incubated into a complete medium (5 min) before extraction. Conditioned media were prepared by immersing material in a low-serum medium (5 %) at a ratio of 100 mg per ml (24 h, 37 °C, 5 % CO<sub>2</sub>). After incubation, supernatants were collected, centrifuged (1100 rpm, 5 min) to discard macroscopic debris, and were immediately used as conditioned media (CM) to treat cells. L929 fibroblasts were seeded into 96 wells culture plate (8.10<sup>3</sup> cells per well) in a complete culture medium. After an overnight adhesion step, the medium was replaced by conditioned media. In addition, we used all the needed control to exclude any cytotoxic effect from our technical procedure: fresh medium (Ctrl) and heated medium (Ctrl37). Moreover, 10 % DMSO was used as a positive control of cytotoxicity (Ctrl+). After 48h of treatment (with CM or control), MTT solution (final concentration 1 mg/ml) was added to cells and incubated for 4 h. The supernatant was then discarded, cells were washed two times with PBS, and formazan crystals were dissolved in 100 μL DMSO. Absorbance at 571 nm was measured with a microplate reader (Multiskan FC, Thermo Scientific). Raw data were obtained from three independent experimentation (n=10 per condition per experimentation). Relative cell viability (%) was expressed as a percentage relative to the non-treated control cells (Ctrl) and calculated by the following formula:

$$Viab. (\%) = \frac{100 * OD_s}{OD_{Ctrl}}$$

Where OD<sub>s</sub> refers to the absorption of the sample, and OD<sub>Ctrl</sub> refers to the absorption of the non-treated control.

#### Proliferation assay

The conditioned media were also used to address the question of their effect on L929 proliferation over time. L929 fibroblasts were seeded into 96 wells culture plate (2.10<sup>3</sup> cells per well) in a complete culture medium. After an overnight adhesion step, the medium was replaced by conditioned media. Same control than previously was used to exclude any cytotoxic effect from our technical procedure: fresh medium (Ctrl-) and heated medium (Ctrl-h, and 10 % DMSO as a positive control of cytotoxicity (Ctrl+). From 0 to 96 h post treatment, cells shape, and confluency status were followed and recorded every 4 h with a live-cell imaging system (IncucyteS3, Sartorius). At each time point, the confluency percentage was analyzed and calculated using the IncuCyte™ Analysis Software (Sartorius). Raw data were obtained from three independent

experimentation (n=10 per condition per experimentation), and the linear part of each proliferation curve were used to determine the proliferation index (i.e., slope).

### Statistical analysis

All data are expressed as a mean  $\pm$  SD. Statistical analyses were performed using one-way analysis of variance followed by a Dunnett's multiple comparison test. All analyses were performed using GraphPad Prism 7 software. Differences were considered as statistically significant \* for  $p < 0.05$ ; \*\* for  $p < 0.01$ ; \*\*\* for  $p < 0.001$ ; \*\*\*\* for  $p < 0.0001$ .

## Results and discussion

Biocompatibility assays are carried out to select the molecules for further grafting based on primary cytotoxicity-free results. The main purpose is to ensure that the molecules are harmless for living cells before exposing them to bacteria strains. Of course, these are preliminary tests to prove biocompatibility based on basic but normative protocols and literature. If any process of marketing is considered, far more tests and validations would be necessary before any clinical trial.

These tests as detailed in this part involve two parameters that were not described earlier, because not kept for the rest of this study as the product were found cytotoxic or not useful; the cytotoxicity being considered when the viability is significantly under 70 %. Firstly, this is the case of another solvent, hexamethylphosphoramide (HMPA) which is cytotoxic, whatever the molecule grafted after (Figure 46). The other one, is the reduction carried out after CHI grafting (ECR, DCR): an additional step of reduction with NaBH<sub>4</sub> was carried out at first to reduce the imine present after functionalization with glutaraldehyde. As no difference was observed at this point compared to the samples with imine (ECI, DCI in Figure 47), we chose to continue the glutaraldehyde grafting without this additional step and simply noting CHI to refer to chitosan grafting. It was also found that imine, notably in chitosan, tend to have antimicrobial properties, among others.<sup>308</sup>



To exclude any cytotoxic effect from the technical procedure, we took as control fresh medium (Ctrl) and heated medium at the temperature used to heat each sample in its medium (Ctrl37).

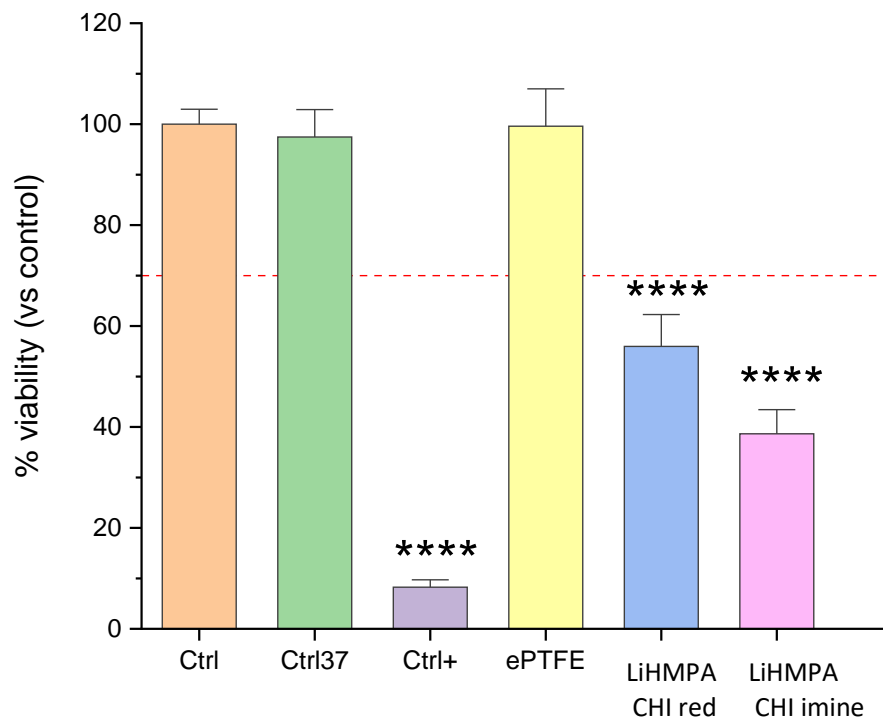


Figure 46. Cell viability of LiHMPA treated samples, with additional grafting of chitosan followed by a reduction (LiHMPA CHI red) or not (LiHMPA CHI imine) with  $\text{NaBH}_4$ . LiHMPA CHI red: sample modified with LiHMPA followed by chitosan grafting and  $\text{NaBH}_4$  reduction. LiHMPA CHI imine: sample modified with LiHMPA followed by chitosan grafting only.

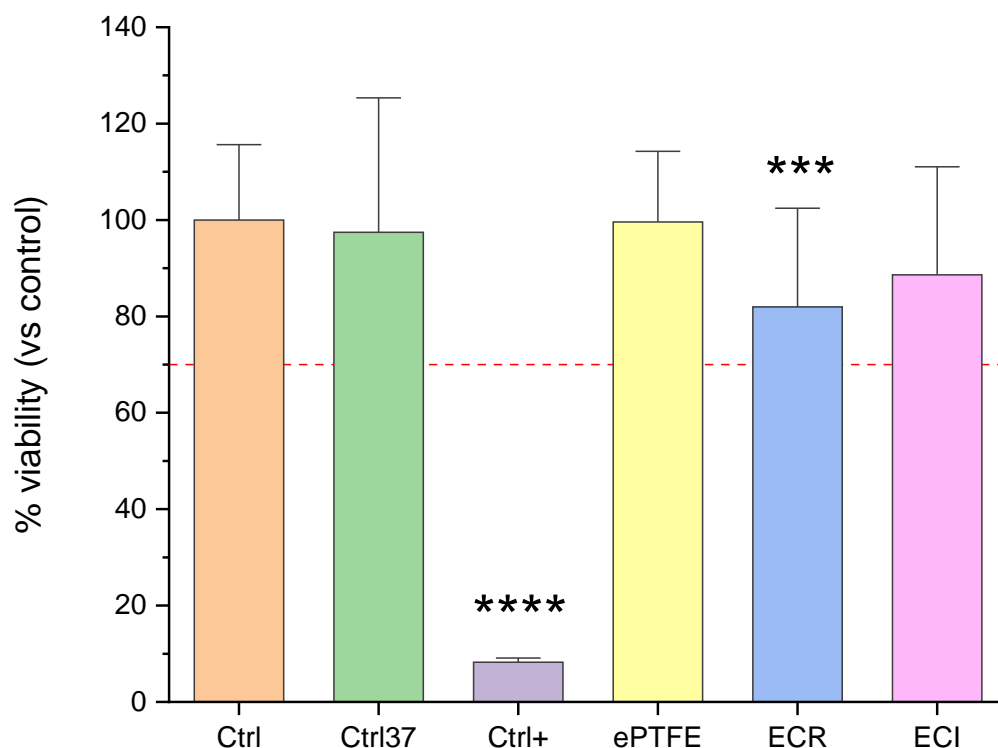


Figure 47. Cell viability of LiEDA treated samples, with additional grafting of chitosan followed by a reduction (ECR) or not (ECI) with NaBH<sub>4</sub>. ECR: sample modified with LiEDA followed by chitosan grafting and NaBH<sub>4</sub> reduction. ECI: sample modified with LiEDA followed by chitosan grafting only.

As we can notice on Figure 48 A and Figure 49 A, no cell viability seems to be significantly under the baseline of 70 % if we consider the confidence interval of 95 % that the error bars represent. The p-values presented for LiEDA and LiDETA samples batches were calculated in comparison to the control with a cell viability of 100 %. These p-values can reach probabilities below 0.0001 but they do not show correlation with the cell confluency speed. ePTFE sample is added to the study to understand the effect of the material alone. With no surprise, the material presents a comparable viability as the control, and a confluency speed resemblant compared to the control, as well as the confluency rate reaching 97 %. The cells from the LiEDA PVP condition seem to grow following the trend for bare ePTFE sample and meet the control near 90 % of confluency, even if their

viability is significantly lower. On the contrary, LiEDA PEI condition has a similar viability as for the control, but it slows considerably the cells' multiplication and their confluency only reached 30 % after 4 days.

Even if the viability against control of the LiEDA PVP and CHI conditions is different, their proliferation present a similar profile compared to the ePTFE trend approaching the 100 % confluency after 4 days. These functionalizations do not seem to alter the properties of ePTFE in term of cell proliferation. However, the LiEDA PVP sample might have a significantly lower viability because of a PVP release when the sample is immersed. A more detailed study about the released agents in solution might be beneficial to improve our understanding.

LiEDA modified sample seem to reduce the confluency speed and rate compared to the bare material. Two of the functionalizations, PVP and CHI, improve these parameters, when PEI reduces them more. The modification of the surface properties, such as porosity and chemical bonds might explain the impact of PEI on the cell confluency.<sup>309-310</sup> The surface treatment with LiEDA coupled with the cross-linking of glutaraldehyde and PEI might lead to the release of inhibiting compounds for cells. It was indeed found that PEI could be cytotoxic as we mentioned in the previous part.<sup>281-282</sup> A study of the tested solution with chromatography could help to understand this phenomenon.

The pictures taken at t=0 and t=4 days by the IncucyteS3 of the cells improves our understanding with visual data. In these pictures, in Figure 50 we can see that for LiEDA PVP condition, even if more cells die at the beginning, the confluence after 4 days looks like the control. For LiEDA PEI, the cells have differentiated but the confluency is not achieved yet. The rest of the pictures are displayed in the annex **A4**.

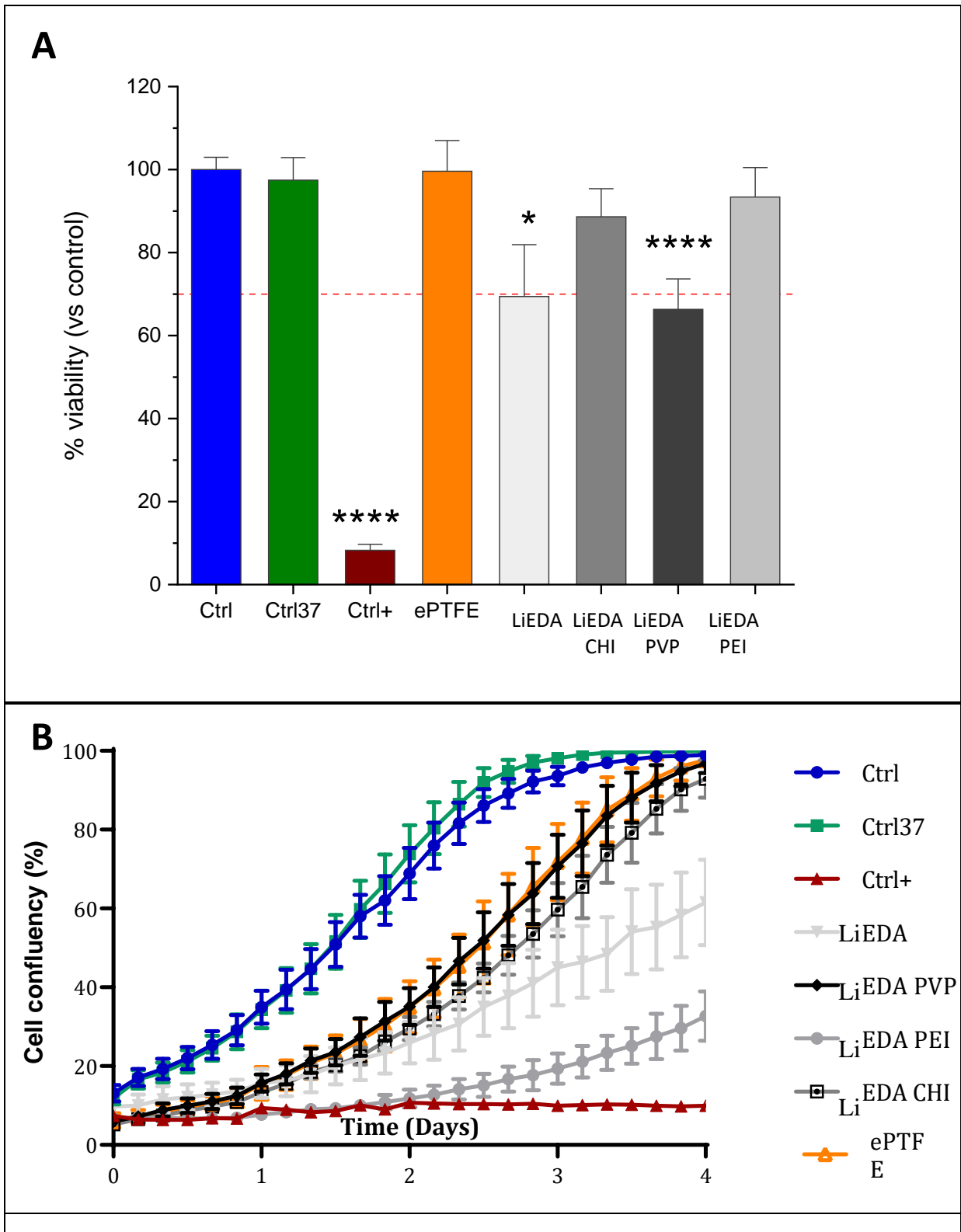


Figure 48. Cell viability vs control (A) and confluency (B) for LiEDA-modified samples. The colors between the two figures correspond.

Regarding LiDETA samples in Figure 49, we can also notice that no samples present viability under 70 %. LiDETA alone and with CHI and PVP functionalizations present similar proliferation profile, even if CHI viability against control is significantly lower. Their confluency after 4 days is high, near 90 %, without reaching the 100 % as some of the samples from LiEDA batch. Indeed, we do not notice a considerably slower confluency speed than the bare ePTFE for LiDETA treated sample, contrary to LiEDA one. Only LiDETA PEI condition presents a slower proliferation with a confluency of 38 % after 4 days.

In a recent study, biocompatibility of ePTFE coated with different gentamicin-based solutions was evaluated. Viability was assessed by WST-1 assay. The authors found a metabolic activity of 122 % for ePTFE, which is 22 % higher than our results here with MTT assay. WST-1 assay is known to be more precise than MTT, which might be a reason for this difference. Even with a higher precision, their coated material presented the same range of viability, between 70 and 100 %. This are encouraging results, even if these alone are not enough to decide on the final biocompatibility of our material.<sup>311</sup>

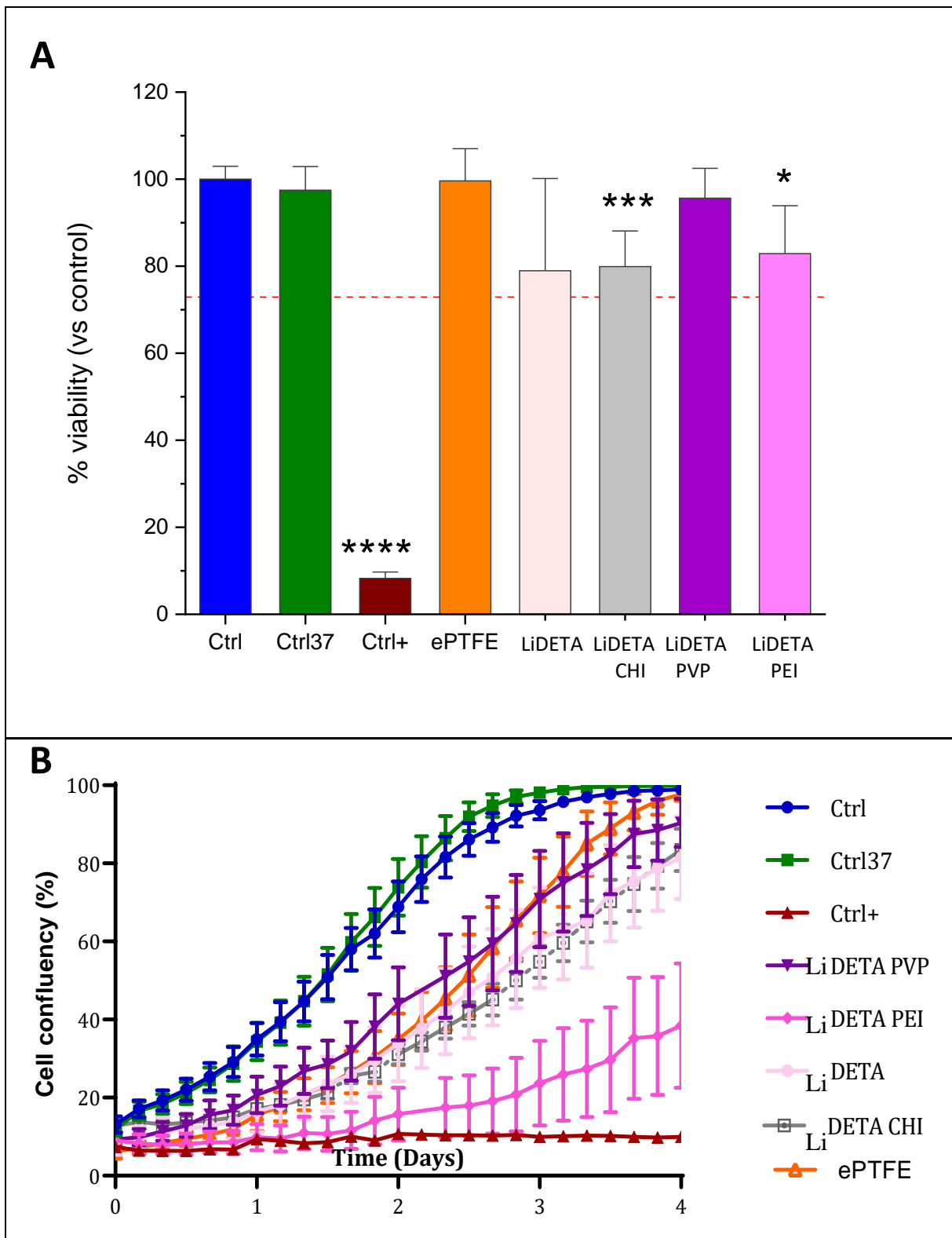


Figure 49. Cell viability vs control (A) and confluency (B) for LiDETA-modified samples. The colors between the two figures correspond.

Thus, the surface modifications of ePTFE appears to enable cell growth, even if some showed a significant speed reduction, unable to reach the full confluency after 4 days. Some modifications as mentioned before lead to a significantly lower viability than the control, which shows that the molecules released in the medium by the samples can be harmful for a non-negligible part of the cells without being cytotoxic, because not under the viability threshold of 70 %. These tests also enabled us to exclude the LiHMPA samples for the rest of our tests as high cytotoxicity was early found.

Further biocompatibility tests and analysis of the compounds released by chromatography would be advisable for a better understanding of the effects of the samples and their potential harm.

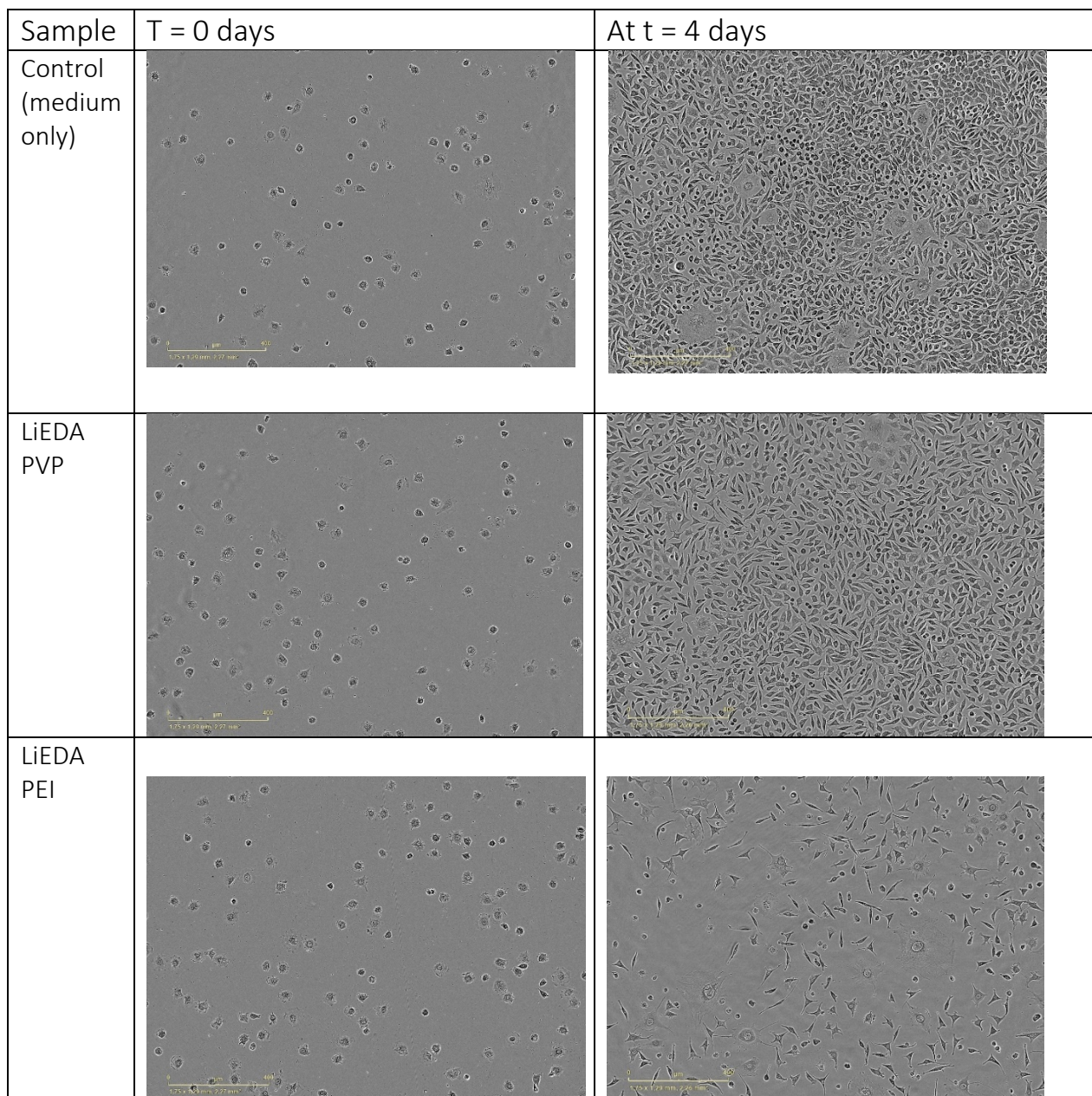


Figure 50. Images obtained from the IncucyteS3 at t=0 and 4 days for 3 conditions

The selected materials considered as not cytotoxic are then tested to evaluate their antibacterial properties according to the protocol presented in the next part.

#### III.4. Antibacterial evaluation of the biomaterials

As presented in the introduction, the materials that were developed here aim to be used against bacterial colonization of implants, biofilm formation and fouling, and consequently avoid the use of antibiotics, which could limit the



apparition of resistant bacteria. Indeed, infections due to resistant bacteria are frequent in nosocomial diseases. It is since the beginning of the 21st century that studies reported cases of patients infected with resistant bacteria strains were more often those who had received prior antimicrobials, compared to control patients.<sup>312</sup>

The transmission of antibiotic-resistance genes in a bacterial community can occur through horizontal and vertical gene transfer. The first type consists in a transfer from one bacterium to another one through a plasmid, the second type is a gene inheritance from a mother to a daughter cell. In presence of trimethoprim, resistant bacteria to this antibiotic increase both vertical and horizontal gene transfer to other bacteria.<sup>313</sup> These mechanisms require efficient strategies to tackle this issue.

Six bacteria mostly found in nosocomial diseases and subject to antibiotic-resistance are used to test our modified ePTFE samples, according to the protocol below. This protocol and the experiments following it were carried out by the hospital hygienist team of Besançon.

## Materials and methods

### Bacterial isolates

We used six bacterial species to test the antibacterial activity of the ePTFE prostheses. For each species, we used one isolate with wild type susceptibility to antibiotics distributed as follows: 1 clinical isolate (*Staphylococcus epidermidis*) and 5 reference isolates ((i) *Staphylococcus aureus* ATCC 6538P, (ii) *Klebsiella pneumoniae* ATCC 4352, (iii) *Escherichia coli* ATCC 25922, (iv) *Enterococcus faecalis* ATCC 29212, (v) *Pseudomonas aeruginosa* ATCC 27853). All these isolates were stored in the Centre de Ressources Biologiques-Filière Microbiologique of Besançon (Biobank number BB 0033 00090). Mueller-Hinton agar (MHA) was used for the cultivation of all isolates after storage.

### Preparation of bacterial inoculum

The tests are performed according to the recommendation of the absorption method described in the standard “NF EN ISO 20743 – Textiles – Détermination de l’activité antibactérienne des produits textiles”. Briefly, after

overnight culture on MHA, one bacterial colony culture was suspended in Tryptone Soy Broth (TSB) medium and incubated at 37°C for 18-24 hours with gentle agitation (160 rpm). Four hundred  $\mu\text{L}$  of this suspension was added to 20 mL of TSB and further incubated with gentle agitation for 2 h at 37°C. Then, the suspension was adjusted to the turbidity of 1 McFarland ( $\sim 10^8$  CFU/ml). The concentration of the suspension of Gram-positive bacteria (*S. epidermidis*, *S. aureus*, *E. faecalis*) were adjusted at  $10^7$  CFU/mL. The inoculum of Gram-negative bacteria (*K. pneumoniae*, *E. coli*, *P. aeruginosa*) were concentrated at  $10^{10}$  UFC/mL by centrifugation (20 min at 3220 x g) and pellet dilution in 3 mL of water.

#### Preparation of ePTFE prostheses samples

For each physicochemical treatment to be evaluated and for each bacterium to be tested, twelve prostheses samples were used (six untreated and six treated). All the samples received were sterilized by autoclave at 121°C for 20 min.

#### Antibacterial activity tests according to the absorption method (NF EN ISO 20743)

A drop of 200  $\mu\text{L}$  of the bacterial inoculum was deposited on each prostheses sample, further dried for 2 h (at room temperature in a biosafety cabinet). Three treated (samples T) and three untreated samples (C, for control) go through the extraction step directly after plating ( $T_{2h}$  and  $C_{2h}$ ). Three other treated and three other untreated samples were incubated at 37°C for 24 h ( $T_{24h}$  and  $C_{24h}$ ).

In the extraction step, each sample was placed in 20 mL of physiological saline extraction solution and vortexed for 30 s. For Gram-negative bacteria, the extract obtained was diluted according to the need. One hundred  $\mu\text{L}$  of the dilution were plated on MHA using a Spiral Plater (easySpiral® Pro, Interscience). The MHA plates were then incubated at 37°C for 24 h before colony counting.

We calculated the antibacterial activity of the chemical treatment (A, Equation 19) by subtracting the bacterial growth after the 22-hour incubation on non-chemically treated samples ( $\log C_{24h} - \log C_{2h}$ ) from that after incubation on chemically-treated samples ( $\log T_{24h} - \log T_{2h}$ ).

Equation 19. Formula of the antibacterial activity of a sample.

$$A = (\log T_{24h} - \log T_{2h}) - (\log C_{24h} - \log C_{2h})$$

## Results and discussion

As mentioned before, the NF EN ISO 20743 standard was used as a pattern to carry out these tests properly. This standard is usually suited for textiles. Even if resemblant to a textile, ePTFE differs mostly because of its hydrophobicity. This required an adaptation of the conditions and thus the protocol. *The recommendations of the standard i.e. i) to have a bacterial concentration between  $1.10^5$  and  $3.10^5$  CFU/mL of the inoculum; ii) to obtain a growth value greater than or equal to 1; iii) to have a difference of common logarithm of the extreme values of the samples, less than 1 and iv) to observe a difference of common logarithm of the extreme values of the samples to be less than 2) could not be respected at the time of each test. Moreover, the sterilization of the samples using an autoclave at  $121^\circ\text{C}$  for 20 min might alter the functionalization obtained, but this possible issue was not considered or evaluated in this study.*

Antibacterial activity is obtained from Equation 19. If the result is negative, the treated samples tested are considered to have an efficient antibacterial activity. Indeed, a negative value results from a lower value of the bacterial growth of the treated samples than the untreated samples.

As we can see on Figure 51, the only condition that present a negative bacterial activity for each species is reached from the LiDETA PEI treatment, which could be considered as the most effective. LiEDA CHI treatment presents only one species touched by a negative growth. Three treatments, LiEDA PEI, PVP and LiDETA CHI, present 5 out of 6 strains responding with negative bacterial activity. *S. aureus* is the one remaining in two of them, *P. aeruginosa* the third one. The other treatments present 3 to 4 negative bacterial activities, which is less interesting to reach the objective to cover as much strains as possible.

Compared to LiEDA CHI and PEI, LiDETA CHI and PEI samples present respectively a higher efficacy in terms of quantity of bacteria strains, as LiDETA CHI presents an antibacterial activity on 5 out of 6 strains, whereas LiEDA CHI presents 1 out of 6. For LiDETA PEI, the treatment is efficient on the 6 strains, and LiEDA PEI on 5 out of 6. We can conclude from these observations that we obtained a different antibacterial property according to the lithium alkylamide used in the first step of our functionalization. The difference in terms of surface properties and chemical composition could be correlated to the difference in antibacterial efficiency.<sup>314</sup>

However, in this study the number of replicates (n=3) recommended by the standard NF EN ISO 20743 impeded robust statistical analysis. Consequently, the results obtained here should be carefully examined as it is only an evaluation without any statistical confirmation.

A bias in the results should be considered: the control samples might present remaining bacteria on the surface because of the porosity of ePTFE. An additional inspection of the samples after the vortex step would be advisable.

Thus, from this first antibacterial evaluation, the LiDETA PEI treatment stands out by its apparent antibacterial efficacy and allows us to conclude that it would be an interesting candidate for further investigations.

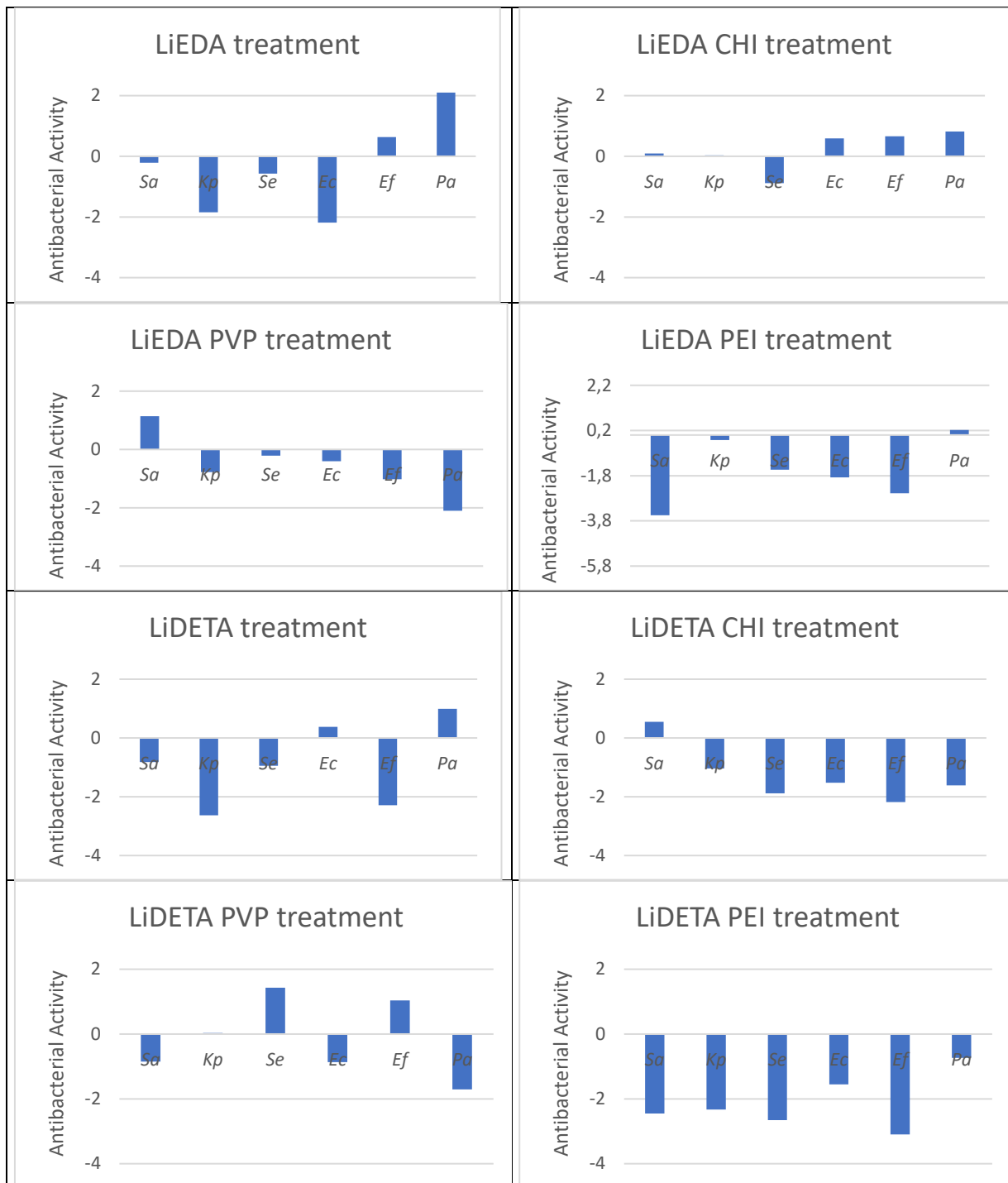


Figure 51. Antibacterial activity of eight treatments applied on ePTFE prostheses and tested against a panel of six bacterial strains. *S. aureus* (Sa), *K. pneumoniae* (Kp), *S. epidermidis* (Se), *E. coli* (Ec), *E. faecalis* (Ef), *P. aeruginosa* (Pa). The antibacterial activity of the chemical treatment (A) was calculated by subtracting the bacterial growth after the 22-hour incubation on non-chemically treated samples ( $\log C_{24h} - \log C_{2h}$ ) from that after incubation on chemically-treated samples ( $\log T_{24h} - \log T_{2h}$ ). Each test was carried out in triplicate.

## Conclusion and outlook

The methods used in this study to modify the surface of ePTFE using LiEDA and LiDETA appear to be very effective to achieve the defluorination of the material and the addition of amine groups on its surface. Indeed, the chemical modification can attack the material on a thickness of several hundreds of  $\mu\text{m}$  if necessary, in a few hours, much more than a treatment by competing plasma. LiEDA solution is found to be an aggressive treatment as the morphology, the structure and the properties of the material have undergone important changes. Indeed, the surface becomes stiffer, with a higher roughness and apparent porosity. The surface energy is also three times higher than the pristine material. LiDETA treatment appears to have a different impact on the material. Morphology and structure seem to be less attacked than by LiEDA treatment, but the surface energy is radically changed, as the material's surface becomes hydrophilic. The atomic ratio of the surfaces' composition can explain the modification of the physical properties of the surface. With the results we obtained, we can suppose that a difference in the C:F ratio, from pristine to LiEDA treated sample (ratios from 1:2 to 1:1), involves a high structure and properties modification of the surface. An even higher difference in this ratio, from 1:2 to 7:1 for LiDETA, presents a surface more different than the original as it becomes hydrophilic, but preserves some of its morphological and structural aspects.

Functionalization after defluorination and amination of the surface was carried out. The success particularly in grafting CHI and PEI is delicate to determine as the IR-ATR spectroscopy hardly enables to distinct precisely the LiEDA or LiDETA treatment from the molecules added in a second time. The penetration depth of the IR beam in the ePTFE is too great compared to the thin film layer resulting from the functionalization to be analyzed. However, structural changes of the ePTFE structure could be observed in LiEDA CHI with a significant reduction of the size of the short fibrils.

The MTT tests carried out for cytotoxicity evaluation shows us that the samples do not have the same effect on cells, which could be due to their different functionalization. But more importantly we were able to select the combination of molecules to functionalize the samples we would study, based on their toxicity for dermal cells. Thus, the following treatments by LiEDA CHI, LiEDA

PEI, LiEDA PVP, LiDETA CHI, LiDETA PEI and LiDETA PVP were chosen to be studied, as they each presented acceptable cell viability for this test. Two functionalization were excluded thanks to this test because of high toxicity for LiHMPA samples and optimization of the sample preparation for LiEDA CHI samples.

These treatments were then used to make 336 samples in total to be tested to evaluate their antibacterial efficiency. The bacterial activity of 6 strains was tested. Based on the data obtained, the treatments were effective on at least 3 bacteria. One treatment stood out with an antibacterial effect on all of the bacteria, LiDETA PEI. These tests, conducted more like a screening method, did not include enough samples per bacteria to conduct any parametric statistics, even though they respected the number of samples advised by the standard used. Non-parametric studies were found to be irrelevant, with no significant difference from one treatment to another, or from any treated sample to pristine material.

The bioactive evaluations carried out in this project did not consider or evaluate the porosity as a particularity of the ePTFE polymer, which can have effects on the results. The differences observed in cell confluency for cytotoxicity tests, as well as the number of bacteria counted in antibacterial tests could be explained or modified by the porosity and the particular surface state of the material. Further studies with more detailed parameters would be necessary to investigate this perspective.

The medical device standards and regulations obviously require far more tests to prove the safety and efficiency of the material presented here. This is supervised by the European regulation (EU) 2017/745, updating the directive 93/42/CEE. A meticulous process is necessary for any device before being ready for human use. For a class III medical device such as surgical membranes, it is necessary to determine the procedure for the evaluation of its conformity to the regulation. Then, the conformity must be proven with an adequate quality management system from the company, meeting the standard ISO 13495 requirements, and the technical documents. These latter need to prove that the device is safe and efficient, using standards such as the ISO 10993. This standard ensures the biocompatibility of the device, requiring -as a non-exhaustive list- *in vitro* evaluations of cytotoxicity, hemocompatibility, mutagenicity and

genotoxicity; as well as *in vivo* ones to evaluate systemic toxicity, intradermal, ocular, and skin tolerance or subcutaneous implantation.



## Résumé en français

### Introduction - Présentation du projet DELPHI

Le travail présenté dans ce manuscrit est le résultat d'une réflexion sur un enjeu majeur concernant les prothèses en polytétrafluoroéthylène expansé (ePTFE) utilisées à des fins chirurgicales. Ceci a nécessité une approche multidisciplinaire, combinant chimie, science des matériaux et biologie. Ce projet a reçu un soutien financier de la part de la région sur les trois ans, dans le cadre du projet de DELPHI, l'abrégié de "Développement de prothèses ePTFE antibactériennes implantables pour les tissus mous".

Le ePTFE est un polymère largement utilisé en chirurgie réparatrice et de remplacement, qui est davantage décrit dans la partie suivante. Ce projet a pour origine un problème observé en chirurgie pédiatrique. Des bactéries multirésistantes aux antibiotiques sont de plus en plus impliquées lors du traitement de laparochisis ou d'omphalocèle chez les nouveaux nés. Il s'agit de malformation de l'abdomen où celui-ci n'est pas refermé. La paroi abdominale reste ouverte pendant la gestation, pendant laquelle les organes se développent à l'extérieur de l'organisme. A la naissance, après avoir replacé les organes, une membrane de ePTFE chirurgicale est placée comme barrière pour délimiter la partie interne de l'organisme. Cette membrane est donc sujette régulièrement à des colonisations bactériennes qui peuvent donner suite à de sévères infections. Cette malformation a une prévalence de 1 pour 10 000 naissances, et 50% de mortalité est observée en cas d'infection.

En cas d'infection de nombreuses interventions sont nécessaires et l'utilisation d'antibiotiques favorise l'émergence des bactéries résistantes. Ceci est le cas dans tous les domaines de la chirurgie utilisant notamment ce matériau. Ce projet a donc pour but de modifier le ePTFE en surface afin d'obtenir un matériau antibactérien, biocompatible sans utilisation d'antibiotiques.

Pour cela, nous avons développé une méthode innovante brevetée permettant de modifier chimiquement la surface du ePTFE en la défluorant et lui ajoutant d'autres fonctions chimiques, et ce en une seule étape expérimentalement. Différentes fonctionnalisations sont ensuite ajoutées pour

espérer obtenir les propriétés antibactériennes souhaitées. Des tests de cytotoxicité ont été réalisés grâce à notre collaboration avec le Dr. Gwenaël Rolin et son équipe. Les matériaux réussissant ces premiers essais sont ensuite testés pour évaluer leur propriété antibactérienne, à l'aide de l'équipe du Pr. Didier Hocquet.

## Présentation du ePTFE

Le polytétrafluoroéthylène expansé (ePTFE) est un polymère obtenu par étirement du PTFE massif, pour obtenir de nombreuses propriétés intéressantes.<sup>315-316</sup> En plus de présenter les propriétés d'inertie chimique, d'anti-adhésion ou encore de résistance thermique inhérentes au PTFE qu'il doit à sa composition chimique, le ePTFE présente des avantages supplémentaires dus à sa structure expansée. En effet, sa structure microporeuse est due à l'expansion du PTFE brut. Pour cela, le PTFE est chauffé à une température supérieure à son point de fusion cristalline le plus bas, puis étiré à haute-vitesse de déformation. Le ePTFE obtenu est alors étiré à 800% sans rupture, ce qui lui confère de meilleures propriétés mécaniques une résistance plus élevée à la traction, et une rigidité plus faible. Ce changement de structure, usuellement décrite comme un réseau de fibrilles interconnectées par des nœuds, le change également en un matériau auxétique. Un tel matériau présente un comportement bien particulier, celui de s'épaissir en largeur lorsqu'il est étiré dans sa longueur (ce qui correspond à un coefficient de Poisson négatif). Ces propriétés supplémentaires confèrent au matériau un intérêt particulier pour les applications biomédicales, car plus léger, flexible, résistant et permettant la croissance tissulaire. L'utilisation du ePTFE montre des améliorations notables en ce qui concerne les greffes vasculaires comparées à celles en PTFE qui se détachent après implantation.<sup>82</sup> Aujourd'hui, il existe des implants médicaux en ePTFE et PTFE pour différentes parties du corps, dont les cathéters pour angioplastie,<sup>317</sup> implants orbitaux stables sur le long terme,<sup>318</sup> remplacement de cordes vocales défectueuses,<sup>319</sup> cartilage,<sup>320</sup> chirurgie plastique faciale ou encore membrane de réparation du péricarde endommagé.<sup>321</sup> De plus, il existe également des dispositifs d'analyses biomédicales du corps humain en PTFE.<sup>322</sup>

## 1. Etat de l'art de la recherche sur le ePTFE dans la littérature : de la chimie aux essais cliniques

La fonctionnalisation de surface du ePTFE a été développée à l'aide de différentes techniques au cours des dix dernières années. Dans le cas du ePTFE, les stratégies choisies sont des fonctionnalisations par liaisons covalentes ou non covalentes. La fonctionnalisation par liaison covalente implique généralement une modification par liaison forte à des espèces très réactive, dû à sa forte inertie chimique de départ. La fonctionnalisation non covalente ou de contact utilise quant à elle les propriétés du matériau, structurelle comme sa porosité ou physique comme son hydrophobicité.

### 1.1. Les améliorations nécessaires des différentes propriétés du ePTFE pour le médical

Le PTFE et ePTFE sont utilisés à des fins médicale variées, et présentent des propriétés particulièrement adaptées à cette fin. Cependant, ce matériau, bien qu'étant très efficace et polyvalent, présente des défauts liés à sa non-spécificité et peut entraîner des complications pour ces raisons. En effet, bien qu'étant un matériau hydrophobe empêchant en théorie l'adhésion bactérienne, le ePTFE est un matériau poreux à pores micrométriques qui permettent en réalité aux bactéries de se loger dans ceux-ci, les rendant inatteignables pour les cellules immunitaires, trop grosses pour les atteindre. Les infections nosocomiales post-implantaires sont reconnues pour être une cause majeure de morbidité et de mortalité. Un tier des maladies nosocomiales post-implantaires de vaisseaux synthétiques sont létales.<sup>13-17</sup> A cela s'ajoute les bactéries résistantes aux antibiotiques qui aggravent ces maladies nosocomiales, les rendant plus difficiles à traiter. Les bactéries résistantes prédominantes étant *Staphylococcus aureus*, *Pseudomonas aeruginosa*, *Klebsiella pneumoniae*, *Escherichia coli*, and *Acinetobacter baumannii*.<sup>12</sup>

Les prothèses vasculaires synthétiques en cas de d'occlusion vasculaire constituent en elles-mêmes un défi particulier que le ePTFE ne relève pas à lui seul. En effet, l'obstruction partielle (sténose) ou totale (thrombose) de ces prothèses est régulièrement rencontré sur le long terme. Ceci est dû à une prolifération cellulaire à l'intérieur de la prothèse, le matériau étant un corps étranger et les vaisseaux sanguins ayant une structure particulière qu'un matériau seul ne permet pas de remplacer. L'adhésion de protéines plasmatiques est également un problème rencontré, car il mène à l'activation du système du

complément faisant partie du système immunitaire inné, à l'adhésion de plaquettes, ou encore à des systèmes de coagulation. Ces mécanismes contribuent également à l'obstruction des vaisseaux synthétiques.

L'inertie chimique du ePTFE ainsi que sa structure microporeuse empêche également l'adhésion cellulaire parfois nécessaire pour certains implants, comme les membranes utilisées en cas de hernie diaphragmatique.<sup>22</sup>

## 1.2. Les différentes modifications de surfaces du ePTFE qui existent dans la littérature, pour des applications médicales

Les modifications de surfaces du ePTFE à des visées thérapeutiques sont nombreuses mais peu ont été testées jusqu'aux essais cliniques. Pour résumer les différentes modifications chimiques existantes dans la littérature, le tableau ci-dessous les présente en les regroupant sous deux catégories : les modifications de surface par liaisons covalentes et celles par liaisons non covalentes. Nous avons publié une revue qui explique avec plus de détails ces réactions.<sup>323</sup> Les fonctionnalisations par liaison covalentes sont moins nombreuses car le PTFE est un matériau dont la composition chimique est difficile à altérer, avec la liaison forte C-F notamment. Des conditions extrêmes doivent donc être employées pour y parvenir, comme l'utilisation d'agent réducteurs ou oxydants puissants, ou encore l'utilisation de gaz plasma. En ce qui concerne les liaisons non covalentes, il s'agit de compter sur l'adhésion et l'affinité plus ou moins forte des molécules intéressantes avec le PTFE. Pour cela, le matériau peut subir différentes méthodes de trempage ou de recouvrement par des molécules adhésives. La colonisation par des cellules ou des tissus est également un moyen de fonctionnaliser le matériau de manière non covalente.

Type de modification	Référence	Méthode de fonctionnalisation	Propriétés bioactives visées
Covalente	32	Reduction chimique de surface et greffage par polymérisation induite sous UV	Anti-inflammatoire et antibactérien
	33-34	Modification de surface par gaz plasma greffage par polymérisation induite sous UV	Eviter l'adhésion et l'activation des plaquettes
	38-39	Gaz plasma et greffage de PEG puis de pénicilline	Antibactérien
	43	Irradiation par rayon gamma et greffage de nanoparticules d'argent sous irradiation	Antibactérien

	45	Oxydation de surface et greffage de nanoparticules de PLGA	Antibactérien et anti-sténose pour prothèses vasculaires
Non-covalente	47-50	Infusion de liquide hydrophobe à la surface de matériaux poreux (Slippery Liquid-Infused Porous Surfaces)	Anti-inflammatoire et antibactérien
	51-52	Trempe dans une solution antibiotique	Antibactérien pour prothèses vasculaire ou reconstruction tissulaire guidée
	53	Trempe dans une solution antibiotique	Antibactérien et anti-sténose pour prothèses vasculaires
	58	Vascularisation autologue	Antibactérien
	59	Vascularisation autologue	Anti-sténose pour prothèses vasculaires
	60	Spin-coating de polyuréthane (PU) suivi d'un dépôt de nanoparticules de PU	Eviter l'adhésion et des plaquettes
	61	Polymère fluoro-tensioactif auto-assemblé avec des molécules bioactives	Anti-sténose pour prothèses vasculaires
	62 64	Traitement au gaz plasma suivi de Layer-by-Layer	Adhésion cellulaire
	65	Héparine/Collagène Layer-by-Layer avec séquence peptidique adhésive Arg-Glu-Asp-Val (REDV)	Anticoagulation et endothélialisation pour réparation cardiaque
	66	Revêtement de poly(1,8-octanediol-co-citrate) (POC) via une méthode de spin-shearing et liaison covalente d'héparine via des réactions EDC/NHS	Anti thrombogène pour les prothèses vasculaires
	67	Cellules endothéliales placentaires humaines cultivées à la surface interne de la prothèse, cellules	Anti-sténose pour prothèses vasculaires

	souches/stromales mésenchymateuses dérivées de l'amnios à la surface externe	
68	Ensemencement cellulaire de cellules endothéliales autologues sur la surface luminale	Anti-sténose pour prothèses vasculaires d'hémodialyse
69	Revêtement par adhésion de protéine de soie 4RepCT contenant le motif de liaison cellulaire RGD de la fibronectine	Inciter l'endothélialisation des prothèses vasculaire
54	Revêtement avec une fine couche de copolymère thermoplastique styrène éthylène propylène styrène (SEPS). Greffage de la couche SEPS et liaison covalente avec des molécules semi- synthétiques de type héparane sulfate. (Brevet EP 1501565 B1)	Anti-adhésion de plaquettes et anti- sténose pour prothèses vasculaires
76	Irradiation de la surface avec des faisceaux d'ions He <sup>+</sup> , Ne <sup>+</sup> , Ar <sup>+</sup> and Kr <sup>+</sup>	Anti-adhésion de plaquettes et adhésion de cellules endothéliales pour prothèses vasculaires
77	Adhésion de polydopamine (PDA) en surface par trempage	Adhésion cellulaire pour réparation du diaphragme
78	Traitement par gaz d'argon plasma suivi de l'adhésion de PDA	-
80	Co-dépôt de polyéthylèneimine (PEI) et de PDA suivi d'un greffage de polymères zwitterioniques sulfatés	Antibactérien
81	Revêtement sous vide de PLCL P- conjugué (SP-PLCL) et/ou de PLCL conjugué à l'héparine (Hep- PLCL)	Anti-thrombogène pour prothèses vasculaires

83-84	Traitement de surface du PTFE suivi d'une pulvérisation magnétron de phosphate de calcium	Ostéoinduction (favoriser la différenciation de cellules souches en cellules osseuses)
85-86	Dopage par plasma pulsé	Ostéoinduction
87	Adsorption de peptide adhésif	Ostéoinduction
88	Autoassemblage de protéines de soie d'araignée avec un motif de liaison cellulaire dans un revêtement nanofibrillaire	Adhésion cellulaire et régénération osseuse

### 1.3. Les différents essais cliniques portant sur l'efficacité des implants en ePTFE existants dans la littérature.

Depuis le début des années 90, les dispositifs médicaux en ePTFE ont été testés cliniquement avec une augmentation au fil des années d'interventions réussies et de suivis post-opératoires. Nous avons publié une revue détaillée des différents essais cliniques existant portant sur l'utilisation d'implants totalement ou partiellement composé de ePTFE dans les différents domaines de la chirurgie.<sup>324</sup> Des avancées significatives ont été réalisées dans les domaines de la régénération vasculaire, osseuse et tissulaire guidée, de la réparation herniaire et de la chirurgie réparatrice cardiaque, même si les taux d'échec des essais cliniques peuvent rester élevés selon les domaines (jusqu'à 40% et plus). De plus, le ePTFE semble être un matériau plus ou tout aussi efficace que d'autres matériaux utilisés aux mêmes fins, tels que le Dacron pour la greffe vasculaire, les polymères bioabsorbables pour la régénération tissulaire guidée pour la reconstruction maxillofaciale ou le nitinol pour les stents. Les essais cliniques portant sur du ePTFE fonctionnalisés maintiennent une présence marginale dans la littérature aujourd'hui.

## 2. Modification chimique de surface directe : une nouvelle méthode combinant métal alcalin et solvant organique.

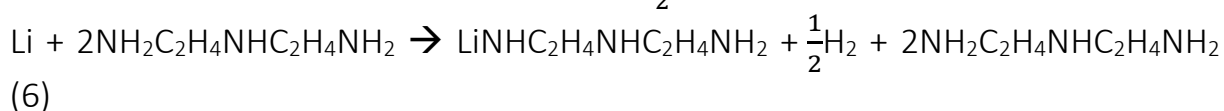
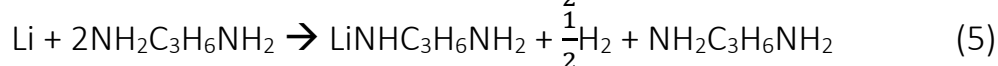
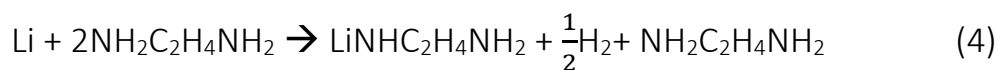
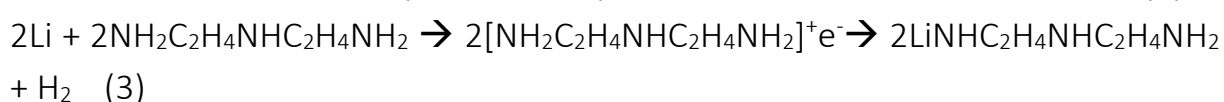
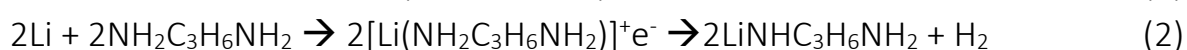
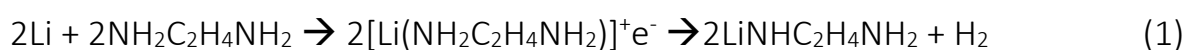
### 2.1. Présentation de la méthode.

Nous avons développé une approche rapide et efficace permettant de fonctionnaliser des fluoropolymères. Un amidure de lithium est produit in situ, dans des conditions douces de températures (20°C) et de pression, sous atmosphère inerte, par la réaction du lithium solide et d'une di ou tri amine. Dans

cette étude, nous nous focalisons sur les applications de l'éthylènediamine (EDA) et de la diéthylènetriamine (DETA), mais nous présentons également ici les résultats pour le 1,3-Diaminopropane (DAP). Ces solvants permettent une bonne solubilisation du lithium ainsi que la formation d'électrons solvatés stables.

D'après les réactions (1), (2) et (3), nous obtenons des amidures de lithium solides en mettant les réactifs en proportions équimolaires.

Équation 1. Réactions (1) à (6). 1 à 3 : réactions en proportions équimolaires, 4 à 6 : en dessous des proportions stœchiométriques.



Ces amidures de lithium, formées dans le milieu réactionnel, permettent de modifier la surface du polymère, en les défluorant, avec les molécules de solvant se greffant à la place du fluor. Quel que soit le solvant utilisé, on observe pour les polymères fluorés que plus la concentration en amidure de lithium est élevée, plus la réaction de modification est rapide à température ambiante. Les analyses XPS ont permis de constater que cette méthode permet une défluoration importante, avec un ratio C:F passant de 1:2 à 7:2 pour DETA et 1:1 pour EDA.

## 2.2. Caractérisations

L'analyse AFM des différentes surfaces montre des formes sphériques à la surface du matériau, le PTFE seul présentant une surface plutôt lisse avec quelques rayures d'usinage. Il semble que le traitement par LiEDA forme des sphères plus petites que LiDETA, avec des diamètres moyens de  $105 \pm 24$  nm et



605 ± 80 nm respectivement. Il apparaît également que le ePTFE modifié par LiEDA présente des sphères de plus grand diamètre que le PTFE, avec 239 ± 61 nm. Des formes particulières appelées « sphérulites » ont déjà été observées à plus petite échelle pour une solution de défluoration à base de naphthalène de sodium ou après irradiation du PTFE.<sup>214, 255-256</sup> Leur morphologie n'est cependant pas similaire car leur apparence n'est pas réellement sphérique et la dimension bien plus grande, de l'ordre de plusieurs micromètres.

Les images MEB montrent que les échantillons de PTFE modifiés présentent une organisation poreuse et fibrillaire, comparées au PTFE vierge apparaissant plutôt lisse. L'échantillon LiEDA présente un plus grand nombre de pores que l'échantillon LiDETA, ce qui pourrait être interprété comme une modification plus intense de surface. Une porosité est également obtenue lorsque le PTFE est irradié, avec une gamme similaire de diamètres entre 50 et 100 nm.<sup>255</sup> Une image de la tranche du matériau montre une épaisseur colorée due à la réaction de l'ordre de 100 µm.

L'énergie de surface du PTFE modifié ou non a également été calculé, utilisant pour cela les mesures d'angles de goutte. La théorie de Fowkes est utilisée, théorie se basant sur l'hypothèse que l'énergie de surface d'un solide peut se définir comme l'addition d'une composante dispersive et d'une composante polaire. La méthode de calcul est tirée de la fiche technique KRUSS TN306e. Les énergies de surface obtenues décrivent une évolution du PTFE, passant d'une surface très hydrophobe à moins hydrophobe pour le LiEDA, et hydrophile pour le LiDETA. En effet, le PTFE massif voit son énergie de surface augmentée de 3 pour LiEDA et de 6 pour LiDETA, avec des valeurs de 12.34±2.45, 32.76±0.51 et 72.90±0.42 mJ/cm<sup>2</sup> respectivement.

Des tests de nanoindentation furent également réalisés sur les échantillons. Le ePTFE et sa structure auxétique particulière ne permet pas d'observer de modification de la rigidité de surface. Les mêmes tests réalisés sur le PTFE ont permis de s'affranchir de la structure pour n'observer que l'effet des traitements. En effet, le PTFE voit sa rigidité de surface augmenter de 1.31±0.10 GPa à 1.73±0.30 GPa pour un traitement LiEDA. Ceci pourrait s'expliquer par le raccourcissement de la longueur des liaisons, remplaçant les liaisons C-F par des

liaisons multiples (Equation 5). Ces liaisons sont plus rigides dans les chaînes moléculaires, ce qui a un impact sur le matériau à grande échelle. Pour LiDETA, il n'y a pas de différence significative avec le PTFE, ce qui en fait un agent de modification respectant davantage ses propriétés de surface.

### 3. Fonctionnalisation secondaire par des molécules antibactériennes

#### 3.1. Présentation des molécules sélectionnées

Le chitosan, la polyéthylèneimine et la povidone iodée sont trois agents antibactériens qui ont fait leur preuve, et que nous utilisons comme molécules de fonctionnalisation. Les deux premières par greffage suite à la modification par LiEDA ou LiDETA, utilisant le glutaraldéhyde, la dernière par immersion dans une solution (voir protocoles en annexe).

En effet, le chitosan est un polysaccharide aminé qui a été très tôt un sujet de d'études pour ses propriétés biocompatibles et antimicrobiennes. Il est utilisé aujourd'hui depuis plus de 20 ans car il a été prouvé sûr et efficace pour des utilisations cliniques et pharmacologiques.<sup>270-273</sup>

La polyéthylèneimine est un polymère organique présentant des amines secondaires pour les structures linéaires et primaires jusqu'à tertiaires pour les chaînes ramifiées. Cette molécule présente des propriétés très différentes en fonction de sa masse moléculaire et de sa concentration. Cependant des propriétés antibactérienne<sup>284</sup> ou encore le fait de favoriser l'attachement de cellules primaires<sup>279</sup> et en fait une molécule intéressante à utiliser pour notre étude.

La povidone iodée est également une molécule étudiée et utilisée il y a plusieurs décennies, et prouvée être efficace sur de nombreuses souches à l'origine de maladies nosocomiales.<sup>292</sup> Cette molécule est un iodophore soluble dans l'eau, capable de relarguer de l'iode ( $I_2$ ) Cette petite molécule pénétrant rapidement à travers les membranes des microorganismes, oxydant leur protéines, nucléotides et acides gras, ce qui mène généralement à la mort cellulaire.<sup>293</sup> Bien que cet antiseptique soit communément utilisé, il doit tout de même être manipulé avec précaution en cas d'utilisation sur des nouveau-nés

car la perméabilité de leur peau les rends plus vulnérable à la diffusion de l'iode et à son accumulation au niveau de la thyroïde. Ceci a été observé notamment chez des patients en soins intensifs,<sup>296</sup> mais des sujets sains ont aussi présenté des quantités anormales d'iode sans dysfonctionnement de la thyroïde.<sup>297</sup> Il est donc recommandé dans ce cas d'utiliser la povidone iodée avec précaution.

### 3.2. Caractérisations

L'imagerie MEB du ePTFE (Figure 38) et des échantillons fonctionnalisés présentés en annexe A3, rapporte des modifications notables de la structure de la surface après traitement. En effet, les fibrilles semblent se casser en certains points, principalement au niveau de leur site d'attache à un nœud. D'autres traitements décrits dans la littérature conduisent à la rupture des fibrilles dans la structure de l'ePTFE, comme le plasma d'argon ou d'oxygène à haute puissance RF.<sup>300-301</sup> Une porosité avec une apparence toile d'araignée telle que décrite par les auteurs peut également être remarquée dans le lot d'échantillons traités au LiEDA.

Dans les échantillons greffés par le glutaraldéhyde, les fibrilles semblent être particulièrement étendues, et les nœuds regroupés. Nous avons mesuré les distances internodales dans chaque image, en considérant deux tailles différentes dans chaque image, un long et une court, comme décrite dans la Figure 38.

Pour une longue distance internodale, seul le traitement avec LiEDA conduit à une distance significativement plus longue que le ePTFE seul. Cependant, ce n'est pas le cas pour les échantillons fonctionnalisés comme LiEDA CHI, PEI et PVP. Cela pourrait être dû à une réticulation avec le glutaraldéhyde pour CHI et PEI qui modifie la structure et implique une variance plus large, notamment avec la rupture des fibrilles. La fonctionnalisation par PVP modifie également la structure, qui présente des nœuds plus resserrés et des fibrilles rompues. L'échantillon LiDETA ne présente pas non plus de différences significatives pour les longues distances internodales malgré l'allongement visible des fibrilles et leur rupture. Cela pourrait être lié au résultat précédent où la structure résultant du traitement LiDETA ne semblait pas impliquer une altération des propriétés mécaniques. La

courte distance internodale est cependant nettement inférieure à l'ePTFE, ce qui pourrait renforcer la structure totale.

Une analyse IR-ATR a été réalisée pour identifier les groupes fonctionnels chimiques résultant de la fonctionnalisation pour chaque échantillon. A première vue, les spectres semblent assez identiques les uns des autres. Nous avons analysé chaque spectre précisément en les comparant au spectre de la molécule seule trouvée dans la littérature. La plupart des bandes chevauchent celles présentes sur les spectres des échantillons LiEDA et LiDETA. Il est donc difficile de se prononcer avec certitude sur les fonctions présentes ou non.

En comparant les 4 spectres du lot LiEDA ensemble, on observe uniquement chez les échantillons fonctionnalisés la présence d'un pic à  $1654\text{ cm}^{-1}$  qui pourrait correspondre à la vibration d'une imine. Ce phénomène est également observé pour le lot d'échantillons LiDETA. Cela peut être dû à la présence d'une imine produite lors du greffage du CHI et de la PEI à l'aide de glutaraldéhyde. La PVP présente également une imine dans ses formes mésomères.

La comparaison des spectres expérimentaux et ceux de la littérature permet de supposer la présence de certaines fonctions chimiques que la surface fonctionnalisée et la molécule étudiée ont en commun, en restant prudent sur l'interprétation puisque chevauchement avec des fonctions existantes. Pour les échantillons fonctionnalisés par PVP, il serait possible de détecter les groupements O-H et C=O. Pour l'échantillon LiDETA PVP, une fonction supplémentaire, le  $\text{CH}_2$  d'un alcane pourrait être détecté également. Pour les échantillons fonctionnalisés par PEI, les fonctions N-H, C-H et  $\text{CH}_2$  pourraient être attribuées. L'échantillon LiEDA PVP présenterait une fonction supplémentaire, la liaison C-N. En ce qui concerne les échantillons fonctionnalisés par CHI, on rencontrerait les groupes O-H et N-H avec liaisons hydrogène intramoléculaire, C-H,  $\text{CH}_2$  et  $\text{CH}_3$ . LiDETA CHI présente également une liaison C-O et LiDETA CHI une liaison N-H.

### 3.3. Tests de cytotoxicité comme premier élément de sélection des fonctionnalisations.

Des tests sont réalisés afin de sélectionner les fonctionnalisations non cytotoxiques. Pour cela les différents échantillons sont trempés dans du milieu de culture à 37°C pendant 24h, puis ce milieu de culture est récupéré et mis au contact de cellules arrivées à confluence dans des puits de culture. Après 24h d'incubation, on ajoute du MTT afin d'évaluer l'activité cellulaire, puis du DMSO 4h plus tard pour permettre des mesures de densité optique. Une expérience en parallèle est réalisée sur 4 jours : les cellules ne sont pas à confluence et on observe leur croissance au cours du temps au contact de chaque milieu de culture. L'objectif principal est de s'assurer que les molécules sont inoffensives pour des cellules vivantes avant de les exposer à des souches bactériennes. Bien sûr, ce sont des tests préliminaires à une preuve de biocompatibilité complète, mais basée sur des protocoles normatifs. Si un quelconque processus de commercialisation est envisagé, bien plus de tests et de validations seraient nécessaires avant tout essai clinique.

Deux fonctionnalisations n'ont pas été retenues rapidement dans notre processus de sélection, celles-ci n'ont donc pas été étudiées selon les caractérisations présentées précédemment. C'est d'abord le cas d'un autre solvant, l'hexaméthylphosphoramidate (HMPA) qui a été prouvé cytotoxique en tant que solvant organique réagissant avec le lithium, et ce quelle que soit la molécule greffée par la suite. L'autre, est la réduction effectuée après greffage de CHI : une étape supplémentaire de réduction avec  $\text{NaBH}_4$  a été effectuée dans un premier temps pour réduire l'imine présente après fonctionnalisation avec le glutaraldéhyde. Comme aucune différence n'a été observée à ce stade par rapport aux échantillons avec imine (Figure 47), nous avons choisi de poursuivre le greffage de glutaraldéhyde sans cette étape supplémentaire. Il a également été constaté que l'imine, notamment dans le CHI, présenterait des propriétés antimicrobiennes.<sup>308</sup>

Comme nous pouvons le remarquer sur les Figure 48A et Figure 49A, aucune viabilité cellulaire ne semble être significativement inférieure au seuil de cytotoxicité de 70 % si l'on considère l'intervalle de confiance de 95 % que représentent les barres d'erreur. Les valeurs p présentées pour les lots d'échantillons LiEDA et LiDETA ont été calculées par rapport au témoin avec une viabilité cellulaire de 100 %. Ces valeurs p peuvent atteindre des probabilités

inférieures à 0,0001 mais elles ne montrent pas de corrélation avec la vitesse de confluence des cellules. Le ePTFE est également ajouté à l'étude pour comprendre l'effet du matériau seul. Sans surprise, le matériau présente une viabilité comparable au témoin, et une vitesse de confluence similaire par rapport au témoin, atteignant 97 % de confluence après les 4 jours que dure l'expérience.

Les cellules en présence du milieu LiEDA PVP semblent croître de manière similaire à celles de l'échantillon de ePTFE seul et arrivent à une confluence de près de 90 %. La viabilité des cellules obtenue par le test MTT est cependant significativement plus faible que celle du témoin négatif. Au contraire, la condition LiEDA PEI a une viabilité similaire à celle du témoin, mais elle ralentit considérablement la multiplication des cellules et leur confluence n'atteint que 30 % après 4 jours.

Même si les viabilités obtenues pour les conditions LiEDA PVP et CHI sont différentes, les proliférations correspondantes présentent un profil similaire au ePTFE seul, approchant les 100 % de confluence après 4 jours. Ces fonctionnalisations ne semblent donc pas altérer les propriétés du ePTFE en termes de prolifération cellulaire.

La condition LiEDA semble réduire la vitesse et le taux de confluence cellulaire par rapport au matériau seul. Les fonctionnalisations PVP et CHI améliorent ces paramètres, alors que PEI les réduit davantage.

En ce qui concerne les échantillons LiDETA de la Figure **49**, nous pouvons également remarquer qu'aucun échantillon ne présente une viabilité inférieure à 70 %. LiDETA seul et avec les fonctionnalisations CHI et PVP présentent un profil de prolifération similaire, même si la viabilité de la condition LiDETA CHI est significativement plus faible. Leur confluence après 4 jours est élevée, proche de 90 %, sans atteindre les 100 % comme certains des échantillons du lot LiEDA. En effet, nous ne remarquons pas une vitesse de confluence considérablement plus lente que le ePTFE seul pour l'échantillon traité avec LiDETA, contrairement à celui avec LiEDA. Seule la condition LiDETA PEI présente une prolifération plus lente avec une confluence de 38 % après 4 jours.

Ainsi, les modifications de surface du ePTFE semblent permettre la croissance cellulaire, même si certaines ont montré une réduction significative de vitesse de croissance, n'atteignant pas de confluence maximale à la fin de l'essai. Certaines modifications comme évoqué précédemment conduisent à une viabilité significativement plus faible que le témoin, ce qui montre que les molécules libérées dans le milieu par les échantillons peuvent être nocives pour une partie non négligeable des cellules sans être cytotoxiques, car au-dessus du seuil de viabilité de 70 %. Ces tests nous ont également permis d'exclure les échantillons traités par LiHMPA pour le reste de nos tests en raison d'une cytotoxicité élevée.

#### 3.4. Tests antibactériens pour évaluer l'efficacité des traitements sélectionnés.

Six souches bactériennes ont été sélectionnées pour tester les propriétés antibactériennes des échantillons fonctionnalisés. Chaque bactérie a été testée sur chaque type d'échantillon. Ce test a pour but d'évaluer l'activité antibactérienne de chaque type de traitement. L'inoculum bactérien est déposé sur six échantillons traités et six non traités, et séché pendant 2h. Trois de chaque échantillon passent directement à l'étape d'extraction. Le reste des échantillons sont incubés pendant 24h à 37°C avant de passer à l'extraction également. L'extraction consiste à mettre les échantillons dans une solution saline d'extraction sous agitation pour récupérer les bactéries en les décollant du matériau. Cette solution est alors répartie sur une gélose de dénombrement et le comptage est réalisé après 24h d'incubation à 37°C. Pour évaluer l'effet antibactérien de nos échantillons, on calcule l'activité antibactérienne de l'échantillon étudié. Pour cela, on soustrait la croissance bactérienne de l'échantillon traité à celle d'échantillon non traité. Une activité antibactérienne négative rapporte donc *a priori* un effet antibactérien efficace de l'échantillon.

Ces tests permettent notamment une appréciation qualitative des effets antibactériens des échantillons. D'après les résultats obtenus, la seule condition présentant une activité bactérienne négative pour chacune des 6 espèces est le traitement LiDETA PEI, qui peut être considéré comme le plus efficace. Le traitement LiEDA CHI ne présente qu'une seule espèce concernée par une

diminution de la croissance bactérienne. Trois traitements, LiEDA PEI, PVP et LiDETA CHI, présentent 5 souches sur 6 avec une activité bactérienne négative. Les autres traitements présentent 3 à 4 activités bactériennes négatives, ce qui est moins intéressant pour atteindre l'objectif de couvrir le plus de souches possibles.

Dans cette étude, le nombre de répétitions (n=3) préconisé par la norme NF EN ISO 20743 n'a pas permis de réaliser une analyse statistique robuste. Par conséquent, les résultats obtenus doivent être examinés attentivement car il ne s'agit d'une évaluation sans confirmation de significativité statistique.

De plus, un biais dans les résultats doit être pris en compte : les échantillons témoins peuvent présenter des bactéries résiduelles en surface du fait de la porosité du ePTFE. Une inspection supplémentaire des échantillons après l'étape d'agitation sous vortex permettrait d'éliminer ce doute.

Ainsi, pour ces tests antibactériens préliminaires, il semble que le traitement LiDETA PEI se distingue par son apparente efficacité antibactérienne, et nous permet de conclure qu'il s'agirait d'un candidat intéressant pour de futures investigations.

## Conclusion et perspectives

Les méthodes de modification de surface du ePTFE, LiEDA et LiDETA semblent être efficaces pour réaliser la défluoruration du matériau et l'ajout de groupes amines à sa surface. LiEDA s'avère être un traitement agressif étant donné les changements importants qu'il occasionne concernant la morphologie, la structure et les propriétés du matériau. En effet, la surface devient plus rigide, avec une rugosité et une porosité apparente plus élevées. L'énergie de surface est également trois fois supérieure à celle du matériau seul. Le traitement LiDETA semble avoir un impact différent sur le matériau. La morphologie et la structure semblent moins affectées qu'avec le traitement LiEDA, mais l'énergie de surface est radicalement modifiée, la surface du matériau devenant hydrophile. La composition atomique de surfaces peut expliquer cette modification de propriétés physiques. Avec les résultats obtenus, nous pouvons supposer qu'une



différence dans le rapport C:F, de l'échantillon seul à l'échantillon traité par LiEDA (rapports passant de 1:2 à 1:1), implique une forte modification de la structure et des propriétés de surface. Une différence encore plus élevée dans ce rapport, de 1:2 à 7:1 pour LiDETA, présente une surface bien plus différente de l'original car hydrophile, mais conserve certains de ses aspects morphologiques et structurels.

La fonctionnalisation de la surface après défluoration et amination a été réalisée. Le succès du greffage de CHI et PEI est délicat à déterminer car la spectroscopie IR ne permet guère de distinguer précisément le traitement LiEDA ou LiDETA des molécules ajoutées dans un second temps. Cependant, des changements structurels du ePTFE ont pu être observés dans LiEDA CHI avec une réduction significative de la taille des fibrilles courtes.

Les tests MTT réalisés pour l'évaluation de la cytotoxicité nous montrent que les échantillons n'ont pas le même effet sur les cellules, et donc indirectement qu'ils présentent des spécificités qui peuvent être expliquées par leur fonctionnalisation. De plus, nous avons surtout pu sélectionner la combinaison de molécules pour fonctionnaliser les échantillons que nous allons étudier, en fonction de leur toxicité pour les cellules dermiques. Ainsi, les traitements LiEDA CHI, LiEDA PEI, LiEDA PVP, LiDETA CHI, LiDETA PEI et LiDETA PVP ont été choisis pour cette étude, car ils présentaient chacun une viabilité cellulaire suffisante pour ce test. Deux fonctionnalisations ont été exclues en raison de la forte toxicité pour les échantillons LiHMPA et de l'optimisation de la préparation des échantillons traités par LiEDA CHI.

Ces traitements ont ensuite été utilisés pour réaliser 336 échantillons au total à tester et évaluer leur efficacité antibactérienne. L'activité antibactérienne de 6 souches à l'origine de maladies nosocomiales a été obtenue à l'issue de ces tests. D'après les données obtenues, les traitements testés ont été efficaces sur au moins 3 bactéries. Un traitement s'est démarqué avec un effet antibactérien sur toutes les bactéries : LiDETA PEI. Ces tests, menés plutôt comme une méthode de criblage, ne comprenaient pas suffisamment d'échantillons par bactérie pour effectuer des statistiques paramétriques, même s'ils respectaient le nombre d'échantillons conseillé par la norme utilisée.

Les évaluations des propriétés bioactives réalisées dans ce projet n'ont pas considéré ou évalué la porosité comme une particularité du polymère ePTFE, ce qui peut avoir des effets sur les résultats. Les différences observées dans la confluence cellulaire pour les tests de cytotoxicité, ainsi que le nombre de bactéries dénombrées dans les tests antibactériens pourraient être expliquées ou modifiées par la porosité et l'état de surface particulier du matériau. D'autres études avec des paramètres plus détaillés seraient nécessaires pour étudier cette perspective.

Les normes et réglementations relatives aux dispositifs médicaux exigent sans aucun doute bien plus de tests pour prouver la sécurité et l'efficacité du matériau présenté ici. La mise sur le marché de tels dispositifs est encadrée par le règlement européen (UE) 2017/745, mettant à jour la directive 93/42/CEE. Un processus méticuleux doit être impérativement suivi avant qu'un dispositif médical (DM) soit prêt pour une utilisation humaine. Pour un DM de classe III comme les membranes chirurgicales, il est nécessaire de déterminer la procédure d'évaluation de sa conformité à la réglementation. Ensuite, la conformité doit être prouvée, avec un système de gestion de la qualité adéquat mis en place par l'entreprise, répondant aux exigences de la norme ISO 13495, et des documents techniques. Ces derniers doivent prouver que le DM est sûr et efficace, en utilisant des normes telles que l'ISO 10993. Cette norme garantit la biocompatibilité du dispositif, nécessitant, comme exemples non exhaustifs, des évaluations *in vitro* de la cytotoxicité, de l'hémocompatibilité, de la mutagénicité et de la génotoxicité ; ainsi que celles *in vivo* pour évaluer la toxicité systémique, la tolérance intradermique, oculaire et cutanée ou l'implantation sous-cutanée.

## Annexes

### A1

#### *LiEDA and LiDETA functionalization protocol*

ePTFE surface modification is obtained with the protocol as follow:

The material is roughly cut into squares of 1 cm. They are wiped with 90° ethanol to remove any dust.

They are then transferred in the glove box transfer cell, within a pressure of -1bar for 1 hour to remove any adsorbed gas.

They are then transferred into the glove box, filled with inert Argon gas.

100 mL of anhydrous organic solvent (EDA, DETA or HMPA) are poured in a bottle with 0.5 g of lithium, reaching a mass fraction of Li in organic solvent of 5.3%w for EDA and 5.2%w for DETA. Mass of EDA and Li used for 10 reactions are presented in Table 5.

The 10 samples are then immersed in the solution obtained and stirred with a glass-coated barrel overnight (between 17 and 18 hours).

Once the stirring step done, the samples are picked up with a glass lab spatula and dried on absorbent paper, and then put in a plastic box.

Then, the samples are directly transferred out of the glove box to a fume hood. They are then put in a glass bottle with 90° ethanol in an ultrasonic cleaner for 10 min. Then the samples are washed twice with ultrapure distilled water in the ultrasonic cleaner for 10min each time.

They are then dried on absorbent paper and left in a plastic box opened to finish the drying of the sample.

No quantification of the grafting on the surface was possible as it would need a precise scale to the microgram.

Table 5. 10 measurements of mass of Li and EDA used to modify 10 samples of ePTFE for each bottle

Bottle n°	Mass of EDA (g)	Mass of Li (g)
1	101,5	0,58
2	102,3	0,579
3	101,4	0,575
4	101,1	0,581
5	101,6	0,583
6	103	0,586
7	101,5	0,579
8	101,7	0,584
9	102,6	0,582
10	101,8	0,576

## A2

### Chitosan grafting protocol

First, 0.2g of chitosan is put in a 30mL volumetric flask with 0.094mL of  $10^{-6}$ M acid acetic solution and filled until the marking with water. The solution is stirred for 15min, then filtered with Büchner filtration. The filtrate containing the soluble fraction of chitosan is kept for the following steps.

10 ePTFE samples are immersed in the solution of chitosan with 0.30mL of glutaraldehyde solution (GA 25 %). The solution is stirred for 2 hours.

This following step is not used for all the samples: the imines reduction with  $\text{NaBH}_4$  solution. The solution of CHI and GA is removed, and the samples are immersed in 30mL of  $\text{NaBH}_4$  solution (2mg/mL). The solution is stirred for 1h30.

Whether the samples are reduced or not, they are finally rinsed three times for 10 min in distilled water with ultrasound cleaner, dried on absorbent paper and put in a box left open to dry under the hood.

### PEI grafting protocol

As the chitosan grafting protocol, a solution of PEI is realized with 0.6g of PEI and 30mL of water. The solution is stirred until homogenous. Then the 10 samples are added to the solution with 0.30mL of GA 25 %. The stirring is continued for 2 hours. No step of reduction has been done. They are finally rinsed three times for 10 min in distilled water with ultrasound cleaner, dried on absorbent paper and put in a box left open to dry under the hood.

### PVP soaking protocol

For this functionalization, the 10 samples are soaked in 15mL of a solution of absolute ethanol and 5 %w of PVP, for 2 hours. They are then rinsed and dried as previous protocols.

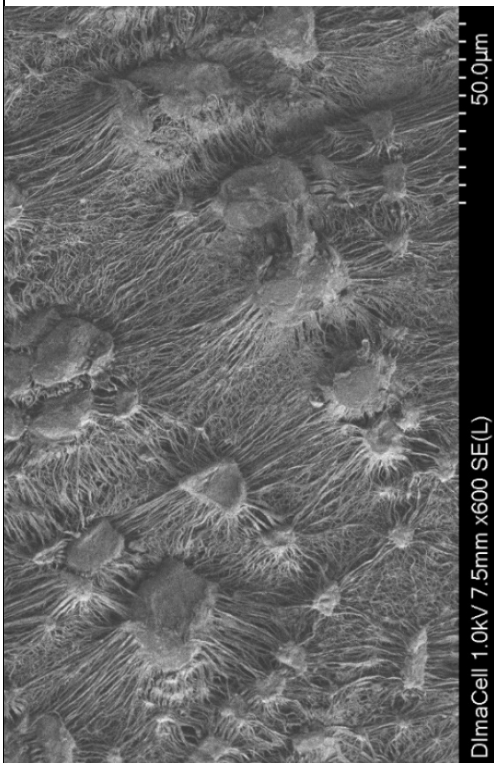
No grafting yield could be obtained as it would need a precise scale to the microgram to measure the weigh differences.

### A3

SEM images of ePTFE treated samples.

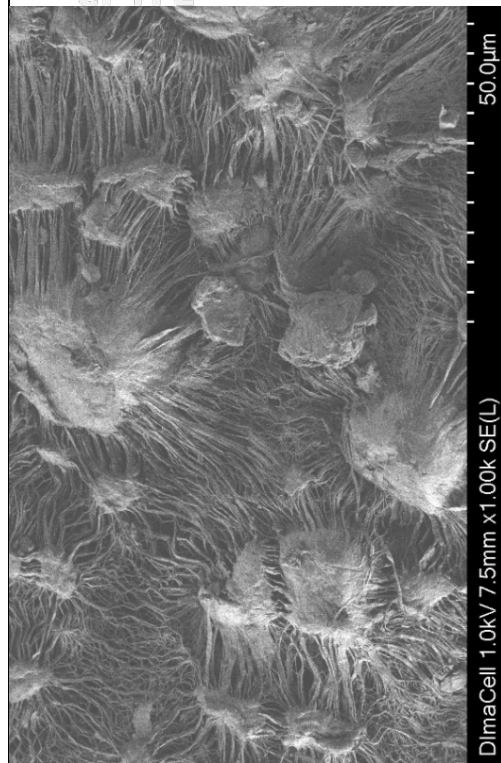
x 500 - 600

ePTFE

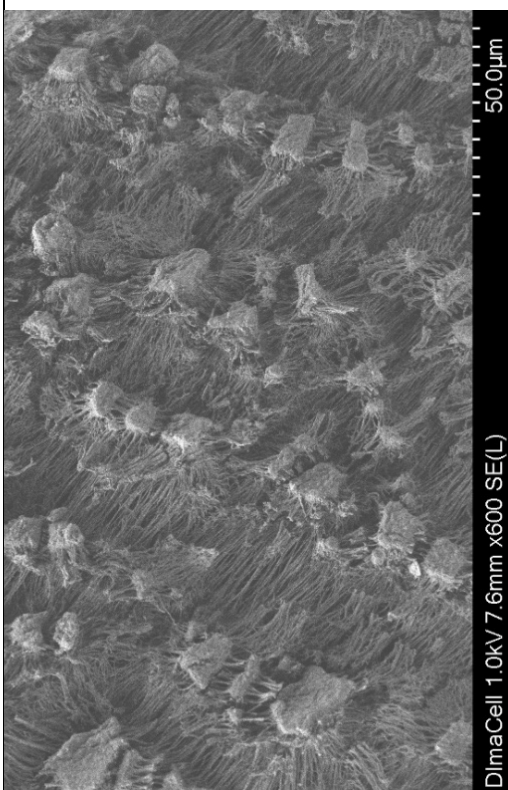


x 1000

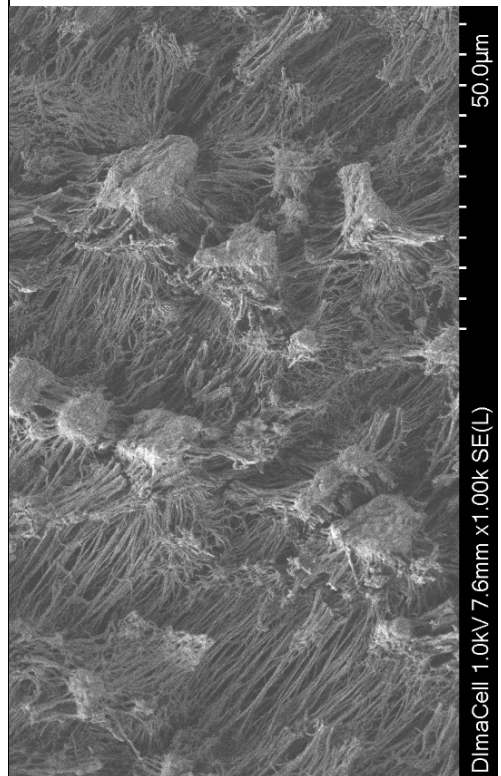
ePTFE



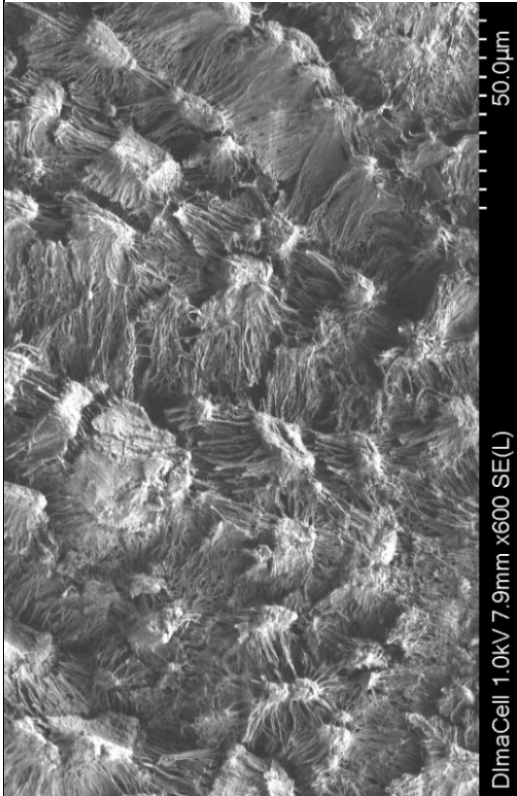
LiEDA



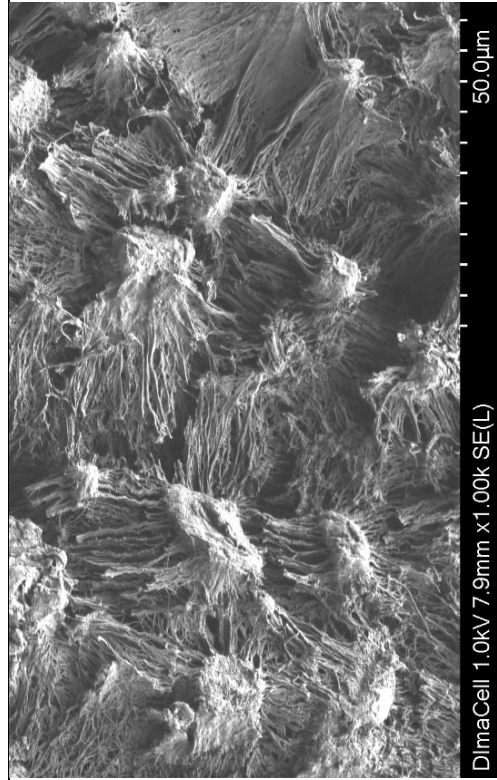
LiEDA



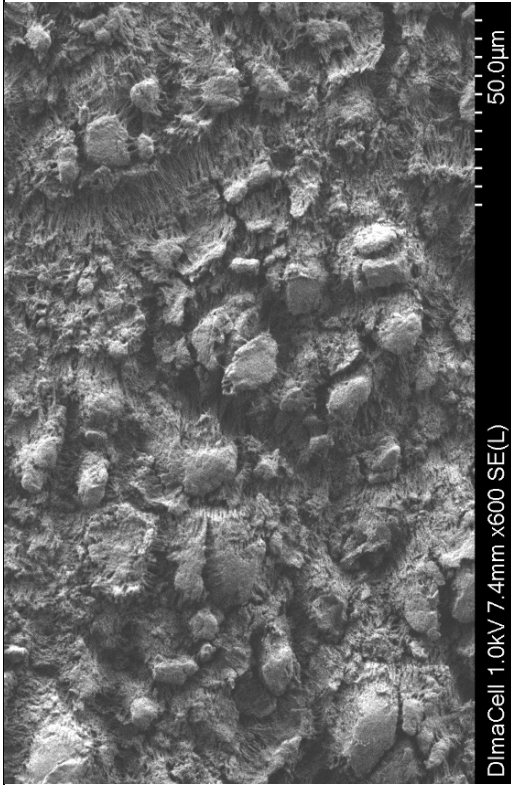
# LIEDA PEI



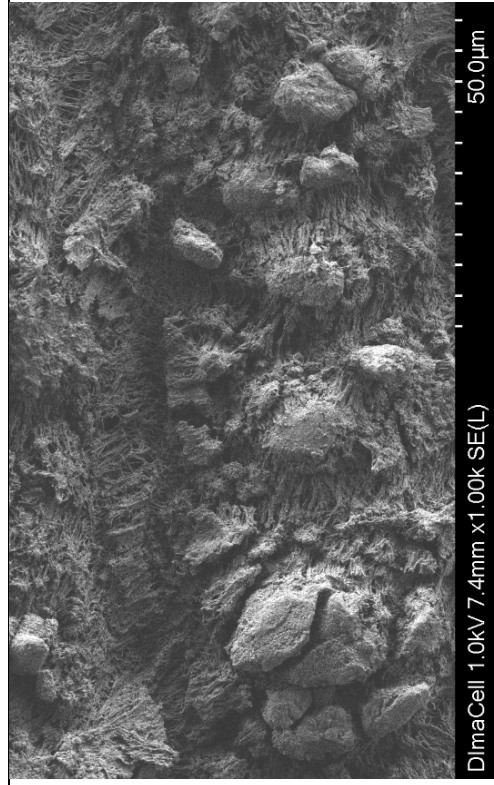
# LIEDA PEI



# LiEDA PVP

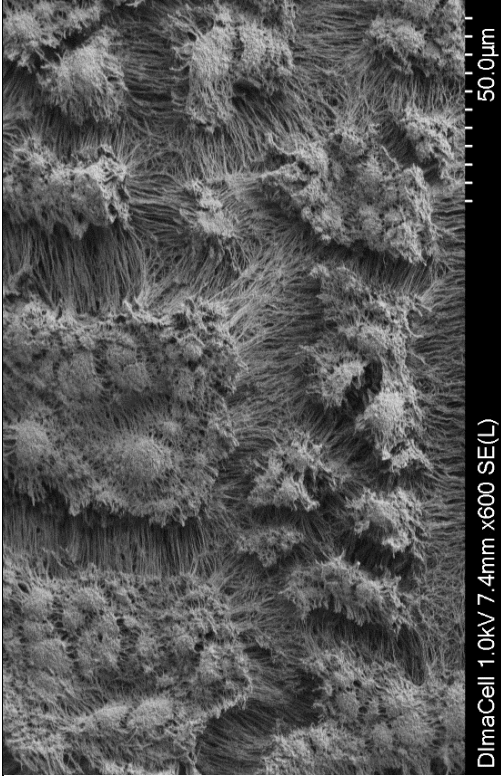


# LiEDA PVP

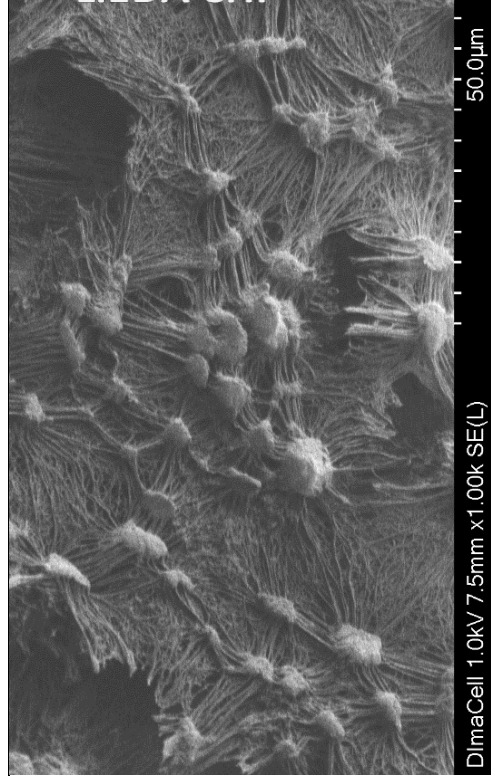




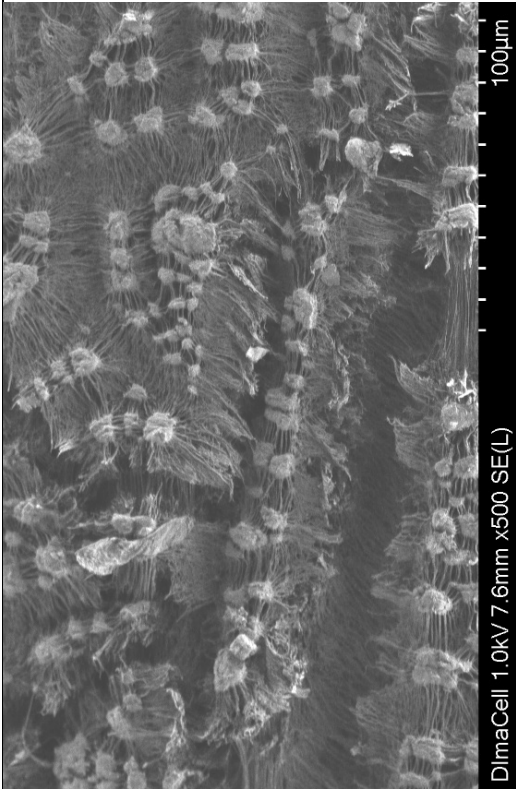
LIEDA CHI



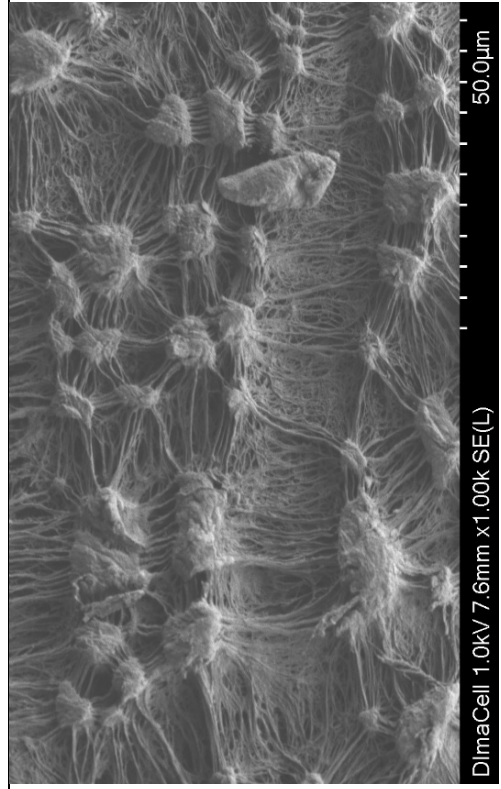
LIEDA CHI



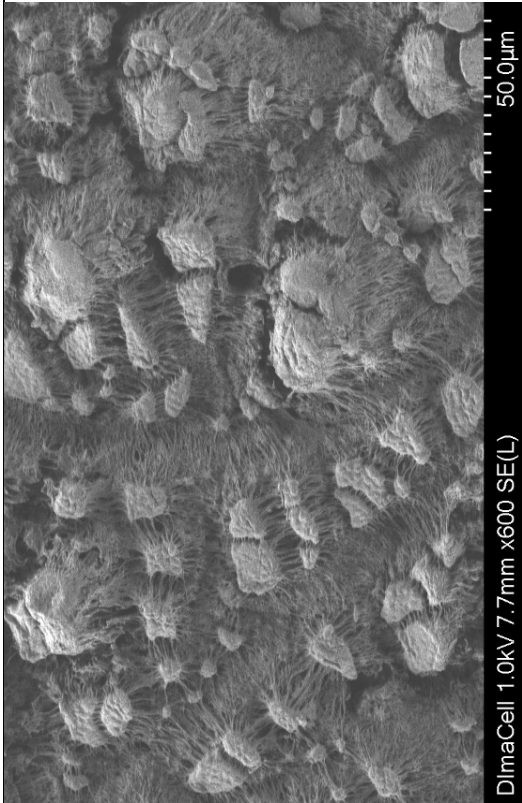
LiDETA



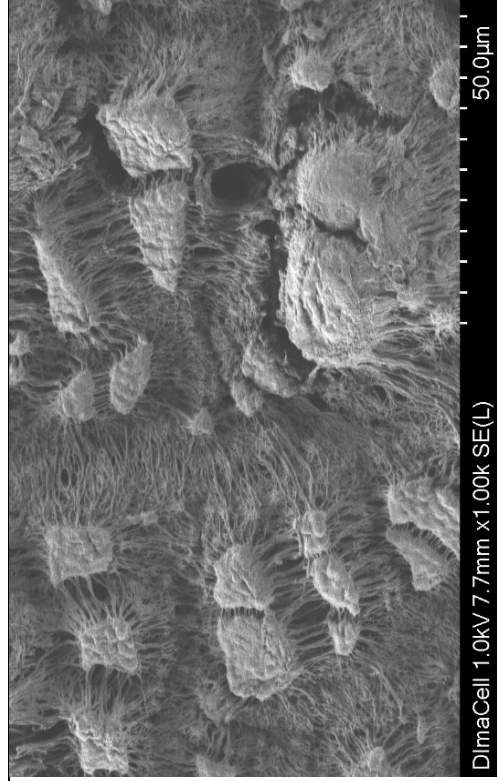
LiDETA



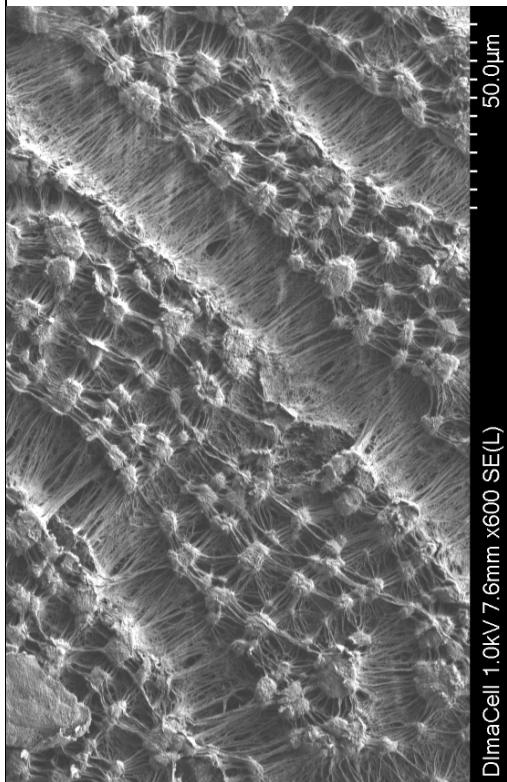
# LiDETA PVP



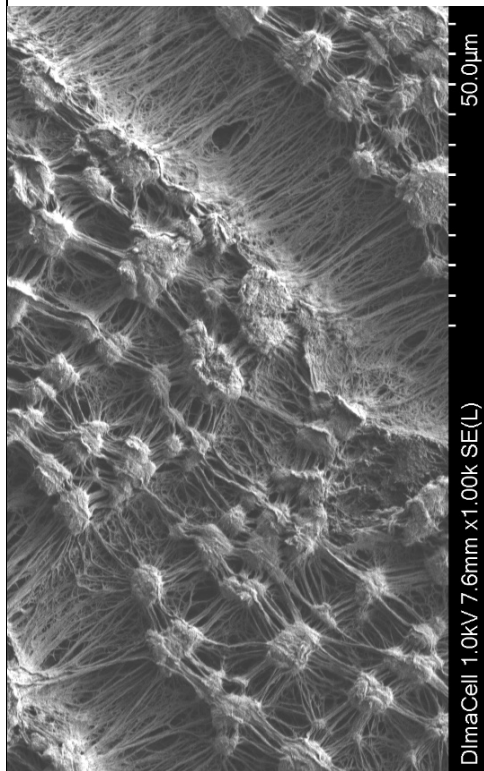
# LiDETA PVP

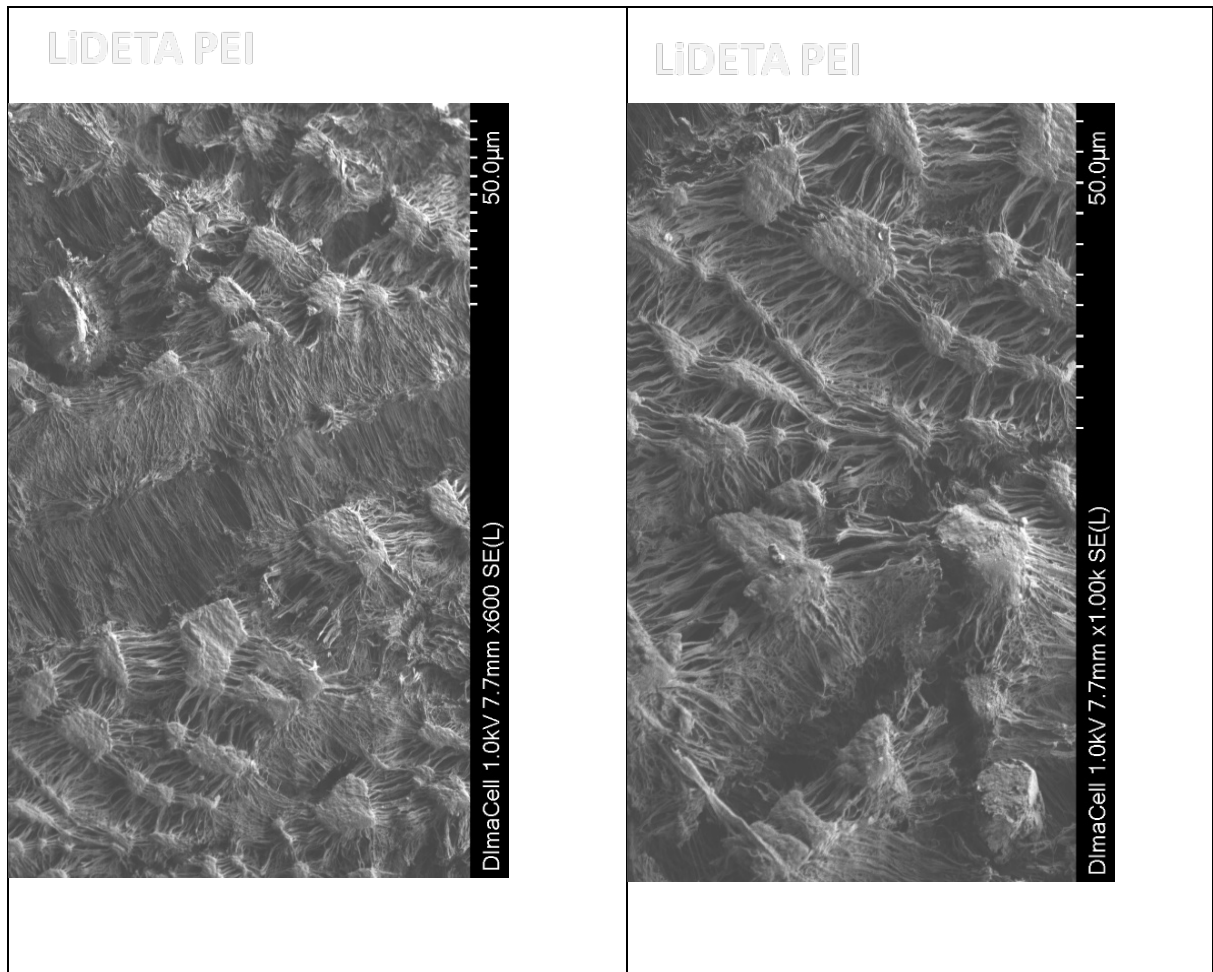


# LiDETA CHI



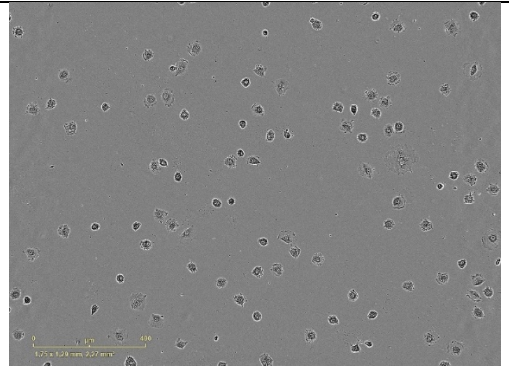
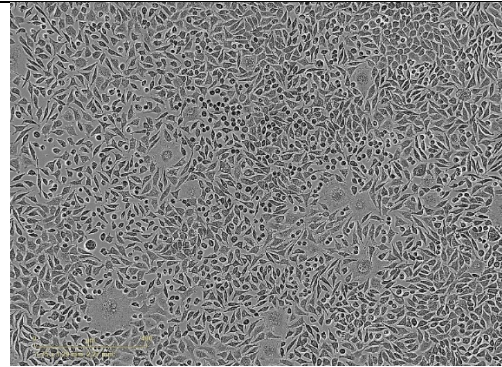
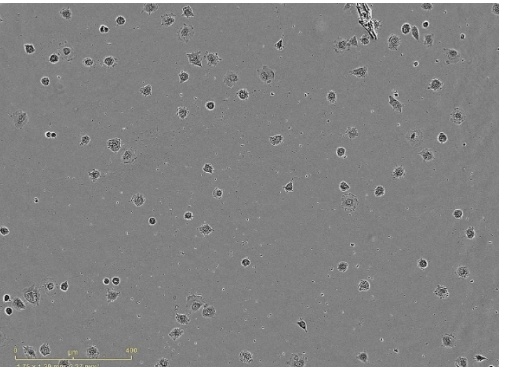
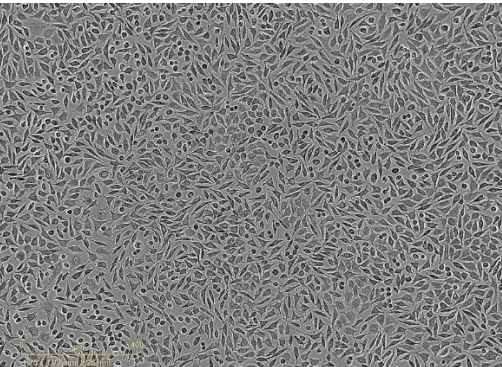
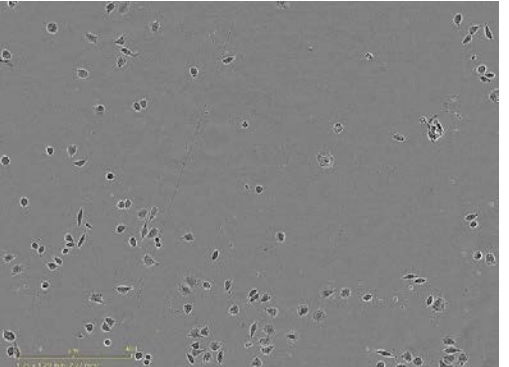
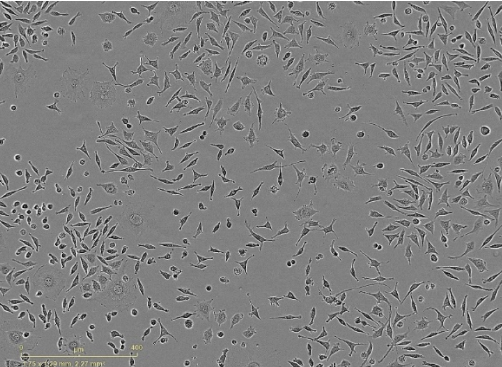
# LiDETA CHI

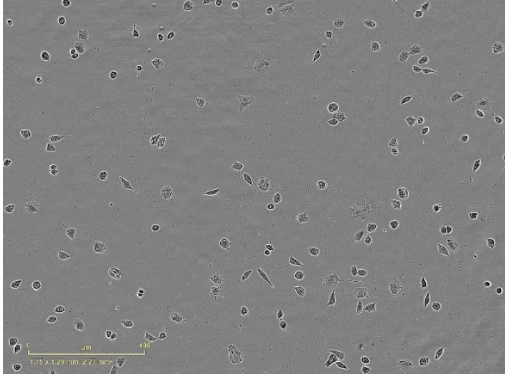
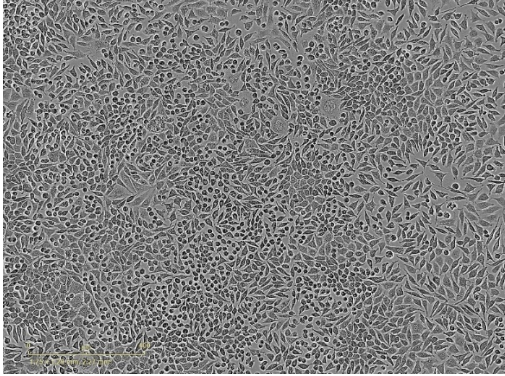
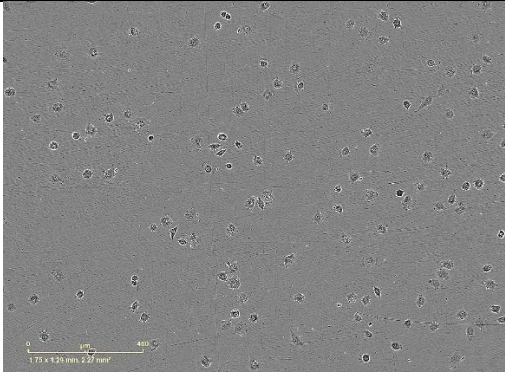
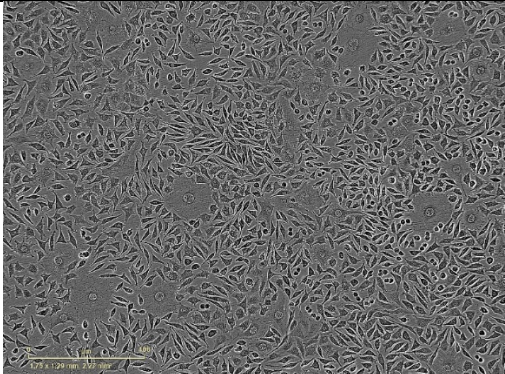
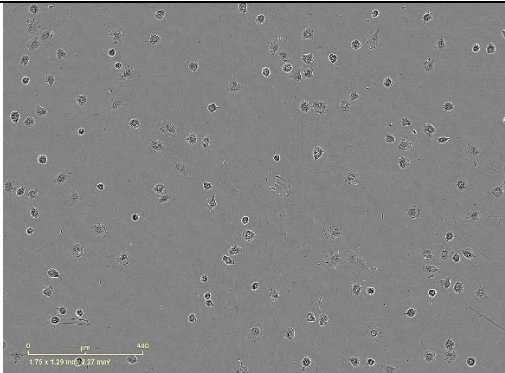
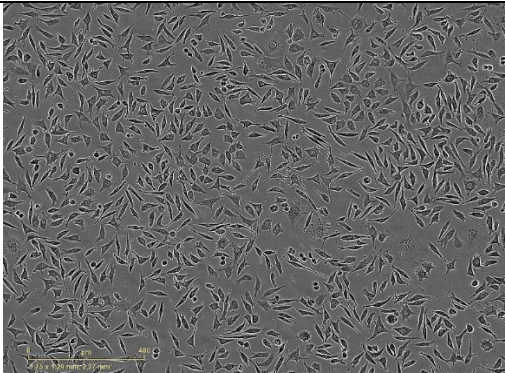




A4

Pictures from the IncucyteS3 in the next page.

Sample	T = 0 days	At t = 4 days
Control (medium only)	 <p>Micrograph showing a sparse population of cells on a dark background. A scale bar at the bottom indicates 100 μm.</p>	 <p>Micrograph showing a dense, confluent layer of cells covering the entire field of view.</p>
LiEDA CHI	 <p>Micrograph showing a sparse population of cells on a dark background. A scale bar at the bottom indicates 100 μm.</p>	 <p>Micrograph showing a dense, confluent layer of cells covering the entire field of view.</p>
LiDETA PEI	 <p>Micrograph showing a sparse population of cells on a dark background. A scale bar at the bottom indicates 100 μm.</p>	 <p>Micrograph showing a dense, confluent layer of cells covering the entire field of view.</p>

<p>LiDETA PVP</p>		
<p>DETA</p>		
<p>EDA</p>		

## References

1. Ebnesajjad, S., Expanded PTFE applications handbook : technology, manufacturing and applications. **2017**.
2. Gore, R. W. Process for producing porous products. 1973.
3. Gore, R. W. Porous products and process therefor. 1977.
4. Clark, E. S., The Crystal Structure of Polytetrafluoroethylene, Forms I and IV. *Journal of Macromolecular Science, Part B* **2006**, *45* (2), 201-213.
5. Clark, E. S., The molecular conformations of polytetrafluoroethylene: forms II and IV. *Polymer* **1999**, *40* (16), 4659-4665.
6. Eby, R. K.; Clark, E. S.; Farmer, B. L.; Piermarini, G. J.; Block, S., Crystal structure of poly(tetrafluoroethylene) homo- and copolymers in the high pressure phase. *Polymer* **1990**, *31* (12), 2227-2237.
7. Chibowski, E., Some problems of characterization of a solid surface via the surface free energy changes. *Adsorption Science & Technology* **2017**, *35* (7-8), 647-659.
8. Améduri, B., The Promising Future of Fluoropolymers. *Macromolecular Chemistry and Physics* **2020**, *221* (8), 1900573.
9. Pelagade, S. M.; Singh, N. L.; Rane, R. S.; Mukherjee, S.; Deshpande, U. P.; Ganesan, V.; Shripathi, T., Investigation of Surface Free Energy for PTFE Polymer by Bipolar Argon Plasma Treatment. **2012**, *2* (2), 132-136.
10. Jie-Rong, C.; Wakida, T., Studies on the surface free energy and surface structure of PTFE film treated with low temperature plasma. *Journal of Applied Polymer Science* **1997**, *63* (13), 1733-1739.
11. Polytetrafluoroethylene. In *Meyler's Side Effects of Drugs (Sixteenth Edition)*, Aronson, J. K., Ed. Elsevier: Oxford, 2016; pp 872-873.
12. Xia, J.; Gao, J.; Tang, W., Nosocomial infection and its molecular mechanisms of antibiotic resistance. *BioScience Trends* **2016**, *10* (1), 14-21.
13. Messina, L. M., Vascular surgery: Basic science and clinical correlations. *Journal of Vascular Surgery* **1996**, *23* (2), 380.



14. Hasse, B.; Husmann, L.; Zinkernagel, A.; Weber, R.; Lachat, M.; Mayer, D. Vascular graft infections *Swiss Med Wkly* [Online], 2013, p. w13754. PubMed. <http://europepmc.org/abstract/MED/23348860>  
<https://doi.org/10.4414/smw.2013.13754> (accessed 2013).
15. Wilson, W.; Bower, T.; Creager, M.; Amin-Hanjani, S.; O’Gara, P.; Lockhart, P.; Darouiche, R.; Ramlawi, B.; Derdeyn, C.; Bolger, A.; Levison, M.; Taubert, K.; Baltimore, R.; Baddour, L., Vascular Graft Infections, Mycotic Aneurysms, and Endovascular Infections: A Scientific Statement From the American Heart Association. *Circulation* **2016**, *134*, CIR.00000000000000457.
16. Gharamti, A.; Kanafani, Z., Vascular Graft Infections. *Infectious Disease Clinics of North America* **2018**, *32*.
17. Kilic, A.; Arnaoutakis, D.; Reifsnnyder, T.; Black, J.; Abularrage, C.; Perler, B.; Lum, Y. W., Management of infected vascular grafts. *Vascular medicine (London, England)* **2015**, *21*.
18. Kirkton, R.; Prichard, H.; Santiago-Maysonet, M.; Niklason, L.; Lawson, J.; Dahl, S., Susceptibility of ePTFE vascular grafts and bioengineered human acellular vessels to infection. *The Journal of surgical research* **2018**, *221*, 143-151.
19. Kannan, R. Y.; Salacinski, H. J.; Butler, P. E.; Hamilton, G.; Seifalian, A. M., Current status of prosthetic bypass grafts: A review. *Journal of Biomedical Materials Research Part B: Applied Biomaterials* **2005**, *74B* (1), 570-581.
20. Ratner, B. D.; Hoffman, A. S.; Schoen, F. J.; Lemons, J. E., *Biomaterials Science : an Introduction to Materials in Medicine*. Elsevier Science: Saint Louis, 2014.
21. Gabriel, M.; Niederer, K.; Becker, M.; Raynaud, C.; Vahl, C.; Frey, H., Tailoring Novel PTFE Surface Properties: Promoting Cell Adhesion and Antifouling Properties via a Wet Chemical Approach. *Bioconjugate chemistry* **2016**, *27*.
22. Talon, I.; Schneider, A.; Ball, V.; Hemmerle, J., Polydopamine Functionalization: A Smart and Efficient Way to Improve Host Responses to e-PTFE Implants. *Frontiers in Chemistry* **2019**, *7* (482).

23. Hidzir, N.; Hill, D.; Martin, D.; Grøndahl, L., In vitro mineralisation of grafted ePTFE membranes carrying carboxylate groups. *Bioactive Materials* **2017**, *2*.
24. Shao, H.-J.; Chen, C.-S.; Lee, I. C.; Wang, J.-H.; Young, T.-H., Designing a Three-dimensional Expanded Polytetrafluoroethylene-Poly(lactic-co-glycolic acid) Scaffold for Tissue Engineering. *Artificial organs* **2009**, *33*, 309-17.
25. Catalá-Icardo, M.; Torres-Cartas, S.; Meseguer-Lloret, S.; Gómez-Benito, C.; Carrasco-Correa, E.; Simó-Alfonso, E. F.; Ramis-Ramos, G.; Herrero-Martínez, J. M., Preparation of organic monolithic columns in polytetrafluoroethylene tubes for reversed-phase liquid chromatography. *Analytica Chimica Acta* **2017**, *960*, 160-167.
26. Sorribes-Soriano, A.; Arráez-González, R.; Esteve-Turrillas, F. A.; Armenta, S.; Herrero-Martínez, J. M., Development of a molecularly imprinted monolithic polymer disk for agitation-extraction of ecgonine methyl ester from environmental water. *Talanta* **2019**, *199*, 388-395.
27. Talon, I.; Schneider, A.; Ball, V.; Hemmerlé, J., Functionalization of PTFE Materials Using a Combination of Polydopamine and Platelet-Rich Fibrin. *YJSRE Journal of Surgical Research* **2020**, *251*, 254-261.
28. Gannot, I.; Harrington, J. A.; Melzer, J. E.; Mitrofanov, O.; Navarro-Cía, M.; Photonics West - Biomedical, O.; BIOS, S.; San Francisco, C. U. S.; Optical, F.; Sensors for Medical, D.; Treatment Applications, X. I. V.; Optical, F.; Sensors, I. V., Silver-coated Teflon hollow waveguides for the delivery of terahertz radiation. **2014**, 8938, 89380I-89380I-10.
29. de los Reyes, C. A.; Smith McWilliams, A. D.; Hernández, K.; Walz-Mitra, K. L.; Ergülen, S.; Pasquali, M.; Martí, A. A., Adverse Effect of PTFE Stir Bars on the Covalent Functionalization of Carbon and Boron Nitride Nanotubes Using Billups–Birch Reduction Conditions. *ACS Omega* **2019**, *4* (3), 5098-5106.
30. Shen, B.; Xiong, B.; Wu, H., Convenient surface functionalization of whole-Teflon chips with polydopamine coating. *Biomicrofluidics* **2015**, *9* (4), 044111.

31. Kwon, I. S.; Bettinger, C. J., Polydopamine nanostructures as biomaterials for medical applications. *Journal of Materials Chemistry B* **2018**, *6* (43), 6895-6903.
32. Jin, Y.; Kang, S.; Park, P.; Choi, D.; Kim, D.; Jung, D.; Koh, J.; Jeon, J.; Lee, M.; Ham, J.; Seo, J.-H.; Jin, H.-R.; Lee, Y., Anti-inflammatory and Antibacterial Effects of Covalently Attached Biomembrane-Mimic Polymer Grafts on Gore-Tex Implants. *ACS Applied Materials & Interfaces* **2017**, *9*.
33. Liu, Y.; Munisso, M. C.; Mahara, A.; Kambe, Y.; Yamaoka, T., Anti-platelet adhesion and in situ capture of circulating endothelial progenitor cells on ePTFE surface modified with poly(2-methacryloyloxyethyl phosphorylcholine) (PMPC) and hemocompatible peptide 1 (HCP-1). *Colloids and Surfaces B: Biointerfaces* **2020**, *193*, 111113.
34. Liu, Y.; Munisso, M. C.; Mahara, A.; Kambe, Y.; Fukazawa, K.; Ishihara, K.; Yamaoka, T., A surface graft polymerization process on chemically stable medical ePTFE for suppressing platelet adhesion and activation. *Biomaterials Science* **2018**, *6* (7), 1908-1915.
35. Kang, E. T.; Tan, K. L.; Kato, K.; Uyama, Y.; Ikada, Y., Surface Modification and Functionalization of Polytetrafluoroethylene Films. *Macromolecules* **1996**, *29* (21), 6872-6879.
36. Gao, A.; Hang, R.; Li, W.; Zhang, W.; Li, P.; Wang, G.; Bai, L.; Yu, X.-F.; Wang, H.; Tong, L.; Chu, P. K., Linker-free covalent immobilization of heparin, SDF-1 $\alpha$ , and CD47 on PTFE surface for antithrombogenicity, endothelialization and anti-inflammation. *Biomaterials* **2017**, *140*, 201-211.
37. Cheng, B.; Inoue, Y.; Ishihara, K., Surface functionalization of polytetrafluoroethylene substrate with hybrid processes comprising plasma treatment and chemical reactions. *Colloids and Surfaces B: Biointerfaces* **2019**, *173*, 77-84.
38. Aumswun, N.; Heinhorst, S.; Urban, M., Antibacterial Surfaces on Expanded Polytetrafluoroethylene; Penicillin Attachment. *Biomacromolecules* **2007**, *8*, 713-8.
39. Aumswun, N.; Danyus, R.; Urban, M. W.; Heinhorst, S.; th Acs National Meeting, S., The effectiveness of antibiotic activity of

penicillin attached to expanded poly (tetrafluoroethylene) (ePTFE) surfaces: A quantitative assessment. *Am Chem Soc Polym Prepr Div Polym Chem American Chemical Society, Polymer Preprints, Division of Polymer Chemistry* **2008**, 49 (1), 1086-1087.

40. Yang, G. H.; Lim, C.; Tan, Y. P.; Zhang, Y.; Kang, E. T.; Neoh, K. G., Electroless deposition of nickel on fluoropolymers modified by surface graft copolymerization. *European Polymer Journal European Polymer Journal* **2002**, 38 (11), 2153-2160.

41. Pino-Ramos, V. H.; Ramos-Ballesteros, A.; López-Saucedo, F.; López-Barriguete, J. E.; Varca, G. H. C.; Bucio, E.; SpringerLink, Radiation Grafting for the Functionalization and Development of Smart Polymeric Materials. **2016**.

42. Taimur, S.; Hassan, M. I. u.; Yasin, T.; Ali, S. W., Synthesis of modified sepiolite-g-polystyrene sulfonic acid nanohybrids by radiation induced graft polymerization. *RPC Radiation Physics and Chemistry* **2018**, 148, 19-24.

43. López-Saucedo, F.; Flores-Rojas, G. G.; Magariños, B.; Concheiro, A.; Alvarez-Lorenzo, C.; Bucio, E., Radiation grafting of poly(methyl methacrylate) and poly(vinylimidazole) onto polytetrafluoroethylene films and silver immobilization for antimicrobial performance. *Applied Surface Science* **2019**, 473, 951-959.

44. Mujgan, K.; Senem Kiralp, K.; Ayhan, B., The synthesis of complex polymer electrolytes based on alginic acid and poly(1-vinylimidazole) and application in tyrosinase immobilization. *Polymer journal / Society of Polymer Science, Japan*. **2009**, 41 (1), 46-50.

45. Al Meslmani, B.; Mahmoud, G.; Bakowsky, U., Development of Expanded Polytetrafluoroethylene Cardiovascular Graft Platform Based on Immobilization of Poly Lactic-co-Glycolic Acid Nanoparticles using a Wet Chemical Modification Technique. *International Journal of Pharmaceutics* **2017**, 529.

46. Kakinoki, S.; Nishioka, S.; Arichi, Y.; Yamaoka, T., Stable and direct coating of fibronectin-derived Leu-Asp-Val peptide on ePTFE using one-pot tyrosine oxidation for endothelial cell adhesion. *Colloids and Surfaces B: Biointerfaces* **2022**, 112576.

47. Chen, J.; Howell, C.; Haller, C.; Patel, M.; Ayala, P.; Moravec, K.; Dai, E.; Liu, L.; Sotiri, I.; Aizenberg, M.; Aizenberg, J.; Chaikof, E., An immobilized liquid interface prevents device associated bacterial infection in vivo. *Biomaterials* **2016**, *113*.
48. Wong, T.-S.; Kang, S. H.; Tang, S. K. Y.; Smythe, E. J.; Hatton, B. D.; Grinthal, A.; Aizenberg, J., Bioinspired self-repairing slippery surfaces with pressure-stable omniphobicity. *Nature* **2011**, *477* (7365), 443-447.
49. Overton, J. C.; Weigang, A.; Howell, C., Passive flux recovery in protein-fouled liquid-gated membranes. *Journal of Membrane Science* **2017**, *539*, 257-262.
50. Villegas, M.; Zhang, Y.; Abu Jarad, N.; Soleymani, L.; Didar, T. F., Liquid-Infused Surfaces: A Review of Theory, Design, and Applications. *ACS Nano* **2019**, *13* (8), 8517-8536.
51. Cheng, C.-F.; Lee, Y.-Y.; Chi, L.-Y.; Chen, Y.-T.; Hung, S.-L.; Ling, L.-J., Bacterial Penetration Through Antibiotic-Loaded Guided Tissue Regeneration Membranes. *Journal of periodontology* **2009**, *80*, 1471-8.
52. Sa, M.; Goksin, I.; Baltarali, A.; Turgut, H.; Sacar, S.; Onem, G.; Ozcan, V.; Adali, F., The Prophylactic Efficacy of Rifampicin-Soaked Graft in Combination with Systemic Vancomycin in the Prevention of Prosthetic Vascular Graft Infection: An Experimental Study. *The Journal of surgical research* **2005**, *129*, 329-34.
53. Fischer, P.; Schroepfel, T.; Fabian, T.; De Rijk, W.; Edwards, N.; Magnotti, L.; Doty, D.; Croce, M., Antibiotic-Coated ePTFE Decreases Graft Colonization and Neointimal Hyperplasia<sup>1</sup>. *The Journal of surgical research* **2009**, *156*, 199-204.
54. Wulff, B.; Stahlhoff, S.; Vonthein, R.; Schmidt, A.; Sigler, M.; Torsello, G. B.; Herten, M., Biomimetic Heparan Sulfate-Like Coated ePTFE Grafts Reduce In-graft Neointimal Hyperplasia in Ovine Carotids. *Annals of Vascular Surgery* **2017**, *40*, 274-284.
55. Prevention., C. f. D. C. a. *Antibiotic Resistance Threats in the United States, 2019 (2019 AR Threats Report)*; 2019.
56. European Centre for Disease, P.; Control; European Medicines, A., *The bacterial challenge : time to react : a call to narrow the gap*

*between multidrug-resistant bacteria in the EU and the development of new antibacterial agents.* Publications Office of the European Union: Luxembourg, 2009.

57. Barnard, J.; Humphreys, J.; Bittar, M., Endovascular versus open surgical repair for blunt thoracic aortic injury. *Interactive cardiovascular and thoracic surgery* **2009**, *9*, 506-9.

58. Lei, Z.-y.; Li, J.; Liu, T.; Shi, X.-h.; Fan, D.-l., Autologous Vascularization: A Method to Enhance the Antibacterial Adhesion Properties of ePTFE. *Journal of Surgical Research* **2019**, *236*, 352-358.

59. Geelhoed, W. J.; van der Bogt, K. E. A.; Rothuizen, T. C.; Damanik, F. F. R.; Hamming, J. F.; Mota, C. D.; van Agen, M. S.; de Boer, H. C.; Restrepo, M. T.; Hinz, B.; Kislaya, A.; Poelma, C.; van Zonneveld, A. J.; Rabelink, T. J.; Moroni, L.; Rotmans, J. I., A novel method for engineering autologous non-thrombogenic in situ tissue-engineered blood vessels for arteriovenous grafting. *Biomaterials* **2020**, *229*, 119577.

60. Zhang, J.; Wang, Y.; Liu, C.; Feng, F.; Wang, D.; Mo, H.; Si, L.; Wei, G.; Shen, J., Polyurethane/polyurethane nanoparticle-modified expanded poly(tetrafluoroethylene) vascular patches promote endothelialization. *Journal of Biomedical Materials Research Part A* **2018**, *106* (8), 2131-2140.

61. Bastijanic, J. M.; Marchant, R. E.; Kligman, F.; Allemang, M. T.; Lakin, R. O.; Kendrick, D.; Kashyap, V. S.; Kottke-Marchant, K., In vivo evaluation of biomimetic fluorosurfactant polymer-coated expanded polytetrafluoroethylene vascular grafts in a porcine carotid artery bypass model. *Journal of Vascular Surgery* **2016**, *63* (6), 1620-1630.e4.

62. Lee, H.; Lee, Y.; Statz, A. R.; Rho, J.; Park, T. G.; Messersmith, P. B., Substrate-Independent Layer-by-Layer Assembly by Using Mussel-Adhesive-Inspired Polymers. *Adv Mater* **2008**, *20* (9), 1619-1623.

63. Ku, S. H.; Ryu, J.; Hong, S. K.; Lee, H.; Park, C. B., General functionalization route for cell adhesion on non-wetting surfaces. *JBMT Biomaterials* **2010**, *31* (9), 2535-2541.

64. Lu, S.; Zhang, P.; Sun, X.; Gong, F.; Yang, S.; Shen, L.; Huang, Z.; Wang, C., Synthetic ePTFE Grafts Coated with an Anti-CD133 Antibody-Functionalized Heparin/Collagen Multilayer with Rapid in

vivo Endothelialization Properties. *ACS Applied Materials & Interfaces* **2013**, *5* (15), 7360-7369.

65. Shan, Y.; Jia, B.; Ye, M.; Shen, H.; Chen, W.; Zhang, H., Application of Heparin/Collagen-REDV Selective Active Interface on ePTFE Films to Enhance Endothelialization and Anticoagulation. *Artificial Organs* **2018**, *42* (8), 824-834.

66. Hoshi, R.; Lith, R.; Jen, M.; Allen, J.; Lapidos, K.; Ameer, G., The blood and vascular cell compatibility of heparin-modified ePTFE vascular grafts. *Biomaterials* **2012**, *34*.

67. Pfeiffer, D.; Wankhammer, K.; Stefanitsch, C.; Hingerl, K.; Huppertz, B.; Dohr, G.; Desoye, G.; Lang, I., Amnion-derived mesenchymal stem cells improve viability of endothelial cells exposed to shear stress in ePTFE grafts. *The International Journal of Artificial Organs* **2018**, *42* (2), 80-87.

68. Tzchori, I.; Falah, M.; Shteynberg, D.; Levin Ashkenazi, D.; Loberman, Z.; Perry, L.; Flugelman, M. Y., Improved Patency of ePTFE Grafts as a Hemodialysis Access Site by Seeding Autologous Endothelial Cells Expressing Fibulin-5 and VEGF. *Molecular Therapy* **2018**, *26* (7), 1660-1668.

69. Tasiopoulos, C. P.; Widhe, M.; Hedhammar, M., Recombinant Spider Silk Functionalized with a Motif from Fibronectin Mediates Cell Adhesion and Growth on Polymeric Substrates by Entrapping Cells During Self-Assembly. *ACS Applied Materials & Interfaces* **2018**, *10* (17), 14531-14539.

70. Preis, M.; Schneiderman, J.; Koren, B.; Ben-Yosef, Y.; Levin-Ashkenazi, D.; Shapiro, S.; Cohen, T.; Blich, M.; Israeli-Amit, M.; Sarnatzki, Y.; Gershtein, D.; Shofty, R.; Lewis, B.; Shaul, Y.; Flugelman, M., Co-expression of Fibulin-5 and VEGF165 increases long-term patency of synthetic vascular grafts seeded with autologous endothelial cells. *Gene Therapy* **2015**, *23*.

71. Weinbaum, J. S.; Haskett, D. G.; Mandelkern, T. F.; Vorp, D. A., Advances in Cell Seeding of Tissue Engineered Vascular Grafts. In *Tissue-Engineered Vascular Grafts*, Walpoth, B. H.; Bergmeister, H.; Bowlin, G. L.; Kong, D.; Rotmans, J. I.; Zilla, P., Eds. Springer International Publishing: Cham, 2020; pp 295-319.

72. Wang, D.; Xu, Y.; Lin, Y.-J.; Yilmaz, G.; Zhang, J.; Schmidt, G.; Li, Q.; Thomson, J. A.; Turng, L.-S., Biologically Functionalized Expanded Polytetrafluoroethylene Blood Vessel Grafts. *Biomacromolecules* **2020**, *21* (9), 3807-3816.
73. Zilla, P.; Bezuidenhout, D.; Human, P., Prosthetic vascular grafts: wrong models, wrong questions and no healing. *Biomaterials* **2007**, *28* (34), 5009-27.
74. Pawlowski, K.; Rittgers, S.; Schmidt, S.; Bowlin, G., Endothelial cell seeding of polymeric vascular grafts. *Frontiers in bioscience : a journal and virtual library* **2004**, *9*, 1412-21.
75. Roland Horres, M. K. L., Michael Hoffmann, Volker Faust, Erika Hoffmann, Donato Di Biase Compounds and method for coating surfaces in a haemocompatible manner 05-09, 2002.
76. Hiruma, H.; Toida, H.; Hanawa, T.; Sakuragi, H.; Suzuki, Y., Ion beam modification of ePTFE for improving the blood compatibility. *Surface & Coatings Technology - SURF COAT TECH* **2011**, *206*, 905-910.
77. Talon, I.; Schneider, A.; Mathieu, E.; Senger, B.; Frisch, B.; Seguin, C.; Ball, V.; Hemmerl' , J., How Polydopamine Modulates Biological Responses to PTFE Prostheses. *Materials Sciences and Applications* **2019**, *Vol.10No.05*, 16.
78. Cheng, B.; Ishihara, K.; Ishihara, K., Formation of stable polydopamine layer on polytetrafluoroethylene substrate by hybrid process involved plasma treatment and spontaneous chemical reactions. *Mater. Today Commun. Materials Today Communications* **2020**, *22*.
79. Liu, Z.; Qu, S.; Weng, J., Application of Polydopamine in Surface Modification of Biomaterials. *Progress in Chemistry* **2015**, *27*, 212-219.
80. Fowler, P. M. P. T.; Dizon, G. V.; Tayo, L. L.; Caparanga, A. R.; Huang, J.; Zheng, J.; Aimar, P.; Chang, Y., Surface Zwitterionization of Expanded Poly(tetrafluoroethylene) via Dopamine-Assisted Consecutive Immersion Coating. *ACS Applied Materials & Interfaces* **2020**, *12* (37), 41000-41010.
81. Kim, D.; Chung, J. J.; Jung, Y.; Kim, S. H., The effect of Substance P/Heparin conjugated PLCL polymer coating of bioinert ePTFE vascular



- grafts on the recruitment of both ECs and SMCs for accelerated regeneration. *Scientific Reports* **2019**, *9* (1), 17083.
82. Cassady, A. I.; Hidzir, N. M.; Grøndahl, L., Enhancing expanded poly(tetrafluoroethylene) (ePTFE) for biomaterials applications. *Journal of Applied Polymer Science* **2014**, *131* (15).
83. Feddes, B.; Wolke, J.; Vredenberg, A. M.; Jansen, J., Adhesion of calcium phosphate ceramic on polyethylene (PE) and polytetrafluoroethylene (PTFE). *Surface and Coatings Technology* **2004**, *184*.
84. Feddes, B.; Wolke, J.; Weinhold, W. P.; Vredenberg, A. M.; Jansen, J., Adhesion of calcium phosphate coatings on polyethylene (PE), polystyrene (PS), poly(tetrafluoroethylene) (PTFE), poly(dimethylsiloxane) (PDMS) and poly-L-lactic acid (PLLA). *Journal of Adhesion Science and Technology* **2004**, *18*.
85. Tong, L.; Kwok, D.; Wang, H.; Wu, L.; Chu, P., Surface Structures and Osteoblast Activity on Biomedical Polytetrafluoroethylene Treated by Long-Pulse, High-Frequency Oxygen Plasma Immersion Ion Implantation. *Advanced Engineering Materials* **2010**, *12*, B163-B169.
86. Wang, H.; Kwok, D.; Xu, M.; Shi, H.; Wu, Z.; Zhang, W.; Chu, P., Tailoring of Mesenchymal Stem Cells Behavior on Plasma-Modified Polytetrafluoroethylene. *Adv Mater* **2012**, *24*, 3315-24.
87. Jiang, Z.; Yu, Y.; Du, L.; Ding, X.; Xu, H.; Sun, Y.; Zhang, Q., Peptide derived from Pvf<sub>1</sub>-1 as bioadhesive on bio-inert surface. *Colloids and surfaces. B, Biointerfaces* **2011**, *90*, 227-35.
88. Tasiopoulos, C. P.; Petronis, S.; Sahlin, H.; Hedhammar, M., Surface Functionalization of PTFE Membranes Intended for Guided Bone Regeneration Using Recombinant Spider Silk. *ACS Applied Bio Materials* **2020**, *3* (1), 577-583.
89. Borhani, S.; Hassanajili, S.; Ahmadi Tafti, S. H.; Rabbani, S., Cardiovascular stents: overview, evolution, and next generation. *Prog. Biomater. Progress in Biomaterials* **2018**, *7* (3), 175-205.
90. Luo, X.; Wang, X.; Zhu, Y.; Xi, X.; Zhao, Y.; Yang, J.; Li, X.; Yang, L., Clinical Efficacy of Transjugular Intrahepatic Portosystemic Shunt Created with Expanded Polytetrafluoroethylene-Covered Stent-Grafts:

8-mm Versus 10-mm. *CardioVascular and Interventional Radiology* **2019**, *42* (5), 737-743.

91. Liu, J.; Meng, J.; Zhou, C.; Shi, Q.; Yang, C.; Ma, J.; Chen, M.; Xiong, B., A New Choice of Stent for Transjugular Intrahepatic Portosystemic Shunt Creation: Viabahn ePTFE Covered Stent/Bare Metal Stent Combination. *Journal of Interventional Medicine* **2020**.

92. Gupta, A. C.; Wang, W.; Shah, C.; Sands, M. J.; Bullen, J.; Remer, E. M.; Bayona, P. M.; Carey, W.; Kapoor, B., Added Value of Covered Stents in Transjugular Intrahepatic Portosystemic Shunt: A Large Single-Center Experience. *CardioVascular and Interventional Radiology* **2017**, *40* (11), 1723-1731.

93. Li, T.; Sun, P.; Belgaumkar, A. P.; Sun, Y.; Cheng, X.; Zheng, Q., Expanded polytetrafluoroethylene (ePTFE)-covered stents versus bare stents for transjugular intrahepatic portosystemic shunt in people with liver cirrhosis. *Cochrane Database Syst Rev* **2016**, *2016* (9), CD012358.

94. Bucsecs, T.; Schoder, M.; Diermayr, M.; Feldner-Busztin, M.; Goeschl, N.; Bauer, D.; Schwabl, P.; Mandorfer, M.; Angermayr, B.; Cejna, M.; Ferlitsch, A.; Sieghart, W.; Trauner, M.; Peck-Radosavljevic, M.; Karner, J.; Karnel, F.; Reiberger, T., Transjugular intrahepatic portosystemic shunts (TIPS) for the prevention of variceal re-bleeding - A two decades experience. *PloS one* **2018**, *13* (1).

95. Paravastu, S. C. V.; Jayarajasingam, R.; Cottam, R.; Palfreyman, S. J.; Michaels, J. A.; Thomas, S. M.; Thomas, S. M., Endovascular repair of abdominal aortic aneurysm. *Cochrane Database of Systematic Reviews* **2014**, (1).

96. Schermerhorn, M. L.; O'Malley, A. J.; Jhaveri, A.; Cotterill, P.; Pomposelli, F.; Landon, B. E., Endovascular vs. Open Repair of Abdominal Aortic Aneurysms in the Medicare Population. *N Engl J Med New England Journal of Medicine* **2008**, *358* (5), 464-474.

97. Peterson, B. G.; Matsumura, J. S.; Brewster, D. C.; Makaroun, M. S., Five-year report of a multicenter controlled clinical trial of open versus endovascular treatment of abdominal aortic aneurysms. *Journal of Vascular Surgery* **2007**, *45* (5), 885-890.

98. Schermerhorn, M. L.; Buck, D. B.; O'Malley, A. J., Long-Term Outcomes of Abdominal Aortic Aneurysm in the Medicare Population. *Journal of Vascular Surgery Journal of Vascular Surgery* **2016**, *63* (1), 280.
99. Patel, R.; Sweeting, M. J.; Powell, J. T.; Greenhalgh, R. M.; investigators, E. t., Endovascular versus open repair of abdominal aortic aneurysm in 15-years' follow-up of the UK endovascular aneurysm repair trial 1 (EVAR trial 1): a randomised controlled trial. *Lancet (London, England)* **2016**, *388* (10058), 2366-2374.
100. Antoniou, G. A.; Antoniou, S. A.; Torella, F., Editor's Choice - Endovascular vs. Open Repair for Abdominal Aortic Aneurysm: Systematic Review and Meta-analysis of Updated Peri-operative and Long Term Data of Randomised Controlled Trials. *European journal of vascular and endovascular surgery* **2020**, *59* (3), 385-397.
101. Kontopodis, N.; Galanakis, N.; Antoniou, S. A.; Tsetis, D.; Ioannou, C. V.; Veith, F. J.; Powell, J. T.; Antoniou, G. A., Meta-Analysis and Meta-Regression Analysis of Outcomes of Endovascular and Open Repair for Ruptured Abdominal Aortic Aneurysm. *YEJVS European Journal of Vascular & Endovascular Surgery* **2020**, *59* (3), 399-410.
102. Jonker, F. H. W.; Trimarchi, S.; Verhagen, H. J. M.; Moll, F. L.; Sumpio, B. E.; Muhs, B. E., Meta-analysis of open versus endovascular repair for ruptured descending thoracic aortic aneurysm. *Journal of Vascular Surgery Journal of Vascular Surgery* **2010**, *51* (4), 1026-1032.e2.
103. Dake, M. D.; Miller, D. C.; Semba, C. P.; Mitchell, R. S.; Walker, P. J.; Liddell, R. P., Transluminal Placement of Endovascular Stent-Grafts for the Treatment of Descending Thoracic Aortic Aneurysms. *The New England Journal of Medicine* **1994**, *331* (26), 1729-1734.
104. Goodney, P. P.; Travis, L.; Lucas, F. L.; Fillinger, M. F.; Goodman, D. C.; Cronenwett, J. L.; Stone, D. H., Survival After Open Versus Endovascular Thoracic Aortic Aneurysm Repair in an Observational Study of the Medicare Population. *Circulation Circulation* **2011**, *124* (24), 2661-2669.
105. Codner, J. A.; Lou, X.; Chen, E. P.; Leshnowar, B. G.; Duwayri, Y. M.; Jordan, W. D.; Binongo, J. N.; Moon, R., The distance of the

- primary intimal tear from the left subclavian artery predicts aortic growth in uncomplicated type B aortic dissection. *J. Vasc. Surg. Journal of Vascular Surgery* **2019**, *69* (3), 692-700.
106. Walschot, L. H.; Laheij, R. J.; Verbeek, A. L., Outcome after endovascular abdominal aortic aneurysm repair: a meta-analysis. *Journal of endovascular therapy : an official journal of the International Society of Endovascular Specialists* **2002**, *9* (1), 82-9.
107. Hong, C.; Heiken, J. P.; Sicard, G. A.; Pilgram, T. K.; Bae, K. T., Clinical Significance of Endoleak Detected on Follow-Up CT After Endovascular Repair of Abdominal Aortic Aneurysm. *American Journal of Roentgenology American Journal of Roentgenology* **2008**, *191* (3), 808-813.
108. England, A.; Mc Williams, R., Endovascular aortic aneurysm repair (EVAR). *Ulster Med J* **2013**, *82* (1), 3-10.
109. Turney, E. J.; Steenberge, S. P.; Lyden, S. P.; Eagleton, M. J.; Srivastava, S. D.; Sarac, T. P.; Kelso, R. L.; Clair, D. G., Late graft explants in endovascular aneurysm repair. *Journal of Vascular Surgery* **2014**, *59* (4), 886-893.
110. Kouvelos, G. N.; Oikonomou, K.; Antoniou, G. A.; Verhoeven, E. L.; Katsargyris, A., A Systematic Review of Proximal Neck Dilatation After Endovascular Repair for Abdominal Aortic Aneurysm. *Journal of endovascular therapy : an official journal of the International Society of Endovascular Specialists* **2017**, *24* (1), 59-67.
111. Savlovskis, J.; Krievins, D.; de Vries, J.-P. P. M.; Holden, A.; Kisis, K.; Gedins, M.; Ezite, N.; Zarins, C. K., Aortic neck enlargement after endovascular aneurysm repair using balloon-expandable versus self-expanding endografts. *Journal of Vascular Surgery* **2015**, *62* (3), 541-549.
112. Swerdlow, N. J.; Lyden, S. P.; Verhagen, H. J. M.; Schermerhorn, M. L., Five-year results of endovascular abdominal aortic aneurysm repair with the Ovation abdominal stent graft. *YMVA Journal of Vascular Surgery* **2020**, *71* (5), 1528-1537.e2.
113. Kocaaslan, C.; Aldag, M.; Kehlibar, T.; Yilmaz, M.; Aydin, E.; Ketenci, B., Open repair of a type Ia endoleak with a giant abdominal aortic aneurysm sac. *Northern clinics of Istanbul* **2018**, *5* (3), 261-263.

114. de Donato, G.; Pasqui, E.; Panzano, C.; Brancaccio, B.; Grottola, G.; Galzerano, G.; Benevento, D.; Palasciano, G., The Polymer-Based Technology in the Endovascular Treatment of Abdominal Aortic Aneurysms. *Polymers* **2021**, *13* (8), 1196.
115. Stollwerck, P. L.; Kozlowski, B.; Sandmann, W.; Grabitz, K.; Pfeiffer, T., Long-term dilatation of polyester and expanded polytetrafluoroethylene tube grafts after open repair of infrarenal abdominal aortic aneurysms. *J Vasc Surg* **2011**, *53* (6), 1506-13.
116. Voûte, M. T.; Bastos Gonçalves, F. M.; van de Luijtgarden, K. M.; Klein Nulent, C. G. A.; Hoeks, S. E.; Stolker, R. J.; Verhagen, H. J. M., Stent graft composition plays a material role in the postimplantation syndrome. *Journal of Vascular Surgery* **2012**, *56* (6), 1503-1509.
117. Dake, M. D.; Miller, D. C.; Semba, C. P.; Mitchell, R. S.; Walker, P. J.; Liddell, R. P., Transluminal placement of endovascular stent-grafts for the treatment of descending thoracic aortic aneurysms. *N Engl J Med* **1994**, *331* (26), 1729-34.
118. Jonker, F. H.; Trimarchi, S.; Verhagen, H. J.; Moll, F. L.; Sumpio, B. E.; Muhs, B. E., Meta-analysis of open versus endovascular repair for ruptured descending thoracic aortic aneurysm. *J Vasc Surg* **2010**, *51* (4), 1026-32, 1032.e1-1032.e2.
119. Mezzetto, L.; Scorsone, L.; Silingardi, R.; Gennai, S.; Leone, N.; Piffaretti, G.; Veraldi, G. F., Early and Long-term Results of ePTFE (Gore TAG®) versus Dacron (Relay Plus® Bolton) Grafts in Thoracic Endovascular Aneurysm Repair. *Annals of Vascular Surgery* **2021**, *71*, 419-427.
120. Laarman, G. J.; Kiemeneij, F.; Mueller, R.; Guagliumi, G.; Cebaugh, M.; Serruys, P. W.; Symbiot, I. I. T. I., Feasibility, safety, and preliminary efficacy of a novel ePTFE-covered self-expanding stent in saphenous vein graft lesions: the Symbiot II trial. *Catheterization and cardiovascular interventions : official journal of the Society for Cardiac Angiography & Interventions* **2005**, *64* (3), 361-8.
121. Turco, M. A.; Buchbinder, M.; Popma, J. J.; Weissman, N. J.; Mann, T.; Doucet, S.; Johnson, W. L., Jr.; Greenberg, J. D.; Leadley, K.; Russell, M. E., Pivotal, randomized U.S. study of the Symbiottrade mark covered stent system in patients with saphenous vein graft

disease: eight-month angiographic and clinical results from the Symbiot III trial. *Catheterization and cardiovascular interventions : official journal of the Society for Cardiac Angiography & Interventions* **2006**, *68* (3), 379-88.

122. Dhondt, E.; Vanlangenhove, P.; Geboes, K.; Vandenabeele, L.; Van Cauwenberghe, L.; Defreyne, L., No evidence of improved efficacy of covered stents over uncovered stents in percutaneous palliation of malignant hilar biliary obstruction: results of a prospective randomized trial. *European Radiology* **2020**, *30* (1), 175-185.

123. Hui, A.; Krokidis, M., ePTFE/FEP stents for malignant biliary obstruction. *BMJ Supportive & Palliative Care* **2020**, bmjspcare-2019-001961.

124. Gwon, D. I.; Ko, G. Y.; Sung, K. B.; Yoon, H. K.; Shin, J. H.; Kim, J. H.; Kim, J.; Oh, J. Y.; Song, H. Y., A novel double stent system for palliative treatment of malignant extrahepatic biliary obstructions: A pilot study. *Am. J. Roentgenol. American Journal of Roentgenology* **2011**, *197* (5), W942-W947.

125. Yi, R.; Gwon, D. I.; Ko, G. Y.; Yoon, H. K.; Kim, J. H.; Shin, J. H.; Sung, K. B., Percutaneous unilateral placement of biliary covered metallic stent in patients with malignant hilar biliary obstruction and contralateral portal vein occlusion. *Acta Radiol. Acta Radiologica* **2012**, *53* (7), 742-749.

126. Gwon, D. I.; Ko, G.-Y.; Kim, J. H.; Yoon, H.-K.; Lee, I. S.; Kim, K.-A.; Sung, K.-B., A Comparative Analysis of PTFE-Covered and Uncovered Stents for Palliative Treatment of Malignant Extrahepatic Biliary Obstruction. *AJR, American journal of roentgenology*. **2010**, *195* (6), W463.

127. Hamada, T.; Isayama, H.; Nakai, Y.; Iwashita, T.; Ito, Y.; Mukai, T.; Yagioka, H.; Saito, T.; Togawa, O.; Ryozaawa, S.; Hirano, K.; Mizuno, S.; Yamamoto, N.; Kogure, H.; Yasuda, I.; Koike, K., Antireflux covered metal stent for nonresectable distal malignant biliary obstruction: Multicenter randomized controlled trial. *Digestive endoscopy* **2019**, *31* (5), 566-574.

128. Jiao, D.; Wang, J.; Han, B.; Li, Z.; Wang, Y.; Han, X., Placement of a newly designed partially covered T- or Y-configured self-expanding

- metallic stent for hilar biliary obstruction: technical note. *La Radiologia medica* **2020**, *125* (10), 999-1007.
129. Sugimoto, M.; Takagi, T.; Suzuki, R.; Konno, N.; Asama, H.; Watanabe, K.; Nakamura, J.; Kikuchi, H.; Waragai, Y.; Takasumi, M.; Sato, Y.; Hikichi, T.; Ohira, H., Predictive factors for the failure of endoscopic stent-in-stent self-expandable metallic stent placement to treat malignant hilar biliary obstruction. *World journal of gastroenterology* **2017**, *23* (34), 6273-6280.
130. Hwang, J. C.; Kim, J. H.; Lim, S. G.; Kim, S. S.; Yoo, B. M.; Cho, S. W., Y-shaped endoscopic bilateral metal stent placement for malignant hilar biliary obstruction: prospective long-term study. *Scandinavian Journal of Gastroenterology* **2011**, *46* (3), 326-332.
131. Kim, D. U.; Kang, D. H.; Kim, G. H.; Song, G. A.; Kim, C. W.; Kim, S.; Jang, A. L., Bilateral biliary drainage for malignant hilar obstruction using the 'stent-in-stent' method with a Y-stent: efficacy and complications. *European journal of gastroenterology & hepatology* **2013**, *25* (1), 99-106.
132. Lee, J. M.; Lee, S. H.; Chung, K. H.; Park, J. M.; Paik, W. H.; Woo, S. M.; Lee, W. J.; Ryu, J. K.; Kim, Y.-T., Small cell- versus large cell-sized metal stent in endoscopic bilateral stent-in-stent placement for malignant hilar biliary obstruction. *dig endosc Digestive Endoscopy* **2015**, *27* (6), 692-699.
133. Naitoh, I.; Nakazawa, T.; Ban, T.; Okumura, F.; Hirano, A.; Takada, H.; Togawa, S.; Hayashi, K.; Miyabe, K.; Shimizu, S.; Kondo, H.; Nishi, Y.; Yoshida, M.; Yamashita, H.; Umemura, S.; Hori, Y.; Kato, A.; Sano, H.; Joh, T., 8-mm versus 10-mm diameter self-expandable metallic stent in bilateral endoscopic stent-in-stent deployment for malignant hilar biliary obstruction. *JHBP Journal of Hepato-Biliary-Pancreatic Sciences* **2015**, *22* (5), 396-401.
134. Heo, J. Y.; Lee, H. S.; Son, J. H.; Lee, S. H.; Bang, S., Clinical Outcomes of Bilateral Stent-in-Stent Placement Using Self-Expandable Metallic Stent for High-Grade Malignant Hilar Biliary Obstruction. *Yonsei Medical Journal* **2018**, *59* (7), 827-833.
135. National Heart, L., and Blood Institute. What to Expect When Getting a Stent 2022. <https://www.nhlbi.nih.gov/health/stents/during>.

136. Giannopoulos, S.; Lyden, S. P.; Bisdas, T.; Micari, A.; Parikh, S. A.; Jaff, M. R.; Schneider, P. A.; Armstrong, E. J., Endovascular intervention for the treatment of Trans-Atlantic Inter-Society Consensus (TASC) D femoropopliteal lesions: A systematic review and meta-analysis. *CARREV Cardiovascular Revascularization Medicine* **2020**.
137. Liu, Y.-H.; Hung, Y.-N.; Hsieh, H.-C.; Ko, P.-J., Impact of Cuffed, Expanded Polytetrafluoroethylene Dialysis Grafts on Graft Outlet Stenosis. *World J. Surg. World Journal of Surgery* **2006**, *30* (12), 2290-2294.
138. Ko, P.-J.; Liu, Y.-H.; Hung, Y.-N.; Hsieh, H.-C., Patency Rates of Cuffed and Noncuffed Extended Polytetrafluoroethylene Grafts in Dialysis Access: A Prospective, Randomized Study. *World Journal of Surgery* **2009**, *33* (4), 846-851.
139. Sawo, P.; Moufarrej, A.; Sloff, M.; Snoeijs, M. G.; Delhaas, T.; Tordoir, J. H. M.; Mees, B. M. E., The Effect of Geometric Graft Modification on Arteriovenous Graft Patency in Haemodialysis Patients: A Systematic Review and Meta-Analysis. *European journal of vascular and endovascular surgery : the official journal of the European Society for Vascular Surgery* **2020**, *60* (4), 568-577.
140. Shemesh, D.; Goldin, I.; Hijazi, J.; Zaghal, I.; Berelowitz, D.; Verstandig, A.; Olsha, O., A prospective randomized study of heparin-bonded graft (Propaten) versus standard graft in prosthetic arteriovenous access. *Journal of Vascular Surgery Journal of Vascular Surgery* **2015**, *62* (1), 115-122.
141. Nissen, A. P.; Sandhu, H. K.; Perlick, A. P.; Saqib, N. U.; Martin, G. H.; Miller, C. C.; Charlton-Ouw, K. M.; Nissen, A. P.; Wong, V. L.; Smith, T. A.; Smeds, M. R.; Charlton-Ouw, K. M., Heparin-bonded versus standard polytetrafluoroethylene arteriovenous grafts: A Bayesian perspective on a randomized controlled trial for comparative effectiveness. *Surgery Surgery (United States)* **2020**.
142. Davidovic, L.; Jakovljevic, N.; Radak, D.; Dragas, M.; Ilic, N.; Koncar, I.; Markovic, D., Dacron or ePTFE graft for above-knee femoropopliteal bypass reconstruction. A bi-centre randomised study. *VASA. Zeitschrift fur Gefasskrankheiten* **2010**, *39* (1), 77-84.



143. Bosiers, M.; Deloose, K.; Verbist, J.; Schroë, H.; Lauwers, G.; Lansink, W.; Peeters, P., Heparin-bonded expanded polytetrafluoroethylene vascular graft for femoropopliteal and femorocrural bypass grafting: 1-year results. *Journal of vascular surgery* **2006**, *43* (2), 313-8.
144. Kaiser, J.; Chen, A.; Cheung, M.; Kfoury, E.; Bechara, C. F.; Lin, P. H., Comparison of propaten heparin-bonded vascular graft with distal anastomotic patch versus autogenous saphenous vein graft in tibial artery bypass. *Vascular* **2017**, *26* (2), 117-125.
145. Samson, R. H.; Morales, R.; Showalter, D. P.; Lepore, M. R.; Nair, D. G., Heparin-bonded expanded polytetrafluoroethylene femoropopliteal bypass grafts outperform expanded polytetrafluoroethylene grafts without heparin in a long-term comparison. *Journal of Vascular Surgery* **2016**, *64* (3), 638-647.
146. Gouëffic, Y.; Favre, J.-P.; Steinmetz, E.; Ordureau, A.; Riche, V.-P.; Guyomarch, B.; Rosset, E., A Randomized Controlled Trial Comparing Crude Versus Heparin-Bonded PTFE Graft in Below the Knee Bypass Surgery for Critical Limb Ischemia (REPLACE Trial): Design and Protocol. *Annals of Vascular Surgery* **2019**, *58*, 115-121.
147. Pontoriero, R.; Lindhe, J.; Nyman, S.; Karring, T.; Rosenberg, E.; Sanavi, F., Guided tissue regeneration in degree II furcation-involved mandibular molars. A clinical study. *Journal of clinical periodontology* **1988**, *15* (4), 247-54.
148. Garrett, S.; Polson, A. M.; Stoller, N. H.; Drisko, C. L.; Caton, J. G.; Harrold, C. Q.; Bogle, G.; Greenwell, H.; Lowenguth, R. A.; Duke, S. P.; DeRouen, T. A., Comparison of a Bioabsorbable GTR Barrier to a Non-Absorbable Barrier in Treating Human Class II Furcation Defects. A Multi-Center Parallel Design Randomized Single-Blind Trial. *Journal of Periodontology* **1997**, *68* (7), 667-675.
149. Anjos, Clinical comparison of cellulose and expanded polytetrafluoroethylene membranes in the treatment of class II furcations in mandibular molars with sixmonth reentry. *JOURNAL-WESTERN SOCIETY OF PERIODONTOLOGY PERIODONTAL ABSTRACTS* **1998**, *46* (4), 102.

150. Hugoson, A.; Raval, N.; Fornell, J.; Johard, G.; Teiwik, A.; Gottlow, J., Treatment of Class II Furcation Involvements in Humans With Bioresorbable and Nonresorbable Guided Tissue Regeneration Barriers. A Randomized Multi-Center Study. *Journal of Periodontology* **1995**, *66* (7), 624-634.
151. Jalaluddin, M.; Patel, R.; Almalki, S.; Nagdev, P.; Roshan, R.; Varkey, R., Assessment of the Efficacy of Periodontal Tissue Regeneration using Non-resorbable and Bioabsorbable GTR Membrane—A Clinical Comparative Study. *The Journal of Contemporary Dental Practice* **2019**, *20*, 675-679.
152. Eickholz, P.; Pretzl, B.; Holle, R.; Kim, T.-S., Long-Term Results of Guided Tissue Regeneration Therapy With Non-Resorbable and Bioabsorbable Barriers. III. Class II Furcations After 10 Years. *Journal of periodontology*. **2006**, *77* (1), 88.
153. Eickholz, P.; Kim, T. S.; Holle, R., Guided tissue regeneration with non-resorbable and biodegradable barriers: 6 months results. *JOURNAL OF CLINICAL PERIODONTOLOGY* **1997**, *24* (2), 92-101.
154. Eickholz, P.; Kim, T.-S.; Holle, R., Regenerative periodontal surgery with non-resorbable and biodegradable barriers: results after 24 months. *JCPE Journal of Clinical Periodontology* **1998**, *25* (8), 666-676.
155. Eickholz, Long-term results of guided tissue regeneration therapy with nonresorbable and bioabsorbable barriers. I. Class II furcations. *JOURNAL- WESTERN SOCIETY OF PERIODONTOLOGY PERIODONTAL ABSTRACTS* **2002**, *50*, 13.
156. Silvestri, M.; Sartori, S.; Rasperini, G.; Ricci, G.; Rota, C.; Cattaneo, V., Comparison of infrabony defects treated with enamel matrix derivative versus guided tissue regeneration with a nonresorbable membrane. *JOURNAL OF CLINICAL PERIODONTOLOGY* **2003**, *30*, 386-393.
157. Sipos, P. M.; Loos, B. G.; Abbas, F.; Timmerman, M. F.; Velden, U. v. d., The combined use of enamel matrix proteins and a tetracycline-coated expanded polytetrafluoroethylene barrier membrane in the treatment of intra-osseous defects. *Journal of Clinical Periodontology* **2005**, *32*, 765-772.

158. Cortellini, P.; Pini Prato, G.; Tonetti, M. S., Periodontal regeneration of human intrabony defects with titanium reinforced membranes. A controlled clinical trial. *Journal of periodontology* **1995**, *66* (9), 797-803.
159. Heden, G., A case report study of 72 consecutive Emdogain-treated intrabony periodontal defects: clinical and radiographic findings after 1 year. *The International journal of periodontics & restorative dentistry* **2000**, *20* (2), 127-39.
160. Sculean, A.; Donos, N.; Windisch, P.; Brex, M.; Gera, I.; Reich, E.; Karring, T., Healing of human intrabony defects following treatment with enamel matrix proteins or guided tissue regeneration. *JRE Journal of Periodontal Research* **1999**, *34* (6), 310-322.
161. Pontoriero, R.; Wennstroem, J.; Lindhe, J., The use of barrier membranes and enamel matrix proteins in the treatment of angular bone defects. A prospective controlled clinical study. *JOURNAL OF CLINICAL PERIODONTOLOGY* **1999**, *26* (12), 833-840.
162. Sculean, A.; Windisch, P.; Chiantella, G. C.; Donos, N.; Brex, M.; Reich, E., Treatment of intrabony defects with enamel matrix proteins and guided tissue regeneration. A prospective controlled clinical study. *J Clin Periodontol Journal of Clinical Periodontology* **2001**, *28* (5), 397-403.
163. Dóri, F.; Kristóf, K.; Gera, I.; Sculean, A.; Eick, S., Bacterial Contamination of ePTFE Membranes Following Regenerative Surgery of Intrabony Defects Treated with Platelet-rich Plasma and Natural Bone Mineral. *Oral Health and Preventive Dentistry* **2019**, *17* (5), 439-445.
164. Rojas, M. A.; Marini, L.; Pilloni, A.; Sahrmann, P., Early wound healing outcomes after regenerative periodontal surgery with enamel matrix derivatives or guided tissue regeneration: a systematic review. *BMC Oral Health* **2019**, *19* (1), 76.
165. Ronda, M.; Rebaudi, A.; Torelli, L.; Stacchi, C., Expanded vs. dense polytetrafluoroethylene membranes in vertical ridge augmentation around dental implants: A prospective randomized controlled clinical trial. *Clinical oral implants research* **2013**, *25*.

166. Trobos, M.; Juhlin, A.; Shah, F. A.; Hoffman, M.; Sahlin, H.; Dahlin, C., In vitro evaluation of barrier function against oral bacteria of dense and expanded polytetrafluoroethylene (PTFE) membranes for guided bone regeneration. *Clinical implant dentistry and related research* **2018**, *20* (5), 738-748.
167. Carbonell, J. M.; Martín, I. S.; Santos, A.; Pujol, A.; Sanz-Moliner, J. D.; Nart, J., High-density polytetrafluoroethylene membranes in guided bone and tissue regeneration procedures: a literature review. *YIJOM International Journal of Oral & Maxillofacial Surgery* **2014**, *43* (1), 75-84.
168. Lee, S.-W.; Kim, S.-G., Membranes for the Guided Bone Regeneration. *Maxillofacial plastic and reconstructive surgery* **2014**, *36* (6), 239-246.
169. Jang, J.-W.; Kim, J.; Kook, M.-S.; Lee, K.-Y.; Original, L., Evaluation of Gellan Gum/Glycol Chitosan Bioabsorbable Membrane for Guided Bone Regeneration. *P'ollimo = Polymer (Korea) = Han'guk Kobunja Hakhoe chi.* **2018**, *42* (5), 874-881.
170. Kim, H. Y.; Park, J. H.; Oh, S. H.; Byun, J. H.; Lee, J. H.; Oh, S. H., BMP-2-Immobilized Porous Matrix with Leaf-Stacked Structure as a Bioactive GBR Membrane. *ACS Appl. Mater. Interfaces ACS Applied Materials and Interfaces* **2018**, *10* (36), 30115-30124.
171. Zhang, H. Y.; Kim, J. E.; Kim, K. M.; Kwon, J. S.; Jiang, H. B.; Zhang, S.; Kim, K. M.; Kwon, J. S., Bioresorbable magnesium-reinforced PLA membrane for guided bone/tissue regeneration. *J. Mech. Behav. Biomed. Mater. Journal of the Mechanical Behavior of Biomedical Materials* **2020**, *112*.
172. Du, X.; Song, Y.; Xuan, X.; Chen, S.; Wu, X.; Jiang, H. B.; Lee, E.-S.; Wang, X., Characterization of a Bioresorbable Magnesium-Reinforced PLA-Integrated GTR/GBR Membrane as Dental Applications. *Scanning* **2020**, *2020*, 6743195.
173. Becker, W.; Dahlin, C.; Lekholm, U.; Bergstrom, C.; Steenberghe, D.; Higuchi, K.; Becker, B. E., Five-Year Evaluation of Implants Placed at Extraction and with Dehiscences and Fenestration Defects Augmented with ePTFE Membranes: Results from a Prospective Multicenter

- Study. *CID Clinical Implant Dentistry and Related Research* **1999**, *1* (1), 27-32.
174. Gananadha, S.; Samra, J. S.; Smith, G. S.; Smith, R. C.; Leibman, S.; Hugh, T. J., LAPAROSCOPIC ePTFE MESH REPAIR OF INCISIONAL AND VENTRAL HERNIAS. *ANS ANZ Journal of Surgery* **2008**, *78* (10), 907-913.
175. Elliott, M. P.; Juler, G. L., Comparison of Marlex mesh and microporous teflon sheets when used for hernia repair in the experimental animal. *American journal of surgery* **1979**, *137* (3), 342-4.
176. Usher, F. C., HERNIA REPAIR WITH KNITTED POLYPROPYLENE MESH. *Surgery, gynecology & obstetrics* **1963**, *117*, 239-40.
177. Alarcón, I.; Balla, A.; Soler Frías, J. R.; Barranco, A.; Bellido Luque, J.; Morales-Conde, S., Polytetrafluoroethylene versus polypropylene mesh during laparoscopic totally extraperitoneal (TEP) repair of inguinal hernia: short- and long-term results of a double-blind clinical randomized controlled trial. *Hernia* **2020**, *24* (5), 1011-1018.
178. Orenstein, S. B., Permanent Prosthetics: Polypropylene, Polyester, ePTFE, and Hybrid Mesh. **2019**, 57-69.
179. Bensaadi, H.; Paolino, L.; Valenti, A.; Polliand, C.; Champault, G.; Barrat, C., Intraperitoneal tension-free repair of a small midline ventral abdominal wall hernia: Randomized study with a mean follow-up of 3 years. *Am. Surg. American Surgeon* **2014**, *80* (1), 57-65.
180. Liang, M. K.; Berger, R. L.; Li, L. T.; Davila, J. A.; Hicks, S. C.; Kao, L. S., Outcomes of Laparoscopic vs Open Repair of Primary Ventral Hernias. *JAMA Surg JAMA Surgery* **2013**, *148* (11), 1043.
181. Hadi, H. I.; Maw, A.; Sarmah, S.; Kumar, P., Intraperitoneal tension-free repair of small midline ventral abdominal wall hernias with a Ventralex hernia patch: initial experience in 51 patients. *HERNIA -PARIS-* **2006**, *10* (5), 409-413.
182. Rodríguez, M.; Gómez-Gil, V.; Pérez-Köhler, B.; Pascual, G.; Bellón, J. M., Polymer Hernia Repair Materials: Adapting to Patient Needs and Surgical Techniques. *Materials* **2021**, *14* (11), 2790.
183. Schumpelick, V.; Fitzgibbons, R. J.; Conze, J., *Hernia repair sequelae*. Springer: Berlin, 2010.

184. Bellon, J. M.; Bujan, J.; Contreras, L. A.; Carrera-San Martin, A.; Jurado, F., Comparison of a New Type of Polytetrafluoroethylene Patch (Mycro Mesh) and Polypropylene Prosthesis (Marlex) for Repair of Abdominal Wall Defects. *Journal of the American College of Surgeons*. **1996**, *183* (1), 11.
185. Bellón, J. M.; Contreras, L. A.; Buján, J.; Martin, A. C.-S., The Use of Biomaterials in the Repair of Abdominal Wall Defects: A Comparative Study between Polypropylene Meshes (Marlex) and a New Polytetrafluoroethylene Prosthesis (Dual Mesh). *J Biomater Appl Journal of Biomaterials Applications* **1997**, *12* (2), 121-135.
186. Harrell, A. G.; Novitsky, Y. W.; Kercher, K. W.; Foster, M.; Burns, J. M.; Kuwada, T. S.; Heniford, B. T., In vitro infectability of prosthetic mesh by methicillin-resistant Staphylococcus aureus. *Hernia : the journal of hernias and abdominal wall surgery* **2006**, *10* (2), 120-4.
187. Gillinov, A. M.; Cosgrove, D. M.; Blackstone, E. H.; Diaz, R.; Arnold, J. H.; Lytle, B. W.; Smedira, N. G.; Sabik, J. F.; McCarthy, P. M.; Loop, F. D., Durability of mitral valve repair for degenerative disease. *The Journal of Thoracic and Cardiovascular Surgery The Journal of Thoracic and Cardiovascular Surgery* **1998**, *116* (5), 734-743.
188. Suri, R. M.; Schaff, H. V.; Dearani, J. A.; Sundt, T. M.; Daly, R. C.; Mullany, C. J.; Enriquez-Sarano, M.; Orszulak, T. A., Survival Advantage and Improved Durability of Mitral Repair for Leaflet Prolapse Subsets in the Current Era. *ATS The Annals of Thoracic Surgery* **2006**, *82* (3), 819-826.
189. Suri, R. M.; Vanoverschelde, J.-L.; Grigioni, F.; Schaff, H. V.; Tribouilloy, C.; Avierinos, J.-F.; Barbieri, A.; Pasquet, A.; Huebner, M.; Rusinaru, D.; Russo, A.; Michelena, H. I.; Enriquez-Sarano, M., Association Between Early Surgical Intervention vs Watchful Waiting and Outcomes for Mitral Regurgitation Due to Flail Mitral Valve Leaflets. *JAMA* **2013**, *310* (6), 609-616.
190. Salvador, L.; Mirone, S.; Bianchini, R.; Regesta, T.; Patelli, F.; Minniti, G.; Masat, M.; Cavarretta, E.; Valfrè, C., A 20-year experience with mitral valve repair with artificial chordae in 608 patients. *YMTCThe Journal of Thoracic and Cardiovascular Surgery* **2008**, *135* (6), 1280-1287.e1.

191. Bhatnagar, G.; Fremes, S. E.; Christakis, G. T.; Goldman, B. S., Early Results Using an ePTFE Membrane for Pericardial Closure Following Coronary Bypass Grafting. *JOCS Journal of Cardiac Surgery* **1998**, *13* (3), 190-193.
192. Harada, Y.; Imai, Y.; Kurosawa, H.; Hoshino, S.; Nakano, K., Long-term results of the clinical use of an expanded polytetrafluoroethylene surgical membrane as a pericardial substitute. *The Journal of Thoracic and Cardiovascular Surgery The Journal of Thoracic and Cardiovascular Surgery* **1988**, *96* (5), 811-815.
193. Jacobs, J. P.; Iyer, R. S.; Weston, J. S.; Amato, J. J.; Elliott, M. J.; de Leval, M. R.; Stark, J., Expanded PTFE Membrane to Prevent Cardiac Injury During Resternotomy for Congenital Heart Disease. *The Annals of Thoracic Surgery* **1996**, *62* (6), 1778-1782.
194. Edwards-Lehr, T.; Franke, J.; Bertog, S. C.; Bäcker, C.; Wunderlich, N.; Hofmann, I.; Wilson, N.; Piechaud, J.-F.; Sievert, H., Safety and performance of the spider patent foramen ovale occluder. *CCD Catheterization and Cardiovascular Interventions* **2013**, *81* (2), 317-323.
195. Hardt, S. E.; Eicken, A.; Berger, F.; Schubert, S.; Carminati, M.; Butera, G.; Grohmann, J.; Höhn, R.; Nielsen-Kudsk, J. E.; Hildick-Smith, D.; Settergren, M.; Thomson, J. D.; Geis, N.; Søndergaard, L., Closure of patent foramen ovale defects using GORE® CARDIOFORM septal occluder: Results from a prospective European multicenter study. *Catheterization and Cardiovascular Interventions* **2017**, *90* (5), 824-829.
196. Kasner, S. E.; Thomassen, L.; Søndergaard, L.; Rhodes, J. F.; Larsen, C. C.; Jacobson, J., Patent foramen ovale closure with GORE HELEX or CARDIOFORM Septal Occluder vs. antiplatelet therapy for reduction of recurrent stroke or new brain infarct in patients with prior cryptogenic stroke: Design of the randomized Gore REDUCE Clinical Study. *Int. J. Stroke International Journal of Stroke* **2017**.
197. Chen, J. Z.-J.; Thijs, V. N., Atrial Fibrillation Following Patent Foramen Ovale Closure Systematic Review and Meta-Analysis of Observational Studies and Clinical Trials. *Stroke* **2021**, *52* (5), 1653-1661.

198. Shadfar, S.; Farag, A.; Jarchow, A. M.; Shockley, W. W., Safety and Efficacy of Expanded Polytetrafluoroethylene Implants in the Surgical Management of Traumatic Nasal Deformity. *JAMA Otolaryngol Head Neck Surg JAMA OtolaryngologyHead & Neck Surgery* **2015**, *141* (8), 710.
199. Lee, T.-Y.; Chung, H.-Y.; Dhong, E.-S.; Jeong, S.-H.; Han, S.-K., Paranasal Augmentation Using Multi-Folded Expanded Polytetrafluorethylene (ePTFE) in the East Asian Nose. *Aesthetic Surgery Journal* **2019**, *39* (12), 1319-1328.
200. Sintler, M.; Mahmood, A.; Smith, S.; Simms, M.; Vohra, R., Randomized Trial Comparing Quixil Surgical Sealant with Kaltostat Hemostatic Dressing to Control Suture Line Bleeding after Carotid Endarterectomy with ePTFE Patch Reconstruction. *World journal of surgery* **2005**, *29*, 1259-62.
201. Saha, S. P.; Muluk, S.; Schenk, W.; Dennis, J. W.; Ploder, B.; Grigorian, A.; Presch, I.; Goppelt, A., A prospective randomized study comparing fibrin sealant to manual compression for the treatment of anastomotic suture-hole bleeding in expanded polytetrafluoroethylene grafts. *YMVA Journal of Vascular Surgery* **2012**, *56* (1), 134-141.
202. Daud, A.; Kaur, B.; McClure, G. R.; Belley-Cote, E. P.; Harlock, J.; Crowther, M.; Whitlock, R. P., Fibrin and Thrombin Sealants in Vascular and Cardiac Surgery: A Systematic Review and Meta-analysis. *European Journal of Vascular and Endovascular Surgery* **2020**, *60* (3), 469-478.
203. Pahor, D.; Pahor, A., E-PTFE Membran für die Behandlung von perforiertem Hornhautulkus. *Klin Monatsbl Augenheilkd Klinische Monatsblätter für Augenheilkunde* **2016**, *233* (10), 1156-1162.
204. Kim, K. W.; Kim, J. C.; Moon, J. H.; Koo, H.; Kim, T. H.; Moon, N. J., Management of complicated multirecurrent pterygia using multimicroporous expanded polytetrafluoroethylene. *British journal of ophthalmology*. **2013**, *97* (6), 694-700.
205. Choi, Y. J.; Kim, C. S.; Ahn, B.-H., A comparison of the clinical effect between e-PTFE membrane-tube implant and Ahmed glaucoma



- valve implant for the treatment of refractory glaucoma. *Korean J Ophthalmol Korean Journal of Ophthalmology* **2003**, *17* (2), 106.
206. Wu, L.; Deng, H., Defluorination of 4-fluorothreonine by threonine deaminase. *Organic & Biomolecular Chemistry* **2020**, *18* (32), 6236-6240.
207. Huang, S.; Jaffé, P. R., Defluorination of Perfluorooctanoic Acid (PFOA) and Perfluorooctane Sulfonate (PFOS) by Acidimicrobium sp. Strain A6. *Environmental Science & Technology* **2019**, *53* (19), 11410-11419.
208. Bentel, M. J.; Yu, Y.; Xu, L.; Li, Z.; Wong, B. M.; Men, Y.; Liu, J., Defluorination of Per- and Polyfluoroalkyl Substances (PFASs) with Hydrated Electrons: Structural Dependence and Implications to PFAS Remediation and Management. *Environmental Science & Technology* **2019**, *53* (7), 3718-3728.
209. Yanagihara, N.; Katoh, T., Mineralization of poly(tetrafluoroethylene) and other fluoropolymers using molten sodium hydroxide. *Green Chemistry* **2022**, *24* (16), 6255-6263.
210. Chaban, V. V.; Prezhdo, O. V., Electron Solvation in Liquid Ammonia: Lithium, Sodium, Magnesium, and Calcium as Electron Sources. *The Journal of Physical Chemistry B* **2016**, *120* (9), 2500-2506.
211. Dye, J. L., The alkali metals: 200 years of surprises. *Philosophical Transactions of the Royal Society A: Mathematical, Physical and Engineering Sciences* **2015**, *373* (2037), 20140174.
212. Birch, A. J., The Birch reduction in organic synthesis. *Pure and Applied Chemistry* **1996**, *68* (3), 553-556.
213. Graziani, E. I.; McKeown, N. B.; Kalman, P. G.; Thompson, M., Surface selective modification of fluoropolymer biomaterial. *International Biodeterioration & Biodegradation* **1992**, *30* (2), 217-231.
214. Roina, Y.; Gonçalves, A.-M.; Fregnaux, M.; Auber, F.; Herlem, G., Sodium Naphthalenide Diglyme Solution for Etching PTFE, Characterizations and Molecular Modelization. *ChemistrySelect* **2022**, *7* (21), e202200153.
215. Liang, F.; Sadana, A. K.; Peera, A.; Chattopadhyay, J.; Gu, Z.; Hauge, R. H.; Billups, W. E., A Convenient Route to Functionalized Carbon Nanotubes. *Nano Letters* **2004**, *4* (7), 1257-1260.

216. Benkeser, R. A.; Lambert, R. F.; Ryan, P. W.; Stoffey, D. G., Reduction of Organic Compounds by Lithium in Low Molecular Weight Amines. IV. The Effect of Nitro and Amino Groups on the Course of the Reduction. *Journal of the American Chemical Society* **1958**, *80* (24), 6573-6577.
217. Benkeser, R. A.; Agnihotri, R. K.; Burrous, M. L., Reduction of organic compounds by lithium in low molecular weight amines. Highly selective lithium-amine reducing systems. *Tetrahedron Letters* **1960**, *1* (37), 1-3.
218. Benkeser, R. A.; Burrous, M. L.; Hazdra, J. J.; Kaiser, E. M., Reduction of Organic Compounds by Lithium in Low Molecular Weight Amines. VII. The Preparation of Dihydroaromatics. A Comparison of the Lithium-Amine and Birch Reduction Systems. *The Journal of Organic Chemistry* **1963**, *28* (4), 1094-1097.
219. Benkeser, R. A.; Agnihotri, R. K.; Burrous, M. L.; Kaiser, E. M.; Mallan, J. M.; Ryan, P. W., Highly Selective Lithium—Amine Reducing Systems. The Selective Reduction of Aromatic Compounds by Lithium in Mixed Amine Solvents<sup>1a</sup>. *The Journal of Organic Chemistry* **1964**, *29* (6), 1313-1316.
220. Benkeser, R. A.; Rappa, A.; Wolsieffer, L. A., Calcium and lithium reductions of epoxides in ethylenediamine. A comparison study. *The Journal of Organic Chemistry* **1986**, *51* (17), 3391-3393.
221. Garst, M. E.; Dolby, L. J.; Esfandiari, S.; Fedoruk, N. A.; Chamberlain, N. C.; Avey, A. A., Reductions with Lithium in Low Molecular Weight Amines and Ethylenediamine. *The Journal of Organic Chemistry* **2000**, *65* (21), 7098-7104.
222. Reggel, L.; Friedel, R. A.; Wender, I., Lithium in Ethylenediamine: A New Reducing System for Organic Compounds<sup>1</sup>. *The Journal of Organic Chemistry* **1957**, *22* (8), 891-894.
223. Xinliang, T.; Qingze, J.; Yong, C.; Pei, Z.; Hongbo, L.; Hongyu, W.; Mingji, Z.; Xuefei, L.; Yun, Z., Reductive Alkylation and Arylation of Single-walled Carbon Nanotubes in Ethylenediamine via Benkeser Reaction. *Chemistry Letters* **2009**, *38* (3), 220-221.

224. Tang, X.; Zhao, Y.; Jiao, Q.; Cao, Y., Hydrogenation of Multi-walled Carbon Nanotubes in Ethylenediamine. *Fullerenes, Nanotubes and Carbon Nanostructures* **2010**, *18* (1), 14-23.
225. Sarkar, A. K.; Saha, S.; Ganguly, S.; Banerjee, D.; Kargupta, K., Hydrogen storage on graphene using Benkeser reaction. *International Journal of Energy Research* **2014**, *38* (14), 1889-1895.
226. Kaiser, E.; Benkeser, R., DELTA-9, 10-OCTALIN. *Organic Syntheses* **1988**, *50*, 852-855.
227. Vesel, A.; Zaplotnik, R.; Primc, G.; Mozetič, M.; Katan, T.; Kargl, R.; Mohan, T.; Kleinschek, K. S., Rapid Functionalization of Polytetrafluorethylene (PTFE) Surfaces with Nitrogen Functional Groups. *Polymers* **2021**, *13* (24), 4301.
228. Coupe, B.; Chen, W., A New Approach to Surface Functionalization of Fluoropolymers. *Macromolecules* **2001**, *34* (6), 1533-1535.
229. Beumel, O. F.; Harris, R. F., The Preparation of Lithium Acetylide-Ethylenediamine. *The Journal of Organic Chemistry* **1963**, *28* (10), 2775-2779.
230. Pettersen, D.; Amedjkouh, M.; Ahlberg, P., Chiral Lithium Amides in Asymmetric Synthesis. In *The Chemistry of Organolithium Compounds*, 2005; pp 411-476.
231. Connelly, N. G.; Geiger, W. E., Chemical Redox Agents for Organometallic Chemistry. *Chemical Reviews* **1996**, *96* (2), 877-910.
232. Reiß, A.; Donsbach, C.; Feldmann, C., Insights into the naphthalenide-driven synthesis and reactivity of zerovalent iron nanoparticles. *Dalton Transactions* **2021**, *50* (44), 16343-16352.
233. Kowach, G. R.; Warren, C. J.; Haushalter, R. C.; DiSalvo, F. J., Synthesis and Structure of the One-Dimensional Polymer Li(NHCH<sub>2</sub>CH<sub>2</sub>NH<sub>2</sub>). *Inorganic Chemistry* **1998**, *37* (1), 156-159.
234. Frisch, M. J.; Trucks, G. W.; Schlegel, H. B.; Scuseria, G. E.; Robb, M. A.; Cheeseman, J. R.; Scalmani, G.; Barone, V.; Petersson, G. A.; Nakatsuji, H.; Li, X.; Caricato, M.; Marenich, A. V.; Bloino, J.; Janesko, B. G.; Gomperts, R.; Mennucci, B.; Hratchian, H. P.; Ortiz, J. V.; Izmaylov, A. F.; Sonnenberg, J. L.; Williams; Ding, F.; Lipparini, F.; Egidi, F.; Goings, J.; Peng, B.; Petrone, A.; Henderson, T.; Ranasinghe, D.;

Zakrzewski, V. G.; Gao, J.; Rega, N.; Zheng, G.; Liang, W.; Hada, M.; Ehara, M.; Toyota, K.; Fukuda, R.; Hasegawa, J.; Ishida, M.; Nakajima, T.; Honda, Y.; Kitao, O.; Nakai, H.; Vreven, T.; Throssell, K.; Montgomery Jr., J. A.; Peralta, J. E.; Ogliaro, F.; Bearpark, M. J.; Heyd, J. J.; Brothers, E. N.; Kudin, K. N.; Staroverov, V. N.; Keith, T. A.; Kobayashi, R.; Normand, J.; Raghavachari, K.; Rendell, A. P.; Burant, J. C.; Iyengar, S. S.; Tomasi, J.; Cossi, M.; Millam, J. M.; Klene, M.; Adamo, C.; Cammi, R.; Ochterski, J. W.; Martin, R. L.; Morokuma, K.; Farkas, O.; Foresman, J. B.; Fox, D. J. *Gaussian 16 Rev. C.01*, Wallingford, CT, 2016.

235. Domingo, L.; Ríos-Gutiérrez, M.; Pérez, P., Applications of the Conceptual Density Functional Theory Indices to Organic Chemistry Reactivity. *Molecules* **2016**, *21*, 748.

236. Parr, R. G. Y. W., Density-functional theory of atoms and molecules. **2020**.

237. Lu, T.; Chen, F., Multiwfn: A multifunctional wavefunction analyzer. *Journal of Computational Chemistry* **2012**, *33* (5), 580-592.

238. Chamorro, E.; Pérez, P.; Domingo, L. R., On the nature of Parr functions to predict the most reactive sites along organic polar reactions. *Chemical Physics Letters* **2013**, *582*, 141-143.

239. Pino-Rios, R.; Inostroza, D.; Cárdenas-Jirón, G.; Tiznado, W., Orbital-Weighted Dual Descriptor for the Study of Local Reactivity of Systems with (Quasi-) Degenerate States. *The Journal of Physical Chemistry A* **2019**, *123* (49), 10556-10562.

240. Garst, J. F.; Barbas, J. T.; Barton, F. E., Radical mechanism of alkylation of sodium naphthalenide. *Journal of the American Chemical Society* **1968**, *90* (25), 7159-7160.

241. Sargent, G. D.; Lux, G. A., Reactions of aromatic radical anions. III. Evidence for an alkyl radical-radical anion combination mechanism for alkylation of sodium naphthalenide with alkyl halides. *Journal of the American Chemical Society* **1968**, *90* (25), 7160-7162.

242. Newcomb, M.; Reeder, R. A., Reactions of trans-2-tert-butyl-3-phenyloxaziridine with lithium amide bases. *The Journal of Organic Chemistry* **1980**, *45* (8), 1489-1493.

243. Renaud, P.; Fox, M. A., Electrochemical behavior of lithium dialkylamides: the effect of aggregation. *Journal of the American Chemical Society* **1988**, *110* (17), 5702-5705.
244. Jahn, U.; Müller, M.; Aussieker, S., The Combination of Anionic and Radical Reactions to Oxidative Tandem Processes Exemplified by the Synthesis of Functionalized Pyrrolidines. *Journal of the American Chemical Society* **2000**, *122* (21), 5212-5213.
245. Yan, H. W. B. Z. X.-K. Y. C. W. J. H. H.-S. Z. W.-X. X. Z., Rare-Earth Metal Boroxide with Formal Triple MetalOxygen Orbital Interaction: Synthesis from  $B(C_6F_5)_3 \cdot H_2O$  and Radical-Anion Ligated Rare-Earth Metal Amides. *CCS Chem CCS Chemistry* **2021**, *3* (11), 2772-2781.
246. Wotiz, J. H.; HUBA, F., Low Temperature Amination of Aromatic Polyhalides. *The Journal of Organic Chemistry* **1959**, *24* (5), 595-598.
247. Leffler, M. T., The Amination of Heterocyclic Bases by Alkali Amides. The Chichibabin Reactions. In *Organic Reactions*, 2011; pp 91-104.
248. Doi, H.; Sakai, T.; Iguchi, M.; Yamada, K.-i.; Tomioka, K., Chiral Ligand-Controlled Asymmetric Conjugate Addition of Lithium Amides to Enoates. *Journal of the American Chemical Society* **2003**, *125* (10), 2886-2887.
249. Tomioka, K.; Sakai, T.; Ogata, T.; Yamamoto, Y., Aminolithiation of carbon-carbon double bonds as a powerful tool in organic synthesis. *Pure and Applied Chemistry* **2009**, *81* (2), 247-253.
250. Cui, X. S. F., *Catalytic Amination for N-Alkyl Amine Synthesis*. Academic Press: 2018.
251. Xu, F.; Peng, L.; Shinohara, K.; Nishida, T.; Wakamatsu, K.; Uejima, M.; Sato, T.; Tanaka, K.; Machida, N.; Akashi, H.; Orita, A.; Otera, J., One-Shot Double Amination of Sondheimer–Wong Dienes: Synthesis of Photoluminescent Dinaphthopentalenes. *Organic Letters* **2015**, *17* (12), 3014-3017.
252. Streckowski, L.; Janda, L.; Patterson, S. E.; Nguyen, J., Amination by lithium alkylamide reagents of ketimines derived from 2-(trifluoromethyl)anilines and methyl halophenyl ketones and their

- cyclization products 2-(halophenyl)quinolin-4-amines. *Tetrahedron* **1996**, 52 (9), 3273-3282.
253. de Jong, J.; Heijnen, D.; Helbert, H.; Feringa, B. L., One-pot, modular approach to functionalized ketones via nucleophilic addition/Buchwald–Hartwig amination strategy. *Chemical Communications* **2019**, 55 (20), 2908-2911.
254. Socrates, G. J. W.; Sons, *Infrared and Raman characteristic group frequencies : tables and charts*. John Wiley & Sons LTD: Chichester [etc.], 2015.
255. Khatipov, S. A.; Serov, S. A.; Sadovskaya, N. V.; Konova, E. M., Morphology of polytetrafluoroethylene before and after irradiation. *Radiation Physics and Chemistry* **2012**, 81 (3), 256-263.
256. Marchesi, J. T.; Keith, H. D.; Garton, A., Adhesion to Sodium Naphthalenide Treated Fluoropolymers. Part III. Mechanism of Adhesion. *The Journal of Adhesion* **1992**, 39 (4), 185-205.
257. Wu, S., *Polymer interface and adhesion*. Dekker: New York; Basel, 1982.
258. Chen, Y.; Zhao, Z.; Liu, Y., Wettability characteristic of PTFE and glass surface irradiated by keV ions. *Applied Surface Science* **2008**, 254 (17), 5497-5500.
259. Kolská, Z.; Řezníčková, A.; Hnatowicz, V.; Švorčík, V., PTFE surface modification by Ar plasma and its characterization. *Vacuum* **2012**, 86 (6), 643-647.
260. Švorčík, V.; Kotál, V.; Siegel, J.; Sajdl, P.; Macková, A.; Hnatowicz, V., Ablation and water etching of poly(ethylene) modified by argon plasma. *Polymer Degradation and Stability - POLYM DEGRAD STABIL* **2007**, 92, 1645-1649.
261. Liu, C. Z.; Wu, J. Q.; Ren, L. Q.; Tong, J.; Li, J. Q.; Cui, N.; Brown, N. M. D.; Meenan, B. J., Comparative study on the effect of RF and DBD plasma treatment on PTFE surface modification. *Materials Chemistry and Physics* **2004**, 85 (2), 340-346.
262. Švorčík, V.; Kolářová, K.; Slepíčka, P.; Macková, A.; Novotná, M.; Hnatowicz, V., Modification of surface properties of high and low density polyethylene by Ar plasma discharge. *Polymer Degradation and Stability* **2006**, 91 (6), 1219-1225.

263. Gerenser, L. J., XPS studies of in situ plasma-modified polymer surfaces. *Journal of Adhesion Science and Technology* **1993**, 7 (10), 1019-1040.
264. Oliver, W. C.; Pharr, G. M., An improved technique for determining hardness and elastic modulus using load and displacement sensing indentation experiments. *Journal of Materials Research* **1992**, 7 (6), 1564-1583.
265. Vanlandingham, M.; Villarrubia, J.; Guthrie, W.; Meyers, G., Nanoindentation of Polymers: An Overview. *Macromolecular Symposia* **2001**, 167.
266. Tan, B.; Stephens, L. S., Evaluation of viscoelastic characteristics of PTFE-Based materials. *Tribology International* **2019**, 140, 105870.
267. Halalay, I. C.; Lukitsch, M. J.; Balogh, M. P.; Wong, C. A., Nanoindentation testing of separators for lithium-ion batteries. *Journal of Power Sources* **2013**, 238, 469-477.
268. Chudoba, T.; Richter, F., Investigation of creep behaviour under load during indentation experiments and its influence on hardness and modulus results. *Surface and Coatings Technology* **2001**, 148 (2), 191-198.
269. Lucas, B.; Rosenmayer, T.; Oliver, W., Mechanical Characterization of Sub-Micron Polytetrafluoroethylene (PTFE) Thin Films. *MRS Proceedings* **2011**, 505.
270. Muzzarelli, R. A.; Pariser, E. R., Proceedings of the First International Conference on Chitin/Chitosan. **1978**.
271. Gooday, G. W.; Jeuniaux, C.; Muzzarelli, R., *Chitin in nature and technology*. Springer Science & Business Media: 2012.
272. Belmonte, M.; Muzzarelli, B.; Muzzarelli, R., Chitin and chitosan in wound healing and other biomedical applications. *Carbohydrates in Europe* **1997**, 30-37.
273. Shigemasa, Y.; Minami, S., Applications of chitin and chitosan for biomaterials. *Biotechnology and Genetic Engineering Reviews* **1996**, 13 (1), 383-420.
274. Gomathysankar, S.; Halim, A. S.; Yaacob, N. S., Proliferation of Keratinocytes Induced by Adipose-Derived Stem Cells on a Chitosan

- Scaffold and Its Role in Wound Healing, a Review. *Arch Plast Surg* **2014**, *41* (05), 452-457.
275. Hosseinnejad, M.; Jafari, S. M., Evaluation of different factors affecting antimicrobial properties of chitosan. *International journal of biological macromolecules* **2016**, *85*, 467-75.
276. Yilmaz Atay, H., Antibacterial Activity of Chitosan-Based Systems. *Functional Chitosan* **2020**, 457-489.
277. Chung, Y.-C.; Chen, C.-Y., Antibacterial characteristics and activity of acid-soluble chitosan. *Bioresource Technology* **2008**, *99* (8), 2806-2814.
278. Eaton, P.; Fernandes, J. C.; Pereira, E.; Pintado, M. E.; Xavier Malcata, F., Atomic force microscopy study of the antibacterial effects of chitosans on *Escherichia coli* and *Staphylococcus aureus*. *Ultramicroscopy* **2008**, *108* (10), 1128-1134.
279. Vancha, A. R.; Govindaraju, S.; Parsa, K. V.; Jasti, M.; González-García, M.; Ballester, R. P., Use of polyethyleneimine polymer in cell culture as attachment factor and lipofection enhancer. *BMC biotechnology* **2004**, *4* (1), 1-12.
280. Ciofani, G.; Raffa, V.; Menciassi, A.; Cuschieri, A., Cytocompatibility, interactions, and uptake of polyethyleneimine-coated boron nitride nanotubes by living cells: Confirmation of their potential for biomedical applications. *Biotechnology and bioengineering* **2008**, *101* (4), 850-858.
281. Brunot, C.; Ponsonnet, L.; Lagneau, C.; Farge, P.; Picart, C.; Grosgeat, B., Cytotoxicity of polyethyleneimine (PEI), precursor base layer of polyelectrolyte multilayer films. *Biomaterials* **2007**, *28* (4), 632-640.
282. Uwem Okon, E.; Hammed, G.; Abu El Wafa, P.; Abraham, O.; Case, N.; Henry, E., In-vitro cytotoxicity of Polyethyleneimine on HeLa and Vero Cells. **2014**.
283. Hernandez-Montelongo, J.; Lucchesi, E. G.; Nascimento, V. F.; França, C.; Gonzalez, I.; Macedo, W.; Machado, D.; Lancellotti, M.; Moraes, Â.; Beppu, M.; Cotta, M., Antibacterial and non-cytotoxic ultra-thin polyethylenimine film. *Materials Science and Engineering C* **2016**, *71*, 718-724.



284. Gibney, K. A.; Sovadinova, I.; Lopez, A. I.; Urban, M.; Ridgway, Z.; Caputo, G. A.; Kuroda, K., Poly(ethylene imine)s as antimicrobial agents with selective activity. *Macromolecular bioscience* **2012**, *12* (9), 1279-89.
285. Mayandi, V.; Sridhar, S.; Fazil, M. H. U. T.; Goh, E. T. L.; Htoon, H. M.; Orive, G.; Choong, Y. K.; Saravanan, R.; Beuerman, R. W.; Barkham, T. M. S.; Yang, L.; Baskaran, M.; Jhanji, V.; Loh, X. J.; Verma, N. K.; Lakshminarayanan, R., Protective Action of Linear Polyethylenimine against Staphylococcus aureus Colonization and Exaggerated Inflammation in Vitro and in Vivo. *ACS Infectious Diseases* **2019**, *5* (8), 1411-1422.
286. Venkatesh, M.; Barathi, V. A.; Goh, E. T. L.; Anggara, R.; Fazil, M. H. U. T.; Ng, A. J. Y.; Harini, S.; Aung, T. T.; Fox, S. J.; Liu, S.; Yang, L.; Barkham, T. M. S.; Loh, X. J.; Verma, N. K.; Beuerman, R. W.; Lakshminarayanan, R., Antimicrobial Activity and Cell Selectivity of Synthetic and Biosynthetic Cationic Polymers. *Antimicrobial Agents and Chemotherapy* **2017**, *61* (10), e00469-17.
287. Kocaçalışkan, I.; Talan, I.; Terzi, I., Antimicrobial activity of catechol and pyrogallol as allelochemicals. *Zeitschrift fur Naturforschung. C, Journal of biosciences* **2006**, *61* (9-10), 639-42.
288. Zhang, Y.; Chen, S.; An, J.; Fu, H.; Wu, X.; Pang, C.; Gao, H., Construction of an Antibacterial Membrane Based on Dopamine and Polyethylenimine Cross-Linked Graphene Oxide. *ACS Biomaterials Science & Engineering* **2019**, *5* (6), 2732-2739.
289. Ren, J.; Kong, R.; Gao, Y.; Zhang, L.; Zhu, J., Bioinspired adhesive coatings from polyethylenimine and tannic acid complexes exhibiting antifogging, self-cleaning, and antibacterial capabilities. *Journal of Colloid and Interface Science* **2021**, *602*, 406-414.
290. Qiu, W.-Z.; Zhao, Z.-S.; Du, Y.; Hu, M.-X.; Xu, Z.-K., Antimicrobial membrane surfaces via efficient polyethyleneimine immobilization and cationization. *Applied Surface Science* **2017**, *426*, 972-979.
291. Tiwari, A. K.; Gupta, M. K.; Pandey, G.; Narayan, R. J.; Pandey, P. C., Molecular weight of polyethylenimine-dependent transfection and selective antimicrobial activity of functional silver nanoparticles. *Journal of Materials Research* **2020**, *35* (18), 2405-2415.

292. Lacey, R., Antibacterial activity of povidone iodine towards non-sporing bacteria. *Journal of Applied Bacteriology* **1979**, *46* (3), 443-449.
293. Lepelletier, D.; Maillard, J. Y.; Pozzetto, B.; Simon, A., Povidone Iodine: Properties, Mechanisms of Action, and Role in Infection Control and Staphylococcus aureus Decolonization. *Antimicrob Agents Chemother* **2020**, *64* (9).
294. Papadopoulou, E. L.; Valentini, P.; Mussino, F.; Pompa, P. P.; Athanassiou, A.; Bayer, I. S., Antibacterial bioelastomers with sustained povidone-iodine release. *Chemical Engineering Journal* **2018**, *347*, 19-26.
295. Xing, C.-M.; Deng, J.-P.; Yang, W.-T., Synthesis of antibacterial polypropylene film with surface immobilized polyvinylpyrrolidone-iodine complex. *Journal of Applied Polymer Science* **2005**, *97* (5), 2026-2031.
296. Chabrolle, J. P.; Rossier, A., Goitre and hypothyroidism in the newborn after cutaneous absorption of iodine. *Archives of Disease in Childhood* **1978**, *53* (6), 495.
297. Pyati, S. P.; Ramamurthy, R. S.; Krauss, M. T.; Pildes, R. S., Absorption of iodine in the neonate following topical use of povidone iodine. *The Journal of pediatrics* **1977**, *91* (5), 825-828.
298. Zhu, Y.; Gao, C.; He, T.; Shen, J., Endothelium regeneration on luminal surface of polyurethane vascular scaffold modified with diamine and covalently grafted with gelatin. *Biomaterials* **2004**, *25* (3), 423-430.
299. Jayakrishnan, A.; Jameela, S. R., Glutaraldehyde as a fixative in bioprostheses and drug delivery matrices. *Biomaterials* **1996**, *17* (5), 471-484.
300. Chien, H.-H.; Ma, K.-J.; Kuo, C.-H.; Huang, S.-W., Effects of plasma power and reaction gases on the surface properties of ePTFE materials during a plasma modification process. *Surface and Coatings Technology* **2013**, *228*, S477-S481.
301. Chien, H. H.; Ma, K. J.; Yeh, Y. P.; Chao, C. L. In *Preparation of superhydrophobic surface for PTFE/ePTFE materials by oxygen plasma treatment*, Proceedings of 2011 International Conference on

Electronic & Mechanical Engineering and Information Technology, 12-14 Aug. 2011; 2011; pp 1215-1218.

302. Shahmiri, M.; Ibrahim, N.; Kamyar, S.; Jahangirian, H.; Zainuddin, N., Synthesis and Characterization of CuO Nanosheets in Polyvinylpyrrolidone by Quick Precipitation Method. *Advanced Science, Engineering and Medicine* **2013**, *5*.

303. Rahma, A.; Munir, M. M.; Khairurrijal; Prasetyo, A.; Suendo, V.; Rachmawati, H., Intermolecular Interactions and the Release Pattern of Electrospun Curcumin-Polyvinyl(pyrrolidone) Fiber. *Biological & pharmaceutical bulletin* **2016**, *39* (2), 163-73.

304. Kasprzak, A.; Popławska, M.; Bystrzejewski, M.; Łabędź, O.; Grudziński, I. P., Conjugation of polyethylenimine and its derivatives to carbon-encapsulated iron nanoparticles. *RSC advances* **2015**, *5* (104), 85556-85567.

305. Fernandes Queiroz, M.; Melo, K. R.; Sabry, D. A.; Sasaki, G. L.; Rocha, H. A., Does the use of chitosan contribute to oxalate kidney stone formation? *Marine drugs* **2014**, *13* (1), 141-58.

306. ISO 10993-12 Biological Evaluation of Medical Devices. Part 5: Tests for in Vitro Cytotoxicity. 2009.

307. ISO 10993-5 Biological Evaluation of Medical Devices. Part 12: Sample preparation and reference materials. 2021.

308. Antony, R.; Arun, T.; Manickam, S. T. D., A review on applications of chitosan-based Schiff bases. *International journal of biological macromolecules* **2019**, *129*, 615-633.

309. Bourkoula, A.; Constantoudis, V.; Kontziampasis, D.; Petrou, P. S.; Kakabakos, S. E.; Tserepi, A.; Gogolides, E., Roughness threshold for cell attachment and proliferation on plasma micro-nanotextured polymeric surfaces: the case of primary human skin fibroblasts and mouse immortalized 3T3 fibroblasts. *Journal of Physics D: Applied Physics* **2016**, *49* (30), 304002.

310. Akther, F.; Yakob, S. B.; Nguyen, N. T.; Ta, H. T., Surface Modification Techniques for Endothelial Cell Seeding in PDMS Microfluidic Devices. *Biosensors* **2020**, *10* (11).

311. Lazic, I.; Obermeier, A.; Dietmair, B.; Kempf, W. E.; Busch, A.; Tübel, J.; Schneider, J.; von Eisenhart-Rothe, R.; Biberthaler, P.;

- Burgkart, R.; Pförringer, D., Treatment of vascular graft infections: gentamicin-coated ePTFE grafts reveals strong antibacterial properties in vitro. *Journal of Materials Science: Materials in Medicine* **2022**, *33* (3), 30.
312. Weber, D. J.; Raasch, R.; Rutala, W. A., Nosocomial Infections in the ICU: The Growing Importance of Antibiotic-Resistant Pathogens. *Chest* **1999**, *115* (3, Supplement 1), 34S-41S.
313. Li, B.; Qiu, Y.; Song, Y.; Lin, H.; Yin, H., Dissecting horizontal and vertical gene transfer of antibiotic resistance plasmid in bacterial community using microfluidics. *Environment International* **2019**, *131*, 105007.
314. Li, W.; Thian, E. S.; Wang, M.; Wang, Z.; Ren, L., Surface Design for Antibacterial Materials: From Fundamentals to Advanced Strategies. *Advanced Science* **2021**, *8* (19), 2100368.
315. McKeen, L. W., 11 - Fluoropolymers. In *Film Properties of Plastics and Elastomers (Third Edition)*, McKeen, L. W., Ed. William Andrew Publishing: Boston, 2012; pp 255-313.
316. Radulovic, L. L.; Wojcinski, Z. W., PTFE (Polytetrafluoroethylene; Teflon®). In *Encyclopedia of Toxicology (Third Edition)*, Wexler, P., Ed. Academic Press: Oxford, 2014; pp 1133-1136.
317. Briguori, C.; Sarais, C.; Sivieri, G.; Takagi, T.; Di Mario, C.; Colombo, A., Polytetrafluoroethylene-covered stent and coronary artery aneurysms. *CCD Catheterization and Cardiovascular Interventions* **2002**, *55* (3), 326-330.
318. Khatskevitch, G.; Soloviev, M.; Onokhova, T.; Nikolaenko, V.; Panova, T., A rare late complication of silicone orbital implant. *Ophthalmology journal* **2016**, *9*, 55-60.
319. Rubin, J. S.; Sataloff, R. T.; Korovin, G. S., *Diagnosis and treatment of voice disorders*. Plural Publishing, Inc.: San Diego, CA, 2014.
320. *Advances in Materials Science and Implant Orthopedic Surgery*. Springer Verlag: 2013.
321. Kornberger, A.; Walter, V.; Khalil, M.; Therapidis, P.; Assmus, B.; Moritz, A.; Beiras-Fernandez, A.; Stock, U. A., Suspected involvement of EPTFE membrane in sterile intrathoracic abscess and pericardial

empyema in a multi-allergic LVAD recipient: a case report. *J Cardiothorac Surg* **2015**, *10*, 99-99.

322. International, A. S. M., *Materials and coatings for medical devices cardiovascular : MPMD Materials and processes for medical devices*. ASM International: Ohio, USA, 2009.

323. Roina, Y.; Auber, F.; Hocquet, D.; Herlem, G., ePTFE functionalization for medical applications. *Materials Today Chemistry* **2021**, *20*, 100412.

324. Roina, Y.; Auber, F.; Hocquet, D.; Herlem, G., ePTFE-based biomedical devices: An overview of surgical efficiency. *Journal of Biomedical Materials Research Part B: Applied Biomaterials* **2022**, *110* (2), 302-320.